Dissertation

submitted to the

Combined Faculties for the Natural Sciences and for Mathematics

of the Ruperto-Carola University of Heidelberg, Germany

for the degree of

Doctor of Natural Sciences

presented by

Diplom-Biologe	Helge Paternoga
Born in:	Berlin, Germany
Oral-examination:	

Ribosome assembly factors Nsa2 and Rsa4 connect the ATPase Rea1 to the maturing catalytic center of the large subunit

Referees: Prof. Dr. Ed Hurt
Prof. Dr. Michael Knop

Summary

Ribosome biogenesis is a highly complex process, which in eukaryotes depends on a myriad of assembly factors, including several energy-consuming enzymes. One of these is the ATPase Rea1, that is necessary for the formation of large ribosomal subunits. Rea1 is responsible for the removal of several assembly factors, including Rsa4, during a late step in 60S biogenesis. This release depends on a Rea1-generated pulling force, that is transmitted to Rsa4 and eventually results in its dissociation from pre-ribosomes. It is therefore of high interest to identify, which proteins or rRNA elements connect Rsa4 to the pre-ribosome, as these could transmit the Rea1 power stroke to the maturing 60S subunit and result in structural rearrangements at their binding site.

This study builds on initial findings, that the 60S assembly factor Nsa2 is a putative interaction partner of Rsa4. Using genetic and biochemical approaches, I was able to verify the interaction and demonstrate, that it is essential for yeast growth. Furthermore, I was able to crystallize the Nsa2-Rsa4 hetero-dimer and the structure was solved in collaboration with the lab of Dr. Irmi Sinning (BZH, Heidelberg). A subsequent structure-function analysis revealed the molecular details of the Nsa2-Rsa4 interaction and its impact on 60S biogenesis. Moreover, I was able to fit the Nsa2-Rsa4 crystal structure in an EM-volume of the Arx1 pre-ribosome, that places Nsa2 and Rsa4 at the nascent peptidyl transferase center (PTC). Here, Rsa4 is bound to the immature central protuberance and Nsa2 is oriented towards the nascent tRNA binding site. Using Nsa2 NMR structures, which were generated in collaboration with the lab of Dr. Elisar Barbar (Oregon State University), and crosslinking data from Dr. Sander Granneman (University of Edinburgh), I propose a model in which the globular C-domain of Nsa2 is located at the maturing peptidyl transferase center and the α-helical N-domain of Nsa2 reaches around immature rRNA helix 89 towards the P stalk region. Nsa2 and Rsa4 therefore connect Rea1 to the maturing PTC, which suggests an additional function of the Rea1-generated pulling force beyond the mere removal of assembly factors. The positioning and functional analysis of Nsa2 implies, that Rea1 exerts a mechanical force on immature helix 89, which is necessary for assembly of the catalytic center during 60S biogenesis.

Zusammenfassung

Die Ribosomenbiogenese ist ein hochkomplexer Vorgang, welcher in Eukaryoten von einer großen Zahl nicht-ribosomaler Proteine abhängt. Eines dieser Proteine ist die ATPase Rea1, welche für die Reifung der großen Untereinheit benötigt wird. Während eines späten Reifungsschrittes entfernt Rea1 eine Reihe von Biogenesefaktoren, einschließlich Rsa4. Es wurde gezeigt, dass für diesen Schritt die ATPase-Aktivität von Rea1 notwendig ist, welche vermutlich eine mechanische Kraft erzeugt, die auf Rsa4 einwirkt und es schließlich vom Prä-Ribosom entfernt. Es ist daher von großem Interesse herauszufinden, welche Proteine, oder Teile der ribosomalen Ribonukleinsäure, Rsa4 mit dem Prä-Ribosom verbinden, da diese an aktiven strukturellen Umlagerungen durch Rea1 beteiligt sein könnten.

Diese Grundlage meiner Doktorarbeit beruht auf vorläufigen Ergebnissen, dass der 60S Biogenesefaktor Nsa2 mit Rsa4 interagiert. Mit Hilfe von genetischen und biochemischen Methoden konnte ich zeigen, dass Nsa2 direkt mit Rsa4 interagiert und dass diese Interaktion für das Wachstum von Hefezellen notwendig ist. Weiterhin habe ich den Nsa2-Rsa4 Hetero-dimer kristallisiert und die Struktur der Interaktion konnte in Zusammenarbeit mit dem Labor von Dr. Irmi Sinning (BZH, Heidelberg) gelöst werden. Daraufhin habe ich die Bedeutung individueller Aminosäuren für die Interaktion untersucht und ihre Rolle in der 60S Biogenese charakterisiert. Außerdem konnte ich die Nsa2-Rsa4 Kristallstruktur in das EM-Volumen des Arx1-Partikels einpassen, was zeigt, dass Nsa2 und Rsa4 am aktiven Zentrum der großen Untereinheit lokalisiert sind. Rsa4 interagiert mit der unreifen Protuberanz und Nsa2 ist zur tRNA-Bindestelle orientiert. Mit Hilfe von NMR Strukturen, welche in Zusammenarbeit mit dem Labor von Dr. Elisar Barbar (Oregon State University) erzeugt wurden, und mit Daten einer Quervernetzungsanalyse von Dr. Sander Granneman (University of Edinburgh), schlage ich ein Modell vor in dem die globuläre C-Domäne von Nsa2 am unreifen aktiven Zentrum gebunden ist während die α-helikale N-Domäne von dort über rRNA helix 89 zum GTPase-Zentrum spannt. Nsa2 und Rsa4 verbinden daher Rea1 mit dem unreifen katalytischen Zentrum der großen Untereinheit, was eine Funktion von Rea1 in der Reifung dieser Region nahelegt. Die Analyse von Nsa2 zeigt, dass Rea1 eine mechanische Kraft auf rRNA helix 89 überträgt, welche für die Bildung des aktiven Zentrums benötigt wird.

Acknowledgements

First and foremost I wish to thank my advisor, Prof. Dr. Ed Hurt for giving me the opportunity to work in his lab and making it possible to follow my curiosity. I would also like to express my gratitude to Dr. Jochen Baßler for his supervision and constructive feedback.

Furthermore, I would like to thank my collaborator, Prof. Dr. Irmi Sinning for advice, encouragement and for making it possible to gain experience in structural biology. I am grateful to all members of the Sinning lab, who handled and shot countless protein (and salt) crystals during the course of the project. Special thanks go out to Dr. Iris Holdermann for solving the structure of the Nsa2-Rsa4 hetero-dimer and to Dr. Domenico Lupo for guiding my first crystallization attempts and his unwavering positive attitude, which significantly affected my approach to science. Furthermore, I would like to thank Gunter Stier and Dr. Yasar Luqman Ahmed for scientifc discussions and know-how. Similarly, I want to thank Dr. Jürgen Kopp and Claudia Siegmann for explanations and all kinds of help with the crystal-growing process.

I would also like to thank my collaborator, Prof. Dr. Elisar Barbar for scientific advice and discussions, as well as Sarah Anna Clark and Dr. Afua Nyarko for solving the structures of the Nsa2 N- and C-domains, respectively.

I am thankful to the members of my thesis committee, Prof. Dr. Michael Knop and Prof. Dr. Tamás Fischer for their scientific input and support throughout the years.

Furthermore, I would like to express my thanks to the members of the Hurt lab for creating a great working atmosphere, especially Martina Kallas for her energetic nature and cheese sandwiches, as well as Ruth Kunze for her comments from the far side of the bench. I am grateful to everybody, who engaged in scientific discussions and helped me navigate the many pitfalls of working in the lab, particularly Dr. Emma Thomson, Matthias Thoms , Dr. Sébastien Ferreira-Cerca, and Dr. Philipp Stelter. Similarly, I would like to express special thanks to my chess-nemesis Dr. Markus Kornprobst for creating an entertaining lab experience. I also want to convey my deepest gratitude to Selene Cordeiro and Jutta Müller for keeping the engine running and always delivering on time.

Finally, I dedicate this thesis to my family, who made me who I am and who are most important to me: Edda, Ralf, Isa, Lucy, and Jana.

Contents

1 Introduction **1**

1.1 Identification and structure of the ribosome 4

1.1.1 Secondary structure of rRNAs 6

1.1.2 The tertiary structure of the ribosome 9

1.1.3 Peptidyl transferase center (PTC) 12

1.2 Evolution of the ribosome 13

1.2.1 Eukaryogenesis and the ribosome 15

1.3 Ribosome biogenesis in *Saccharomyces cerevisiae* 17

1.3.1 Initial stages of ribosome formation occur in the nucleolus 20

1.3.2 rRNA modification 22

1.3.3 rRNA processing 25

1.3.4 Integration of r-proteins into nascent pre-ribosomes 27

1.3.5 Comparison of ribosome biogenesis in bacteria and eukaryotes . 29

1.3.6 Small subunit assembly 31

1.3.7 Large subunit assembly 32

2 Results **44**

2.1 Nsa2 interacts with Rsa4 44

2.1.1 Nsa2 binds to the pore of the Rsa4 β-propeller 47

2.2 The functional context of the Nsa2-Rsa4 interaction 52

2.2.1 The Nsa2 Y90A mutant arrests 60S biogenesis 53

2.2.2 Rsa4 point mutants disrupt the interaction with Nsa2 56

2.3 Structural studies of Nsa2 domains 59

2.3.1 The N-domain of Nsa2 consists of flexible α-helices 60

2.3.2 The C-domain of Nsa2 is highly similar to Rps8 61

2.4 Localization of Nsa2 and Rsa4 on the pre-ribosome 64

2.4.1 Nsa2 and Rsa4 associate with the maturing A-site 65

2.5 Nsa2 associates with pre-ribosomes via the N-domain 68

3 Discussion **72**
3.1 The role of Nsa2 in Rea1 function . . . 73
3.1.1 A counterforce model for Rea1 activation . . . 76
3.2 Additional functions of Nsa2 in 60S subunit assembly . . . 77
3.2.1 rRNA domain stabilization by Nsa2 . . . 77
3.2.2 The role of Nsa2 in helix 89 maturation . . . 79
3.3 Recruitment of Nsa2 to the pre-ribosome . . . 80
3.4 Does Rsa4 have an extra-ribosomal function? . . . 82
3.5 Evolutionary origins of Nsa2 . . . 83

4 Materials and Methods **87**
4.1 Molecular biology techniques . . . 87
4.1.1 Cloning . . . 87
4.1.2 Plasmid construction . . . 87
4.2 Yeast techniques . . . 92
4.2.1 Yeast strains . . . 92
4.2.2 Yeast media . . . 92
4.2.3 Growth assays . . . 93
4.2.4 Non-radioactive pulse chase . . . 93
4.3 Biochemical techniques . . . 93
4.3.1 Tandem affinity purification . . . 93
4.3.2 Western blotting . . . 94
4.3.3 Purification of recombinantly expressed proteins from *E.coli* . . . 94
4.3.4 *In vitro* reconstitution of the Nsa2-Rsa4 interaction . . . 95
4.3.5 Crystallization of the minimal Rsa4-Nsa2 complex . . . 96
4.3.6 Sucrose gradient analysis . . . 96
4.4 *In silico* analysis . . . 98

Bibliography **100**

Appendix **124**
A.1 Salt stability of the Nsa2-Rsa4 interaction . . . 125
A.2 *In vitro* degradation of ctNsa2 . . . 126
A.3 Crystallization finescreen for the Nsa2-Rsa4 complex . . . 127
A.4 Rsa4 alignment . . . 128
A.5 The S8E family . . . 129
A.6 S8E family alignment . . . 130
A.7 Nsa2 alignment . . . 132

A.8 The β-barrel insertion and the linker of Nsa2 are essential 133
A.9 Nog1 N-domain alignment 134
List of abbreviations 135
List of figures 136

1 Introduction

Ribosomes are essential macromolecules, whose function, translation of the genetic code, is conserved in all life. They are large ribonucleoprotein particles that are composed of two thirds RNA and one third protein and contain a catalytic domain, called the 'ribosomal core', that is invariant from bacteria to humans (Kurland 1960; Mears et al. 2002; Melnikov et al. 2012; Schnare et al. 1996; Winker and Woese 1991). Nevertheless, ribosomes have acquired new structural features in evolution and sequence analysis of the ribosomal RNAs can be used to infer similarities between species, which is being used to define the universal tree of life (Woese 1987; Woese 2000).

Ribosomes are ancient ribozymes that produce proteins by a RNA-catalyzed mechanism without the contribution of proteins in the active center (Ban et al. 2000; Khaitovich et al. 1999). Because RNA is essential for protein synthesis, ribosomes are central to the RNA-world hypothesis, which states, that early biologic reactions were catalyzed by RNA-based enzymes, that were outcompeted by proteins in the course of evolution, and that RNA-encoded transmission of genetic information predates DNA (Crick 1968; W. Gilbert 1986; Orgel 1968; Rich 1962; Woese 1967). As the function of the ribosome is conserved, it is seen as proof that ribozymes preceded protein enzymes, because translation does not rely on proteins, but instead uses RNAs in all reaction steps. The genetic code is delivered to the ribosome in the form of messenger RNA (mRNA) and decoding is achieved by transfer RNAs (tRNA), that associate specifically with the mRNA while it is bound to the decoding site of the ribosomal RNA (rRNA). The tRNAs carry specific amino acids, that are incorporated into nascent polypeptides at the site of peptide bond formation, which is also formed by rRNA (Brenner et al. 1961; Gros et al. 1961; Hoagland et al. 1958; Hoagland et al. 1957; Monro 1967; Nirenberg and Matthaei 1961). Today, the genetic code is first copied from a DNA template to create the mRNA, that is then used to translate all DNA-encoded proteins in the cell. Translation is therefore indispensable for cellular activity, as proteins are involved in all cellular processes, including cell division, the formation of organelles, metabolism, and adaptation to external stimuli.

The ribosome is composed of two subunits, the large subunit, which contains the peptidyl transferase center (PTC), that is the site of peptide bond formation, and the small subunit, which binds the messenger RNA (mRNA) and enables the decoding of

the genetic code into a specific polypeptide chain (Monro 1967; Nirenberg and Matthaei 1961). Both subunits contain large single-stranded RNAs, which assume compact three-dimensional structures, that are decorated by ribosomal proteins (r-proteins). Although RNA makes up a large portion of the ribosome and is solely responsible for peptide bond formation, the ribosomal proteins are essential constituents of the ribosome, that are stabilizing the structure of the rRNA through unique RNA binding domains.

Because ribosomes are fundamental components of the cell, they are embedded in a network of signaling and regulatory pathways (reviewed in Mahoney et al. 2009). The nutrient state of the cell is especially important, as ribosome biogenesis consumes a large portion of cellular resources, and starvation has been shown to induce turnover of mature ribosomes (Iadevaia et al. 2014; Kraft et al. 2008). Together, these two processes define the number of ribosomes in the cell, which is a key determinant of cell proliferation, as the number of ribosomes has to double before each cell division (Kief and Warner 1981). Therefore, ribosome biogenesis plays a major role in cell growth, as well as in cancer progression, and is frequently upregulated in cells with deregulated proto-oncogenes (Markman et al. 2010; Rosen and She 2006; Ruggero et al. 2004).

Aberrations in ribosome assembly lead to an arrest at distinct biogenesis steps, which can disturb the steady state levels of ribosomal components and biogenesis factors. Because ribosomal proteins are produced in large numbers, they often accumulate in a free form as a result of impaired ribosome biogenesis, which has been termed 'ribosomal stress'. This accumulation has been shown to have negative effects on the cell and induces cellular degradation mechanisms that remove excess r-proteins (Lam et al. 2007; Sung, Porras-Yakushi, et al. 2016; Sung, Reitsma, et al. 2016). However, several ribosomal proteins have acquired extra-ribosomal functions when they are not incorporated into ribosomes (reviewed in Warner and McIntosh 2009; Zhou et al. 2015). One very important example is the regulation of the MDM2-p53 feedback loop by RPL5 (uL18) and RPL11 (uL5), which inhibit the degradation of p53 in stressed cells and therefore enable the cell to undergo p53-mediated apoptosis (Dai and Lu 2004; Lohrum et al. 2003; Marechal et al. 1994; Nicolas et al. 2016; Y. Zhang et al. 2003).

Misassembled, or non-functional ribosomes result in various detrimental effects to the organism, including cell death by lack of protein synthesis, or cellular deregulation and cancer, which are associated with the accumulation of aberrant translation products. There are a number of rare human diseases, that have been connected to mutations in ribosomal components and biogenesis factors, which have been therefore named 'ribosomopathies'. Ribosomopathies display distinct phenotypes, that are summarized in Table 1.1. Clinical effects are highly diverse, yet several ribosomopathies share phenotypes, for example anemia is found in Diamond-Blackfan Anemia and 5q-syndrome,

craniofacial defects in Diamond-Blackfan Anemia and Treacher Collins syndrome, and short stature in Diamond-Blackfan Anemia and Shwachman-Diamond Syndrome (Burwick et al. 2011; Collins 1900; Ellis 2014; Glader et al. 1983; Halperin and Freedman 1989). This suggests, that developmental pathways are affected by individual r-proteins, whose mutations generate tissue specific phenotypes, with varying phenotypic range, and that there is not one 'mutated ribosome' phenotype. All known ribosomopathies are heterozygous, which suggests that associated mutations would be inviable in the homozygous state (Narla and Ebert 2010). In line with this observation, it has been shown in animal models of Diamond-Blackfan Anemia that homozygous loss of function of affected ribosomal proteins is lethal (Matsson et al. 2004; McGowan et al. 2008). Many ribosomopathies additionally increase the risk of certain cancers in the affected individuals (Table 1.1). This highlights the connection between ribosomal stress and cancer development and emphasizes that somatic ribosome defects are emerging as a common occurrence in cancers (Kandoth et al. 2013).

One explanation for the diverse phenotypes of ribosomopathies, that has been emerging recently, is that ribosome composition can vary. Most r-proteins in *Saccharomyces cerevisiae* are encoded by two genes, which in many cases do not produce identical proteins. In humans, it has been shown, that specific variants of r-proteins are expressed in different tissues, as RPL3L is specifically transcribed in muscle and RPL10L in testis (Gupta and Warner 2014). Furthermore, the human malaria parasite *Plasmodium falciparum* expresses different isoforms of rRNA at different stages of the parasitic life cycle (Gunderson et al. 1987). Additionally, rRNA modifications are not applied to all rRNAs uniformly and consequently lead to heterogeneity in the ribosome population (reviewed in Lafontaine 2015), which is further increased by different possible cleavage products of rRNA, as seen in the 5.8S rRNA in yeast. Therefore, it has been suggested, that the combination of individual components can lead to specialized ribosomes with varying translational capacity (Dinman 2016; W. V. Gilbert 2011; Xue and Barna 2012). Ribosomopathies might therefore reflect this specialization, as they show tissue specific phenotypes, which could be caused by a specialized subset of ribosomes that is present in these tissues.

Therefore, when ribosomes are formed, the biogenesis machinery has to ensure, that functioning components are incorporated into nascent ribosomes, which is controlled throughout the maturation process. Alterations in assembly lead to severe phenotypes, which are still not fully understood and necessitate further studies, that will elucidate the role of ribosome biogenesis in development and disease.

Table 1.1: Ribosomopathies and associated phenotypes MDS = myelodysplastic syndrome, AML = acute myeloid leukaemia; taken from Narla and Ebert 2010.

Disease	Gene Defect	Clinical Features	Cancer Risk
Diamond Blackfan anemia	RPS19, RPS24, RPS17, RPL35A, RPL5, RPL11, RPS7, RPL36, RPS15, RPS27A	Macrocytic anemia Short stature Craniofacial defects Thumb abnormalities	?osteosarcoma ?MDS
5q-syndrome	RPS14	Macrocytic anemia Hypolobulated micromegakaryocytes	10% progression to AML
Shwachman-Diamond syndrome	SBDS	Neutropenia/infections Pancreatic insufficiency Short stature	MDS and AML
X-linked dyskeratosis congenita	DKC1	Cytopenias Skin hyperpigmentation Nail dystrophy Oral leukoplakia	AML Head+neck tumors
Cartilage hair hypoplasia	RMRP	Hypoplastic anemia Short limbed dwarfism Hypoplastic hair	Non-Hodgkin lymphoma Basal cell carcinoma
Treacher Collins syndrome	TCOF1	Craniofacial abnormalities	None reported

1.1 Identification and structure of the ribosome

The first hint that RNA is involved in producing proteins was reported in the 1940s by Jean Brachet and Torbjörn Caspersson, who independently showed that cells which are actively synthesizing proteins are rich in RNA (Brachet 1942; Caspersson 1941). The site of protein synthesis was narrowed down in the following years to the cytoplasm of the cell (Caspersson 1947) and in 1950 it was reported that the newly-defined microsomal fraction incorporates labeled amino acids into proteins *in vivo* (Borsook et al. 1950). Microsomes are generated from the endoplasmic reticulum (ER) after cell lysis, when pieces of the ER reform into small vesicles. Therefore, they contain a mixture of ER components which are very heterogeneous. Further analysis of microsomal components revealed in 1953, that a ribonucleoprotein particle is responsible for the demonstrated protein synthesis activity (Allfrey et al. 1953).

This work was the basis for first structural studies on microsomes (Porter 1954; Sjostrand and Hanzon 1954; Slautterback 1953), which were greatly improved by advances in electron microscopy and centrifugation techniques in the lab of Albert Claude. Together, these two methods enabled the analysis of defined cellular components, which allowed the determination of molecular structures at an unprecedented resolution, which marked the beginning of modern molecular cell biology. George Palade in the Claude lab was the first to describe the structure of the microsomal ribonucleoprotein particles in 1955, which were renamed to 'ribosomes' in 1958 (Palade 1955). He was awarded for this discovery, together with Albert Claude, with the Nobel Prize for Physiology or Medicine in 1974. The name 'ribosome' was given by editor Richard B. Roberts in a collection of papers from the first symposium of the Biophysical Society in 1958:

> *"During the course of the symposium a semantic difficulty became apparent. To some of the participants, microsomes mean the ribonucleoprotein particles of the microsome fraction contaminated by other protein and lipid material; to others, the microsomes consist of protein and lipid contaminated by particles. The phrase "microsomal particles" does not seem adequate, and "ribonucleo-protein particles of the microsome fraction" is much too awkward. During the meeting the word "ribosome" was suggested; this seems a very satisfactory name, and it has a pleasant sound. The present confusion would be eliminated if "ribosome" were adopted to designate ribonucleoprotein particles in the size range 20 to 100 S."* Roberts 1958, preface

After ribosomes had been discovered, it was quickly realized, that they are responsible for producing protein and that they are present in all biological organisms with highly similar structures (Littlefield et al. 1955; Ts'o et al. 1958). In the following years, the RNA content of ribosomes was analyzed and two major RNA components were identified (Hall and Doty 1959; Littauer and Eisenberg 1959; Timasheff et al. 1958). These were shown to be part of specific subunits that together form the whole ribosome in *Escherichia coli*, with the 16S rRNA being present in the 30S subunit and the 23S rRNA in the 50S subunit (Kurland 1960). The association of these subunits into 70S ribosomes could be controlled by the amount of magnesium that was added to the buffer, which demonstrated the importance of Mg^{2+} for RNA folding (Tissieres and Watson 1958). In 1963, it was shown, that multiple ribosomes can bind to the same mRNA during translation, forming higher ordered structures called 'polysomes' (Warner et al. 1963).

1.1.1 Secondary structure of rRNAs

Ribosomal RNA makes up two thirds of the ribosome and folds into a compact three-dimensional arrangement, that was already observed by early electron microscopic studies (Kurland 1960; Palade 1955). Folded rRNAs form the body of ribosomal subunits, which are associated, mostly at the exterior, by ribosomal proteins. Because rRNA is single stranded, it can form intermolecular contacts that create an elaborate secondary structure with a plethora of RNA helices, pseudoknots and other structural elements. The determination of the secondary structure of rRNAs was therefore a major undertaking, which relied on data from chemical modifications and nuclease susceptibility of rRNA, as well as a phylogeny-based approach, that was first described in the structure prediction of 5S rRNA (Fox and Woese 1975). The secondary structure of larger rRNAs could only be determined after the sequencing and the subsequent sequence comparison of *E. coli* 16S (Brosius et al. 1978) and 23S rRNA (Brosius et al. 1980) to mitochondrial rRNAs from mouse and human (Eperon et al. 1980; Van Etten et al. 1980). This led to the first phylogeny-based models of 16S and 23S rRNA secondary structures and unraveled their evolutionary relationships at the same time (Glotz and Brimacombe 1980; Glotz et al. 1981; Stiegler et al. 1980; Woese et al. 1980).

The phylogeny-based secondary structure prediction proved to be quite accurate when the crystal structure of the ribosome was solved, yet did not accurately depict the exact base-pairing of all rRNA nucleotides. Recently, the secondary structure models of rRNAs from *Escherichia coli, Thermus thermophilus, Haloarcula marismortui, Saccharomyces cerevisiae, Drosophila melanogaster*, and *Homo sapiens* have been updated with the knowledge gained from available three-dimensional structures, which allow a more accurate view of rRNA folding in the ribosome (Petrov, Bernier, Gulen, et al. 2014; Petrov et al. 2013).

The updated rRNA secondary structures of yeast ribosomal subunits are shown in Figure 1.1 (small subunit) and Figure 1.2 (large subunit). RNA helices and expansion segments are labeled according to Gerbi 1996; Petrov, Bernier, Gulen, et al. 2014. Expansion segments are rRNA elements, that have emerged since the common ancestor and are evidence for the ongoing evolution of the ribosome (section 1.2). Each subunit consists of rRNA domains, that can be considered as modules that make up the ribosome. The small subunit consists of four subdomains, which are arranged around the central pseudoknot at helix 2, that connects all four domains and is conserved in evolution (Gutell et al. 1994). The large subunit contains seven rRNA domains, plus the 5S and 5.8S rRNAs. It is organized around domain 0, which connects the remaining six domains, similarly to the central pseudoknot in the small subunit (Petrov et al. 2013).

Domain 0 has been defined as an additional seventh domain, compared to pre-existing phylogeny-based models, as it is evident from three-dimensional structures that the rRNA in this region is compact and double helical, which opposes the extended single-stranded conformation in the phylogeny based model (Petrov et al. 2013). In addition, it has been shown by the Mfold software, that domain 0 folds into its native structure *in silico* (Petrov et al. 2013; Zuker 2003). This establishes domain 0 as a novel, autonomous seventh rRNA domain of the large subunit.

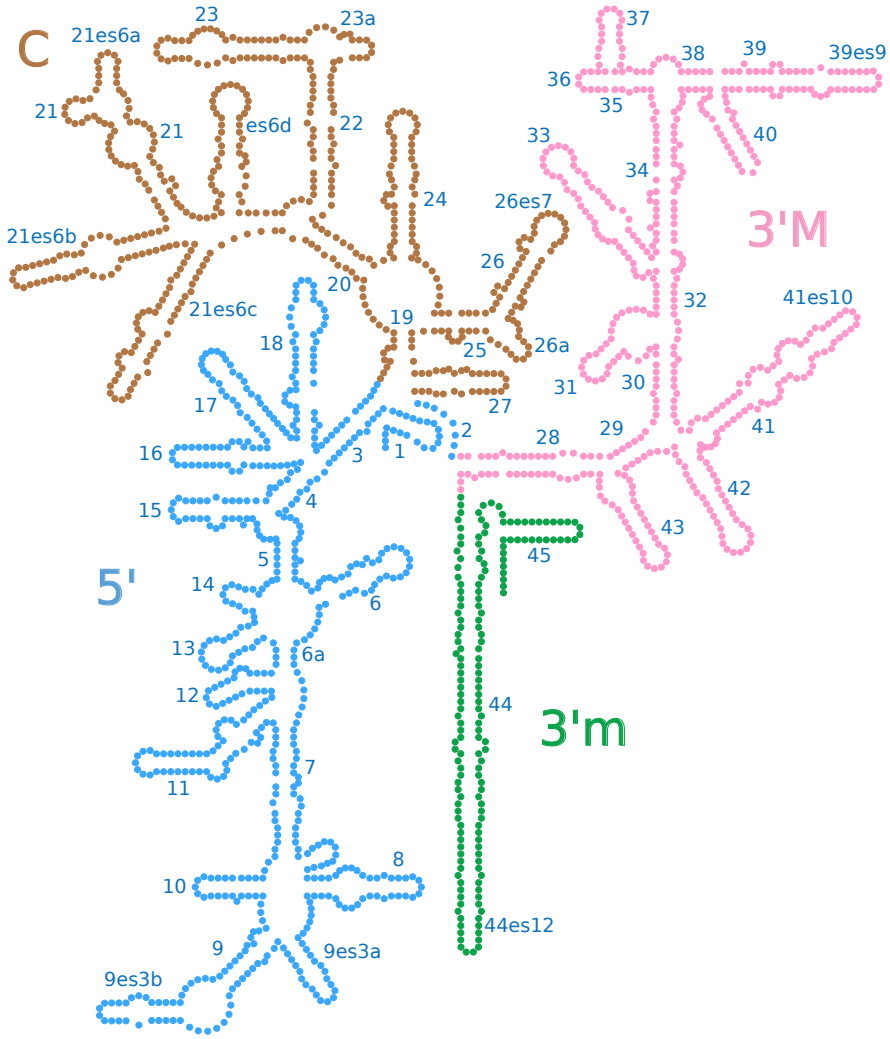

Figure 1.1: Secondary structure of the small subunit of *Saccharomyces cerevisiae* Each circle represents one nucleotide. Helices and expansion segments are labeled according to Gerbi 1996; Petrov, Bernier, Gulen, et al. 2014, es = expansion segment.

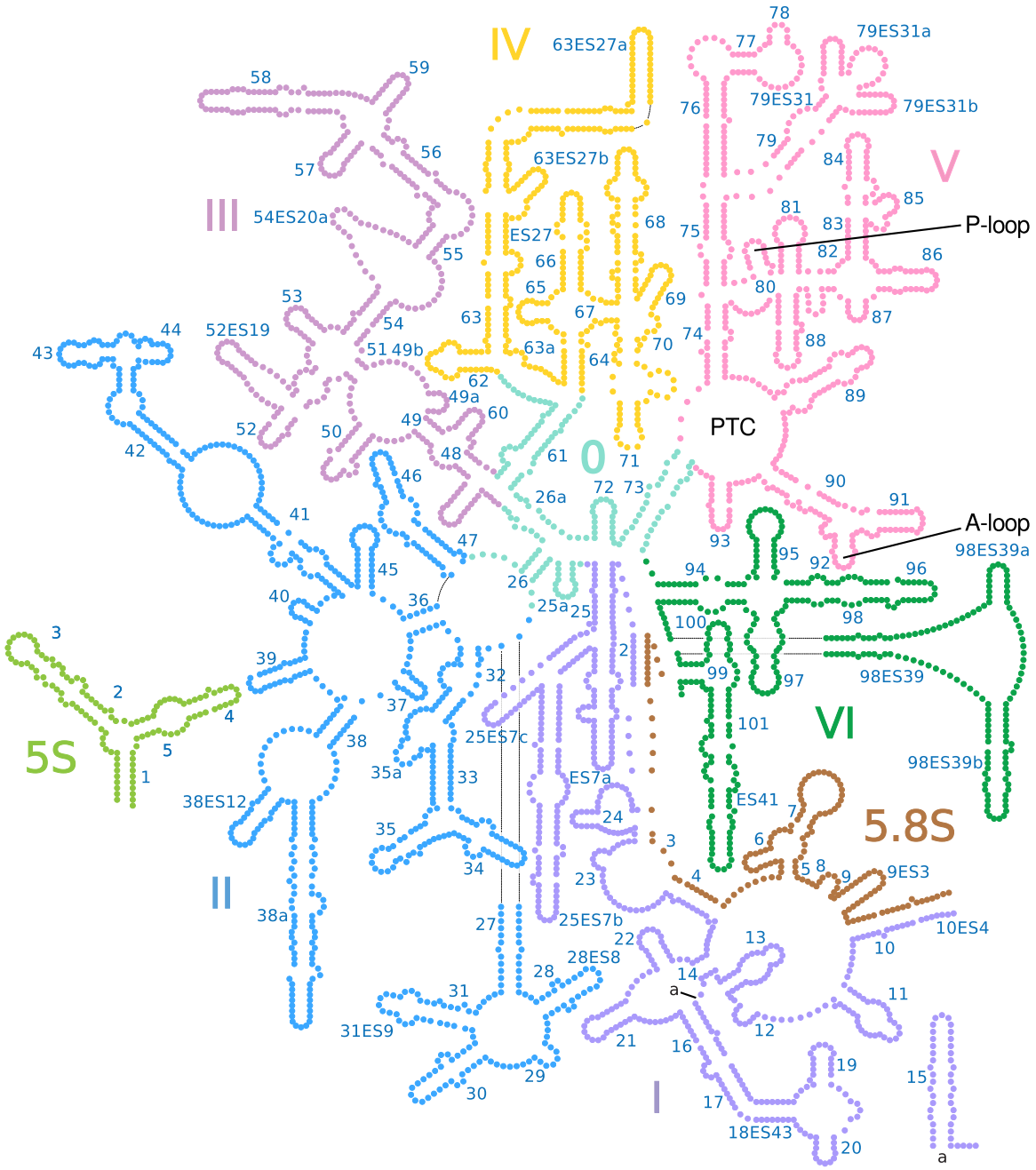

Figure 1.2: Secondary structure of the large subunit of *Saccharomyces cerevisiae* Each circle represents one nucleotide. Helices and expansion segments are labeled according to Gerbi 1996; Petrov, Bernier, Gulen, et al. 2014, es = expansion segment. The A- and P-loop contribute to tRNA binding in the A- and P-site, respectively. PTC = Peptidyl Transferase Center.

1.1.2 The tertiary structure of the ribosome

The ribosome is a huge macromolecular assembly, with a molecular weight of 2.3 MDa in bacteria, 3.3 MDa in lower eukaryotes, like *S. cerevisiae*, and up to 4.3 MDa in higher eukaryotes, like humans. Bacterial ribosomes are made up of three rRNAs and 54 r-proteins (21 small subunit proteins + 33 large subunit proteins), whereas eukaryotic ribosomes contain four separate rRNAs and 80 proteins (79 in yeast) of which 33 are small subunit proteins and 47 are large subunit proteins (46 in yeast). The rRNA contributes greatly to the size difference of bacterial and eukaryotic ribosomes, as it has grown considerably in the course of evolution. Bacterial ribosomes contain ~4500 nucleotides, whereas lower and higher eukaryotic ribosomes contain ~5500 and ~7200 nucleotides, respectively. The ribosomal RNA assembles with r-proteins to build the small and large ribosomal subunits, which are called 30S + 50S in bacteria and 40S + 60S in eukaryotes. Together they form the ribosome, which sediments at 70S in bacteria and 80S in eukaryotes. Although they differ in size, the bacterial and eukaryotic ribosome share a common core of 34 conserved proteins, 15 in the small subunit and 19 in the large subunit and about ~4400 nucleotides, which include the major functional sites of the ribosome: the peptidyl transferase center and the decoding center (Melnikov et al. 2012). This common core is basically invariant in evolution and is at the center of all cellular life on earth.

The complexity of the ribosome was only fully understood, when the first high resolution crystal structures of bacterial ribosomal subunits were published in 2000. The structure of the small subunit was solved independently in the labs of Ada E. Yonath and Venkatraman Ramakrishnan and the large subunit was solved in the lab of Thomas A. Steitz (Ban et al. 2000; Schluenzen et al. 2000; Wimberly et al. 2000). As this was a major step for the analysis of large biological macromolecules and because ribosomes are essential for life, these discoveries were awarded with the Nobel Prize for Chemistry in 2009. In the following years more structures were published, which elucidated the functional aspects of the ribosome. The first complete structure of bacterial 70S ribosomes was solved in 2001 at a resolution of 5.5 Å, which was improved in 2005 to 3.5 Å (Schuwirth et al. 2005; Yusupov et al. 2001). This allowed the detailed study of how the ribosomal subunits interact and was the basis for analyzing the complete ribosome together with tRNAs and mRNA, which was first achieved in 2006 (Korostelev et al. 2006; Selmer et al. 2006; Yusupova et al. 2006). The first structure of the complete eukaryotic 80S ribosome was solved in 2010, when the group of Marat Yusupov published the structure of the *S. cerevisiae* 80S ribosome at 4.15 Å. The resolution could be improved by the same group one year later to 3.0 Å (Ben-Shem et al. 2011; Ben-Shem et al. 2010).

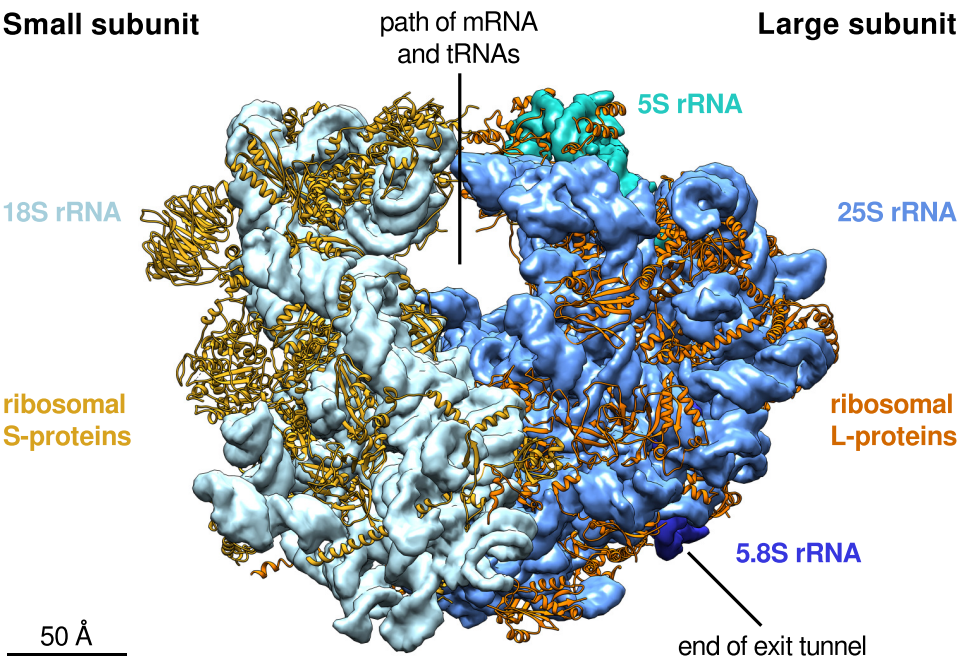

Figure 1.3: 80S ribosome of *Saccharomyces cerevisiae* The rRNAs are shown as volumes (light blue = 18S rRNA, medium blue = 25S rRNA, dark blue = 5.8S rRNA, and light sea green = 5S rRNA). R-proteins are shown in ribbon representation (orange = S-proteins and orange-red = L-proteins). PDB code: 4V88.

Recently, the structure of the human 80S was solved, as well as the 80S of *Drosophila melanogaster* and the human parasite *Trypanosoma brucei* (Anger et al. 2013; Hashem et al. 2013). These structures reveal the extent of ribosomal evolution from bacteria to higher eukaryotes and highlight the intricate arrangement of the ribosomal proteins on the rRNAs.

The 80S ribosome has a compact globular structure, which is defined by the ribosomal RNAs. This rRNA scaffold is bound by ribosomal proteins, that often possess long extensions, which wrap around the ribosome and enclose the rRNA like a net (Figure 1.3). The active site of the ribosome is formed at the subunit interface in the 80S, it is devoid of r-proteins and does not participate in forming intersubunit bridges (Figure 1.4A,B). Instead, the two subunits cooperate to form an opening in the 80S, which is oriented perpendicular to the intersubunit surface and allows the movement of mRNA and tRNAs through the ribosome during translation. This movement is necessary for the processivity of the ribosome in forming polypeptides, that are subsequently released from the ribosome through a tunnel in the 60S subunit, which has been named 'exit tunnel' (Figure 1.3 and Bernabeu and Lake 1982). The exit tunnel spans from the peptidyl transferase center to the solvent side of the 60S subunit and is about ~80 Å in length. During translation, it can accommodate 30-40 amino acids of the nascent chain (Malkin and Rich 1967). These numbers indicate, that the nascent chain is at least partially folded inside the exit

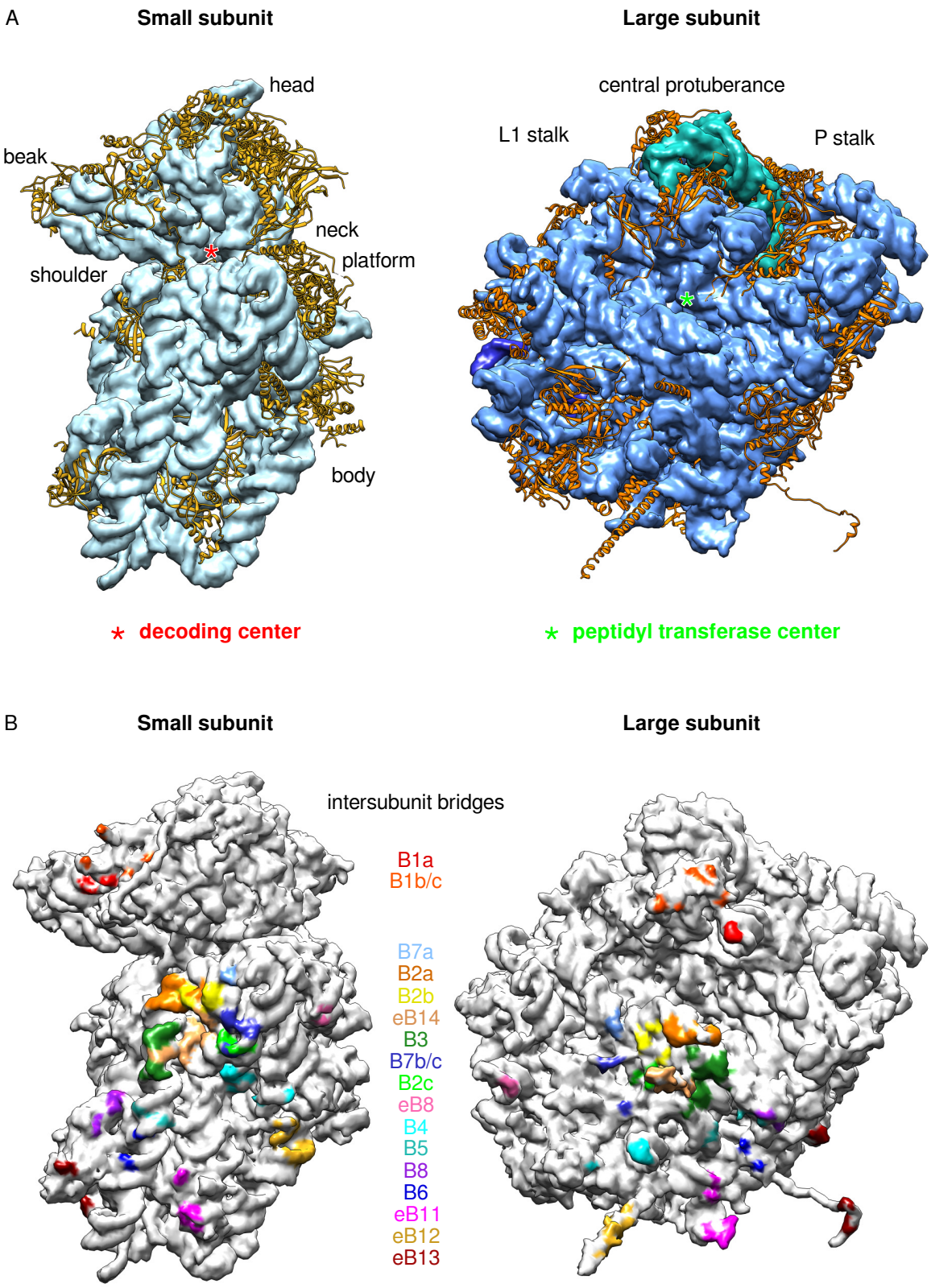

Figure 1.4: Ribosomal subunits of *Saccharomyces cerevisiae* 40S and 60S subunit interfaces are shown, PDB code: 4V88. A) Structural features of ribosomal subunits. The rRNA is shown as a volume and ribosomal proteins are shown as ribbon representation. Features of the small subunit are labeled according to Wimberly et al. 2000. The decoding center and peptidyl transferase center are indicated with a red and a green asterisk, respectively. B) Eukaryotic intersubunit bridges. Ribosomal proteins and rRNA are shown as one volume. Subunit bridges are depicted according to Ben-Shem et al. 2011.

tunnel, because an unfolded chain of 30 amino acids would have a length of 105 Å (Voss et al. 2006). The largest continuous diameter of the exit tunnel is 13.7 Å, which allows only α-helices, but not larger structures, to fit inside (Voss et al. 2006). Therefore, it has been suggested, that the nascent chain can fold into α-helices in the exit tunnel, at least partially, when some bending of the helix axis is permitted (Voss et al. 2006).

The ribosomal subunits are held together by multiple contact sites, which are called 'intersubunit bridges' (Figure 1.4B). These are located all over the subunit interfaces and are formed by both rRNA and r-proteins. They are important for the stability of the 80S and at the same time have to allow the movement of the subunits relative to each other during translation. The B2a and B2b bridges on the large subunit form an important pivoting point for the small subunit, which is necessary for the ratcheting movement of the small subunit during translation.

The ribosomal subunits are highly asymmetric and possess a number of structural features, that have been initially defined by electron microscopy. The small subunit consists of a body and a head, which are further divided into shoulder, platform, neck and beak (Figure 1.4A). The mRNA wraps around the neck of the small subunit during translation which together with the platform, forms the decoding center of the SSU. The large subunit has a globular structure with three protruding features, which are visible in the so called 'crown view' of the LSU and are located at the intersubunit side, above the peptidyl transferase center. They are called L1 stalk, central protuberance, and P stalk in eukaryotes (Figure 1.4A), and are important for the selection, movement and release of tRNAs during translation.

1.1.3 Peptidyl transferase center (PTC)

The PTC is the site of peptide bond formation, a process which involves the binding and movement of peptidyl-tRNAs through distinct sites on the large subunit. The large subunit can accommodate three tRNAs at the same time, two binding sites are located directly at the PTC and one is located adjacent to the PTC (Rheinberger et al. 1981; Wettstein and Noll 1965). The initial binding site is called the A site, because it recruits aminoacyl-tRNA, that is then moved to the P site (for peptidyl-tRNA), where it is covalently attached to the nascent polypeptide. After peptide bond formation, the empty tRNA is moved to the E site (for exit site) and released from the ribosome at the next translation step.

The PTC is assembled by 25S rRNA helices 74, 80, and 89-93 of domain V, that are arranged around a central opening, which forms the beginning of the exit tunnel (Figure 1.5). It possesses an internal symmetry, as helices 74, 80, and 89 can be superimposed with helices 90-93, which is very unusual because the remaining parts

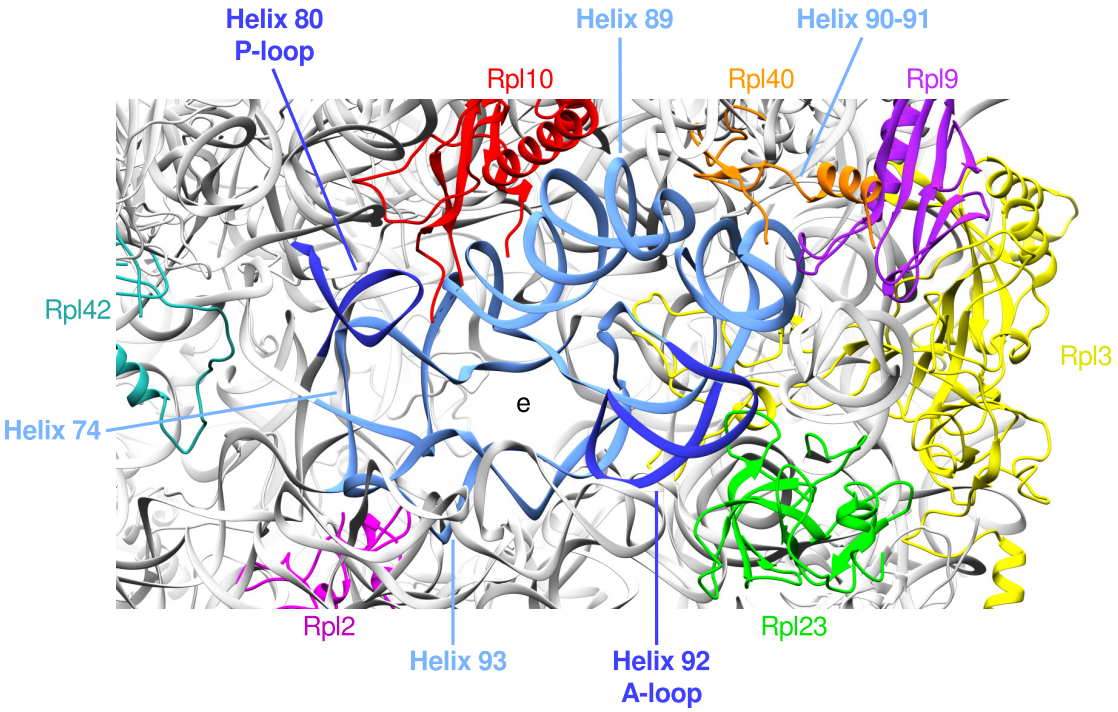

Figure 1.5: Peptidyl transferase center of *Saccharomyces cerevisiae* The PTC is shown from the subunit interface. It is organized by several rRNA helices which are colored in blue. The active site is free of proteins, adjacent r-proteins are indicated. e = exit tunnel. PDB code: 4V88.

of the ribosome are highly asymmetric (reviewed in Agmon et al. 2005). Helices 89-91 form the A-site and helix 80, 89, and 93 the P-site, which is the site of peptide bond formation and is located directly above the exit tunnel (marked 'e' in Figure 1.5). The closest r-proteins are ~18 Å away from the active site, which highlights the rRNA as the major factor in peptide bond formation (Nissen et al. 2000). Nevertheless, r-proteins surround the PTC from all sides and project their extensions towards the active site (see Figure 1.5).

1.2 Evolution of the ribosome

It has been postulated, that the last universal common ancestor of all cells (LUCA), which lived around ~4 billion years ago, already possessed a fully developed ribosome, that was highly similar to ribosomes from extant bacteria and archaea (Forterre 2015; Fox 2010). Therefore, the ribosome is thought to have originated in a prebiotic environment, which is often referred to as the 'RNA world'. The RNA world hypothesis states, that RNA-catalyzed reactions predate protein enzymes and that RNA was able to copy itself via a ribozyme based polymerization reactions which allowed the accumulation of activity-

enhancing mutations by natural selection (Crick 1968; W. Gilbert 1986; Orgel 1968; Rich 1962; Woese 1967).

As ribosomes produce protein, it is thought that polypeptides could only become large and acquire sophisticated enzymatic functions after the inception of the proto-ribosome. This marked the change from the 'RNA world' to the 'Protein and RNA world' and gave rise to a replacement of RNA-based reactions by more efficient and adaptable protein enzymes. Francis Crick therefore hypothesized in 1968, that *"It is tempting to wonder if the primitive ribosome could have been made entirely of RNA"*. In contrast to this view, it is thought today, that the primitive ribosome evolved together with co-factors that could stabilize the rRNA fold or could enhance ribozyme activity (reviewed in C. W. Carter 2015). It is possible, that simple polypeptides, that had been created by abiotic processes, were incorporated into the ribosome from the very beginning and would be replaced by the first ribosomal proteins, after the invention of coded protein synthesis.

Studies of how the ribosome emerged have been hampered by the fact, that LUCA already contained the extant ribosomal core, which means, that nucleotide sequences can only be used to infer ribosome evolution post LUCA. Nevertheless, models have been proposed, that describe the growth of ribosomal RNA in evolution. The most accepted model, which is called the 'accretion model', is based on a study by Bokov and Steinberg, that used A-minor interactions in the large subunit to assign relative ages to the rRNA subdomains (Bokov and Steinberg 2009; Hsiao and L. D. Williams 2009; Petrov, Bernier, Hsiao, et al. 2014; Petrov et al. 2015). An A-minor interactions is a RNA structure motif that is formed between a double helical RNA and an adenosine-rich patch of a second RNA which binds to the minor grove of the double helix (Cate et al. 1996; Nissen et al. 2001). Because RNA helices can exist without the adenosine patch, it is assumed, that the helix has to be present before the adenosine patch can form the A-minor interaction, which identifies the helix as older. Bokov and Steinberg used this assumption to map the oldest part of the large ribosomal subunit, which appears to be the PTC in domain V. Strikingly, this region contains only double helix portions of inter-domain A-minor interactions, which suggests, that it was already present when the remaining rRNA domains formed (Bokov and Steinberg 2009). Recently, the accretion model has been greatly expanded to explain the origin of the ribosome at higher resolution (Petrov, Bernier, Hsiao, et al. 2014; Petrov et al. 2015). In these analyses, Petrov and colleagues define detailed steps in the accretion of rRNA elements of both ribosomal subunits. The steps of large subunit evolution can be summarized as follows: 1) Formation of the PTC 2) Formation of an exit pore + exit tunnel extension 3) Acquisition of the SSU interface 4) Acquisition of the P stalk and central protuberance 6) late tunnel extensions 7) eukaryotic extension of rRNA and proteins. Strikingly, these steps

resemble the order in which the large subunit is assembled during ribosome biogenesis, which is reminiscent of the principle of 'ontogeny recapitulates phylogeny' in embryology (see subsection 1.3.7).

It is thought that the PTC is older than coded protein, and that it is a remnant of the proto-ribosome (Belousoff et al. 2010; Bokov and Steinberg 2009; Hsiao et al. 2009; Hury et al. 2006). This is further supported by a striking internal symmetry, which splits the PTC in two halves that can be superimposed (Agmon et al. 2005). This strongly suggests, that the initial PTC was a dimer of one RNA molecule (Bokov and Steinberg 2009). Furthermore, it has been shown, that PTC-sized ribozymes can catalyze peptide bond formation *in vitro* and that core rRNAs can specifically associate with r-protein derived peptides, which supports the proto-PTC as a possible independent and small transpeptidase (Cech and B. Zhang 1997; Hsiao et al. 2013).

The evolutionary expansion of the ribosome is still ongoing, and it is thought that the ribosome acquires new rRNA in the form of insertions, which add new features on top of existing structures (Petrov, Bernier, Hsiao, et al. 2014; Petrov et al. 2015). Comparison of ribosomes from bacteria to humans shows that, concerning the extant ribosomal core, these insertions are absent in bacteria and first seen in archaea (see Figure 1.6). It is thought, that the insertions convey new functionality while preserving existing functions, which is highlighted by recent eukaryotic insertions, that are arranged at the surface of the ribosome, where they form long, flexible, and sometimes branched extensions. They have been termed 'expansion segments' and contribute greatly to the size difference of ~2700 nucleotides between bacterial and human ribosomes. They were first described in 1984 in the lab of Susan A. Gerbi, who defined the nomenclature that is still used today (Clark et al. 1984; Gerbi 1986; Gerbi 1996). As parts of the ribosome they take part in biogenesis and are assumed to contribute to the higher complexity of the translational apparatus in eukaryotes (Petrov, Bernier, Hsiao, et al. 2014; Ramesh and Woolford 2016).

1.2.1 Eukaryogenesis and the ribosome

Eukaryotes have emerged out of prokaryotes in the course of evolution, which led to an increase in cellular complexity, including the translational machinery. The genome of eukaryotes contains hints on the origin of the eukaryotic cell, as it is a chimeric assembly of an archaeal and a bacterial genome (Rivera et al. 1998). It is assumed today, that eukaryotes emerged from an archaeal host cell, which acquired an α-proteobacterium, that became the mitochondrion (Spang et al. 2015). This is supported by analysis of the translational machinery in eukaryotes, as eukaryotic ribosomes contain 33 archaeal

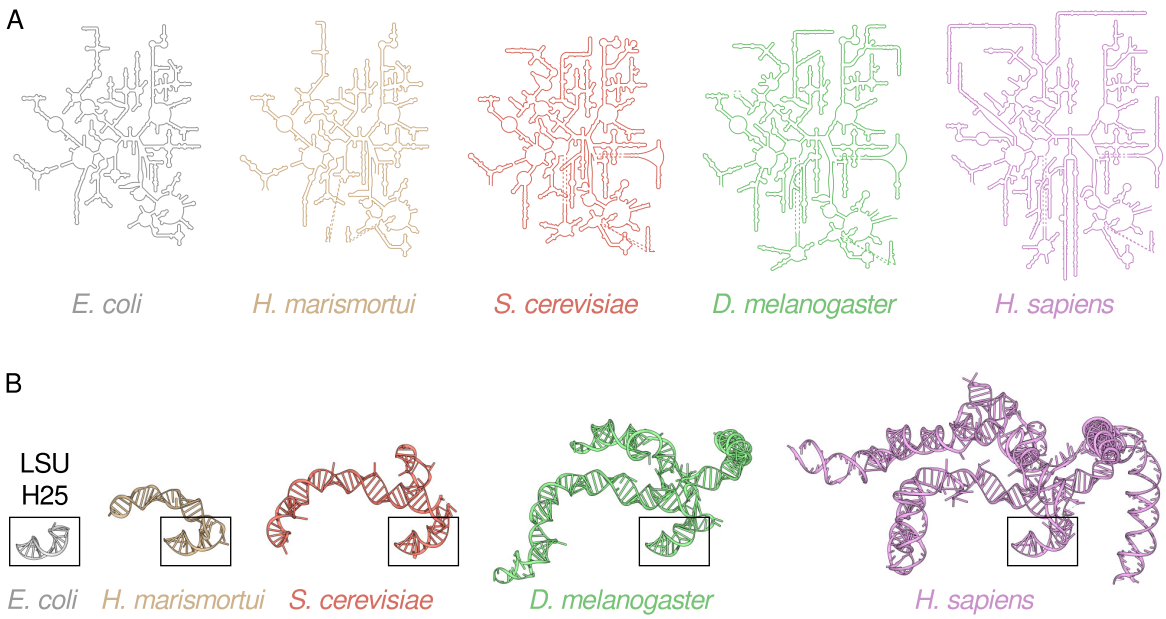

Figure 1.6: Expansion of rRNA in evolution A) Large subunit rRNA secondary structures of *Escherichia coli* (bacteria), *Haloarcula marismortui* (archaea), *Saccharomyces cerevisiae* (eukaryota), *Drosophila melanogaster* (eukaryota), and *Homo sapiens* (eukaryota) demonstrate the growth of rRNA in evolution. Modified from Petrov, Bernier, Gulen, et al. 2014. B) Serial accretion of rRNA at helix 25 of the large subunit forms expansion segment 7 around a common core. Each growth step builds on and does not alter existing structures. LSU = large subunit. After Petrov, Bernier, Hsiao, et al. 2014.

and no bacterial exclusive r-proteins (Lecompte et al. 2002). Additionally, archaea and eukaryotes contain the 'snoRNA' system for rRNA modifications, that is absent in bacteria and several eukaryote specific ribosome assembly factors have been identified in archaea, including archaeal homologs of Dim2, Rio2, Nob1, Nep1/Emg1, Nmd3, and SBDS/Sdo1 (Aravind and Koonin 2000; Boocock et al. 2002; Eschrich et al. 2002; Jia et al. 2010; Malyutin et al. 2017; Shammas et al. 2005; Veith, Martin, et al. 2011; Veith, Wurm, et al. 2011; Wurm et al. 2010). Furthermore, tRNA binding at the E-site differs between kingdoms and separates bacterial from archaeal and eukaryotic ribosomes (Steitz 2008).

Phylogenetic analyses support the origin of eukaryotes as a sister clade to, or from within, the archaeal 'TACK' superphylum (Cox et al. 2008; Foster et al. 2009; Guy et al. 2014; Lasek-Nesselquist and Gogarten 2013; T. A. Williams et al. 2012). TACK stands for *Thaumarchaeota*, *Aigarchaeota*, *Crenarchaeota*, and *Korarchaeota*, which contain many eukaryotic signature proteins (Guy and Ettema 2011). Among these are distant archaeal variants of actin, tubulin, ESCRT proteins, and proteins involved in transcription and translation (Ettema et al. 2011; Guy and Ettema 2011; Koonin and Yutin 2014; Lindås et al. 2008; T. A. Williams et al. 2013; Yutin and Koonin 2012). Therefore, the

archaea and eukaryotes have been grouped together in what has been referred to as the 'Arkarya' (Forterre 2015).

Recently, a new sister group of the TACK superphylum has been defined by metagenome analysis, which contains the closest known archaeal relatives of eukaryotes to date. The new phylum is called 'Asgard archaea' and consists of the *Lokiarchaeota*, *Thorarchaeota*, *Odinarchaeota*, and *Heimdallarchaeota* (Zaremba-Niedzwiedzka et al. 2017). The Asgard archaea contain an unusually high number of eukaryotic signature proteins, which suggests that they are highly similar to the host cell, that acquired the α-proteobacterium and gave rise to eukaryotes (Spang et al. 2015; Zaremba-Niedzwiedzka et al. 2017). One member of the Asgard archaea, called '*Lokiarchaeum*', possesses the most eukaryotic-like ribosome of all archaea (Spang et al. 2015). It contains nearly all (14 out of 15) homologs of eukaryotic ribosomal proteins, that have been identified across multiple members of the TACK superphylum and even a putative distant homolog of eL22 (Spang et al. 2015; Yutin et al. 2012). This data indicates that much of the extant ribosomal complexity was present at the inception of eukaryotes and that eukaryotes share their evolutionary path after LUCA with the archaea.

1.3 Ribosome biogenesis in *Saccharomyces cerevisiae*

The growth of all cells depends on the generation of ribosomes, as the number of ribosomes has to double before each cell division (Kief and Warner 1981). Growing yeast cells produce 2000 ribosomes per minute, which consumes a significant amount of cellular resources (Warner 1999). 60 % of all transcription is devoted to ribosome formation, which includes 50 % of RNA pol II transcription (Warner 1999). *S. cerevisiae* possesses 139 r-protein genes (102 with introns) which account for 20 of the 30 most abundant mRNAs in yeast and are responsible for 90 % of mRNA splicing (Nerurkar et al. 2015; Velculescu et al. 1997; Warner 1999). This results in the production of ~160,000 r-proteins per minute, that have to be imported into the nucleus, where they are assembled into pre-ribosomes and subsequently exported to the cytoplasm. It has been estimated, that each nuclear pore has to export a ribosome every 2 seconds, which highlights the essential role of efficient nuclear transport in ribosome biogenesis, both in importing r-proteins and biogenesis factors and in exporting pre-ribosomes to the cytoplasm (Warner 1999).

Eukaryotic ribosome biogenesis starts in the nucleolus, which contains the rDNA repeats and a large portion of the ribosome assembly machinery. rRNA precursors are co-transcriptionally associated with r-proteins, modified, and processed. This is

necessary, as RNAs readily acquire secondary and tertiary structures in the presence of magnesium, which leads to a variety of folds in the case of rRNA (Ramaswamy and Woodson 2009a; Ramaswamy and Woodson 2009b). Therefore, the assembly machinery ensures correct folding by stabilizing intermediates, that enable the ordered assembly of mature ribosomes (Kovacs et al. 2009; Semrad et al. 2004; Woodson 2011). Both ribosomal subunits are produced from a single rRNA precursor, which is processed early on to release the pre-43S and pre-66S particles, that independently mature to 40S and 60S subunits (Figure 1.7). Additionally, the 60S subunit contains the 5S rRNA, that is transcribed from a separate rDNA gene and is recruited to the pre-60S at an early maturation step (see subsection 1.3.7). During biogenesis the pre-ribosomes move from the nucleolus to the nucleus and finally to the cytoplasm, where final maturation steps occur (reviewed in Woolford and Baserga 2013).

Early studies of ribosome formation focused on the reconstitution of bacterial ribosomal subunits from purified components, which was achieved in the late 1960s and early 1970s in the labs of Masayasu Nomura and Ferdinand Dohme, who reconstituted *E. coli* 30S and 50S subunits, respectively (Held et al. 1974; Held et al. 1973; Mizushima and Nomura 1970; Nierhaus and Dohme 1974; Nomura 1973; Traub and Nomura 1968). These studies suggested, that the assembly of ribosomes is a simple process, that does not rely upon extra non-ribosomal factors, and that the information for the assembly is contained in the structure of the subcomponents. The simplicity of this suggestion was challenged in the following years, when biogenesis factors were identified, that facilitate efficient ribosome formation *in vivo* and by the greater complexity of eukaryotic ribosome biogenesis, which could not be recapitulated *in vitro*. Nevertheless, these studies unraveled the order of r-protein assembly in bacteria, that depends on the initial binding of primary r-proteins, which facilitate the subsequent assembly of secondary and even tertiary binders. The 'Nomura' and 'Nierhaus' assembly maps have changed little since they were first postulated and still illustrate the common aspects of ribosome formation.

Studies on yeast ribosomes showed, that it is not possible to reconstitute eukaryotic ribosomal subunits *in vitro* in a similar way to bacterial ones. Early studies on eukaryotic r-protein assembly therefore relied on studies using radioactively labeled amino acids, which were applied to yeast protoplasts, that revealed the existence of 90S, 66S, and 43S pre-ribosomes (Kruiswijk et al. 1978).

In contrast to bacterial pre-ribosomes, it was realized early on, that eukaryotic pre-ribosomes contain a higher ratio of protein to rRNA than mature ribosomes, which suggested that a significant number of non-ribosomal factors are involved in the maturation process (Trapman et al. 1975). The discovery of these factors was greatly accelerated by the tandem-affinity tag (TAP tag), that became available in the early 2000s, which

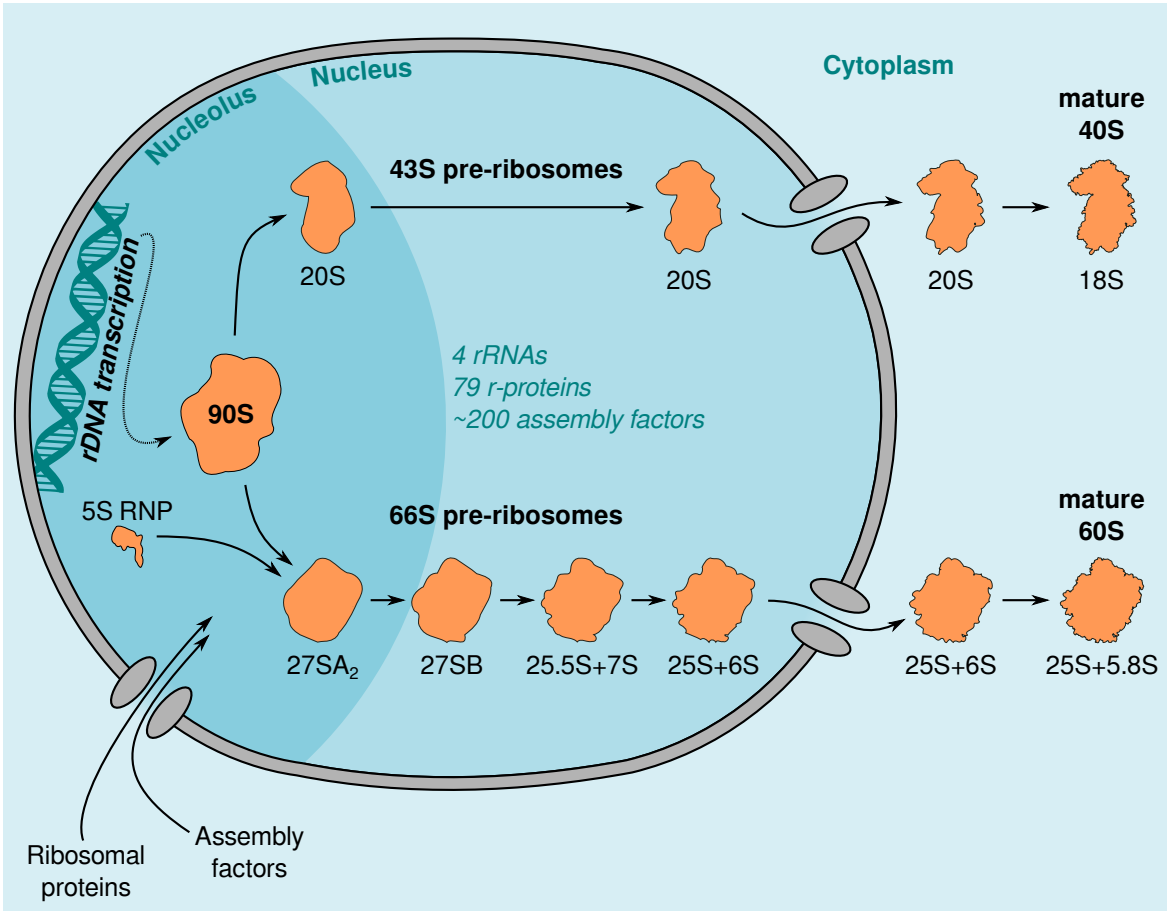

Figure 1.7: Ribosome biogenesis in *Saccharomyces cerevisiae* Simplified overview of ribosome biogenesis in yeast. Biogenesis involves the intial formation of pre-ribosomes in the nucleolus and subsequent maturation steps in the nucleus and cytoplasm. The rDNA is transcribed in the nucleolus to rRNA by Pol I and associates with ribosomal proteins and assembly factors to form the 90S pre-ribosome. The 90S is associated with modification and folding of the small subunit rRNA and gives rise to 43S pre-ribosomes, that mature independently to 40S subunits. Transcription continues and produces the rRNA precursor of the large subunit, which associates with the 5S RNP to form 66S pre-ribosomes, that mature independently to 60S subunits. Maturation of both subunits includes nuclear export and final maturation steps in the cytoplasm, which concludes ribosome biogenesis. The rRNA content and processing steps of 43S and 66S pre-ribosomes are indicated, also see subsection 1.3.3.

allowed the isolation of pre-ribosomes by tagging known biogenesis factors (Rigaut et al. 1999). These purifications contained a large number of novel factors, that could be subsequently identified by mass spectrometry (Baßler et al. 2001; Fatica et al. 2002; Harnpicharnchai et al. 2001; Schaper et al. 2001). In the following years, reverse tagging of these newly identified factors lead to the identification of multiple biogenesis intermediates, which are defined by specific subsets of associated biogenesis factors (reviewed in Kressler et al. 2010). Today, there are >200 known assembly factors, excluding snoRNAs, that contribute to the formation of the eukaryotic ribosome, which

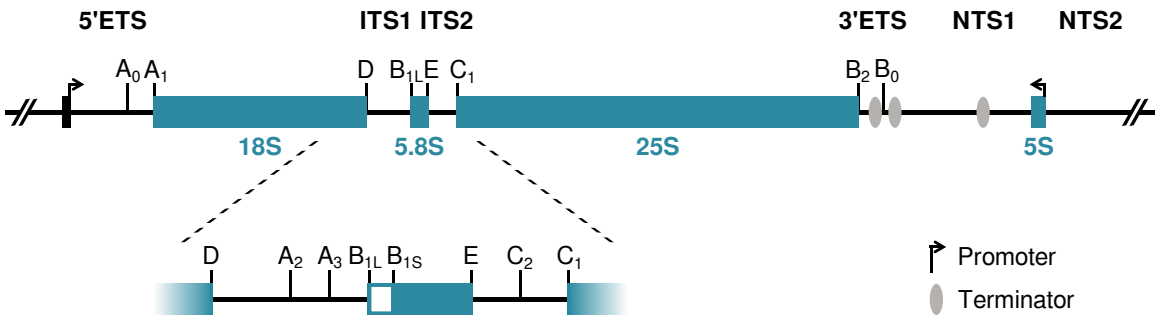

Figure 1.8: rDNA gene of *Saccharomyces cerevisiae* One of the ~100-200 rDNA genes is depicted. The 5S rRNA is transcribed in anti-sense direction to the 35S rRNA, which contains the coding sequence for 18S, 5.8S, and 25S rRNA. rRNA cleavage sites are indicated with capital letters. ETS = external transcribed spacer, ITS = internal transcribed spacer, NTS = non-transcribed spacer.

illustrates the increased complexity of ribosome formation in eukaryotes, compared to bacteria (see subsection 1.3.5).

1.3.1 Initial stages of ribosome formation occur in the nucleolus

The nucleolus is a subcompartment of the nucleus, that is associated with biogenesis of most cellular ribonucleoprotein particles (Thiry and Lafontaine 2005). It contains the rDNA repeats as well as a large portion of the ribosome assembly machinery and is the site of initial ribosome formation, which involves transcription, modification and processing of the 35S precursor rRNA. In yeast it is crescent shaped and located at the nuclear periphery, opposite the spindle pole body, where it takes up one third of the nuclear volume (Bystricky et al. 2005; Yang et al. 1989). The nucleolus is a dynamic structure, which reacts to the cell cycle or nutrient availability and the size and shape of the nucleolus are being used as markers for cellular deregulation and cancer (Hernandez-Verdun et al. 2010; Orsolic et al. 2016; Thiry and Lafontaine 2005).

The nucleolus is membrane-less and it has been demonstrated, that it assembles solely through phase separation from the nucleoplasm (Falahati et al. 2016; Feric et al. 2016). This is achieved by the accumulation of nucleolar macromolecules, that causes a differential surface tension within the nucleus, which creates the nucleolar boundary (Falahati et al. 2016; Falahati and Wieschaus 2017; Feric et al. 2016). This behavior can be reconstituted *in vitro* with individual nucleolar proteins and suggests, that the biophysical properties of nucleolar components are the driving force behind nucleolus formation (Feric et al. 2016). Additionally, it has been demonstrated, that rDNA plays a pivotal role in formation of the nucleolus *in vivo*, as rDNA transcription precedes the

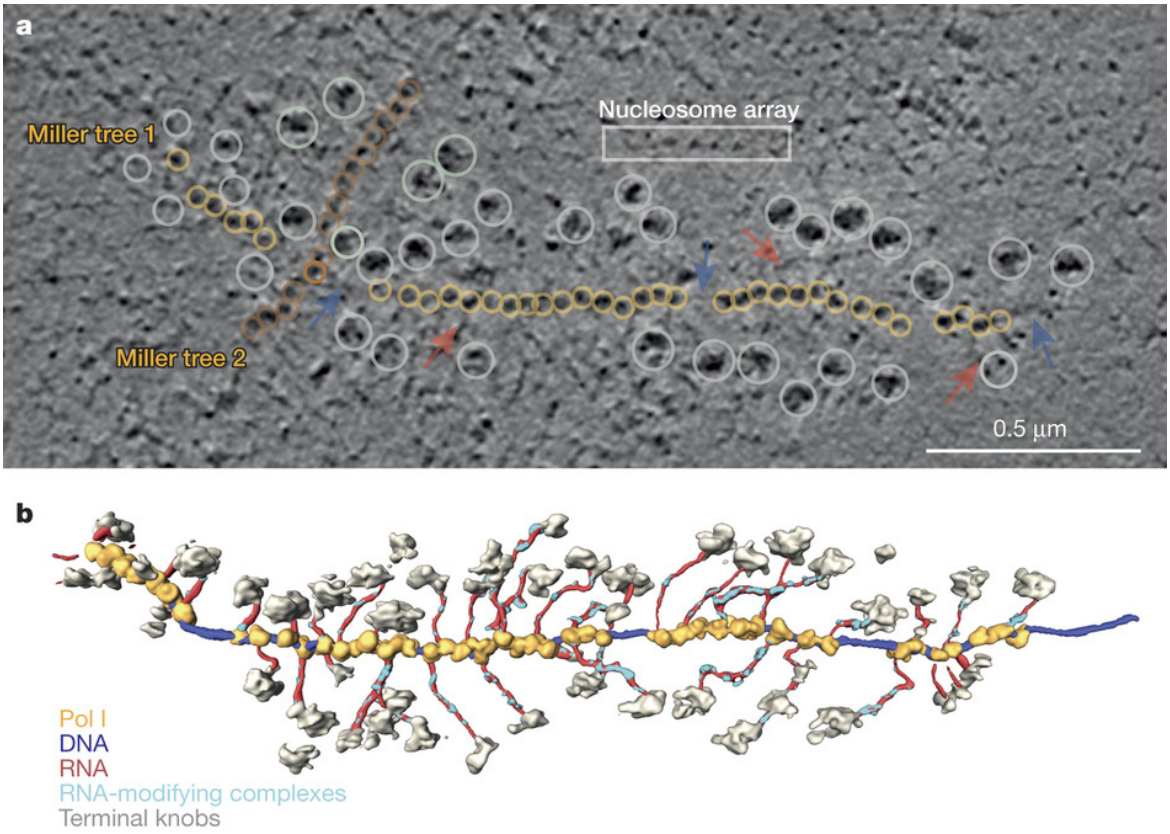

Figure 1.9: cryo-EM tomography analysis of rDNA transcription A) cryo-EM image of two rDNA genes with associated transcription units, containing Pol I and the ribosomal precursors (Miller tress). Yellow circles = Pol I. Gray circles = Terminal knobs. Blue arrow = rDNA. Red arrow = RNA. For comparison a nucleosome array is indicated by a white box. B) Three-dimensional surface representation of Miller tree 1 (see above). Yellow = Pol I. Gray = Terminal knobs. Blue = rDNA. Red = RNA. Cyan = RNA-modifying complexes. Adapted by permission from Macmillan Publishers Ltd: Nature (Neyer et al. 2016), copyright 2016.

assembly of a visible nucleolus and the absence of rDNA leads to a loss of spatiotemporal precision in nucleolar assembly (Falahati et al. 2016; Falahati and Wieschaus 2017).

The ribosomal RNA is encoded on rDNA genes, that are present in multiple copies in the genome of most cells. *E. coli* has seven rDNA genes, that are found all over the circular genome, but are preferentially located close to origins of replication (Ellwood and Nomura 1982). The rDNA of *S. cerevisiae* is organized in ~100-200 copies per haploid cell, which are located on the right arm of chromosome XII (Venema and Tollervey 1999). Each rDNA repeat consists of 9.1 kB, which contain the rRNA genes, as well as spacer regions, called external, internal and non-transcribed or intergenic spacers (ETS, ITS, and NTS/IGS, see Figure 1.8). The 18S, 5.8S, and 25S rRNA are produced as one transcript by RNA polymerase I, which transcribes from the 5' ETS to the 3' ETS (Figure 1.8).

Transcription is stopped at two terminators, one at ~100 nucleotides downstream of the 3' ETS, which terminates the majority of transcripts and the second one at ~250 nucleotides downstream of the 3' ETS (Figure 1.8). The 5S rRNA is transcribed separately in anti-sense direction by RNA polymerase III (Figure 1.8). Additionally, multiple genes for 5S rRNA variants are located at the end of the rDNA repeats, that is closest to the telomere (M. E. McMahon et al. 1984).

rDNA transcription is the first step in ribosome biogenesis and is therefore rate limiting for all subsequent steps. In yeast, Pol I transcribes the rDNA at a rate of 40-60 nt/s, which leads to the production of 35S rRNA precursors, that are co-transcriptionally processed and modified (Kos and Tollervey 2010). This is significantly faster than the elongation rate of RNA Polymerase II, which is about ~35 nt/s in yeast (Mason and Struhl 2005).

Transcription at rDNA loci can be visualized by electron microscopy (Miller and Beatty 1969). Miller and Beatty demonstrated in 1969, that it is possible to extract rDNA repeats from the nucleolus, which still contain the transcription machinery and associated pre-ribosomes (Miller and Beatty 1969). The samples were applied to EM grids and analyzed by electron microscopy, which revealed the characteristic christmas tree like shape of these 'Miller spreads' (Miller and Beatty 1969 and Figure 1.9). In growing yeast, each rDNA gene is associated with ~50 transcription units, which form the branches of the christmas tree (French et al. 2003). The terminal knobs of these structures contain the assembly machinery for the first steps of ribosome biogenesis, that are predominantly associated with rRNA modifications, processing, and folding of the small subunit (Mougey et al. 1993).

1.3.2 rRNA modification in *Saccharomyces cerevisiae*

RNA modifications exist in all three domains of life, and so far over 110 types of modifications have been identified (reviewed in Machnicka et al. 2014; S. Sharma and Lafontaine 2015). Surprisingly, the rRNA of *S. cerevisiae* contains only 12 types of modifications, whereas 25 types have been identified on yeast tRNAs.

rRNA modifications in yeast include: Methylations at the sugar backbone or the nucleobase of nucleosides, isomerization of uridines to pseudouridines (Ψ), acetylation of cytidines, and aminocarboxypropylation of pseudouridine (reviewed in S. Sharma and Lafontaine 2015). There are only two acetylated cytidines and one hypermodified pseudouridine in the ribosome, which are found in the small subunit (ac^4C_{1280}, ac^4C_{1773} and $m^1acp^3\Psi_{1191}$), whereas most modifications are 2'-O-ribose methylations (55 sites in yeast) and pseudouridines (45 sites in yeast). In total, the ribosomal RNA is modified at 112 positions, which amounts to ~2 % of the entire rRNA (S. Sharma and Lafontaine

2015).

The rRNA modifications are produced by a set of nine methyltransferases and one acetyltransferase (that also catalyzes the formation of $m^1acp^3\Psi_{1191}$), and by a RNP-based modification system, which uses small nucleolar RNAs (snoRNAs) for targeting the modification enzyme to rRNA (Meyer et al. 2016; S. Sharma and Lafontaine 2015).

There are two classes of snoRNAs, the box C/D and H/ACA snoRNAs, which have been grouped by conserved sequence elements and secondary structure predictions (Figure 1.10). The snoRNAs are involved in catalyzing the bulk of rRNA modifications, as the C/D box snoRNAs are involved in all 2'-O-ribose methylations and the H/ACA box snoRNAs in all pseudouridylations (Ganot et al. 1997; Kiss-László et al. 1996; J. Ni et al. 1997; Nicoloso et al. 1996). They are thought to act very early in ribosome biogenesis, as it has been demonstrated, that most 2'-O-ribose methylations and pseudouridylations are performed already during transcription of the precursor rRNA (Kos and Tollervey 2010; Turowski and Tollervey 2014).

The snoRNAs are part of a RNP and each class of snoRNAs interacts with a core set of proteins, that are highly conserved in evolution and have been identified in archaea and eukaryotes (Gaspin et al. 2000; Omer et al. 2000). The snoRNA organizes the RNP by forming a scaffold for proteins, including the modification enzyme, and also recognizes the rRNA substrate by base pairing with the target site (Figure 1.10).

The box C/D RNP contains a single snoRNA and two copies each of the core proteins Snu13 (L7Ae in archaea), Nop56 (Nop5 in archaea), Nop58 (no archaeal orthologue), and the methyltransferase Nop1 (fibrillarin in archaea). In H/ACA RNPs, the snoRNA is associated with one copy each of Nhp2 (L7Ae in archaea), Nop10 (Nop10 in archaea), Gar1 (Gar1 in archaea), and the Ψ synthetase Cbf5 (Cbf5 in archaea).

The biological relevance of snoRNAs is, for example, highlighted by depletion studies in zebrafish embryos, where knockdown of a single snoRNA is sufficient to alter development (Henras et al. 2015; Higa-Nakamine et al. 2011). Additionally, the expression of H/ACA snoRNAs is commonly altered in human cancers, especially in many types of leukemia, and it has been shown, that human breast cancer cells produce aberrant rRNA modifications, which result in ribosomes with altered translational capabilities (Belin et al. 2009; M. McMahon et al. 2014).

The rRNA modifications are located at functionally important regions of the ribosome, as they are present at the PTC, the subunit interface, and even inside the ribosome exit tunnel, whereas no modifications have been identified at the solvent-exposed side of the ribosome (S. Sharma and Lafontaine 2015). Many of the modifications are conserved positionally from bacteria to human (Bachellerie et al. 2002; Lestrade and Weber 2006), which is highlighted by the high conservation of base modifications in the small subunit

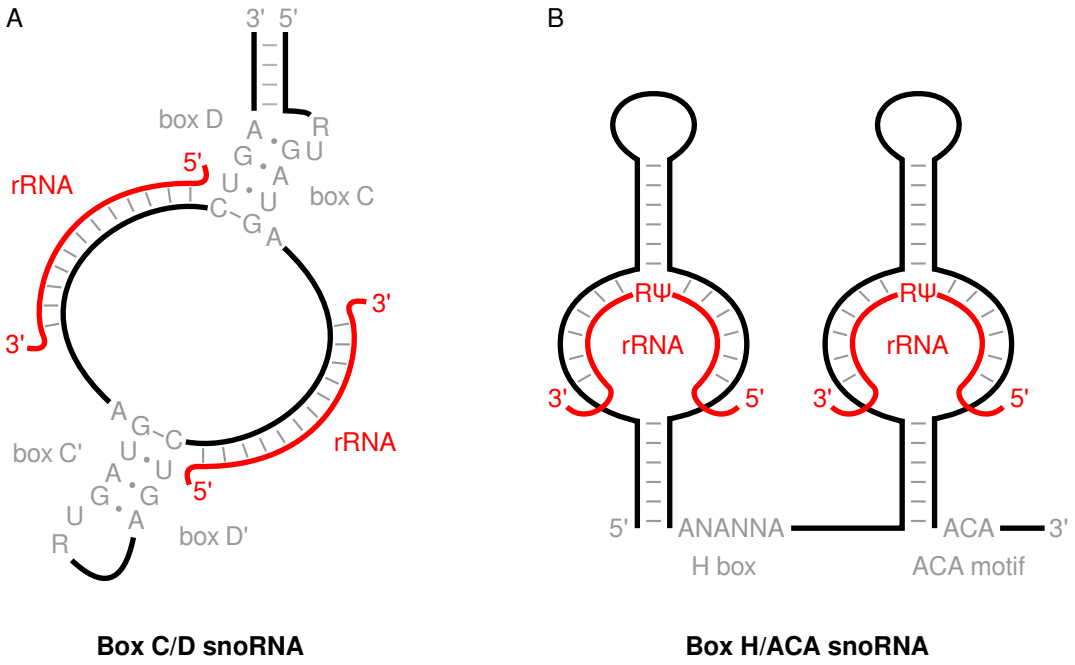

Figure 1.10: Box C/D and H/ACA snoRNAs Schematic depiction of Box C/D (left side) and Box H/ACA (right side) snoRNAs. Conserved sequence motifs are indicated in gray and target rRNAs are shown as red lines. After Watkins and Bohnsack 2011.

(S. Sharma and Lafontaine 2015).

It has been suggested, that rRNA modifications act by stabilizing unfavorable RNA folds through alteration of the electrostatic potential, and therefore the hydrogen-bonding capability, of local rRNA environments (Chawla et al. 2015). Indeed, many modifications are located in clusters, and it has been shown, that those exert a synergistic effect on the structure of the ribosome (Baxter-Roshek et al. 2007; Gigova et al. 2014; Liang et al. 2007; Piekna-Przybylska, Przybylski, et al. 2008). Furthermore, modifications have been shown to be important for ribosome activity or even biogenesis (Gigova et al. 2014; King et al. 2003; Liang et al. 2007; Liang et al. 2009). For example, the hypermodified uridine in the decoding region of the small subunit ($m^1acp^3\Psi_{1191}$) is important for efficient formation of the 18S rRNA (Liang et al. 2009), and cells lacking base modifications at the subunit interface show an increased sensitivity towards anisomycin, which is consistent with subunit joining defects (Gigova et al. 2014; S. Sharma et al. 2013). Moreover, numerous modifications are found inside the exit tunnel, where they are thought to prevent interactions of the nascent polypeptide with the interior of the tunnel during translation (Decatur and Fournier 2002).

Therefore, rRNA modifications have emerged as important elements of the translation machinery, which highlight the role of RNA fine tuning for cellular growth.

1.3.3 rRNA processing in *Saccharomyces cerevisiae*

In yeast, the rRNA transcript associates with ribosomal proteins and assembly factors already during transcription, whereas rRNA processing can occur either during or after transcription. It has been demonstrated, that in exponentially growing cells ~70 % of rRNAs are processed co-transcriptionally at the A_0, A_1, and A_2 sites, which results in the production of separate 20S and 27SA2 pre-rRNAs (Axt et al. 2014; Osheim et al. 2004). Post-transcriptional processing starts with cleavage at the B_0 site, which releases the full 35S rRNA transcript, that contains the 5' ETS, the 18S, 5.8S, and 25S rRNAs, as well as the 3' ETS (Kufel et al. 1999). The 35S rRNA is further processed from the 5' end via subsequent cleavages at the A_0, and A_1 sites, that remove the 5' ETS (Figure 1.11). The co- and post-transcriptional processing pathways converge after A_2 cleavage, which separates the ribosomal subunits and enables individual maturation and export of each pre-ribosome (Lygerou et al. 1996; Udem and Warner 1972).

These initial processing steps are associated with the 90S pre-ribosome, which is assembled around the 5' ETS and the 20S rRNA (Chaker-Margot et al. 2016; Kornprobst et al. 2016; Sun et al. 2017). The 90S is a large macromolecular structure, that contains an assembly factor scaffold, which directs the processing of the 5' ETS and the initial folding of the 20S rRNA. It contains the U3 snoRNA, which is necessary for cleavages at the A_0 and A_1 sites in the 5' ETS (Dragon et al. 2002; Grandi et al. 2002; Hughes and Ares 1991; Osheim et al. 2004). The U3 snoRNA is bound near the A_0 and A_1 sites in the 90S and it has been demonstrated, that it facilitates the processing at these sites by hybridization with pre-rRNA (Borovjagin and Gerbi 2001; Chaker-Margot et al. 2016; Henras et al. 2015; Hughes 1996; Kent et al. 2008; Kornprobst et al. 2016; Marmier-Gourrier et al. 2011; Méreau et al. 1997; K. Sharma and Tollervey 1999; Sun et al. 2017). After the nascent SSU is released from the 90S pre-ribosome, it contains the 20S rRNA and a large portion of ribosomal proteins and it is quickly exported from the nucleus to the cytoplasm, where final maturation steps occur (Figure 1.11). In the cytoplasm, the 20S rRNA is processed to mature 18S rRNA through endonucleolytic cleavage by Nob1, which cleavages at site D and concludes small subunit rRNA processing (Lebaron et al. 2012; Pertschy et al. 2009).

The large subunit is separated from the small subunit by cleavage at site A_2, which results in 27SA2 pre-rRNA, that is a constituent of 66S pre-ribosomes and which is further processed by multiple endo- and exonucleases (Trapman et al. 1975; Udem and Warner 1973 and Figure 1.11). The 5' end of the 27SA2 rRNA, which contains the 5.8S rRNA, is trimmed either by cleavage at site A_3 or B_{1L}, which results in a short or long variant of the mature 5.8S, that are both found in mature ribosomes (Figure 1.11). The

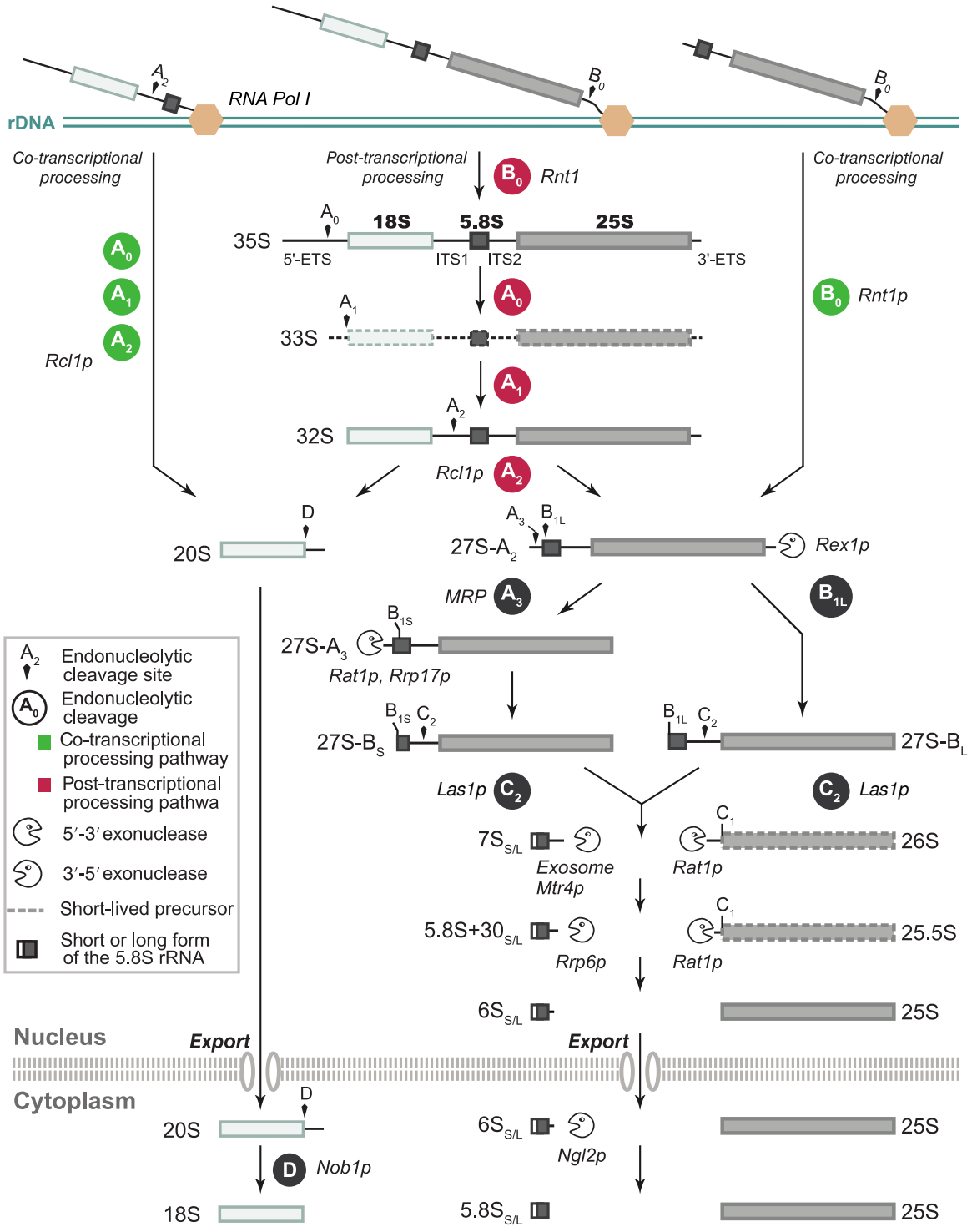

Figure 1.11: rRNA processing in *Saccharomyces cerevisiae* Processing steps from transcription to mature ribosomes are shown. Endo- and exonucleolytic cleavages are indicated with the corresponding enzymes (when known). Both co- and post-transcriptional pathways are shown. The short (85 % of transcripts) and long (15 % of transcripts) forms of 5.8S rRNA are shown as one. Modified from Henras et al. 2015 with data on C_2 cleavage added from Gasse et al. 2015.

short form is present in 85 % of mature ribosomes, whereas 15 % contain the long form (Henras et al. 2015). Furthermore, the processing of the 5' end of the 27SA2 rRNA is coupled to the processing of the 3' ETS by Rex1, because mutations in the 3' ETS impair endonucleolytic cleavages at sites A_3 and B_{1L} (Henras et al. 2015; Kempers-Veenstra et al. 1986; Kufel et al. 1999).

The 27SA2 rRNA is further cleaved in the ITS2 spacer, but only after the 5' and 3' ends are matured (Allmang et al. 1999; Henras et al. 2015). This cleavage at site C_2 separates the 7S rRNA (5.8S rRNA precursor) from the 26S rRNA (25S rRNA precursor) (Figure 1.11). Afterwards, the 26S rRNA is processed to mature 25S rRNA, and the 7S rRNA to 6S rRNA in the nucleus, whereas the final maturation steps of 6S rRNA occur after nuclear export in the cytoplasm (Figure 1.11). Here, the exonuclease Ngl2 removes the 3' end of the 6S pre-rRNA, which produces mature 5.8S rRNA, and concludes large subunit rRNA maturation (Faber et al. 2006; Henras et al. 2015; Thomson and Tollervey 2009).

1.3.4 Integration of r-proteins into nascent pre-ribosomes

Ribosomal proteins are essential components of the ribosome, that interact with the ribosomal RNA through unique RNA binding domains. Many r-proteins are deeply inserted between rRNA helices and form extensive protein:RNA contacts, which stabilize the fold of the rRNA. It is thought, that the association with r-proteins contributes to the formation of correct rRNA intermediates, which therefore confers directionality to the assembly process (reviewed in de la Cruz et al. 2015). The recruitment of r-proteins proceeds in an evolutionary conserved way, which is illustrated by the similar assembly of yeast S-proteins to the SSU rRNA *in vivo*, compared to the *in vitro* assembly of bacterial small subunits (Dutca and Culver 2008; Karbstein 2011; Mulder et al. 2010. Additionally, S-protein assembly in yeast is similar in mammals, which suggests, that formation of the small subunit is conserved in evolution (O'Donohue et al. 2010).

It has been shown, that the association of many r-proteins with rRNA is strengthened as biogenesis proceeds, which is consistent with the incorporation of initially bound r-proteins during compaction or rearrangement of the ribosomal RNA (de la Cruz et al. 2015). These steps are important biogenesis events, that involve biogenesis factors, and can therefore be seen as check points in ribosome formation (Leidig et al. 2014; Loc'h et al. 2014; Mitterer, Murat, et al. 2016; Schäfer et al. 2006; Strunk et al. 2011). An important example is the initial association of the complete 5S RNP with the pre-60S, which associates in a reversed conformation, that is rotated about ~180° from the mature state (Leidig et al. 2014). The turning of the 5S RNP is an essential step in the formation

of the central protuberance and involves a multitude of biogenesis factors, including the large ATPase Rea1 (Barrio-Garcia et al. 2016; Leidig et al. 2014).

The consecutive association of rRNA with r-proteins creates a hierarchical assembly pathway, which involves 'primary binding' r-proteins, that organize the binding of subsequent 'secondary' and 'tertiary binders' (de la Cruz et al. 2015). Therefore, the depletion of individual r-proteins can cause delays or assembly defects of downstream maturation steps, which leads to the accumulation of free r-proteins and ribosomal stress. Unbound r-proteins are toxic for the cell, as they are highly charged and often unstructured, which leads to aggregation and nonspecific interactions with nucleic acids (Jäkel et al. 2002). Consequently, dedicated degradation pathways have evolved, that remove excess r-proteins from the cell (Lam et al. 2007; Sung, Porras-Yakushi, et al. 2016; Sung, Reitsma, et al. 2016). Additionally, it has been demonstrated, that cellular chaperone systems are very important for the solubility of r-proteins, as simultaneous inactivation of the nascent polypeptide-associated complex (NAC) and the yeast Hsp70/40 system (SSB/RAC) leads to aggregation of 52 of the 79 ribosomal proteins in yeast (Koplin et al. 2010).

It has therefore been suggested, that r-proteins are generally unstable until they are incorporated into the ribosome, which requires transport from the site of translation in the cytoplasm to the nucleolus of the cell. Additionally, nuclear import determines the rate of r-protein incorporation into pre-ribosomes, as it controls the amount of r-proteins, that can enter the nucleus. Although most r-proteins can pass through the nuclear pore by passive diffusion due to their small size, r-proteins are actively imported by nuclear transporter proteins (importins), that recognize and associate with nuclear localization signals (NLS) (Bange et al. 2013). Most NLS-containing r-proteins are imported by the β-karyopherin Kap123, but there is a functional overlap with other β-karyopherins, like Kap121 and Kap108 (Rout et al. 1997). Additionally, these importins protect both histones and r-proteins from degradation and can therefore be seen as chaperones of these proteins (Jäkel et al. 2002).

In addition to the general protection of r-proteins by cytoplasmic chaperones and importins, it has been shown recently, that specific 'assembly chaperones' exist, that are involved in the protection and targeting of individual r-proteins to pre-ribosomes (reviewed in Pillet et al. 2016). The protein Yar1 binds to Rps3 (uS3), which is imported into the nucleus in a dimerized state (Holzer et al. 2013; Koch et al. 2012; Mitterer, Gantenbein, et al. 2016; Mitterer, Murat, et al. 2016). Tsr2 binds to Rps26 (eS26) after nuclear import and guides the r-protein to the pre-ribosome (Schütz et al. 2014). Sqt1 has been implicated in the cytoplasmic assembly of Rpl10 (uL16) (Eisinger et al. 1997; West et al. 2005), and Rrb1, Acl4, and Bcp1 have been identified as chaperones of Rpl3

(uL3), Rpl4 (uL4), and Rpl23 (uL14), respectively (Iouk et al. 2001; Pillet et al. 2015; Schaper et al. 2001; Stelter et al. 2015; Ting et al. 2016). A special case is the assembly factor Syo1, which is involved in the simultaneous nuclear import of two r-proteins, Rpl5 (uL18) and Rpl11 (uL5) (Calviño et al. 2015; Kressler, Bange, et al. 2012). Both proteins are part of the 5S RNP, and Syo1 has been shown to be directly involved in 5S RNP assembly by accommodating the RNA binding surface of Rpl11 (uL5) during import and facilitating a handover to the 5S rRNA (Calviño et al. 2015; Kressler, Bange, et al. 2012).

Depletion or deletion of these assembly chaperones has been shown to reduce the cellular levels of the associated r-proteins, which suggests, that these factors have evolved to protect r-proteins from degradation (reviewed in Pillet et al. 2016). This protection function is further highlighted by the co-translational association of Yar1, Rrb1, Acl4, Syo1, and Sqt1 with their respective r-protein targets (Pausch et al. 2015; Pillet et al. 2015). In addition to the chaperones described above, Fap7 and Rrp7 have been described as potential assembly chaperones of Rps14 (uS11) and Rps27 (eS27), respectively (Baudin-Baillieu et al. 1997; de la Cruz et al. 2015; Hellmich et al. 2013; Loc'h et al. 2014; Pillet et al. 2016). Further studies are therefore necessary, to answer the question, if every r-protein requires an associated assembly chaperone, or if those have evolved to stabilize only the most delicate ones.

1.3.5 Comparison of ribosome biogenesis in bacteria and eukaryotes

The complexity of ribosome biogenesis increased significantly in the course of evolution, which is illustrated by the number of assembly factors, that are present in prokaryotes and eukaryotes. Efficient ribosome synthesis in *E. coli* requires ~20 biogenesis factors, whereas ~200 assembly factors have been identified in *S. cerevisiae* (for a review on bacterial ribosome assembly see Shajani et al. 2011, additional assembly factors have been described in Sato et al. 2005; X. Zhang et al. 2014); for a review on eukaryotic ribosome assembly, see Woolford and Baserga 2013). Furthermore, *E. coli* assembly factors are non-essential at optimal growth temperature, whereas most eukaryotic assembly factors are required for maturation (Shajani et al. 2011; Woolford and Baserga 2013). Eukaryotic ribosome biogenesis is a highly regulated process, which depends on the successful completion of each assembly step and contains stringent check points that do not allow faulty pre-ribosomes to enter translation (Dez et al. 2006; Hage and Tollervey 2004; LaRiviere et al. 2006).

The evolution of ribosomes is driven by the accretion of new rRNA elements onto existing structures (see section 1.2). These rRNA expansion segments are not present

in bacteria and are first seen as small additions in archaea (Figure 1.6). In eukaryotes, they have been suggested to participate in ribosome biogenesis and bind additional r-proteins and assembly factors in the process (Ramesh and Woolford 2016). Additionally, eukaryotes have evolved specific rRNA elements, that are removed during biogenesis. For example, the ITS2 is bound by multiple biogenesis factors in yeast, that are necessary for cleavage at the C_2 site, which is located in the ITS2 and is a pre-requisite for subsequent ITS2 removal (Gasse et al. 2015; Wu, Tan, et al. 2016).

Another difference between bacterial and eukaryotic ribosomes is the number of rRNA modifications, which has been increasing in the course of evolution. Bacterial ribosomes contain 35 rRNA modifications, 60 % of which are base methylations, whereas budding yeast contains 112 and vertebrates >200 rRNA modifications, 95 % of which are pseudouridines and ribose methylations (Piekna-Przybylska, Decatur, et al. 2008; S. Sharma and Lafontaine 2015). The increased number of pseudouridylations and ribose methylations in eukaryotes is achieved by a dedicated modification system, which utilizes 'snoRNAs' (for small nucleolar RNA) that target the modification enzymes to specific rRNA sites, whereas all rRNA modifications in bacteria are performed by proteins without the assistance of RNA (Piekna-Przybylska, Decatur, et al. 2008). Eukaryotes have inherited snoRNAs from the archaeal host, that formed the first eukaryote (see subsection 1.2.1) and retain a highly similar core snoRNA system to the archaea (see subsection 1.3.2). In all organisms, rRNA modifications cluster around functionally important regions of the ribosome, the PTC, the decoding center and the subunit interface, and some are conserved positionally from bacteria to humans (Bachellerie et al. 2002; Lestrade and Weber 2006).

A major difference between bacteria and eukaryotes is the presence of the nucleus, which separates most of eukaryotic ribosome formation from the cytoplasm, where translation occurs. When eukaryotes emerged and the nucleus was formed, nuclear transport had to be integrated into the process of ribosome formation, as r-proteins and biogenesis factors have to be imported and pre-ribosomes have to be exported from the nucleus. Therefore, eukaryotes have evolved nuclear localization signals (NLS) on r-proteins and import receptors that recognize these signals, as well as several export receptors for pre-ribosomes, that bind to correctly folded and export competent pre-ribosomal subunits and facilitate their export from the nucleus to the cytoplasm. Analysis of nuclear localization signals of conserved ribosomal proteins has revealed, that many NLS have evolved on rRNA binding surfaces of r-proteins, which highlights a dual function of these regions in nuclear import and rRNA folding, that is realized by the same basic amino acids (Melnikov et al. 2015). In bacteria, r-proteins are incorporated into pre-ribosomes shortly after their translation, whereas nuclear separation in eukaryotes poses a problem

for eukaryotic cells, because free r-proteins are toxic, as they are highly charged, which leads to aggregation and nonspecific interactions with nucleic acids (Jäkel et al. 2002; Lam et al. 2007; Sung, Porras-Yakushi, et al. 2016; Sung, Reitsma, et al. 2016). This is exacerbated by the fact, that many eukaryotic r-proteins have acquired long unstructured and highly charged extensions. Therefore, eukaryotes have evolved specialized chaperone biogenesis factors, that facilitate nuclear import and assembly of many eukaryotic r-proteins (see subsection 1.3.4).

1.3.6 Small subunit assembly

Small subunit biogenesis is associated with initial transcription of the rDNA, and the 5' ETS is the first part of the transcript that is bound by ribosome assembly factors of the UTP-A and UTP-B subcomplexes (Chaker-Margot et al. 2015; Hunziker et al. 2016; Kornprobst et al. 2016; L. Zhang et al. 2016). The 5' ETS is subsequently incorporated into 90S pre-ribosomes and organizes the formation of a scaffold structure, which is involved in the initial folding of the 20S rRNA (Chaker-Margot et al. 2016; Kornprobst et al. 2016; Sun et al. 2017). The 90S strikingly contains only assembly factors and r-proteins of the small subunit, which indicates that it is solely dedicated to SSU formation (Dragon et al. 2002; Grandi et al. 2002). This includes the U3 snoRNA, which is necessary for cleavages at the A_0 and A_1 sites, that are located in the 5' ETS (Dragon et al. 2002; Grandi et al. 2002; Hughes and Ares 1991; Osheim et al. 2004). Furthermore, it is thought, that the terminal knob structures, which are seen in Miller spreads (see Figure 1.9), resemble these initial stages of ribosome biogenesis (Mougey et al. 1993).

The 90S contains a subset of ribosomal S-proteins, which have been associated with early and middle SSU assembly steps by depletion analysis in yeast (Figure 1.12). Their depletion blocks assembly at the early cleavage sites A_0 and A_1, which are located in the 5' ETS and are necessary for formation of the mature 5' end of the 20S rRNA (Figure 1.11 and Ferreira-Cerca et al. 2005; Ferreira-Cerca et al. 2007). The early binding S-proteins are associated with the 5' and central domains of the 20S rRNA, which form the body of the small subunit (Figure 1.13). Interestingly, in the 90S structure, the 5' domain is already folded into a nearly mature state, whereas the central domain and the 3' domain are unfolded and arrested into an open conformation by the 90S scaffold (Chaker-Margot et al. 2016; Kornprobst et al. 2016; Sun et al. 2017). This rRNA conformation is readily accessible to modification enzymes and the 90S scaffold is therefore thought to coordinate the modification and folding of the SSU (Kornprobst et al. 2016). Furthermore, the rRNA state in the 90S RNP illustrates, that the small subunit is generated in a sequential manner, with the body and platform being formed before the

head and its characteristic beak structure (Figure 1.12 and Figure 1.13).

After the processing and modification steps, the 90S pre-ribosome is disassembled, which includes the removal of the U3 snoRNA by the helicase Dhr1 (Sardana et al. 2015; Zhu et al. 2016). The pre-40S is released from the 90S scaffold, which separates it from the 5' ETS, that is subsequently degraded by the nuclear exosome and the exonucleases Xrn1 and Rat1 (Allmang et al. 2000; Petfalski et al. 1997; Thoms et al. 2015). Small subunit maturation continues in the nucleus, which is characterized by a novel set of assembly factors, including Ltv1, that is bound at the region of the beak, Rio2, Tsr1, and Dim1, which are bound at the subunit interface, and Nob1, which is bound at the platform (reviewed in de la Cruz et al. 2015; Schäfer et al. 2003; Strunk et al. 2011). These pre-43S particles are quickly exported from the nucleus, which requires the presence of a subset of head-binding S-proteins (Rps3 (uS3), Rps15 (uS19), Rps18 (uS13), and Rps19 (eS19); Ferreira-Cerca et al. 2007).

In the cytoplasm, the final S-proteins are thought to assemble and form part of the mRNA-binding channel, which suggests, that mRNAs are unable to bind to upstream pre-ribosomes (reviewed in de la Cruz et al. 2015). Additionally, the pre-40S undergoes maturation of the beak structure, that also contributes to mRNA binding in mature 40S subunits, and which involves the phosphorylation of Ltv1 by Hrr25 (Ghalei et al. 2015; Schäfer et al. 2006). Subsequently, the pre-40S subunit associates with 60S subunits to form an 80S-like particle, which involves the dissociation of assembly factors Rio2, Tsr1, and Dim1, that are located at the subunit interface (Strunk et al. 2012). The 80S-like particle is thought to perform a functional test of the pre-40S in a translation-like cycle and additionally is associated with the final processing step of 20S rRNA, which is cleaved by the endonuclease Nob1 at site D (Lamanna and Karbstein 2009; Lebaron et al. 2012; Pertschy et al. 2009; Strunk et al. 2012). Subsequently, small subunit biogenesis is thought to end with the assembly of Rps26 (eS26), which is assumed to assemble after the 20S rRNA has been processed (de la Cruz et al. 2015; Strunk et al. 2011).

1.3.7 Large subunit assembly

Maturation of the large subunit is dependent on successful transcription of the 5' ETS and 18S rRNA of the small subunit, as well as the ITS1, which are located upstream of the 5.8S rRNA, ITS2, and 25S rRNA in the rDNA gene (Figure 1.8). Therefore, nascent transcripts of the large subunit are still covalently connected to the pre-40S subunit and the subunits are separated by A_2 cleavage, which occurs during co-transcriptional processing when Pol I has progressed ~1-1.5 kB downstream of the A_2 site (Axt et al.

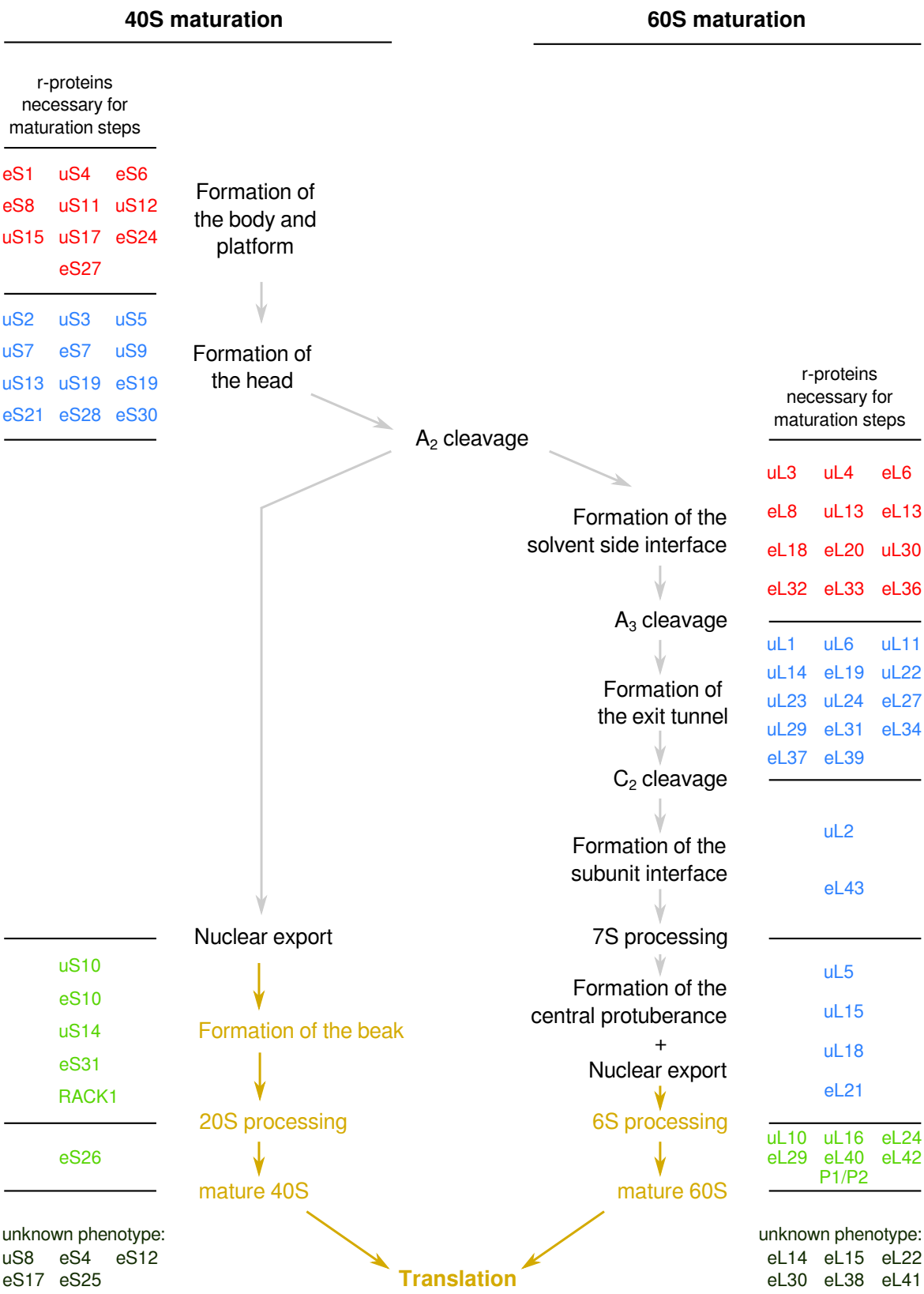

Figure 1.12: Major steps in eukaryotic ribosome assembly Ribosomal subunits mature separately after A_2 cleavage, which requires the presence of additional r-proteins and assembly factors. Major assembly steps for both subunits are indicated in the center and r-proteins needed for each step are listed at the sides. Universal names are used for r-proteins. The proteins are colored by their phenotype, according to de la Cruz et al. 2015. Red = Early, Blue = Middle, Green = Late. Black = Unknown. Cytoplasmic maturation steps are indicated in yellow. The data on r-protein phenotypes was taken from de la Cruz et al. 2015 and integrated with SSU assembly steps derived from Kornprobst et al. 2016; Schäfer et al. 2006 and LSU assembly steps defined in Gamalinda et al. 2014.

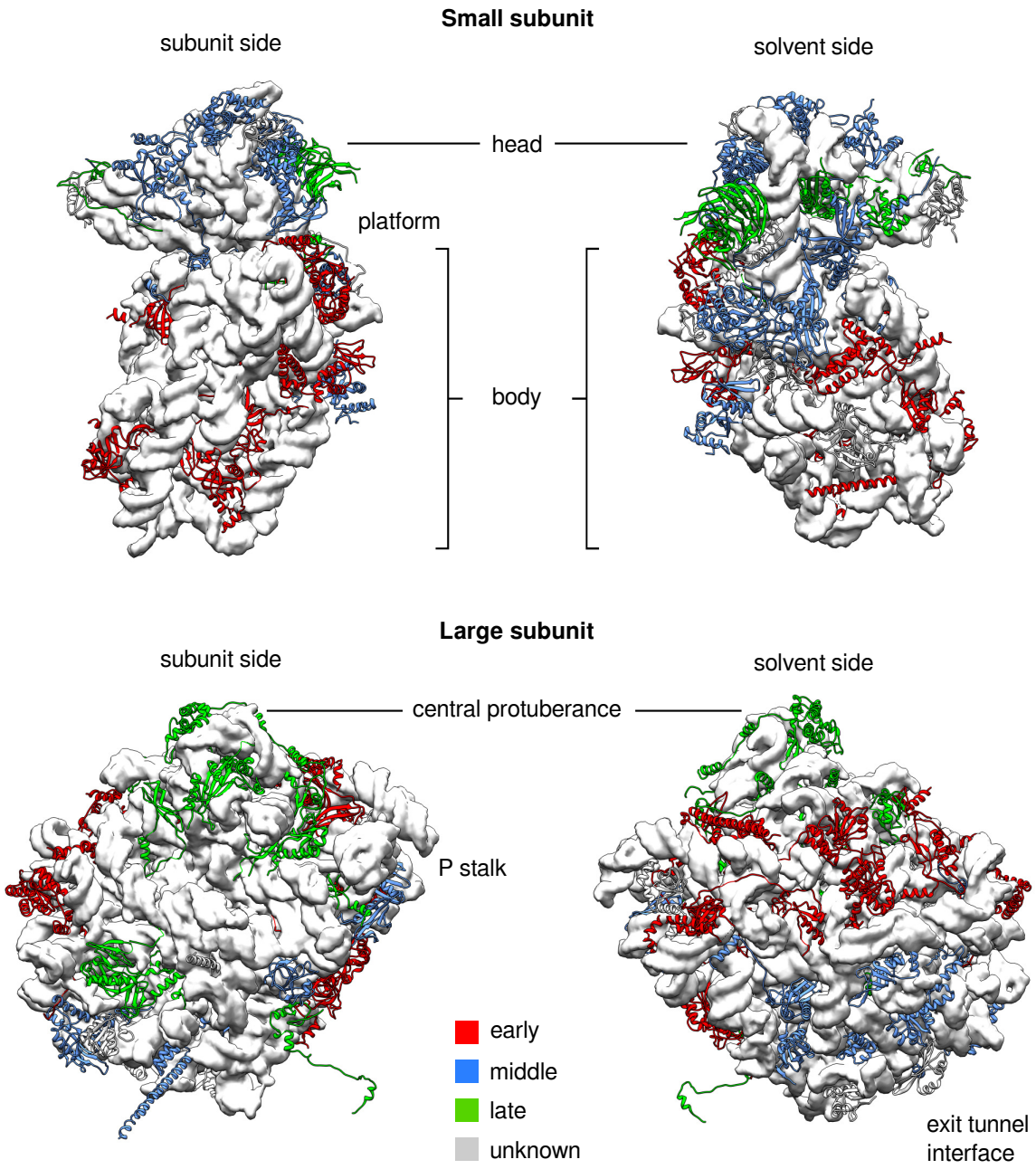

Figure 1.13: Depletion phenotypes of ribosomal proteins correlate with their location on the ribosome Early-acting, middle-acting, and late-acting r-proteins (as shown in Figure 1.12) are mapped onto the crystal structure of yeast ribosomal subunits. rRNAs are shown as white surface. Red = Early acting. Blue = Middle acting. Green = Late acting. Gray = Unknown phenotype. PDB code: 4V88. After de la Cruz et al. 2015; Gamalinda et al. 2014.

2014; Kos and Tollervey 2010; Osheim et al. 2004). Therefore, the initial folding and modification steps of the large subunit are not independent from the small subunit, which is highlighted by assembly factors Rrp5 and Has1, that have dedicated functions in the maturation of both ribosomal subunits (Dembowski et al. 2013; Emery et al. 2004; Hierlmeier et al. 2013; Khoshnevis et al. 2016; Lebaron, Å. Segerstolpe, et al. 2013; Venema and Tollervey 1996). Rrp5 is a large protein of ~193 kDa, which is thought to connect the small to the large subunit with its N- and C-domains and it has been demonstrated, that the C-domain is necessary for A_0 to A_2 cleavage, whereas the N-domain is needed for A_3 cleavage on pre-60S subunits (Lebaron, Å. Segerstolpe, et al. 2013). After A_2 cleavage, the ribosomal subunits mature independently and Rrp5 is found on pre-60S subunits, which explains its requirement for 60S maturation (Hierlmeier et al. 2013; Khoshnevis et al. 2016).

Large subunit maturation involves three major phases, which are thought to occur sequentially (Gamalinda et al. 2014). Assembly proceeds from formation of the solvent side interface to the exit tunnel and finally the subunit interface (Figure 1.12 and Figure 1.13). The early formation of the solvent exposed surface involves domains I and II of the 25S rRNA, whereas subsequent formation of the exit tunnel interface is defined by 25S rRNA domains I and III and the 5.8S rRNA (Gamalinda et al. 2014). This illustrates the early assembly hierarchy, which appears to follow the order in which the rRNA is transcribed. This hierarchy is highly similar to the assembly of 50S subunits in *E. coli*, which highlights the conserved aspects of the assembly process (Chen and Williamson 2013). Assembly depends on the association of the rRNA with ribosomal proteins, which are incorporated into the rRNA fold (subsection 1.3.4). Strikingly, systematic depletion studies of r-proteins have revealed, that the lack of individual L-proteins corresponds to assembly defects of their rRNA neighborhood, which highlights the immediate structural requirements of these r-proteins during maturation (Figure 1.13 and reviewed in de la Cruz et al. 2015).

In addition to the 5.8S rRNA and 25S rRNA, which are part of the 35S rRNA precursor, the 5S rRNA is transcribed from an individual gene by Pol III and subsequently incorporated into the pre-60S subunit as a RNP (J. Zhang et al. 2007). The 5S RNP, which consists of 5S rRNA, Rpl5 (uL18), and Rpl11 (uL5), is assembled in the nucleus, after nuclear import of Rpl5 (uL18), and Rpl11 (uL5), which is facilitated by the assembly chaperone Syo1 and the import receptor Kap104 (Calviño et al. 2015; Kressler, Bange, et al. 2012). Syo1 associates with Rpl5 (uL18) co-transcriptionally and subsequently recruits Rpl11 (uL5) for a coordinated nuclear import of both proteins (Calviño et al. 2015; Kressler, Bange, et al. 2012; Pausch et al. 2015). Additionally, it has been demonstrated, that Syo1 is a RNA mimic, which accommodates the rRNA binding

surface of Rpl11 (uL5), that is necessary for initial docking of the 5S RNP to the large subunit (Calviño et al. 2015). After assembly, the 5S RNP is recruited to the pre-60S and incorporated bound to the trans acting factors Rpf2 and Rrs1 (Asano et al. 2015; Kharde et al. 2015; Madru et al. 2015; J. Zhang et al. 2007). This assembly takes place at early stages in 60S maturation, as both Rpl5 (uL18) and Rpl11 (uL5), as well as Rpf2 and Rrs1 precipitate 35S rRNA, 27SA2 rRNA and 27SB rRNA from yeast, which are the first rRNA precursors of the large subunit (J. Zhang et al. 2007).

During assembly, the pre-60S subunit is associated with >75 non-ribosomal factors, which can be present on a wide range of pre-ribosomes or on distinct particles (reviewed in de la Cruz et al. 2015; Nerurkar et al. 2015). The complexity of pre-ribosomes decreases during maturation, as most biogenesis factors are found on early intermediates (Kressler et al. 2008; Nerurkar et al. 2015; Trapman et al. 1975). Nevertheless, most assembly factors are essential, even late binders, which indicates that all assembly steps are important. Ribosome formation is coordinated by many energy-consuming enzymes, like GTPases, helicases, and AAA-ATPases, which are thought to advance biogenesis by removing other assembly factors or by remodeling the pre-ribosome. These checkpoint functions involve ATP or GTP hydrolysis, which conveys directionality to the assembly process (Nerurkar et al. 2015).

Purification of individual assembly factors precipitates a complex mixture of rRNAs, r-proteins, and additional trans acting factors, which established the time line of 60S maturation. Recently, several distinct late pre-60S particles have been analyzed by cryo-EM, which revealed the structural organization of associated assembly factors with the ribosomal components (Barrio-Garcia et al. 2016; Leidig et al. 2014; Ma et al. 2017; Malyutin et al. 2017; Wu, Tutuncuoglu, et al. 2016). An overview of the Nog2, Rix1/Rea1, and Nmd3 particles is depicted in Figure 1.14, and major structural features are compared to mature 60S subunits. These particles contain compacted rRNAs, which are arranged highly similar to the mature state. The Nog2-particle contains the 5S RNP, which is bound in an inverted conformation from the mature state and assembly factor Arx1, that is prominently visible at the end of the exit tunnel (Bradatsch et al. 2012; Leidig et al. 2014; Wu, Tutuncuoglu, et al. 2016). Arx1 is homologous to methionine aminopeptidases, but enzymatically inactive, and is instead thought to protect the exit tunnel interface during biogenesis. Furthermore, it has been implicated in nuclear export of pre-60S subunits and therefore serves multiple roles during maturation (Bradatsch et al. 2007). Additionally, the Nog2 particle contains a prominent structure, called the 'foot', which forms around the ITS2 and consists of assembly factors Nsa3, Nop7, Nop15, and Nop53 (Tutuncuoglu et al. 2016; Wu, Tan, et al. 2016; Wu, Tutuncuoglu, et al. 2016). ITS2 processing depends on cleavage at site C_2, which is an important

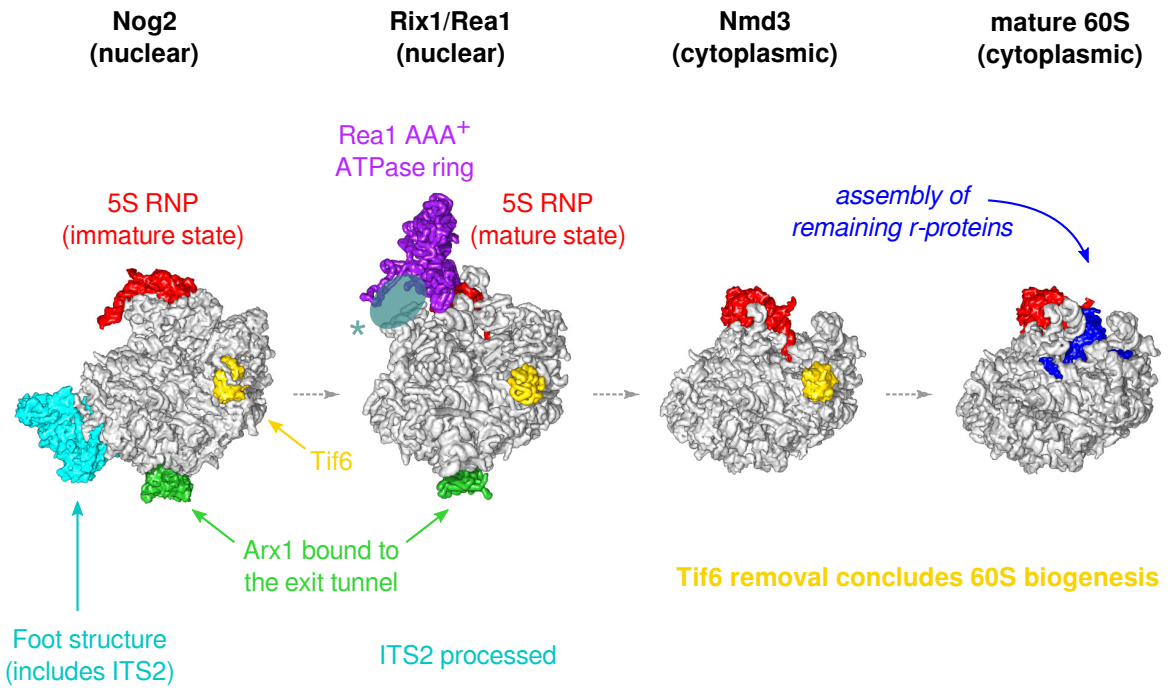

Figure 1.14: Late steps in 60S subunit assembly The structure models of Nog2, Rix1/Rea1, Nmd3, and mature 60S particles are depicted, arranged from earlier to later maturation steps. Proteins and rRNAs are shown as surface representation. Major structural features and rearrangements are indicated by colors: Red = 5S RNP. Cyan = Foot structure. Green = Arx1. Yellow = Tif6. Purple = Rea1 AAA$^+$-ring. Blue = Rpl10 (uL16), Rpl40 (eL40), and Rpl41 (eL41). The location of the Rix1-Ipi1-Ipi3 complex is indicated in sea green and by an asterisk. PDB codes: 3JCT (Nog2), 5JCS (Rix1/Rea1), 5H4P (Nmd3), 4V88 (mature).

step in 60S maturation, that involves the coordinated action of the Las1-Grc3-Rat1-Rai1 complex (Gasse et al. 2015). Las1 is the endonuclease, that cleaves the 27SB rRNA at site C_2, whereas Grc3 phosphorylates the resulting 26S rRNA, which is subsequently processed by Rat1 and Rai1 (Gasse et al. 2015). The ITS2 is then processed by the nuclear exosome, which is recruited to the assembly factor Nop53, that is part of the foot structure (Thoms et al. 2015). As the foot is disassembled and the ITS2 is processed in the Rix1/Rea1 particle, these assembly steps are thought to occur between the Nog2 and the Rix1/Rea1 stage (Barrio-Garcia et al. 2016).

The Rix1/Rea1 particle represents a maturation step downstream of the Nog2 particle (Figure 1.14 and Barrio-Garcia et al. 2016). It is defined by the Rix1-Ipi1-Ipi3 complex of assembly factors, that binds to the pre-ribosome and subsequently recruits the giant AAA-ATPase Rea1 (Barrio-Garcia et al. 2016). Here, the foot structure is missing and the 5S RNP is turned to its mature position (Figure 1.14). This rotation depends on the stable association of Rea1 to the pre-ribosome, which is mediated by the Rix1-Ipi1-Ipi3 complex and assembly factor Rsa4 and is coupled to upstream processing of the

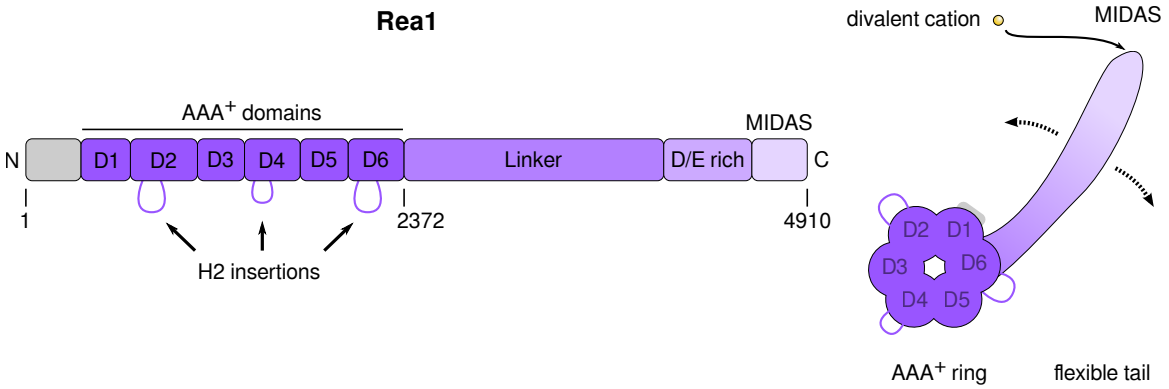

Figure 1.15: The AAA-ATPase Rea1 Rea1 consists of six tandem AAA-ATPase domains in the N-terminal region, which are connected to a C-terminal tail extension. The tail contains a linker region of low complexity, which is enriched in aspartate and glutamate residues (D/E rich). The linker is connected to a C-terminal MIDAS domain (metal ion-dependent adhesion site). The Helix insertion at ATPase domain D2 interacts with Rix1 and is important for recruitment of Rea1 to the pre-ribosome. After Barrio-Garcia et al. 2016.

ITS2 through r-protein Rpl8 (eL8) (Barrio-Garcia et al. 2016; Tutuncuoglu et al. 2016). The rearrangement of the 5S RNP is subsequently coupled to the release of assembly factors Rpf2 and Rrs1 from the 5S RNP, which allows the 5S rRNA to insert into its mature conformation.

Rea1 (also called Midasin or Mdn1) is a huge essential AAA-ATPase, which is related to dynein heavy chain and is conserved from yeast to human. It is the largest protein in yeast, with a molecular weight of ~550 kDa and is divided into several domains (Garbarino and Gibbons 2002; Nissan et al. 2002). It contains a less conserved N-terminal region of ~35 kDa, which is followed by a tandem array of six AAA-ATPase domains, that range from 28 to 40 kDa, each (Figure 1.15). The ATPase domains form a ring, which is readily visible by electron microscopy and is often seen in hexameric assemblies of AAA-ATPases (Ulbrich et al. 2009). The ring is connected to a C-terminal linker domain, which is about ~260 kDa in size and is connected to a region of ~70 kDa, that is rich in aspartic and glutamic acid (D/E rich) (Figure 1.15). The last, C-terminal domain of Rea1, which has a size of 30 kDa, is the, so called, 'metal ion-dependent adhesion site' (MIDAS) (Garbarino and Gibbons 2002). Electron microscopy shows, that the C-terminal linker of Rea1 adopts a flexible, tail-like structure, which protrudes from the AAA-ATPase ring and can move at defined hinge points (Ulbrich et al. 2009).

Rea1 binds to pre-60S subunits via its ATPase domains, which allows free motion of the C-terminal linker, that can reach defined locations on the pre-ribosome, as seen by electron microscopy (Barrio-Garcia et al. 2016; Ulbrich et al. 2009). The C-terminal

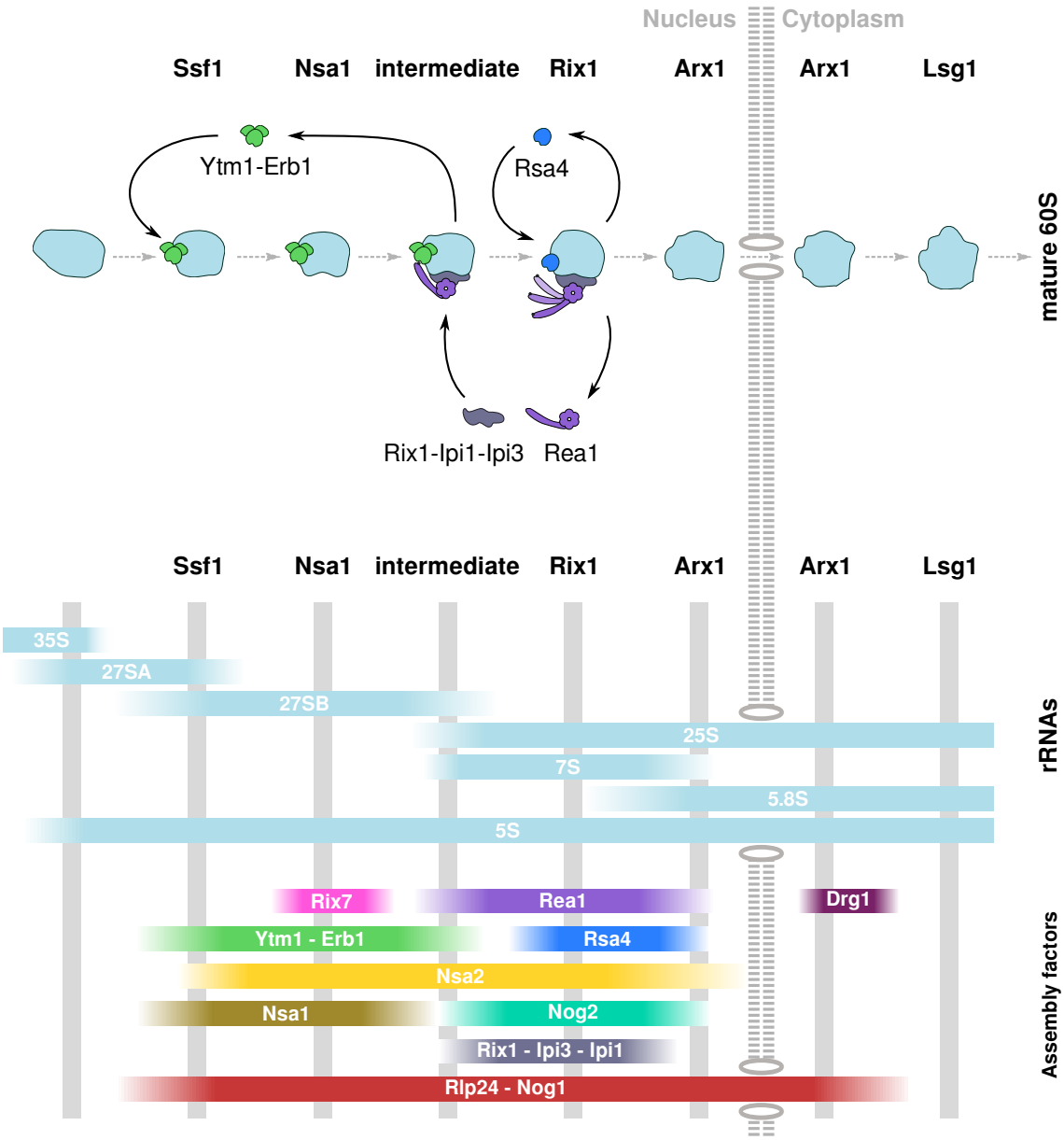

Figure 1.16: The role of Rea1 in 60S biogenesis The Ssf1, Nsa1, Rix1, Arx1, and Lsg1 pre-ribosomes are placed on the 60S maturation time line. The rRNA composition and association of selected assembly factors during biogenesis is shown in the lower panel. 60S maturation includes the action Rea1, a huge AAA-ATPase, which has been implicated in the removal of the Ytm1-Erb1 subcomplex and Rsa4 and the Rix1-Ipi1-Ipi3 complex from pre-ribosomes (Bassler et al. 2010; Ulbrich et al. 2009). After Kressler et al. 2010 and Kressler, Hurt, Bergler, et al. 2012 with data on Nsa2 association added from Ulbrich et al. 2009.

MIDAS domain was found to interact with two adapter proteins, which are called Ytm1 and Rsa4 (Figure 1.16). Ytm1 and Rsa4 are two essential ribosome biogenesis factors, which associate with the pre-60S subunit at different maturation steps. Ytm1 is found on early pre-ribosomes, whereas Rsa4 associates with late nucleoplasmic pre-60S subunits (Bassler et al. 2010; Ulbrich et al. 2009). Furthermore, Ytm1 depletion accumulates small amounts of 27SA2 and large amounts of 27SA3 rRNA, whereas Rsa4 depletion accumulates 27SB rRNA, which suggests, that the two proteins function at separate maturation steps (de la Cruz et al. 2005; Miles et al. 2005). Ytm1 and Rsa4 share a common domain organization. Both proteins consist of a WD40 repeat β-propeller, which contains an additional N-terminal domain, that is homologous in both proteins (Bassler et al. 2010; de la Cruz et al. 2005; Harnpicharnchai et al. 2001; Miles et al. 2005; Royet et al. 1998). The N-domain interacts with the Rea1 MIDAS and is therefore called 'MIDAS interacting domain' (MIDO). It contains a conserved glutamic acid (Glu80 in Ytm1 and Glu114 in Rsa4), which is essential for interaction with Rea1 (Bassler et al. 2010; Ulbrich et al. 2009). This glutamic acid complements the metal binding site of the Rea1 MIDAS, which is formed analogously to the MIDAS in integrins (Bassler et al. 2010; Garbarino and Gibbons 2002; Ulbrich et al. 2009). In integrins, the metal ion is coordinated by six residues, five of which are found in the MIDAS and one, which is provided by the ligand, similar to the Rea1-Ytm1 and Rea1-Rsa4 dimers (Arnaout et al. 2005; Luo et al. 2007; Takagi 2007). *In vitro* release assays have shown, that Rea1 releases both Ytm1 and Rsa4 and additional assembly factors from purified pre-ribosomes upon ATP treatment (Figure 1.16). On early Rix1 particles, that have been purified from a Rea1 depletion background, the addition of wild type Rea1 and ATP releases Ytm1, its binding partner Erb1, and to a lesser extent, the assembly factor Nop7 (Bassler et al. 2010). ATP treatment of late nucleoplasmic Rix1-particles, however, releases Rsa4, Rea1, and the Rix1-Ipi1-Ipi3 subcomplex (Matsuo et al. 2014; Ulbrich et al. 2009). These release steps depend on the interaction of Rea1 with the adapter protein, which is necessary for the ATPase activity of Rea1 and suggests a mechanochemical assembly role for Rea1 (Bassler et al. 2010; Ulbrich et al. 2009). It has therefore been proposed, that Rea1 generates mechanochemical energy, that is transferred via the Ytm1 and Rsa4 adapters to the pre-ribosome, which induces two distinct maturation steps, that lead to possible rearrangements of the pre-ribosome together with the release of the Ytm1 and Rsa4 adapters and associated assembly factors.

The second release step of Rea1 occurs on late nucleoplasmic particles, and is an essential requirement for subsequent nuclear export of pre-60S subunits (Figure 1.16 and Matsuo et al. 2014; Ulbrich et al. 2009). This is regulated by the GTPase Nog2, which binds to the PTC region of 60S pre-ribosomes, at an overlapping location with the

important export adapter Nmd3 (Ma et al. 2017; Malyutin et al. 2017; Matsuo et al. 2014; Wu, Tutuncuoglu, et al. 2016). Nmd3 contains a nuclear export sequence (NES), which interacts with the nuclear export receptor Crm1 and contributes significantly to the export competence of pre-60S subunits (Gadal et al. 2001; Ho et al. 2000; F. Thomas and Kutay 2003; Trotta et al. 2003). Nmd3 can only associate with pre-60S subunits after Nog2 has been released, which requires GTP hydrolysis by Nog2 and ATP hydrolysis by Rea1 (Matsuo et al. 2014). The subsequent export of pre-60S subunits depends on further export adapters, which are recruited to specific locations on the pre-ribosome. Arx1 has been described as an export adapter, which is located at the exit tunnel interface and interacts directly with FG repeats of the nuclear pore complex (Bradatsch et al. 2007; Hung et al. 2007). Additionally, it has been demonstrated that the RNA-export receptor Mex67/Mtr2 facilitates nuclear export of pre-60S subunits by interacting with the premature P stalk region (Sarkar et al. 2016; Yao et al. 2007). Further export adapters have been described, including Bud20, Npl3, and Ecm1, which contribute to the export of pre-60S subunits, but have not been investigated in detail (Altvater et al. 2012; Bassler et al. 2012; Gadal et al. 2001; Hackmann et al. 2011; Ho et al. 2000; Hung et al. 2007; Yao et al. 2007).

After nuclear export, the final maturation steps occur in the cytoplasm, which involves the removal of remaining trans acting factors, the assembly of r-proteins including Rpl10 (uL16), Rpl12 (uL11), Rpl24 (eL24), Rpl40 (eL40), Rpl41 (eL41), and P0 (uL10), the processing of 6S rRNA to 5.8S rRNA by the exonuclease Ngl2, as well as structural probing of the nascent peptidyl transferase center, which is coupled to the release of anti-association factor Tif6 (the yeast eIF6 homolog) (Bussiere et al. 2012; Fernandez-Pevida et al. 2012; Hedges et al. 2005; Kappel et al. 2012; Lo et al. 2010; Ma et al. 2017; Malyutin et al. 2017; Pertschy et al. 2007; Thomson and Tollervey 2009; Weis et al. 2015).

The last steps of cytoplasmic maturation have been analyzed in detail through recent cryo-EM structures of late Nmd3 particles (Figure 1.14 and Ma et al. 2017; Malyutin et al. 2017). These late pre-ribosomes contain only four assembly factors, Nmd3, Lsg1, Tif6, Reh1, and are still lacking the r-proteins Rpl10 (uL16), Rpl12 (uL11), Rpl40 (eL40), Rpl41 (eL41), and P0 (uL10) (Ma et al. 2017; Malyutin et al. 2017). It has been demonstrated, that maturation proceeds with the removal of Nmd3 by the GTPase Lsg1, which requires the association of Rpl10 (uL16) and Rpl40 (eL40) (Bussiere et al. 2012; Fernandez-Pevida et al. 2012; Hedges et al. 2005; West et al. 2005). This frees the PTC interface, which is subsequently thought to assemble with the trans acting factors Sdo1 and Efl1, a paralog of translation elongation factor EF2, that cooperate to release Tif6, which concludes 60S maturation (Ma et al. 2017; Malyutin et al. 2017; Senger et al.

2001; Weis et al. 2015). It has therefore become clear, that maturation of the peptidyl transferase center is the last step in 60S biogenesis and that the PTC is thoroughly tested by a multitude of assembly factors prior to the first round of translation.

Aim of the project

Previous and ongoing research in the Hurt group focuses on the large ATPase Rea1, which is essential for maturation of the large ribosomal subunit. Rea1 binds to the pre-ribosome with its AAA-ATPase ring and contacts additional adapter proteins, Ytm1 and Rsa4, through its C-terminal MIDAS domain (Barrio-Garcia et al. 2016; Bassler et al. 2010; Ulbrich et al. 2009). The interaction with Rsa4 is necessary for an ATP dependent release step by Rea1, which removes Rsa4, Rea1, and the Rix1-Ipi1-Ipi3 complex from late nucleoplasmic pre-ribosomes. It remained unclear, whether this release involves a pulling force by Rea1, that might result in structural rearrangements of the pre-ribosome. It is therefore of high interest to identify the position as well as protein and rRNA contacts of Rsa4 on pre-ribosomes, which would provide insight into the molecular details of Rea1 function.

Recent work has identified a yeast two-hybrid interaction between Rsa4 and the 60S assembly factor Nsa2 (Chantha and Matton 2007; Schraivogel 2009). Furthermore, genetic studies from the Hurt lab suggest, that Rsa4 is functionally linked to Nsa2, which implies, that Nsa2 might be involved in Rea1 activity. Therefore, I sought to identify the molecular details of the Rsa4-Nsa2 interaction and its impact on 60S biogenesis. I aimed to analyze the interaction of Rsa4 and Nsa2 both structurally and functionally in the yeast *Saccharomyces cerevisiae* and to identify the binding site of Rsa4 and Nsa2 on the pre-ribosome. For this, I sought to reconstitute the interaction *in vitro* and to crystallize the hetero-dimer for high-resolution structure determination and a subsequent structure-function analysis *in vivo*. Furthermore, I intended to fit the crystal structure into recent cryo-EM volumes of pre-60S subunits, to identify the position of Rsa4 and Nsa2 on the pre-ribosome, which would unravel the functional neighborhood and possible rRNA targets of Rea1. I expected, that the combination of genetic, biochemical, structural, and functional data would elucidate the extent and molecular details of the Rea1-Rsa4-Nsa2 network and determine its role in 60S biogenesis.

2 Results

2.1 Nsa2 interacts with Rsa4

It has been shown previously, that Nsa2 interacts with Rsa4 in a yeast two-hybrid screen (Chantha and Matton 2007; Schraivogel 2009). Therefore, Nsa2 might be rearranged by the Rea1 power stroke through the interaction with Rsa4 and could direct the Rea1-generated force to further locations on the pre-ribosome. To understand, which part of Nsa2 might be affected by Rea1, I intended to identify the exact binding site of Rsa4 on Nsa2. Therefore, I performed binding assays with recombinant proteins. I purified MBP-tagged variants of Nsa2 and incubated them with His_6-tagged versions of Rsa4. Thus, I could confirm the interaction *in vitro* and I was able to restrict the binding sites on Nsa2 and Rsa4, respectively (Figure 2.1A). Nsa2 interacts with Rsa4 through a small stretch of 13 amino acids in its middle domain (amino acids 84-96). This short linear motif binds to the predicted β-propeller of Rsa4 (Figure 2.1A), which constitutes the minimal Nsa2-Rsa4 complex.

To further characterize the interaction, I checked the stability of the complex by increasing salt concentration in the buffer. I co-expressed Nsa2 with Rsa4 in *E. coli* and purified the complex in buffers containing 250, 600, and 1000 mM NaCl, respectively. The results show, that the interaction between Nsa2 and Rsa4 is resistant to high salt concentrations, including 1000 mM NaCl (appendix Figure A.1).

Due to the fact that a short motif of Nsa2 is sufficient to bind to Rsa4 *in vitro*, I tested if it is also necessary *in vivo*. I used sequence alignment to define two deletion mutants, $Nsa2^{\Delta 85\text{-}98}$ and $Nsa2^{\Delta 86\text{-}90}$. The first mutant removes the complete interaction motif, whereas the shorter one removes only the N-terminal part of the motif. Next, I created a co-expression plasmid with GST-TEV-tagged variants of the deletion mutants and His_6-tagged Rsa4 for heterologous expression in *E. coli*. After expression and purification, I could show that both Nsa2 deletion mutants disrupt the interaction, while the wild type protein still interacts with Rsa4 (Figure 2.2A). To check, if the interaction is necessary for the growth of *S. cerevisiae*, I cloned the deletion mutants into yeast vectors. After transformation of these plasmids into a *NSA2* shuffle strain, I plated the transformants

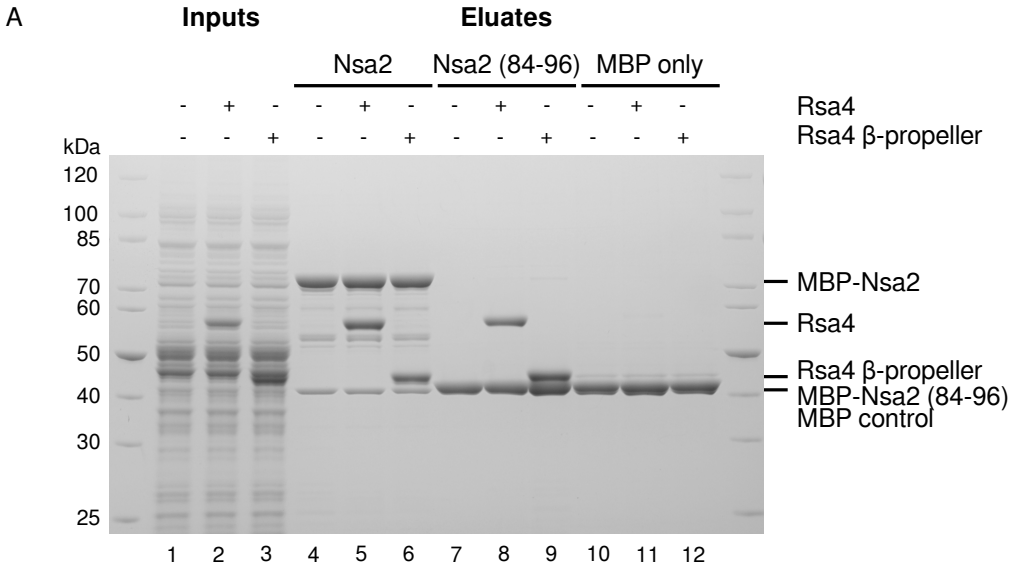

Figure 2.1: 13 amino acids of Nsa2 interact with the Rsa4 β-propeller A) *In vitro* binding assay of Nsa2 and Rsa4. MBP-tagged variants of Nsa2 were immobilized on amylose resin and incubated with *E. coli* lysate containing Rsa4 wild type or β-propeller, respectively. Rsa4 interacts with a short linear motif of Nsa2, which is formed by amino acids 84-96. B) Multiple sequence alignment of the Rsa4 interacting motif of Nsa2. SACCE = *Saccharomyces cerevisiae*, CANAL = *Candida albicans*, CHATH = *Chaetomium thermophilum*, NEUCR = *Neurospore crassa*, CAEEL = *Caenorhabditis elegans*, DROME = *Drosophila melanogaster*, DANRE = *Danio rerio*, MUSMU = *Mus musculus*, HOMSA = *Homo sapiens*.

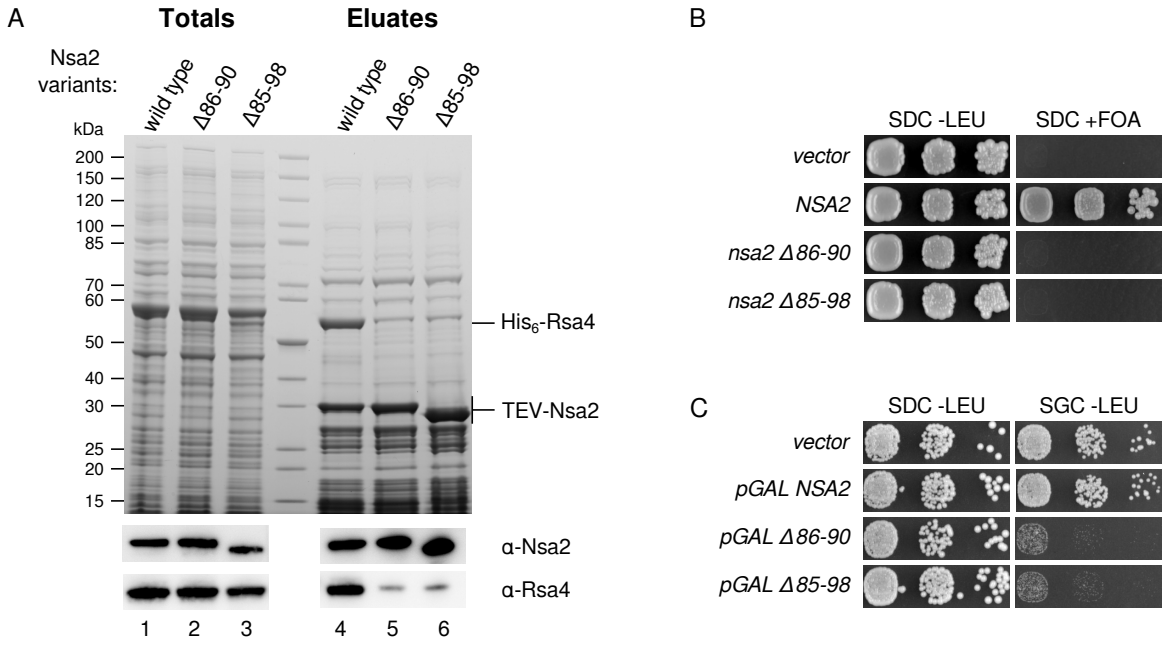

Figure 2.2: The Rsa4-interacting motif of Nsa2 is essential for cell growth A) The Nsa2 motif is necessary for interaction with Rsa4. Co-expression of GST-TEV-Nsa2 wild type and deletion variants Δ86-90 and Δ85-98 with His_6-TEV-Rsa4 in *E. coli*. Nsa2 variants and associated proteins were eluted from GSH-beads by TEV-cleavage. Deletion of the interacting motif in Nsa2 prevents complex formation, which was confirmed by Western blotting. B) The Nsa2 motif is essential for cell growth in *S. cerevisiae*. A *NSA2* shuffle strain was transformed with plasmids expressing *NSA2* wild type and deletion variants Δ86-90 and Δ85-98 under control of the endogenous *NSA2* promoter. Transformants were spotted on plates containing 5-FOA and grown for three days at 30 °C . The deletion mutants fail to support growth in the absence of the wild type protein. C) The Nsa2 deletion mutants exhibit a strong dominant negative growth effect. A wild type yeast strain was transformed with plasmids expressing indicated Nsa2 variants under control of the inducible *GAL1-10* promoter. Transformants were spotted on plates containing galactose and grown for two days at 30 °C .

on 5-FOA, which results in the loss of wild type containing plasmids, that carry the *URA3* marker. This demonstrated, that the interaction is essential for yeast viability, because the deletion mutants can not support growth in the absence of wild type Nsa2 (Figure 2.2B). Additionally, I generated yeast vectors containing the deletion mutants under control of the inducible *GAL1-10*-promoter, which was used for overexpression in *S. cerevisiae*. To asses the effects of the overexpression, the mutants were transformed into a wild type yeast strain and grown on plates containing galactose as the carbon source. Here, the mutants showed a strong dominant-negative growth phenotype, indicating a toxic effect for yeast viability, which suggests, that the mutant protein is still partially functional and interferes with cell growth (Figure 2.2B).

2.1.1 Nsa2 binds to the pore of the Rsa4 β-propeller (in collaboration with Dr. Irmi Sinning)

To understand the molecular structure of the binding motif and how it is embedded between the N- and C-terminal domains of Nsa2, I intended to crystallize full-length Nsa2 in collaboration with the lab of Dr. Irmi Sinning. For crystallization trials, I used the crystallization facility at the Biochemistry Center Heidelberg (BZH) and initial crystallization attempts yielded diffracting crystals, but the dataset could not be solved. Subsequently, I analyzed the crystals by SDS-PAGE, which showed that they contained only a fragment of the full-length protein. Mass spectrometric analysis revealed, that this fragment consisted of the C-terminal domain of Nsa2 (data not shown). This was confirmed by *in vitro* degraded Nsa2, which produced fragments of the same size as the crystal-fragment, that also contained the C-terminal domain (appendix Figure A.2).

Therefore, I concentrated further crystallization attempts on the Nsa2-Rsa4 heterodimer. Because a small peptide of Nsa2 interacts with the β-propeller of Rsa4, I sought to understand which part of the propeller is binding to the peptide. As crystallization of full-length Nsa2 had been unsuccessful, I decided to focus on the minimal complex of Nsa2 and Rsa4 (as defined in section 2.1).

For heterologous expression in *E. coli*, I cloned the coding sequence of the Rsa4-interacting peptide of scNsa2 (amino acids 81-101) in frame, after a modified version of the Maltose-binding protein gene (MBP). This enables visualization of the Nsa2 peptide by standard SDS-PAGE, as the peptide alone is too small to be detected. Additionally, the MBP-tag has been shown to increase the expression of heterologous proteins in *E. coli* and it allows subsequent purification by binding to amylose resin. Furthermore, I used a modified version of the MBP-tag, which carried several point mutations that have been shown to increase crystallization efficiency by surface entropy reduction (Moon et al. 2010).

To reconstitute the minimal complex, the MBP-scNsa2$^{81\text{-}101}$ fusion protein was bound to amylose resin and then incubated with an *E. coli* lysate, containing the heterologously-expressed β-propeller of scRsa4 (scRsa4$^{\Delta 136}$). After washing steps, the complex was eluted with maltose and further purified by size-exclusion chromatography (Figure 2.3B). The fractions containing the complex were collected, concentrated and finally used for crystallization trials (Figure 2.3C,D).

Initial screens were set up at the crystallization facility of the BZH and yielded needle-shaped crystals in one drop-condition (200 mM ammonium sulfate and 20% polyethylene glycol 3350). Since these crystals were too fragile for further analysis, I sought to improve the shape of the crystals by screening around the initial drop condition. Therefore,

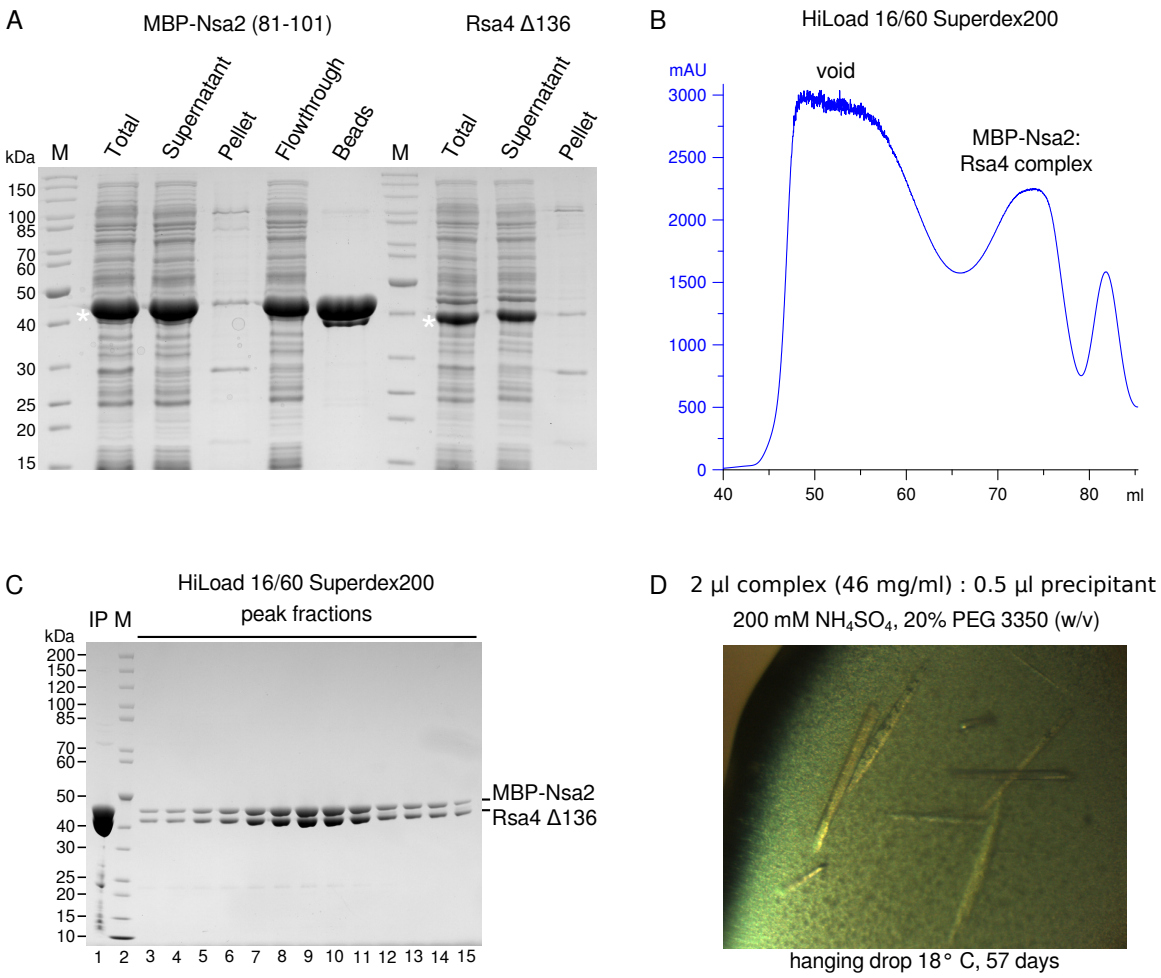

Figure 2.3: Crystallization of the Nsa2-Rsa4 minimal complex A) *In vitro* assembly of the Nsa2-Rsa4 heterodimer. A MBP tagged peptide of Nsa2 (amino acids 81-101) was expressed in *E. coli*, bound to amylose resin, and subsequently incubated with *E. coli* lysate from Rsa4 Δ136 expressing cells. MBP-Nsa2$^{81\text{-}101}$ and Rsa4 Δ136 are indicated with asterisks. B) Size exclusion chromatography of the assembled Nsa2-Rsa4 heterodimer. The complex was concentrated and loaded onto a HiLoad 16/60 Superdex200 column. C) Purified Nsa2-Rsa4 complex after size exclusion chromatography. Peak fractions were collected, concentrated, and used for crystallization trials. D) The purified complex was concentrated to 46mg/ml and hanging drops were set up with 2 µl complex and 0.5 µl precipitant. After 57 days at 18 °C , needle shaped crystals were discovered. The precipitant solution consisted of 200 mM NH_4SO_4 and 20 % PEG 3350 (w/v).

I performed a fine screen with variable ammonium sulfate and polyethylene glycol 3350 concentrations. In addition, I used the remaining protein material to set up a second screen with hanging drops at the initial drop condition, but with varying ratios of protein solution to precipitant. Both screens were incubated at 18 °C and regularly checked for crystals.

The fine screen produced needle-shaped crystals at various conditions, which appeared after one week and were too fragile for analysis (appendix Figure A.3). The second screen did not produce any crystals in the same time interval as the fine screen, but after 57 days, I discovered thicker needles, which could be cryo-protected and analyzed at the European Synchrotron Radiation Facility (ESRF) by members of the lab of Dr. Irmi Sinning. The best crystal diffracted to 3.2 Å and the dataset could be solved by Dr. Iris Holdermann using molecular replacement.

The resulting model of the structure contains both the MBP-Nsa2 fusion protein and the Rsa4 β-propeller domain (Figure 2.4 and PDB code: 4WJV). The β-propeller domain is fully resolved, it consists of an eight bladed WD40 β-propeller and one α-helical insertion of ~45 amino acids at blade five. This insertion is located at the bottom side of the β-propeller and spans across the central pore. The MBP-Nsa2 fusion protein, on the other hand, is not completely resolved. While the MBP-tag is fully present, only amino acids 85-96 of the Nsa2 peptide are seen in the model (The expressed construct contains amino acids 81-101, PDB code: 4WJV). These form a short helical stretch of one turn, which is bound to the top side of the Rsa4 β-propeller and is inserted into the central pore with amino acids 86 to 94 (for a multiple sequence alignment of the motif, see Figure 2.1B).

The peptide enters the central pore with alanine 86 at blade one and leaves on the opposite side with arginine 94 between blades five and six (Figure 2.4). The shape of the peptide perfectly complements the central cavity of the β-propeller and it contacts seven of the eight blades of the propeller through a multitude of hydrophobic and polar interactions. This is achieved by a helical turn of the peptide, which projects the side chains of the amino acids towards the inner side of the propeller. The turn is preceded by the highly conserved proline 88, which also contacts the inner side of the β-propeller at leucine 147 and tyrosine 490 (Figure 2.1 and Figure 2.5). The hydrophobic side chains of alanine 86, leucine 87, leucine 91, and leucine 92 are matched by a hydrophobic ring in the β-propeller, which is formed predominantly by hydrophobic (leucine 147, leucine 190, isoleucine 232, and leucine 404) and aromatic residues (tryptophan 188, tryptophan 231, tryptophan 322, phenylalanine 422, tyrosine 448, and tyrosine 490) (Figure 2.5).

The interaction is further stabilized by threonine 89 and tyrosine 90 of the Nsa2 peptide, which are buried in the central cavity of the β-propeller and are each contacted by multiple amino acids. The methyl group of threonine 89 is probed by leucine 190, cysteine 191, isoleucine 232, and threonine 233 of the β-propeller and the side chain of tyrosine 90 is probed by asparagine 406, tyrosine 448, glutamine 449, and tyrosine 490 (Figure 2.5). The remaining amino acids of the peptide, aspartic acid 93 and arginine 94 are engaged in ionic interactions with lysine 256 and aspartic acid 379 of the β-propeller, respectively.

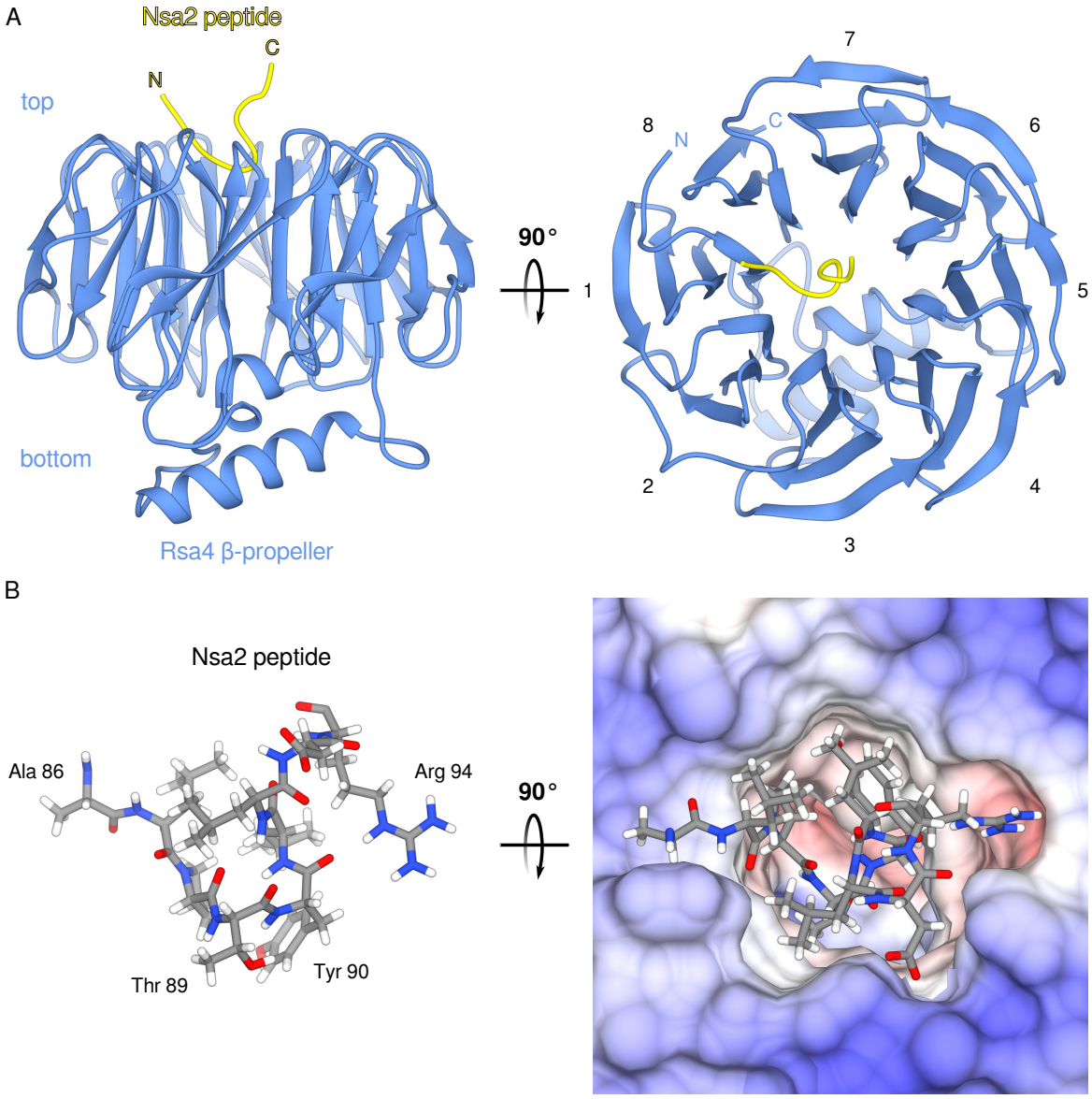

Figure 2.4: Crystal structure of the Nsa2-Rsa4 complex A) Ribbon diagram of the Rsa4 β-propeller with bound Nsa2 peptide at the top side. Amino acids alanine 86 to arginine 94 of Nsa2 are displayed. Left panel = side view, right panel = top view. Individual β-propeller blades are indicated by numbers. N = N-terminus. C = C-terminus. PDB code: 4WJV. B) The Nsa2 peptide binds intimately to the inner surface of the Rsa4 β-propeller. The peptide is shown in the same side and top view as above in A. Left panel = the bound part of the Nsa2-peptide is shown as atoms/bonds representation. White = Hydrogen. Gray = Carbon. Blue = Nitrogen. Red = Oxygen. Nsa2 enters the β-propeller with alanine 86 and leaves at arginine 94. The middle part of the peptide, containing the invariant tyrosine 90, inserts into the pore of the β-propeller. Right panel = top view of the Nsa2 peptide bound to Rsa4. Rsa4 is depicted as electrostatic surface, colors indicate the electrostatic potential. Blue = Positively charged. Red = negatively charged. White = uncharged/hydrophobic. The β-propeller displays a hydrophobic ring, that is associated with the Nsa2 peptide.

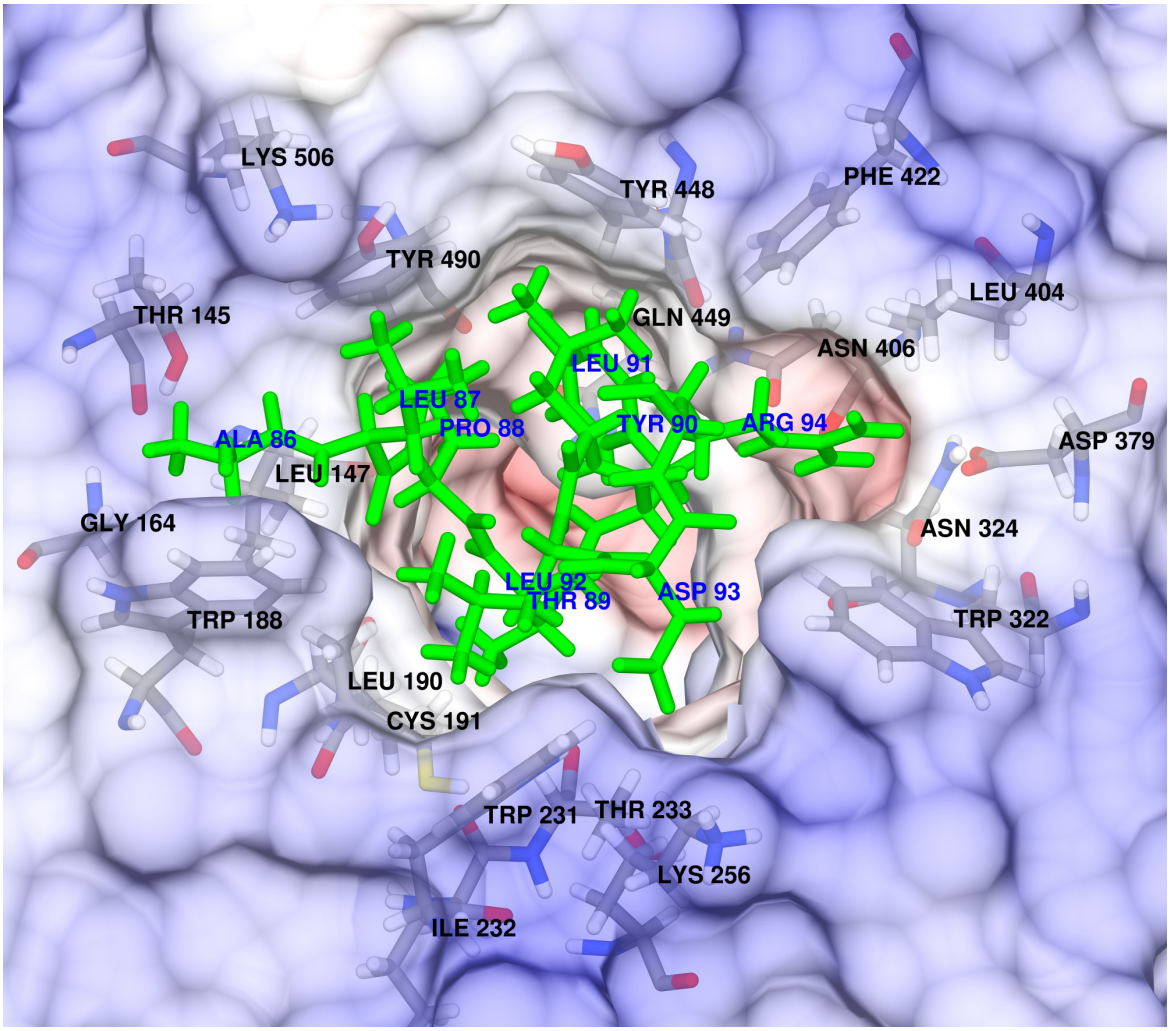

Figure 2.5: Interaction of the Nsa2 peptide with the Rsa4 β-propeller Top view of the Nsa2 peptide and the Rsa4 β-propeller. The Nsa2 peptide and corresponding interacting amino acids of Rsa4 are displayed in atoms/bonds representation. The Nsa2 peptide is colored in green, whereas the residues of Rsa4 are colored according to their elements. White = Hydrogen. Gray = Carbon. Blue = Nitrogen. Red = Oxygen. Yellow = Sulfur. Amino acid labels are displayed in black for the β-propeller and in blue for Nsa2. The picture is overlayed with a surface representation of Rsa4, which is colored according to electrostatic potential. Blue = Positively charged. Red = negatively charged. White = uncharged/hydrophobic. The β-propeller displays a hydrophobic ring, that is associated with the Nsa2 peptide, as well as a salt bridge between aspartic acid 379 and arginine 94 of the Nsa2 peptide. PDB code: 4WJV.

All these interactions lead to a very specific fit of the peptide into the central pore. The shape of the bound peptide closely follows the shape of the β-propeller, leaving no space at the rim or in the middle of the pore. The importance of each residue for the interaction is emphasized by the nearly complete sequence conservation of the motif and the corresponding amino acids in the β-propeller, which highlights the significance of the interaction for eukaryotic ribosome biogenesis (Figure 2.1B and appendix Figure A.4).

2.2 The functional context of the Nsa2-Rsa4 interaction

To study the function of the interaction, I first characterized the pre-ribosomes, that are associated with Nsa2 and Rsa4. It has been demonstrated, that Nsa2 joins the pre-ribosome at an earlier stage than Rsa4, which suggests, that it might be involved in recruiting Rsa4 to the pre-ribosome (Ulbrich et al. 2009). To understand the composition of Nsa2 and Rsa4 particles, I performed tandem affinity purifications (Figure 2.6). Initial purifications with a standard C-terminal TAP-tag showed, that Nsa2-TAP fails to associate with the calmodulin resin at the second purification step (data not shown). This result indicates, that the calmodulin binding part of the TAP tag is not accessible, which suggests, that the C-terminus of Nsa2 is buried in the pre-ribosome. Therefore, I introduced and tested multiple linkers between Nsa2 and the TAP-tag to enable purification (data not shown). With this analysis, I could identify a linker, that allows efficient purification of Nsa2, which I then used for all further purifications from yeast (amino acid sequence 'ASSYTAPQPGLGGS').

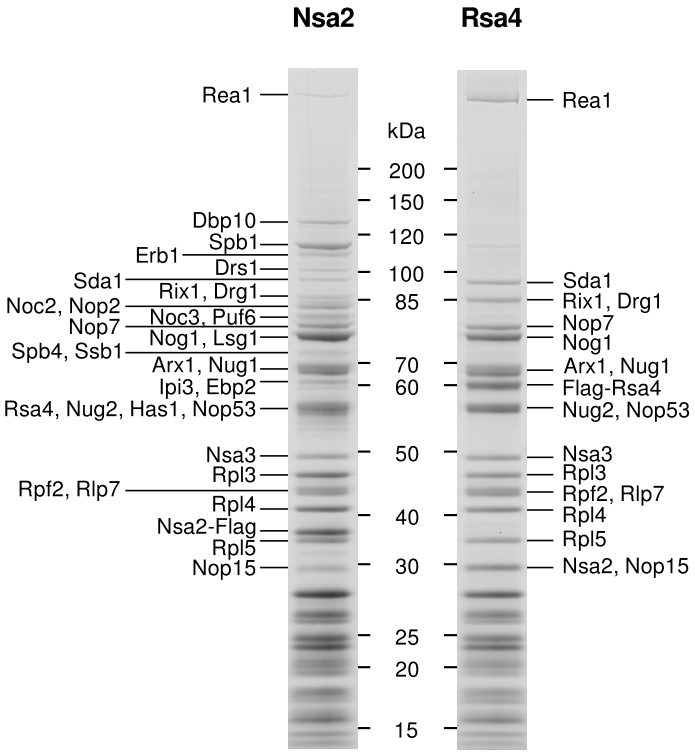

Figure 2.6: Tandem affinity purification of Nsa2 and Rsa4 Yeast strains Nsa2-FTpA and TAP-FLAG-Rsa4 were grown in YPD medium and used for purification. Nsa2 purifies a range of intermediate and late assembly factors, whereas Rsa4 contains only a late acting subset of these factors. Indicated bands were identified by mass spectrometry.

The Nsa2 purification contains both early and late 60S biogenesis factors, whereas the Rsa4 purification contains a subset of these factors, that is associated with late 60S maturation steps (Figure 2.6). The early factors of the Nsa2-particle include Noc2, Noc3, Erb1, Drs1, Has1, Dbp10, Nop2, Puf6, Spb4, Ebp2, and Spb1. The remaining factors, which are involved in later maturation steps and which are shared with the Rsa4 purification are Rea1, Sda1, Rix1, Drg1, Nop7, Nog1, Arx1, Nug1, Rsa4, Nug2, Nop53, Nsa3, Rpf2, Rlp7, and Nop15. Therefore, the interaction of Nsa2 with Rsa4 occurs on late nucleoplasmic pre-ribosomes, that are defined by the presence of the foot structure, that is involved in ITS2 processing, which consists of Nsa3, Nop7, Nop15, and Nop53 (Tutuncuoglu et al. 2016; Wu, Tan, et al. 2016; Wu, Tutuncuoglu, et al. 2016), and the Rix1-complex with its binding partners Sda1 and Rea1. Additionally, the presence of early assembly factors in the Nsa2 purification hints at additional functions of Nsa2 in 60S maturation (see discussion section 3.2).

2.2.1 The Nsa2 Y90A mutant arrests 60S biogenesis at a distinct maturation step

To understand the function of the Nsa2-Rsa4 interaction, I sought to create point mutants, that abolish the interaction and to analyze these for their effect on 60S biogenesis and the recruitment of Rsa4. I chose to create point mutants over the existing deletion mutants (see section 2.1) because it is possible, that the deletion of multiple amino acids affects the fold of Nsa2, which might disrupt the binding to Rsa4 and therefore increase the importance of the interaction motif. Because the shorter deletion mutant Nsa2$^{\triangle 86\text{-}90}$ already disrupts the interaction, I focused on amino acids 86 to 90 of the peptide. I generated yeast vectors, which expressed the Nsa2 mutants L87A, P88A, T89L, and Y90A under control of the endogenous *NSA2* promoter. When checked for complementation in a *NSA2* shuffle strain, only the P88A and Y90A mutant showed a growth phenotype (data not shown). The P88A mutant displayed a slow growth phenotype and the Y90A mutant was inviable (Figure 2.7B). When overexpressed from a *GAL1-10*-promoter, both mutants showed a dominant negative effect on the growth of a wild type yeast strain, with the effect of the P88A mutant being less pronounced than that of the Y90A mutant (Figure 2.7B).

For further analysis, I focused on the lethal Y90A mutant. To check, if the aromatic ring of tyrosine 90 is necessary for the interaction, I generated the Y90F mutant, which is aromatic but lacks the hydroxyl group of tyrosine. Complementation analysis in a *NSA2* shuffle strain revealed, that the Y90F mutant is able to support growth (Figure 2.7B). To check, which mutants can still bind to Rsa4, I created *E. coli* expression plasmids

with MBP-tagged variants of wild type Nsa2, the Y90A mutant, and the Y90F mutant. I used these constructs for an *in vitro* binding assay with His_6-tagged Rsa4. After binding to amylose resin, I incubated the Nsa2 variants with *E. coli* lysate, containing purified His_6-Rsa4 and eluted the proteins with maltose after washing. The results show, that the Y90A mutant prevents the binding to Rsa4, whereas the wild type protein and the Y90F mutant both interact with Rsa4 (Figure 2.7A).

Next, I sought to understand the functional consequence of the mutations *in vivo*. Therefore, I performed tandem affinity purifications (TAP) from *S. cerevisiae* to compare the mutant particles to the wild type. Because the Y90A mutant is not viable, I expressed TAP-tagged variants of the mutants in a wild type yeast strain. I purified the P88A mutant, the Y90A mutant, and the Y90F mutant and compared them to the wild type. The results show very similar gel-patterns for all Nsa2 variants analyzed (Figure 2.7C). The mutants purified pre-ribosomes of highly similar composition to the wild type, the major bands for assembly factors include Spb1, Sda1, Nop7, Nog1, Arx1, Nug1, Rsa4, Nug2, Nsa3, and Nsa2. Further western blotting showed, that Rsa4 is present in similar amounts on all mutant particles, indicating that the interaction with Nsa2 is not necessary for docking of Rsa4 to the pre-ribosome (Figure 2.7C and see discussion section 3.1).

As the mutants were purified under steady state conditions and Nsa2 is associated with a wide spectrum of pre 60S particles (Ulbrich et al. 2009), it is possible that the phenotype of the mutants is only visible on a fraction of the purified particles and could therefore be masked by other, more abundant and wild type like, pre-ribosomes. Therefore, I sought to analyze the Y90A mutant by a pulse chase experiment, which would allow a more dynamic picture of the phenotype. Together with our lab technician Ruth Kunze, I performed non radioactive pulse-chase epitope labeling, according to Stelter and Hurt 2014. The pulse-chase experiment allows the identification of ribosome biogenesis defects, which accumulate after overexpression of a mutant biogenesis factor. For this, I generated overexpression plasmids with Rpl25 (uL23) as the bait protein combined with Nsa2 wild type or the Nsa2 Y90A mutant, that were expressed under control of the inducible *GAL1-10* promoter. Rpl25 (uL23) is generally present in mature ribosomes under normal growth conditions, whereas it shifts to pre-ribosomes when ribosome biogenesis is disturbed (Stelter et al. 2012). Since Rpl25 (uL23) joins very early in ribosome biogenesis, nearly the full range of 60S biogenesis can be analyzed. For the experiment, I defined the pulse and chase time-points and Ruth performed the pulse-chase and subsequent tandem affinity purifications. The results show that the Y90A mutant stalls ribosome biogenesis and leads to a shift of Rpl25 (uL23) from mature to pre-ribosomes (Figure 2.7D). The biogenesis factors associated with the stalled pre-ribosomes include Spb1, Nop2, Nop7, Nog1, Nug1, Ebp2, Nug2, Rsa4, Nsa3, Rpf2,

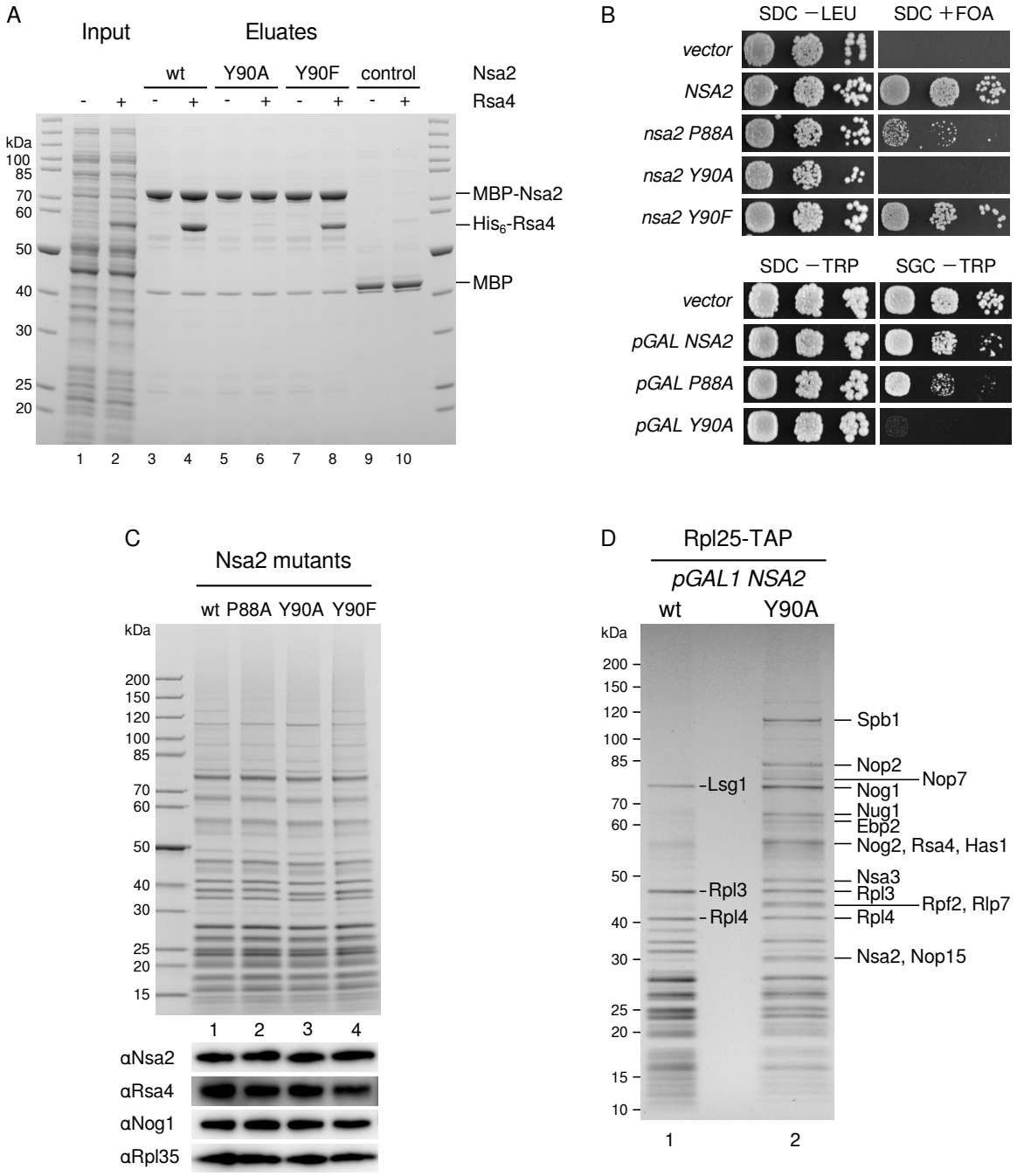

Figure 2.7: The Y90A mutant of Nsa2 abolishes the interaction with Rsa4 A) *In vitro* binding assay of Nsa2 point mutants with Rsa4. MBP-tagged variants of Nsa2 were bound to amylose resin and incubated with *E. coli* lysate containing His_6-Rsa4. B) Upper panel: The P88A mutant of Nsa2 displays a slow growth phenotype, whereas the Y90A mutant is lethal. A *NSA2* shuffle strain was transformed with plasmids expressing indicated Nsa2 variants under control of the endogenous *NSA2* promoter. Transformants were spotted on plates containing 5-FOA and grown for two days at 30 °C . Lower panel: The P88A and Y90A mutant are dominant negative. A wild type yeast strain was transformed with plasmids expressing indicated Nsa2 variants under control of the inducible *GAL1-10* promoter. Transformants were spotted on plates containing galactose and grown for three days at 30 °C . C) TAP of Nsa2 point mutants. A wild type yeast strain was transformed with plasmids expressing FTpA-tagged variants of Nsa2 from the endogenous *NSA2* promoter. The P88A and Y90A mutants contain similar amounts of Rsa4 and Nog1, as indicated by Western blotting. D) Non-radioactive pulse chase of Rpl25-TAP in the presence of the Nsa2 Y90A mutant arrests 60S maturation at a distinct biogenesis step. Indicated Bands were analyzed by mass spectrometry.

Rlp7, Nop15, and Nsa2. The wild type purification also contains extra bands, although in under-stoichiometric amounts. The most prominent band is Lsg1, which has been previously associated with the Rpl25 pulse chase method and is therefore not an effect of the *NSA2* overexpression (Stelter and Hurt 2014).

In summary, the Nsa2-Rsa4 interaction is essential for viability and is involved in a distinct ribosome assembly step, that is downstream of Rsa4 recruitment to the pre-ribosome. The interaction depends on tyrosine 90 of Nsa2, as the Y90A point mutant abolishes the interaction with Rsa4, similar to deletion mutants of the interacting motif.

2.2.2 Rsa4 point mutants disrupt the interaction with Nsa2

To understand the functional implications of the interaction from the side of Rsa4 and to check if a single point mutation in the β-propeller could mimic the phenotype of the Nsa2 Y90A mutation, I created several Rsa4 mutations. Because the Nsa2 peptide interacts with the pore of the β-propeller, a multitude of amino acids are closely located to the bound peptide (see Figure 2.5). Therefore I generated several mutations to disrupt the interaction (Figure 2.8A). Glycine 164 was mutated to leucine (G164L), leucine 190 to isoleucine (L190I), lysine 256 to alanine (K256A), aspartic acid 379 to arginine (D379R), asparagine 406 to lysine and glutamine, respectively (N406K and N406Q), tyrosine 448 to glutamic acid (Y448E), and tyrosine 490 to glutamic acid (Y490E). Two additional mutations are presented in Figure 2.8A, the K130E/K134E and T175R/T177R double mutants, which were generated to disrupt the potential interaction with Rpl5 (uL18) and are explained below in subsection 2.4.1.

I cloned the mutants into yeast vectors and transformed them into a *RSA4* shuffle strain to check for complementation. After plating the cells on 5-FOA, the Rsa4 L190I, K256A, D379R, and N406Q mutants complemented the lack of *RSA4*, therefore I excluded them from further analysis (data not shown). The G164L, N406K, Y448E. and Y490E mutants failed to support growth, equivalent to the Nsa2 Y90A mutant. Because tyrosine 448 and tyrosine 490 are adjacent to each other on two consecutive blades in the β-propeller (Figure 2.8A), and both mutants are lethal, I excluded the Y490E mutant from further analysis. Next, I created overexpression plasmids with the Rsa4 G164L, N406K, and Y448E mutants under control of the inducible *GAL1-10*-promoter. After transformation into a wild type yeast strain, all three mutants showed a dominant negative effect when grown on galactose containing plates (Figure 2.9A).

To check the binding of the Rsa4 mutants to Nsa2 *in vitro*, I generated *E. coli* expression plasmids with His_6-tagged versions of the mutants. I used MBP-tagged wild type Nsa2 as the bait protein and after binding to amylose resin, I incubated Nsa2 with *E. coli*

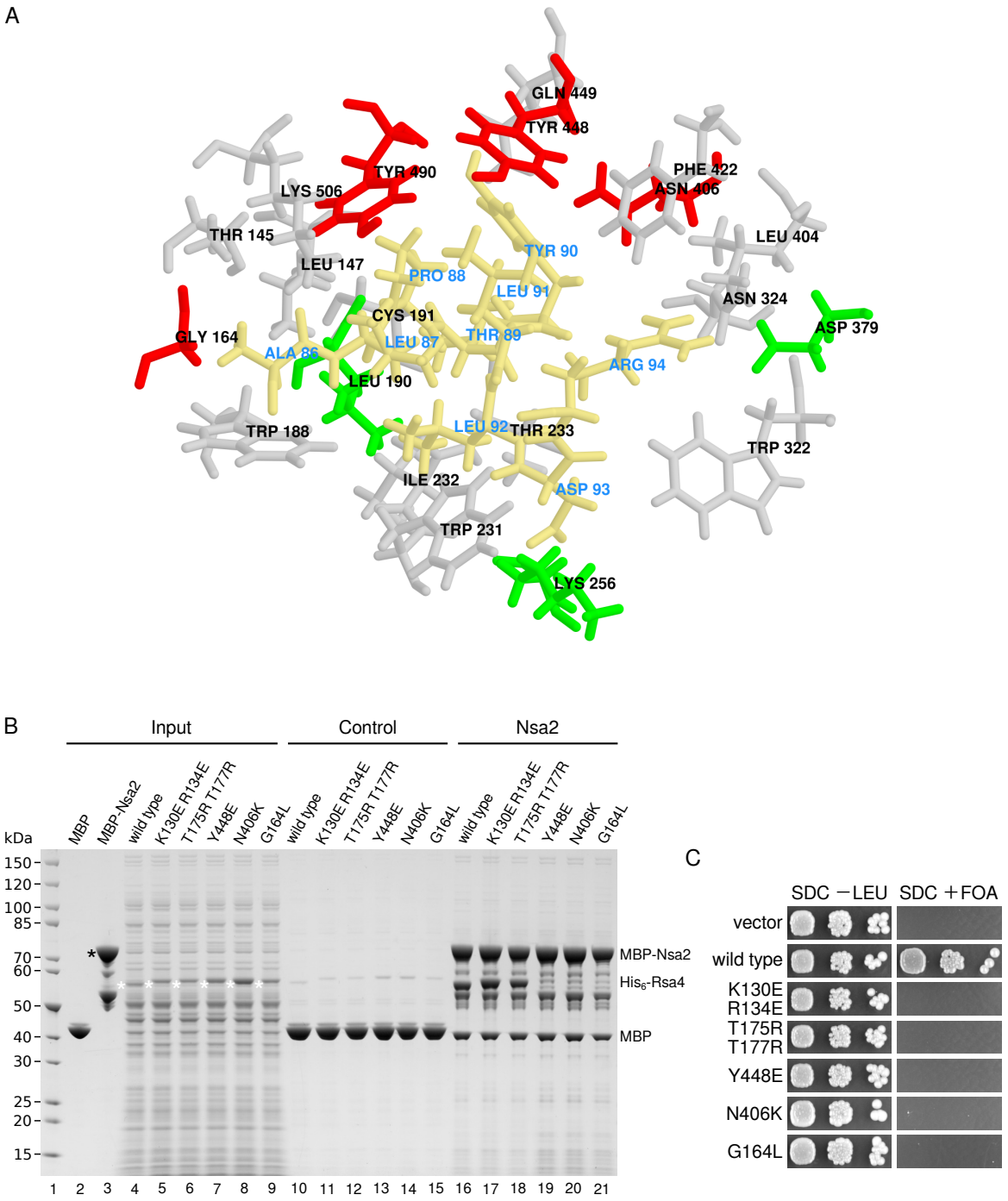

Figure 2.8: Mutations in the Rsa4 β-propeller disrupt the interaction with Nsa2 A) Interactions of the Rsa4 β-propeller with the Nsa2 peptide. Gray, red, green = amino acids of the β-propeller, that interact with Nsa2. Red = lethal mutations. Green = viable mutations. Gray = not mutated. Yellow = Nsa2 peptide. Amino acids labels for the β-propeller are displayed in black, labels of the Nsa2 peptide in blue. B) *In vitro* binding assay of Rsa4 point mutants with Nsa2. The Y448E, N406K, and G164L mutants abolish the interaction with Nsa2. MBP-Nsa2 was bound to amylose resin and incubated with *E. coli* lysate containing His_6-Rsa4 variants. Black asterisk = MBP-Nsa2. White asterisk = Rsa4 variants. C) The Rsa4 mutants are inviable. A *RSA4* shuffle strain was transformed with plasmids expressing Rsa4 variants under control of the endogenous *RSA4* promoter. Transformants were spotted onto plates containing 5-FOA and grown for three days at 30 °C .

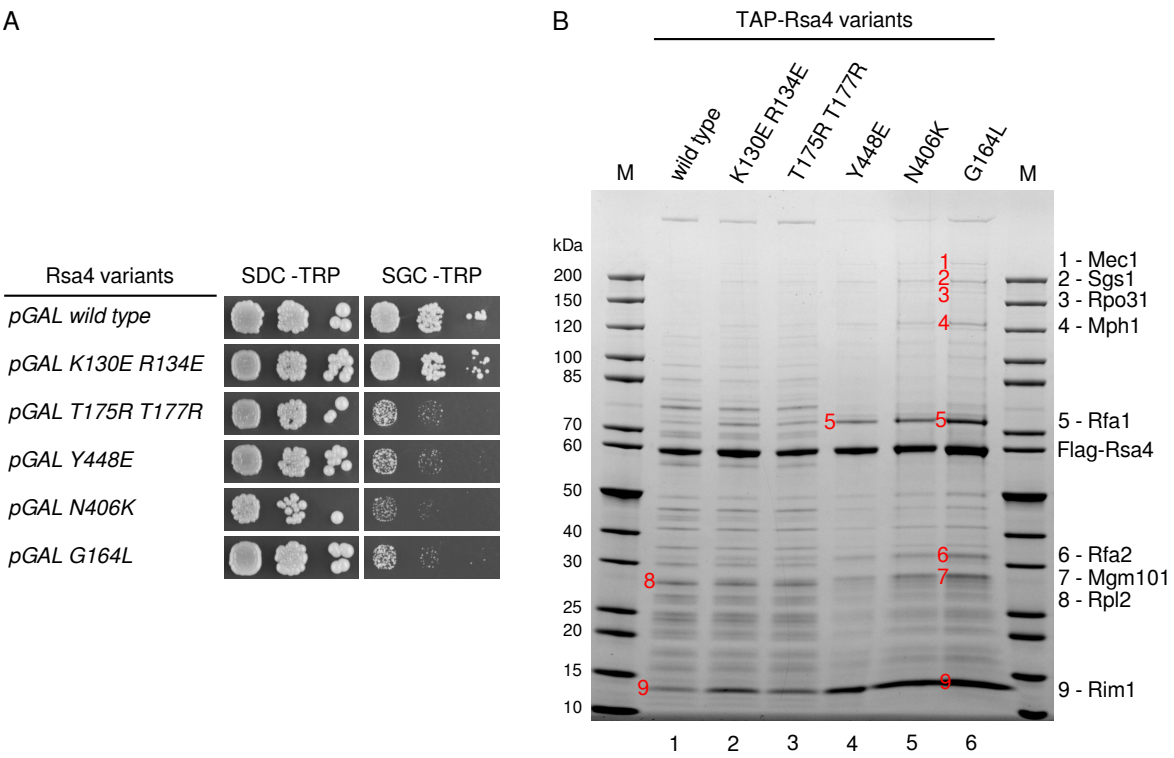

Figure 2.9: Rsa4 point mutants are associated with DNA damage repair factors A) Overexpression phenotype of Rsa4 point mutants. A wild type yeast strain was transformed with plasmids expressing Rsa4 variants under control of the inducible *GAL1-10* promoter. Transformants were spotted on plates containing galactose and grown for three days at 30 °C . B) TAP of Rsa4 point mutants. The K130E/R134E and T175R/T177R double mutants associate with pre-ribosomes like the wild type, whereas the point mutants which disrupt the interaction with Nsa2, Y448E, N406K, and G164L display reduced pre-ribosome binding. Bands indicated by numbers were analyzed by mass spectrometry. The mutants co-purify various non-ribosomal factors, which are involved in DNA related pathways.

lysate containing the His_6-Rsa4 variants. The results show, that the three mutants, that were designed to disrupt the interaction with Nsa2 (G164L, N406K, and Y448E) can not bind to Nsa2, whereas the two mutants, that were designed to disrupt the interaction with Rpl5 (uL18) can still bind to Nsa2 (Figure 2.8B).

To identify the associated proteins of the Rsa4 mutants *in vivo*, I performed tandem affinity purifications from *S. cerevisiae*. For this, I expressed TAP-tagged variants of the Rsa4 mutants in a wild type yeast strain. I purified the G164L, N406K, and Y448E mutants, as well as the K130E/K134E and T175R/T177R double mutants mentioned above and in subsection 2.4.1, and compared them to the wild type. The results show, that the double mutants purify similar particles to the wild type, whereas the single mutants show more distinct phenotypes (Figure 2.9B). The Y448E mutant purifies significantly less pre-ribosomes than the wild type and is associated with two proteins, Rfa1 and Rim1. The other two mutants N406K and G164L purify ribosomal particles, although

smaller amounts of biogenesis factors are visible on the gel, especially above 60 kDa. All mutants purify additional proteins, that are not found in the wild type, which can be seen at higher molecular weights. These were analyzed, exemplary for the G164L mutant, by mass spectrometry in house at the BZH (Figure 2.8B). The bands were identified as Mec1 (genome integrity checkpoint protein and PI kinase superfamily member), Sgs1 (RecQ family nucleolar DNA helicase), Rpo31 (RNA polymerase III largest subunit C160), and Mph1 (3'-5' DNA helicase involved in error-free bypass of DNA lesions). Furthermore, additional bands were identified in the mutants, that are enriched, when compared to the wild type. These were identified by mass spectrometry in the G164L mutant as Rfa1 and Rfa2 (subunits of heterotrimeric Replication Protein A, RPA), Mgm101 (Mitochondrial Genome Maintenance protein), and Rim1 (ssDNA-binding protein essential for mitochondrial genome maintenance) (definitions from SGD).

In summary, the Rsa4 mutants towards the Nsa2 peptide abolish the interaction with Nsa2, which leads to a reduced presence in pre-ribosomes and a co-purification of DNA-repair factors (for a discussion see section 3.4). The mutants do not mimic the Nsa2 Y90A point mutation, as Nsa2 Y90A still associates with pre-ribosomes like wild type, whereas Rsa4 appears to rely on the interaction not for its recruitment, but for subsequent stable association with the pre-ribosome (see discussion section 3.1).

2.3 Structural studies of Nsa2 domains

The functional analysis of Nsa2 and Rsa4 point mutations demonstrated the importance of the Nsa2 motif for ribosome biogenesis, but did not reveal how Nsa2 and Rsa4 bind to pre-ribosomes. Because the motif is located in the middle part of Nsa2, it is important to understand the molecular structure of the N- and C-domains, as these are likely involved in interactions with the pre-ribosome. Additionally, the conformation of the N- and C-domains could reveal if Nsa2 is an elongated or globular protein, which has implications for its functionality. It has been demonstrated, that many eukaryotic ribosomal proteins possess long α-helical extensions, that span around the ribosome in a net-like arrangement (see Figure 1.3). It is therefore interesting, that secondary structure prediction of Nsa2 shows, that the N-domain of Nsa2 is likely α-helical, whereas the C-domain is composed of β-strands (appendix Figure A.7).

Therefore, I intended to crystallize individual Nsa2 domains, which would reveal the high resolution structure of Nsa2 and also enable rigid body fitting of these generated models into recent cryo-EM maps of pre-60S subunits (Bradatsch et al. 2012). For analysis, I chose the Nsa2 homolog of the thermophilic fungus *Chaetomium thermophilum*,

whose proteins have been shown to possess favorable biophysical properties (Amlacher et al. 2011). First, I focused on the C-domain, as it had been established as a stable domain in crystallization attempts of the full-length protein, as well as in an *in vitro* degradation experiment (see subsection 2.1.1 and appendix Figure A.2). I designed the ctNsa2$^{\Delta 167}$ truncation, based on mass spectrometry data of the fragment (appendix Figure A.2) and submitted it to crystallization trials. These attempts yielded crystals, which turned out to be poly-crystalline and consequently could not be used for structure determination. Further optimization trials were unsuccessful as all crystals, that appeared, were poly-crystalline as well.

Because of the unsuccessful crystallization attempts of the C-domain, we started a collaboration with the lab of Dr. Elisar Barbar at Oregon State University, which is focused on structure determination by nuclear magnetic resonance spectroscopy (NMR spectroscopy). Full-length ctNsa2 (30 kDa) is at the size limit for NMR spectroscopy, so we split the sequence of ctNsa2 and analyzed the N-domain and the C-domain separately. The analysis of the N-terminal fragment was performed by Sarah Anna Clark (see subsection 2.3.1) and the C-terminal fragment by Dr. Afua Nyarko (see subsection 2.3.2). These structures have been published in collaboration with Dr. Elisar Barbar in Baßler et al. 2014.

2.3.1 The N-domain of Nsa2 consists of flexible α-helices (in collaboration with Dr. Elisar Barbar)

To define the N-domain of Nsa2, I utilized secondary-structure prediction and sequence alignment of Nsa2 (Figure 2.10A and appendix Figure A.7). I cloned the ctNsa2$^{1\text{-}84}$ truncation, which includes the whole α-helical part of the N-domain up to an unconserved and likely unstructured region. I cloned this truncation into an *E. coli* expression vector, with a N-terminal His_6-tag and sent it to the lab of Dr. Barbar for purification and analysis.

Sarah Anna Clark was able to solve the structure by NMR and the results are shown in Figure 2.10B. The N-domain consists of three α-helices, a short one followed by two longer ones, that are connected by flexible hinge regions. The first two helices, designated h1 and h2, are invariant and have been used to align the four displayed intermediates of the NMR ensemble in Figure 2.10B. The third α-helix (h3) on the other hand differs in length and position relative to h1 and h2. The rest of the N-domain after h3 is unstructured in solution and is therefore highly flexible in relation to h3.

Overall, the flexibility of the N-domain is restricted because the α-helices are looping back and are touching each other in all four states analyzed. Therefore the N-domain does not appear to exist in a completely elongated conformation in solution. Neverthe-

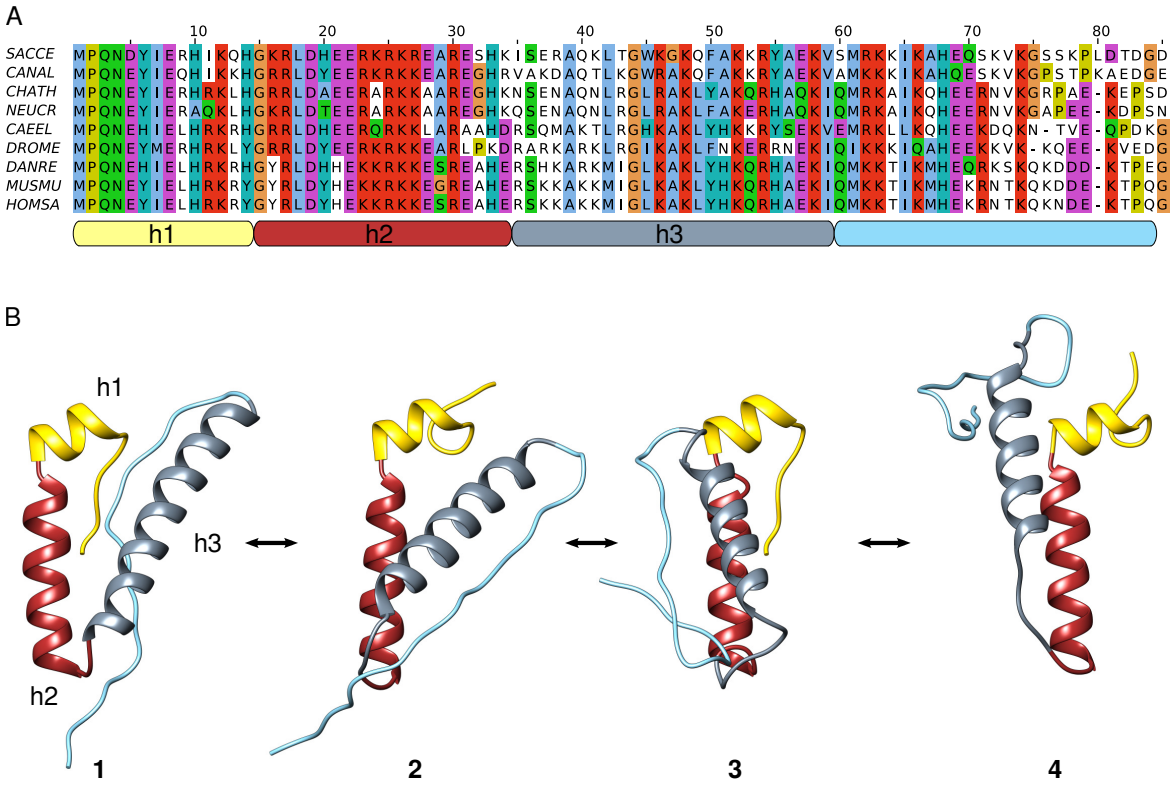

Figure 2.10: NMR structure of the Nsa2 N-domain A) Multiple sequence alignment of the Nsa2 N-domain with individual α-helices indicated below. SACCE = *Saccharomyces cerevisiae*, CANAL = *Candida albicans*, CHATH = *Chaetomium thermophilum*, NEUCR = *Neurospore crassa*, CAEEL = *Caenorhabditis elegans*, DROME = *Drosophila melanogaster*, DANRE = *Danio rerio*, MUSMU = *Mus musculus*, HOMSA = *Homo sapiens*. B) Ribbon style depiction of NMR structures for four identified solution states of the ctNsa2 N-domain. Helices are labeled h1-h3. The orientation of h1 to h2 is invariant in solution, whereas h3 displays flexibility in length and orientation, but always assumes a compact, scissor-like conformation together with h1 and h2.

less, the NMR structure reveals, that the Nsa2 N-domain possesses several hinge points, that allow rotation of individual α-helices.

2.3.2 The C-domain of Nsa2 is highly similar to Rps8 (in collaboration with Dr. Elisar Barbar)

For structural analysis of the C-domain by NMR, I used the Δ167 truncation of ctNsa2, which had been defined as a stable degradation product by mass spectrometry (see subsection 2.1.1). This truncation contains all predicted β-strands of the C-terminal part of ctNsa2 and is resistant to degradation (see appendix Figure A.2). I cloned it into an *E. coli* expression plasmid, with a N-terminal His_6-tag and sent it to the lab of Dr. Barbar for purification and analysis.

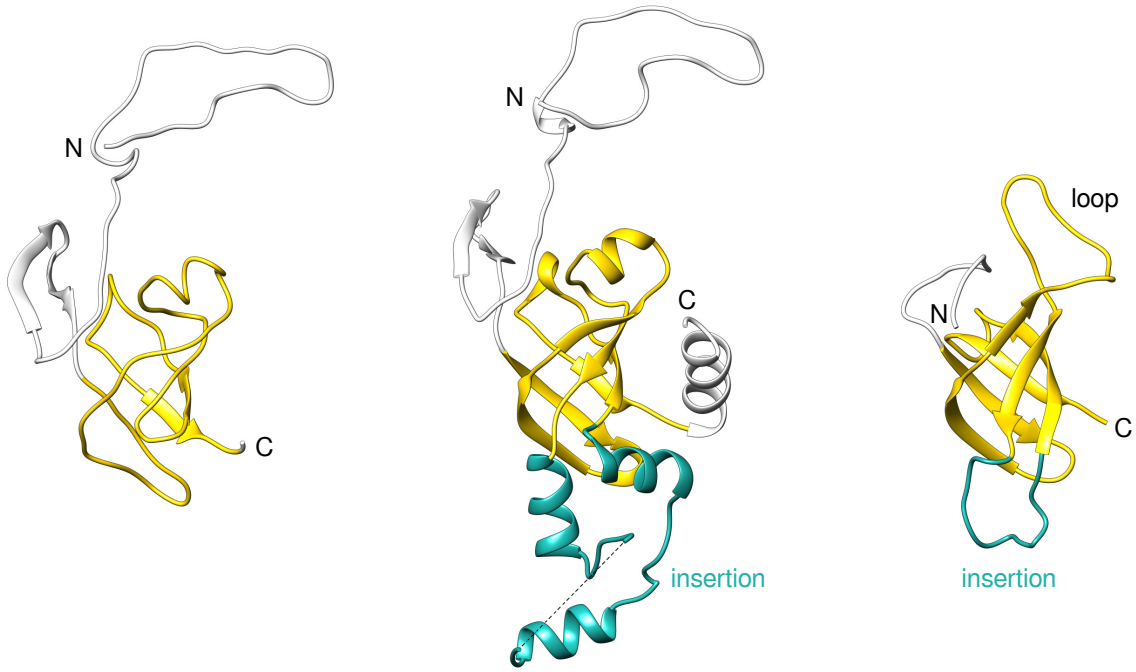

Figure 2.11: The C-domain of Nsa2 forms the S8E family β-barrel The NMR structure of the ctNsa2 C-domain (PDB code: 2MVF) is depicted side by side to full-length Rps8e from the archaeon *Pyrococcus furiosus* (PDB code: 4V6U) and full-length Rps8A from the eukaryote *Saccharomyces cerevisiae* (PDB code: 4U4R). loop = unstructured β-barrel insertion in ctNsa2. Yellow = β-barrel. Cyan = eukaryotic insertions. N- and C-termini are indicated by N and C, respectively.

Dr. Afua Nyarko was able to solve the structure by NMR with support from Dr. Woonghee Lee (National Magnetic Resonance Facility at Madison, University of Wisconsin Madison) and the results are shown in Figure 2.11. The C-domain consists of six β-strands, which form a small β-barrel. The barrel contains two prominent insertions between β-strands, which are labeled 'loop' and 'insertion' in Figure 2.11. These are about ~15 amino acids long and appear to be flexible in solution.

This fold is nearly identical to the β-barrel of Rps8, which is a ribosomal protein of the small subunit. Rps8 is conserved from archaea to eukaryotes and the structure of Rps8 is known from published structures of archaeal and eukaryotic ribosomes (PDB codes: 4V6U and 4U4R). Figure 2.11 shows, that the β-barrel of Rps8 is conserved from archaea to eukaryotes and that the C-domain of Nsa2 assumes a highly similar fold, which only differs in two insertions in the β-barrel (referred to as 'loop' and 'insertion' above). The loop forms an α-helical turn in both Rps8 homologs, but is unstructured in Nsa2, whereas the second insertion is present only in eukaryotic Rps8 and Nsa2, but

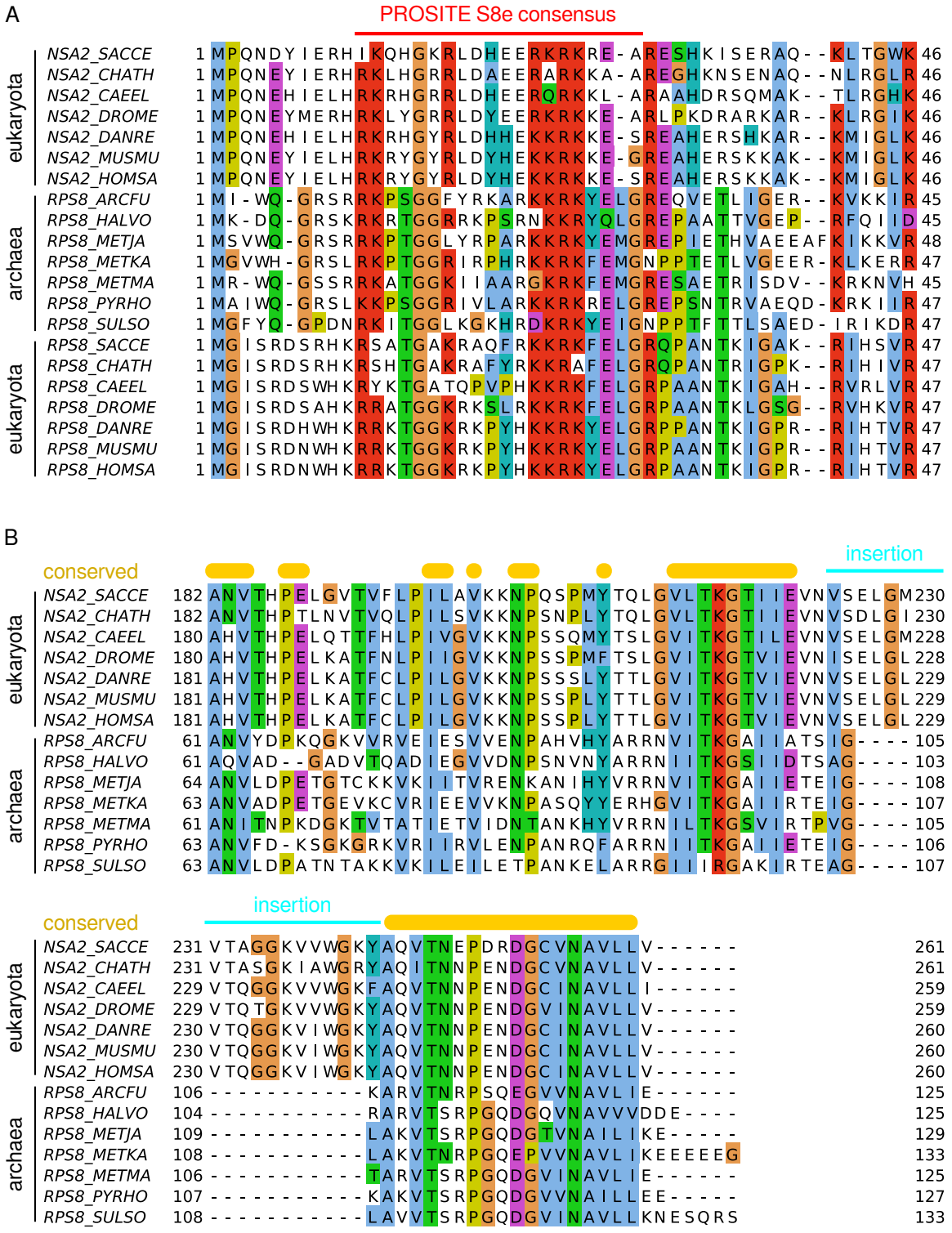

Figure 2.12: Sequence alignment of defining features of the S8e family A) Basic stretch in the N-domain of S8e family members, according to Engemann et al. 1995. B) The C-domain of Nsa2 displays sequence similarity to archaeal Rps8. It forms a β-barrel (see Figure 2.11), which contains an insertion in Nsa2, indicated in cyan. Yellow bars = conserved sequences. SACCE = *Saccharomyces cerevisiae*, CHATH = *Chaetomium thermophilum*, CAEEL = *Caenorhabditis elegans*, DROME = *Drosophila melanogaster*, DANRE = *Danio rerio*, MUSMU = *Mus musculus*, HOMSA = *Homo sapiens*, ARCFU = *Archaeoglobus fulgidus*, HALVO = *Haloferax volcanii*, METJA = *Methanocaldococcus jannaschii*, METKA = *Methanopyrus kandleri*, METMA = *Methanosarcina mazei*, PYRHO = *Pyrococcus horikoshii*, SULSO = *Sulfolobus solfataricus*.

does not contain any sequence similarity between the two (appendix Figure A.6).

It has been mentioned previously, that Nsa2 is part of the S8e superfamily of proteins, which is named after the ribosomal protein Rps8 (Lebreton et al. 2006; H. Zhang et al. 2010). This family contains archaeal and eukaryotic homologs of Rps8 as well as Nsa2, which is only present in eukaryotes (appendix Figure A.5). Family members were grouped based on a consensus sequence in the N-domain, which is located at a similar distance from the start codon (Engemann et al. 1995 and PROSITE entry PDOC00918). The consensus sequence has been defined as '[KR]-x(2)-[ST]-G-[GAR]-x(5,6)-[KRHSA]-x-[KRT]-x-[KR]-x-[EA]-[LIMPA]-G' and a multiple sequence alignment consequently shows this stretch in the N-domain of archaeal and eukaryotic homologs of Rps8 (Figure 2.12A and appendix Figure A.5). Interestingly, Nsa2 homologs do not possess the full consensus sequence, but share a stretch of basic amino acids with Rps8, that is part of the consensus sequence and is located at a similar distance from the start codon. Furthermore, the NMR structure of the Nsa2 N-domain and the structures of Rps8 homologs demonstrate, that there is no structural similarity between the N-domains of Nsa2 and Rps8 (Figure 2.10 and Figure 2.11). This raises the question, of how Nsa2 was grouped with Rps8 in the S8e family, as it is not evident from the PROSITE documentation.

Nevertheless, the NMR structure of the β-barrel argues for a similarity between the C-domains of Nsa2 and Rps8, as the fold is nearly identical in both proteins (Figure 2.11). Additionally, I discovered, that the Nsa2 β-barrel shares significant sequence similarity with archaeal, but not eukaryotic, homologs of Rps8 (Figure 2.12B and appendix Figure A.6). Therefore, these findings suggest, that Nsa2 and Rps8 indeed belong to a protein family and that *NSA2* might have originated from a duplicated *RPS8*-gene in evolution (see discussion section 3.5).

2.4 Localization of Nsa2 and Rsa4 on the pre-ribosome

The structural analysis of Nsa2 revealed, that it consists of an α-helical N-domain, which appears highly flexible and similar to α-helical extensions of r-proteins, as well as a globular C-domain, which is similar to Rps8. As both domains share similarity with r-proteins and contain many basic amino acids (appendix Figure A.7), it is possible, that both engage in rRNA interactions, possibly on separate regions of the pre-ribosome. These interactions might be direct targets of the Rea1 power-stroke and it is therefore important, to identify the position of Nsa2 and Rsa4 on the pre-ribosome. Therefore, I intended to identify the Nsa2 domains and the Nsa2-Rsa4 heterodimer in a cryo-electron

microscopy reconstruction of the Arx1-particle, which represents a nucleoplasmic step in 60S biogenesis (Bradatsch et al. 2012). The Arx1-particle is suitable for analysis, because it contains both Nsa2 and Rsa4 (Bradatsch et al. 2012). The resolution of the reconstruction is 11.9 Å, which allowed the identification of Arx1 at the exit tunnel and additional densities, that were attributed to biogenesis factors (EMDB code 5513). By looking at the electron density map, I could identify an unallocated density, that closely resembles a β-propeller. This density likely represents Rsa4, because Rsa4 is the only β-propeller-containing protein on the Arx1-particle. Therefore, Rsa4 is located at the right shoulder of the maturing 60S, between the central protuberance and the Rpl12 (uL11) stalk (Figure 2.13). This was later confirmed by Leidig and coworkers, who refined the reconstruction of the Arx1-particle to 8.7 Å, and assigned a computer model of Rsa4 to the mentioned location (Leidig et al. 2014, EMDB code 2528, PDB code 4V7F).

2.4.1 Nsa2 and Rsa4 associate with the maturing A-site on the Arx1-particle

When the cryo-EM density of the refined Arx1-particle became available, I used it to fit the crystal structure of the Rsa4 β-propeller with the bound Nsa2 peptide to the P stalk region of the pre-ribosome (Figure 2.13A,B). The fit structure aligns perfectly with the EM volume, including the α-helix at the bottom side of the β-propeller. Next, I looked for traces of Nsa2 in the EM volume. Interestingly, I could identify extra electron density at the top of the Rsa4 β-propeller, where Nsa2 is bound in the crystal structure. This density corresponds perfectly to the Nsa2 peptide, as it follows its shape and shares the same break-off points with the N- and C-termini of the resolved peptide (Figure 2.13B). Therefore, the Nsa2 peptide is located away from the solvent side and points towards the rRNA at the right shoulder and the maturing A-site of the pre-ribosome (Figure 2.13A).

Because Leidig and co-workers had already modeled most of the Arx1-particle and could fit many assembly factors, the neighborhood of Rsa4 and Nsa2 has been well characterized. Rsa4 is located between the immature central protuberance, which is defined by a reversed position of the 5S RNP that is bound facing the L1 stalk. Here, Rsa4 contacts Rpl5 (uL18) on one side of its β-propeller and Rpl12 (uL11) on the other (Figure 2.13A,B). To address the importance of additional contacts of Rsa4 on the pre-ribosome, I generated mutations based on the fit of the β-propeller. To disrupt the interaction with Rpl5 (uL18), I used the K130E/R134E and T175R/T177R double mutations and towards Rpl12 (uL11), the S275H/T278H double mutation. When checked for complementation, only the two mutations towards Rpl5 (uL18) failed to support growth of the *RSA4* shuffle strain (Figure 2.8C and data not shown). Tandem affinity purifications

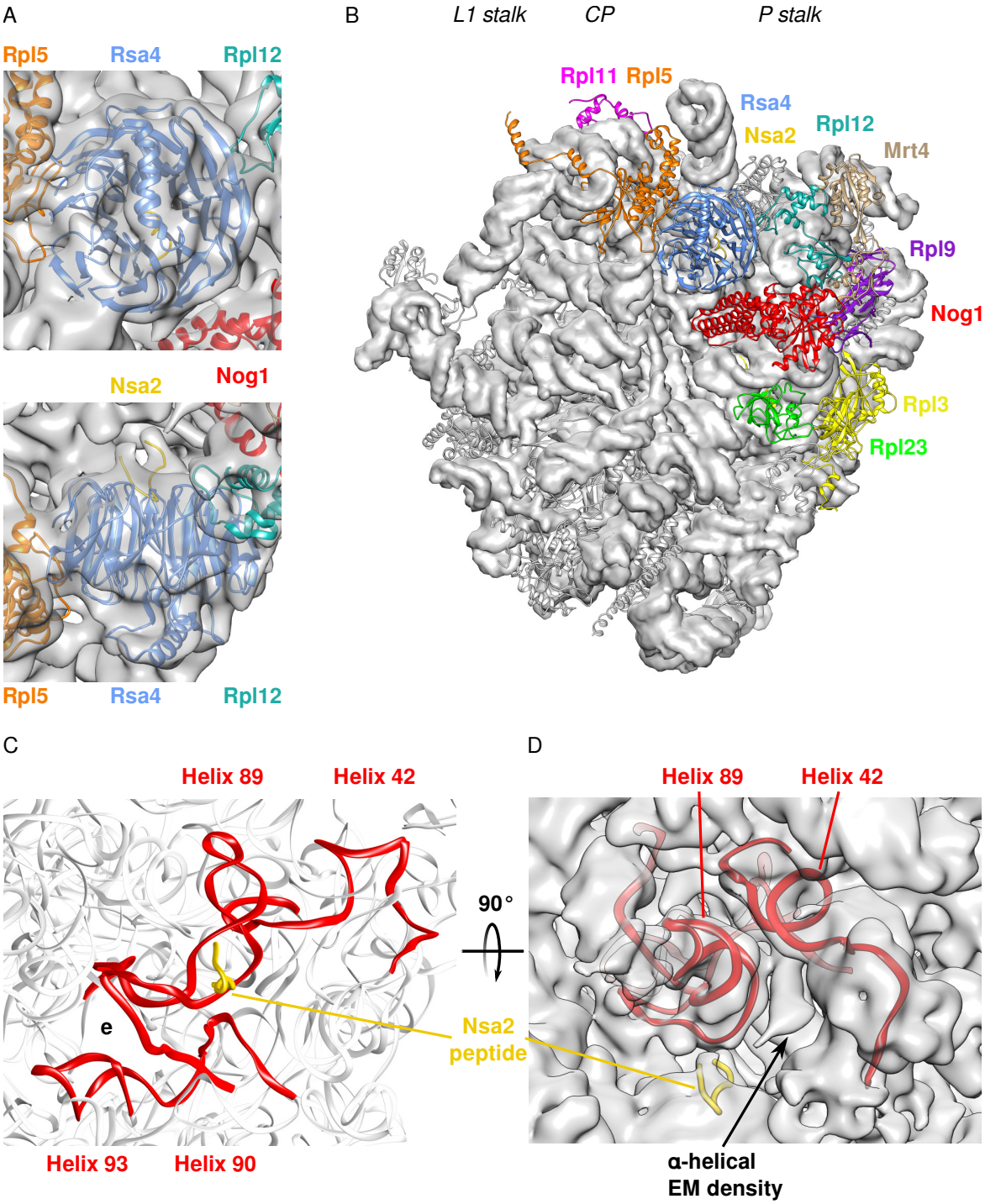

Figure 2.13: Location of Nsa2 and Rsa4 on the Arx1-particle A) Fit of the Nsa2-Rsa4 crystal structure into the electron density of the Arx1-particle. Upper panel: The β-propeller of Rsa4 fits in an electron density next to Rpl5 (uL18) and Rpl12 (uL11). The α-helical insertion is resolved in the EM density. Lower panel: The Nsa2 peptide is located at the same position in the Nsa2-Rsa4 crystal structure and the EM density. The adjacent regions of the peptide are not resolved in the EM density and appear therefore to be flexible. EMDB code: 2528. B) Overview of the neighborhood of Nsa2 and Rsa4 on the Arx1-particle. PDB code: 4V7F. CP = central protuberance. Nsa2 is located next to Nog1, Rpl12 (uL11), and Mrt4. C) CRAC hits of Nsa2 mapped to rRNA of the Arx1-particle. Nsa2 crosslinks to the maturing A-site and parts of the P stalk rRNA. e = exit tunnel. D) Location of the unmapped EM density, which presumably represents an α-helix and is located between Nsa2 CRAC hits.

revealed, that these mutations are still associated with the pre-ribosomes, in similar amounts to the wild type protein (Figure 2.9B), which highlights that Rsa4 association likely depends on multiple binding partners (see discussion section 3.1).

The Nsa2 peptide is oriented towards the pre-ribosomal surface, but because the electron density is not continuous at the N- and C-terminal ends of the peptide, I could not identify the rest of the protein and therefore its binding partners on the pre-ribosome. Nevertheless, the Nsa2 peptide is located in the vicinity of Nog1, Rpl12 (uL11), and Mrt4. To identify the exact binding site of Nsa2 on the pre-ribosome, Dr. Sander Granneman (Centre for Synthetic and Systems Biology, University of Edinburgh) performed crosslinking and analysis of cDNA (CRAC). This method identifies RNA sequences that are bound by a bait-protein and can therefore be crosslinked to the bait. The results are shown in Figure 2.13 and have been published in collaboration with Dr. Granneman in Baßler et al. 2014. Nsa2 crosslinks with four helices of the 25S rRNA, helix 89, helix 90 and helix 93 of the peptidyl transferase center and helix 42 of the P stalk (Figure 2.13C and Baßler et al. 2014). These rRNA elements are concentrated at the maturing A-site of the peptidyl transferase center. (Figure 2.13C). This is consistent with the fit of the crystal structure in the EM volume of the Arx1-particle (see above). The CRAC results demonstrate, that Nsa2 extends from the peptidyl transferase center to the P stalk, but do not reveal the orientation of the N- and C-terminal domains.

With the CRAC data available, I intended to identify the location of individual Nsa2 domains in the EM volume. Therefore, I checked for unassigned densities next to the CRAC hits in the electron microscopy volume of the Arx1-particle. I identified a density in the shape of an α-helix, in close proximity to helix 89 (Figure 2.13D). This density projects from the Nsa2 peptide at the Rsa4 β-propeller towards helix 42, which had been identified as a CRAC hit for Nsa2 (Figure 2.13C). Therefore, I hypothesized, that this density corresponds to the α-helical N-domain of Nsa2, which would put the N-domain next to the P stalk and helix 89 and the C-domain to the maturing A-site. Unfortunately, I could not identify a convincing fit for the C-domain at the A-site, because the resolution of the EM-volume was too low to identify individual β-strands. Nevertheless it appears, that the N- and C-domain of Nsa2 are located at separate locations on the pre-ribosome, which indicates, that Rea1 could act both on the maturing A-site and P stalk rRNA through individual domains of Nsa2 (see discussion section 3.1 and section 3.2).

2.5 Nsa2 associates with pre-ribosomes via the N-domain

Because Nsa2 is bound to both the maturing A-site and the P stalk, I intended to find out how Nsa2 recognizes and is recruited to the pre-ribosome. It has been demonstrated, that Nsa2 is present on early pre-60S particles, that are purified by the biogenesis factor Ssf1 (Ulbrich et al. 2009). To understand the composition of the earliest Nsa2 particle, I performed split tandem affinity purifications. I purified Ssf1 for the first step, followed by Nsa2 as the second. This purified the Nsa2-fraction of the Ssf1-particles. For comparison I used the unbound fraction of the Nsa2-step and a standard Ssf1 purification (Figure 2.14A). The results show, that some biogenesis factors are split between the fractions, very early 60S biogenesis factors like Rrp5, Noc1, and Urb1 do not purify with Nsa2, whereas Dbp10 is found exclusively on the Nsa2 fraction. These results suggest, that Nsa2 is not present on the earliest pre-60S particles, but joins after further maturation steps have occurred.

It has been suggested that the recruitment of Nsa2 depends on the GTPase Nog1 and the helicase Dbp10, but the molecular details of how Nsa2 initially interacts with the pre-ribosome are unknown (Lebreton et al. 2006; Talkish et al. 2012). Nsa2 binds to rRNA directly next to Nog1, as demonstrated by cryo-EM and the CRAC analysis (subsection 2.4.1). Because I hypothesized, that the N-domain of Nsa2 is located at the P stalk rRNA, next to Nog1 (see above), I sought to understand the contribution of the N-domain in the recruitment of Nsa2 to the pre-ribosome. I used the NMR structures of the N-domain and a multiple sequence alignment to define truncation mutants (Figure 2.10 and appendix Figure A.7). For this, I removed the α-helices of the N-domain one by one to generate the Nsa2$^{\Delta 14}$, Nsa2$^{\Delta 34}$, and Nsa2$^{\Delta 59}$ mutants (see appendix Figure A.7). In addition to the Nsa2$^{\Delta 59}$ mutant, I also removed the unconserved linker between the N-domain and the Rsa4-binding motif to create the Nsa2$^{\Delta 84}$ mutant. For comparison, I created the Nsa2$^{1\text{-}14}$, Nsa2$^{1\text{-}34}$, Nsa2$^{1\text{-}59}$, and Nsa2$^{1\text{-}84}$ fragments, as well as the full N-domain together with the Rsa4 binding motif (Nsa2$^{1\text{-}98}$). The *in vivo* analysis of these truncations is feasible, as they can enter the nucleus by passive diffusion (in the case, that no importin recognizes them) and additionally it has been demonstrated, that N-terminal truncations as well as N-terminal fragments of human Nsa2 still enter the nucleus in HeLa cells (H. Zhang et al. 2010).

When checked for complementation, all truncation mutants failed to support growth of the *NSA2* shuffle strain in the absence of wild type *NSA2* (Figure 2.14B). The Nsa2$^{1\text{-}59}$ and Nsa2$^{1\text{-}84}$ mutants displayed a dominant negative growth effect under these conditions

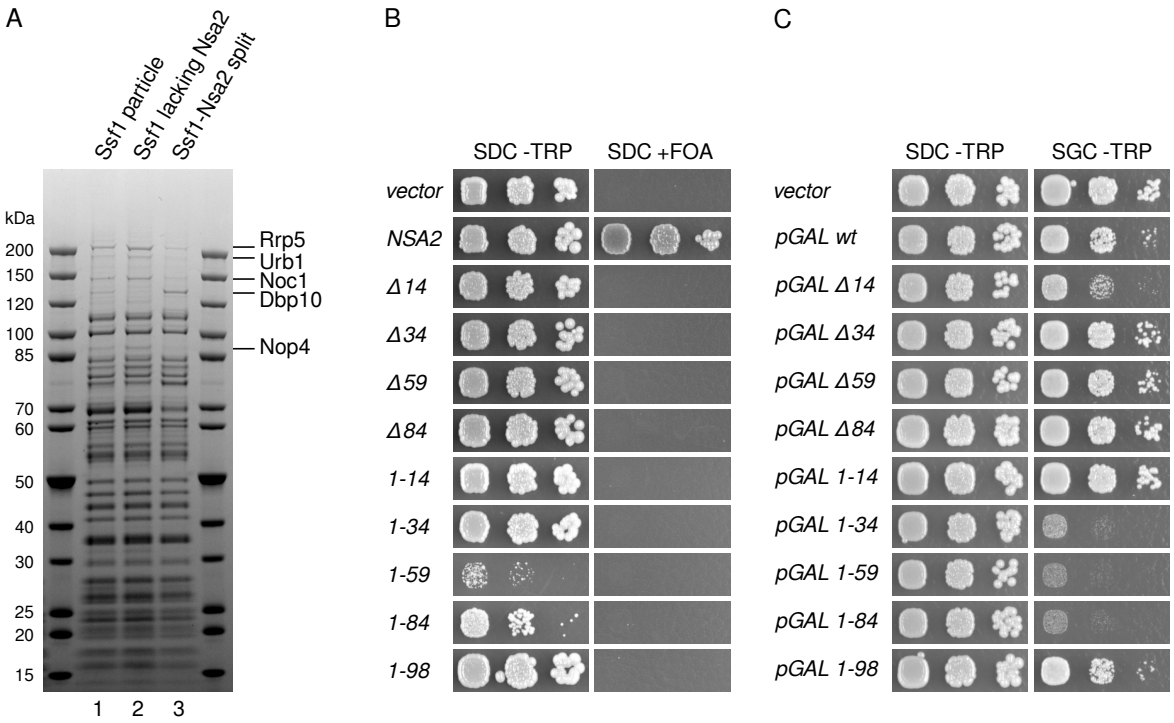

Figure 2.14: Nsa2 association to Ssf1-particles and truncation analysis of the N-domain A) TAP of a *SSF1-TAP NSA2-Flag* strain reveals that Nsa2 is associated with a subpopulation of Ssf1-particles. Normal TAP of Ssf1 is compared to a Ssf1 particle depleted for Nsa2 and a Ssf1-Nsa2 split purification. This reveals, that Nsa2 does not associate with early 60S factors, like Rrp5, Urb1, and Noc1. B) N-terminal truncations of Nsa2 are inviable. A *NSA2* shuffle strain was transformed with plasmids expressing indicated Nsa2 variants under control of the endogenous *NSA2* promoter. Transformants were spotted on 5-FOA containing plates and grown for three days at 30 °C . C) N-terminal fragments of Nsa2 and the Δ14 truncation are dominant negative. A wild type yeast strain was transformed with plasmids expressing indicated Nsa2 variants under control of the inducible *GAL1-10* promoter. Transformants were spotted on plates containing galactose and grown for three days at 30 °C .

(expressed on a single copy plasmid from the endogenous *NSA2* promoter). Additionally, when overexpressed under control of the inducible *GAL1-10*-promoter, the Nsa2$^{1\text{-}34}$, Nsa2$^{1\text{-}59}$, and Nsa2$^{1\text{-}84}$ mutants display a strong dominant negative phenotype, whereas the Nsa2$^{\Delta 14}$ mutant displays a weak dominant negative phenotype. Surprisingly, the Nsa2$^{1\text{-}98}$ mutant, which includes the Rsa4 binding motif, rescues the dominant negative effect of shorter fragments (Figure 2.14C).

To understand which fragments of Nsa2 can still interact with pre-ribosomes, I performed a sedimentation analysis. I prepared lysates of cells expressing HA-tagged variants of the truncation mutants and loaded them onto sucrose gradients followed by a spin in the ultracentrifuge. Afterwards, the gradients were fractionated and the fractions were analyzed by Western blotting (Figure 2.15A,B). Antibodies against Rpl35 (uL29) and Rpl3 (uL3) were used to identify fractions that contain polysomes and free 60S

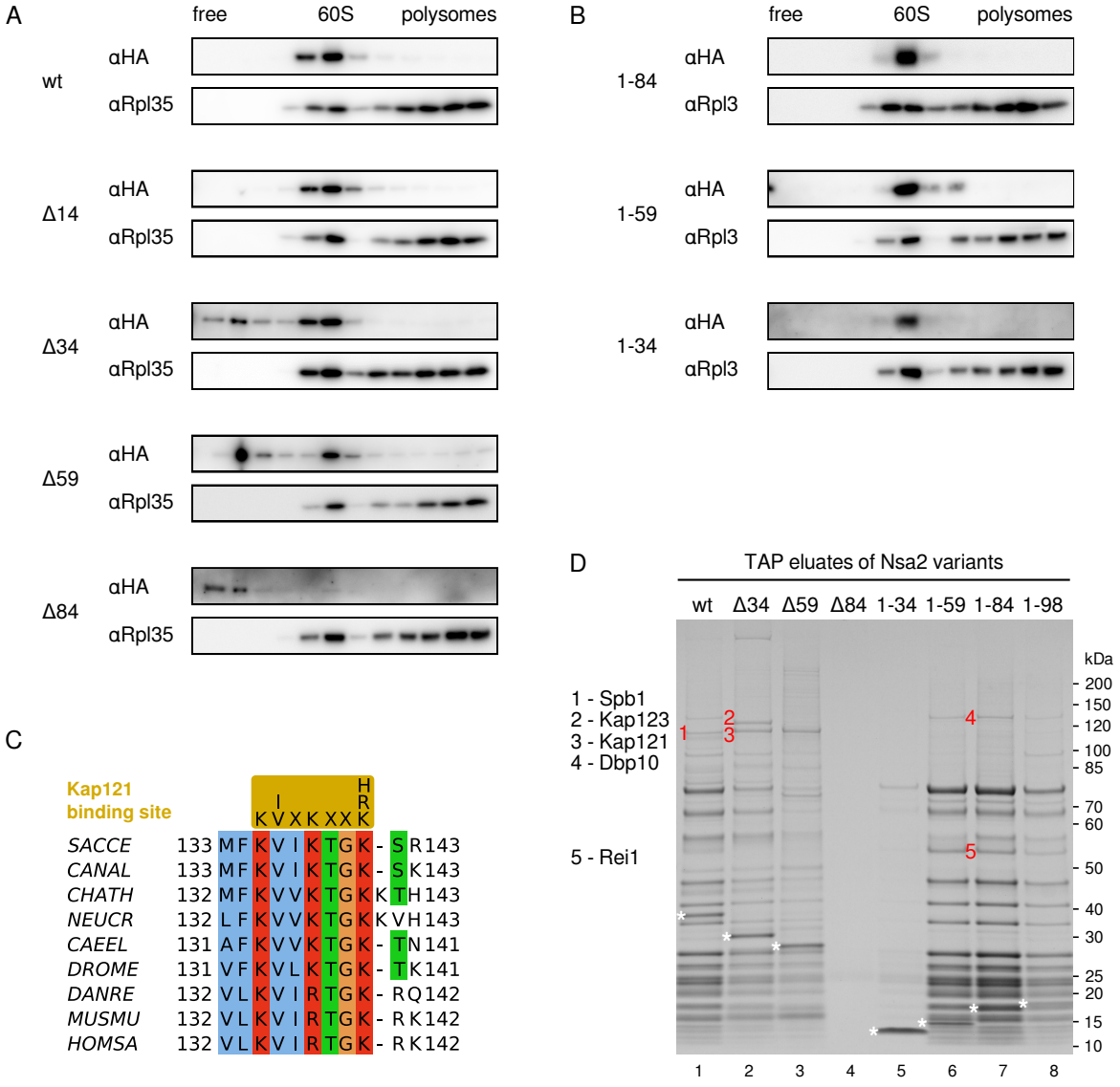

Figure 2.15: Pre-ribosome association of Nsa2 depends on its N-domain A) Gradient analysis of N-terminal truncations of Nsa2. HA-tagged variants of Nsa2 were expressed in wild type yeast cells and lysate was analyzed by high-speed centrifugation on sucrose gradients. Gradient fractions were analyzed by Western blotting, αRpl35 antibody was used as a marker for large subunits. B) N-terminal fragments of Nsa2 migrate with large ribosomal subunits. HA-tagged variants of Nsa2 were expressed in wild type yeast cells and lysate was analyzed by high-speed centrifugation on sucrose gradients. Gradient fractions were analyzed by Western blotting, αRpl3 antibody was used as a marker for large subunits. C) Nsa2 contains a conserved consensus sequence for Kap121 association, according to Kobayashi and Matsuura 2013. SACCE = *Saccharomyces cerevisiae*, CANAL = *Candida albicans*, CHATH = *Chaetomium thermophilum*, NEUCR = *Neurospore crassa*, CAEEL = *Caenorhabditis elegans*, DROME = *Drosophila melanogaster*, DANRE = *Danio rerio*, MUSMU = *Mus musculus*, HOMSA = *Homo sapiens*. D) TAP of Nsa2 N-terminal truncations and fragments. A wild type yeast strain was transformed with plasmids expressing FTpA-tagged variants of Nsa2 from the endogenous *NSA2* promoter. N-terminal truncations display a reduced pre-ribosome association, which coincides with the presence of Kap121 and Kap123. N-terminal fragments purify late 60S pre-ribosomes, which are characterized by the presence of Rei1. Individual bait proteins are indicated by an asterisk. Bands indicated by numbers were analyzed by mass spectrometry.

subunits. The results show, that wild type Nsa2 is exclusively associated with particles resembling the large ribosomal subunit. Removing the first α-helix does not change this association pattern, but with the removal of the second α-helix (Nsa2$^{\Delta 34}$), a free pool of Nsa2 appears, that is not associated with the larger molecular weight fractions. This pattern persists for the longer truncations (Nsa2$^{\Delta 59}$ and Nsa2$^{\Delta 84}$), where only a small amount of the Nsa2$^{\Delta 84}$ mutant migrates with larger molecular weights (Figure 2.15A).

Because the ribosome association is lost, when the N-terminal α-helices of Nsa2 are missing, I wanted to understand if the N-terminal domain is sufficient for targeting. Therefore, I checked the sedimentation pattern of the Nsa2$^{1\text{-}34}$, Nsa2$^{1\text{-}59}$, and Nsa2$^{1\text{-}84}$ fragments (Figure 2.15B). The results show, that all three fragments are found in a fraction resembling large ribosomal subunits, and no free pool can be observed. The binding appears to be specific to large ribosomal subunits, as the bulk of the protein is found in one fraction and does not extend to fractions of the small ribosomal subunit.

In order to understand, if the Nsa2 fragments associate with mature or pre-ribosomes, I performed tandem affinity purifications. The results demonstrate, that the N-terminal fragments purify stoichiometric pre-ribosomes, which are highly similar to the wild type purification (Figure 2.15D). These particles show characteristics of late biogenesis steps, as earlier factors are reduced, compared to the wild type, and additionally they contain stoichiometric amounts of Rei1, which is associated with late biogenesis steps (Figure 2.15D). The N-terminal truncations, on the other hand, display a reduced association with pre-ribosomes and contain additional bands in the higher molecular range, which were identified by mass spectrometry as Kap121 and Kap123. Interestingly, subsequent *in silico* analysis revealed a Kap121 binding site in Nsa2, which suggests that Kap121 is the importin for Nsa2 (Figure 2.15C).

In summary, the N-domain appears to be highly important for the recruitment of Nsa2 to pre-ribosomes and the data indicates, that it can associate even independently from the C-domain.

3 Discussion

The rearrangement of pre-ribosomes by the ATPase Rea1 is a major step in 60S biogenesis, that has been studied from the side of Rea1 and its adapter Rsa4, but knowledge about the targets of Rea1 activity on the pre-ribosome is still incomplete. Rea1 is thought to apply a pulling force on its adapter protein Rsa4, that is transmitted to the pre-ribosome through Rsa4 associated factors, which include the assembly factor Nsa2.

This study provides evidence for the functional relevance of the Rsa4-Nsa2 interaction, which is involved in Rea1 mediated remodeling steps. Moreover, the localization of the Rsa4-Nsa2 crystal structure on the pre-ribosome unraveled the functional neighborhood of Rea1 and target sites of Rea1 action. Nsa2 binds to rRNA at the maturing A-site and it is therefore intimately bound to rRNA and appears to be the final link in the Rea1-Rsa4-Nsa2 chain, which has the potential to rearrange rRNA elements during Rea1 ATP hydrolysis. Furthermore, analysis of Nsa2 truncation mutants highlights an important role of the Nsa2 N-domain in the recruitment of Nsa2 to the pre-ribosome, which emphasizes the precise requirements for the assembly of ribosome biogenesis factors. Nsa2 represents a highly specialized RNA binding protein, that has originated in evolution from archaeal ribosomal protein S8, which highlights one strategy of how the eukaryotic translation machinery acquired its complexity.

3.1 The role of Nsa2 in Rea1 function

Nsa2 is likely affected by late steps in 60S maturation, that include the action of Rea1, as the neighborhood of Nsa2, which includes the central protuberance, the peptidyl transferase center, and the P stalk, undergoes large rearrangements at the transition from nuclear to early cytoplasmic pre-ribosomes (Barrio-Garcia et al. 2016; Leidig et al. 2014; Wu, Tutuncuoglu, et al. 2016). Nsa2 is present on pre-ribosomes before and after the Rea1 power stroke, which raises the question of how it is rearranged by Rea1 and how it could transmit the pulling force of Rea1 to the pre-ribosome.

On pre-Rea1 particles, which are represented by the Arx1-particle and a recent high-resolution structure of the Nog2-particle, Nsa2 is bound to rRNA at the A-site and the P stalk and contacts assembly factors, Rsa4, Rrs1, Nog2, Nog1, Mrt4, and ribosomal protein Rpl9 (uL6) (Figure 3.1A,B). On these particles, the 5S RNP with Rpl5 (uL18) and Rpl11 (uL5) is associated in an immature state, which forms the initial binding surface for Rsa4. Bound Rsa4 contacts Rpl5, Rrs1, Rpf2, Nog2, and Nsa2, and the Nsa2 Y90A mutant demonstrates, that Rsa4 recruitment does not depend on the interaction of the Nsa2 peptide with the pore of the Rsa4 β-propeller (Figure 2.7C). Instead, Rsa4 recruitment most likely depends on the interaction with Rpl5 (uL18), Rrs1, Rpf2, Nog2, and potentially a second binding site on Nsa2, that is formed by an essential loop insertion in the Nsa2 β-barrel (Figure 3.1A and appendix Figure A.8A). Therefore, it is possible, that the Nsa2-Rsa4 interaction at the pore of the β-propeller is necessary for a subsequent maturation step, which likely involves the Rea1 power stroke. Interestingly, this interaction appears to be regulated in human homologs of Nsa2 by phosphorylation at threonine 81, which highlights a possible relevance in cellular signaling (neXtProt identifier: NX_O95478, Gaudet et al. 2015).

It has been shown recently, that the association of Rea1 and the Rix1-complex induces large rearrangements on the pre-ribosome, that are demonstrated by the cryo-EM structure of the Rix1-particle (Barrio-Garcia et al. 2016). Here, the 5S RNP has been turned into its mature position, which involves the release of associated biogenesis factors Rrs1 and Rpf2. Therefore, the association of Nsa2 with Rrs1 is broken at this step (Contact I and II in Figure 3.1B,C). This implies, that it is important for earlier steps in 60S biogenesis, maybe for stabilizing immature rRNA helix 86, which is enclosed by Rrs1, Nsa2 and Rsa4 on the Nog2-particle, or by restricting the flexibility of Nsa2 and Rsa4 (Figure 3.1A,B and Leidig et al. 2014). The latter aspect is highlighted by the fact, that Rsa4 undergoes a drastic rearrangement upon Rea1 recruitment. It is moved and turned around a hinge point, that is formed by Nsa2. Therefore, Nsa2 has to permit these movements, which is illustrated by the presence of a linker region before the Rsa4

binding motif (appendix Figure A.8B). The linker is not resolved in the cryo-EM structures and the Nsa2-Rsa4 crystal structure, which implies that it is indeed flexible in solution. Additionally, the N-terminal domain of Nsa2 is not rearranged, after Rea1 recruitment, which suggests that it is stably associated and might form an anchor point for Rsa4 movement (Barrio-Garcia et al. 2016; Wu, Tutuncuoglu, et al. 2016). The turning of the 5S RNP and the release of Rrs1 and Rpf2, all three of which form a large portion of the Rsa4 binding surface, strongly affect the association of Rsa4 with the pre-ribosome. At this stage in maturation, the Rsa4-Nsa2 interaction might become relevant, as it can keep Rsa4 in place when the other binding sites are lost. Therefore, Rsa4 might be bound in a labile conformation in the Nsa2 Y90A mutant, that would be most pronounced after the initial association of Rea1 and the Rix1-complex. Therefore, the Nsa2-Rsa4 interaction could be necessary for the subsequent stable association of Rea1 to the pre-ribosome, as it has been demonstrated, that Rea1 recruitment depends on the interaction with Rsa4 (Barrio-Garcia et al. 2016). This hypothesis is supported by the Rpl25 pulse chase analysis of the Nsa2 Y90A mutant, as the Y90A mutant arrests 60S biogenesis before the association of Rea1 (Figure 2.7D).

On wild type pre-ribosomes, following Rea1 activation, force is applied to Nsa2 through Rsa4, which is transmitted to the N- and C-terminal domains of Nsa2, followed by the coordinated release of Rsa4 and Nog2. As a consequence, the Nsa2-Rsa4 interaction is disrupted, together with the contacts of Nog2, that include an interaction with Nog1 (III in Figure 3.1B,C). It is likely, that Nsa2 is rearranged upon such drastic changes to its binding region, but no structural data is available to prove this yet. The N-terminal domain of Nsa2 is a promising candidate for Rea1-induced rearrangement, as it forms one endpoint of the Rea1-Rsa4-Nsa2 axis. It contacts rRNA helix 89, which is stabilized in an immature conformation by Nsa2, Nog1, Nug1, and Nog2 and extends to helix 42 of domain II and helix 95+97 of domain VI (Figure 3.2B,C and PDB code: 3JCT). Therefore, Rea1 could contribute to maturation of these rRNA elements by removing Nog2 and potentially the Nsa2 N-domain. Alternatively, Rea1 could apply a pulling force on the N-domain, which could lead to structural rearrangements of helix 89 or the P stalk rRNA. Interestingly, the truncation analysis of the Nsa2 N-domain suggests, that Rea1 is indeed functionally linked to the N-domain, because the strong dominant negative growth effect of the Nsa2$^{1\text{-}84}$ fragment is rescued by the addition of the Rsa4 binding motif in the Nsa2$^{1\text{-}98}$ truncation (Figure 2.14C). This suggests, that Rea1 is directly involved in the release or rearrangement of the Nsa2 N-domain during biogenesis. Furthermore, on Nog2 particles, the Nsa2 N-domain contacts the GTPase domain of Nog1 and it is therefore possible, that Rea1 could induce Nog1 GTPase activity through Nsa2 (see subsection 3.2.2).

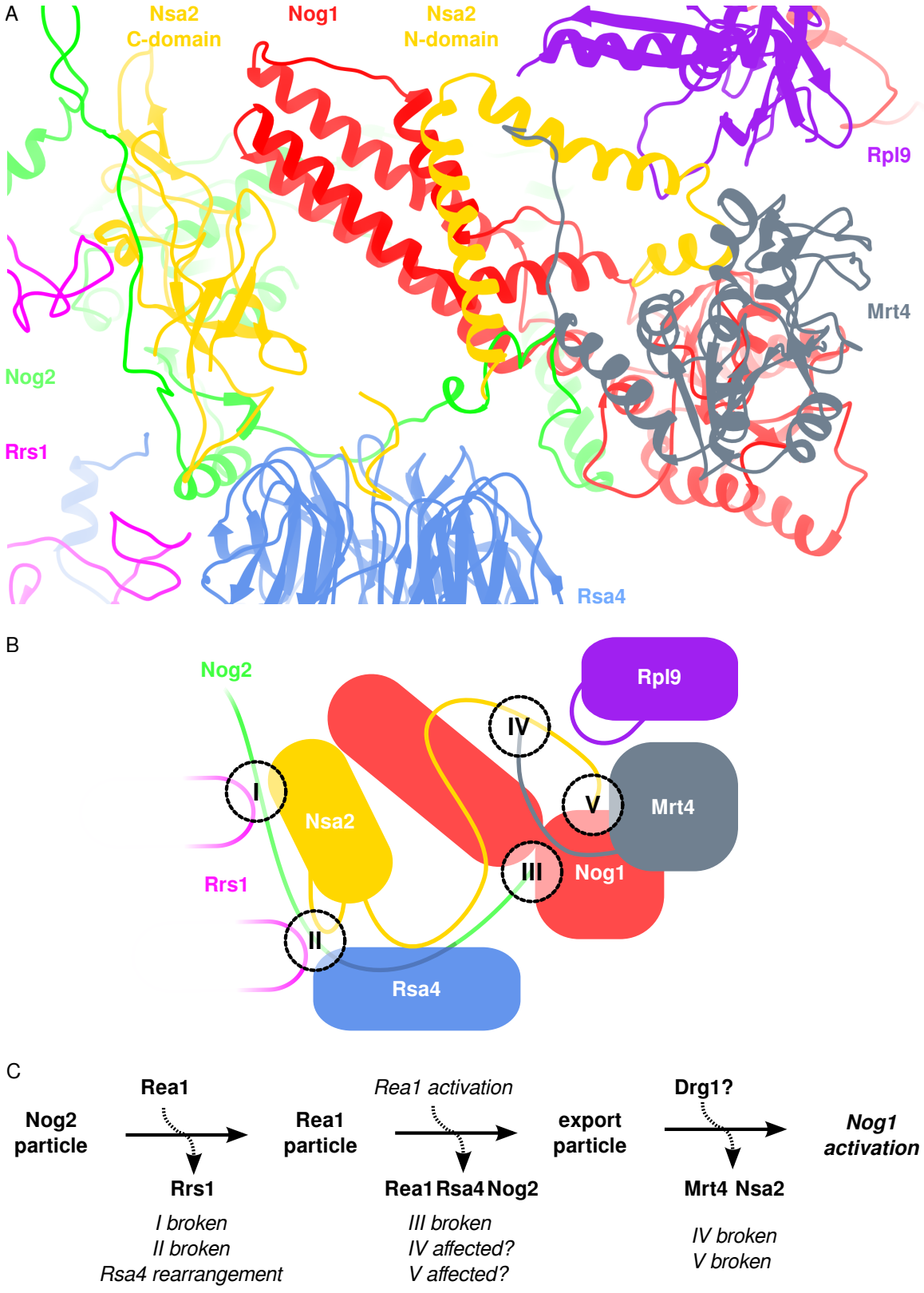

Figure 3.1: Assembly factor network of Nsa2 on late 60S pre-ribosomes A) Nsa2 contacts multiple assembly factors on the Nog2-particle (PDB code: 3JCT). B) Schematic of the Nsa2 contacts. I-V = Relevant interactions of the Nsa2 associated assembly factor network. C) Proposed sequence of maturation events related to Nsa2, starting from the Nog2-particle. The removal of Nsa2 releases the potential inhibition of Nog1 by the Nsa2 N-domain (V).

3.1.1 A counterforce model for Rea1 activation

Rea1 applies mechanical force on Rsa4, which redirects and splits it to its binding partners Nsa2 and Nog2, that in turn reach multiple locations on the pre-ribosome. These contacts might be involved in force transduction in both directions, which raises the possibility of Rea1 regulation by its assembly factor network. It is possible, that multiple structural signals converge to allow Rea1 activation by the means of providing a counterforce at correctly assembled rRNA structures (see below).

Rea1 is related to cytoplasmic dynein heavy chain and contains similar structural features. Dynein has a stalk insertion in its hexameric ring, which binds to microtubules and is necessary for its association and motility on microtubules (reviewed in A. P. Carter and Vale 2010). Similarly, Rea1 contacts the N-domain of Rsa4 with its ATPase-ring (Barrio-Garcia et al. 2016). Additionally, both proteins contain long linker regions, which connect to the ATPase domain ring. In dynein the linker connects to the N-terminus and in Rea1 to the C-terminus of the ATPase domains. Furthermore, dynein and Rea1 contain six ATPase domains in one protein chain, which has led to structural heterogeneity and therefore specialization of individual ATPase domains in evolution, compared to homo-hexameric ATPases, like Cdc48, or Drg1.

In dynein, ATPase domain I is considered the main force generating ATPase domain, which is regulated by ATP hydrolysis in ATPase domain III (Nicholas et al. 2015). It has been shown, that mechanical force, which is applied to the linker region, leads to an altered release pattern from microtubules, that depends on the ATP or ADP state of ATPase domain III (Nicholas et al. 2015). Therefore, the internal strain of the ATPase domain ring might be an important determinant for ATPase activity, as ATP hydrolysis depends on the correct conformation of two adjacent ATPase domains. In dynein, the linker is connected to cargo and to a second dynein, which together forms the processive dynein dimer. In Rea1, the linker loops back to its ATPase ring and binds to the N-domain of Rsa4. Thus, Rsa4 is bound two times by Rea1, which possibly creates a closed feedback loop, that depends on movement of Rsa4 (Barrio-Garcia et al. 2016; Ulbrich et al. 2009).

It is therefore possible, that Rea1 generates an initial mechanical force with one ATPase domain, which is transmitted through Rsa4 and could probe the Rsa4 connected assembly network. By such a mechanism, the individual interactions of Nsa2, Rsa4, Nog2 with their binding partners on the pre-ribosome (either rRNA or protein) will each deliver small counterforces, that are integrated through Rsa4 into one larger force, that is applied to Rea1. If this tension is too weak, which might be caused by unstable rRNA elements or loose or wrongly associated assembly factor domains, Rea1 will not

progress to ATP hydrolysis in the next ATPase domain. If the counterforce is strong enough, the tension in the Rea1 ATPase ring could gate ATPase hydrolysis in a second ATPase domain, which might subsequently facilitate the major Rea1 release step. This mechanism would directly tie Rea1 activation to probing of connected rRNA elements and ensure, that only correctly folded pre-ribosomes are matured by Rea1.

3.2 Additional functions of Nsa2 in 60S subunit assembly

3.2.1 rRNA domain stabilization by Nsa2

Nsa2 is associated with a range of pre-ribosomes, which implies, that it might be involved in multiple maturation steps. The most clear one to date is the involvement in the second Rea1 reaction step via Rsa4, which has been discussed in section 3.1. Apart from that, Nsa2 might stabilize rRNA domains during its association with the pre-ribosome, as it is bound to two separate location at its N- and C-domain, respectively. The N-domain is bound to helix 42 of domain II, helix 89 and 91 of domain V, as well as helix 95 and 97 of domain VI. The C-domain is located away from the N-domain and is bound to helix 39 of domain II and helix 86 and 89 of domain V (Figure 3.2A, Figure 3.3B and PDB code: 3JCT). Therefore, Nsa2 connects multiple rRNA domains, which are significantly rearranged during 60S formation (Barrio-Garcia et al. 2016; Leidig et al. 2014; Wu, Tutuncuoglu, et al. 2016). Interestingly, these regions are flexible on bacterial pre-ribosomes, as cryo-EM structures of stalled late pre-50S subunits display a loss of resolution and electron density at the central protuberance and the GTPase center (Jomaa et al. 2014; Li et al. 2013; X. Ni et al. 2016). As bacteria do not possess stabilizing biogenesis factors, like Nsa2, this phenotype highlights the inherent flexibility of this region, which cannot be resolved by cryo-EM. The flexibility of rRNA helices might be important for the folding of ribosomal RNA, which appears to possess the potential for self organization. As eukaryotic ribosome biogenesis involves significantly more assembly steps than bacterial ribosome formation, the stabilization of rRNA domains might have become relevant to prevent the mis- or disassembly of pre-ribosomes, which exist in a prolonged labile conformation during eukaryotic ribosome biogenesis. Therefore, eukaryotes have evolved assembly factors, including Nsa2, Cgr1, and Nog2, which, in addition to other functions, could stabilize the pre-ribosome in a compact arrangement and prevent the disassociation of rRNA domains II and V (Figure 3.2A).

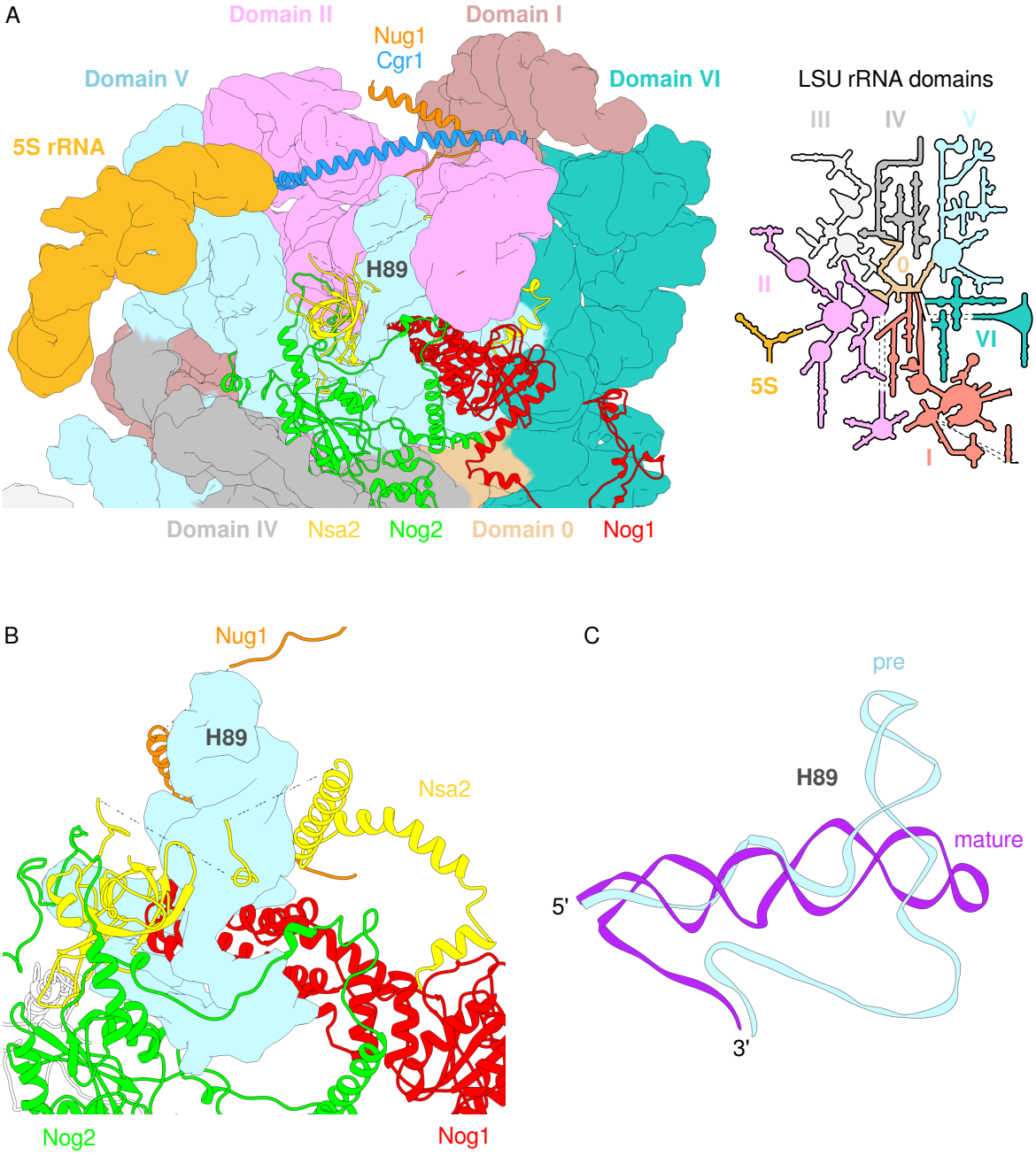

Figure 3.2: Nsa2 functions in rRNA domain stabilization and helix 89 maturation A) rRNA neighborhood of Nsa2 on the Nog2-particle. Nsa2 bridges rRNA domain II and V, potentially stabilizing them during maturation. Right side = Large subunit secondary structure diagram with colored rRNA domains. PDB code: 3JCT. B) Nsa2 is part of an assembly factor cage, that arrests helix 89 in an immature upward state. The Nsa2 β-barrel is wedged against one side of helix 89, whereas the middle domain wraps around helix 89 and is stabilized by the N-domain, which interacts with rRNA domain II. C) Comparison of helix 89 in the immature and mature state. The 5' and 3' ends of the immature state converge into the mature conformation, which indicates, that helix 89 is most likely rearranged locally.

3.2.2 The role of Nsa2 in helix 89 maturation

Another important function of Nsa2 is suggested by its contacts to helix 89 on the pre-ribosome. Nsa2 is part of a protein-cage that is formed around helix 89, together with assembly factors Nog1, Nog2, and Nug1 (Figure 3.2B). This state is characterized by an upward arrangement of helix 89, that is prevented from assuming its mature position by Nog1 and stabilized on all sides by Nsa2, Nug1, and Nog2 (Figure 3.2B,C). This suggests, that helix 89 can likely assume its mature position on its own, similarly as in bacterial ribosome biogenesis, and that the cage has evolved to prevent this from happening too early in 60S biogenesis. An explanation for this is, that mature helix 89 is important for tRNA binding at the A-site, which has to be prevented in pre-ribosomes, as it could block further maturation steps and lead to stalled intermediates. This is relevant, because nuclear pre-tRNAs should be competent to bind to 60S subunits, as the CCA-tail, which is important for ribosome association, is added in the nucleus (reviewed in Graifer and Karpova 2015; Hopper 2013). Therefore, in eukaryotes helix 89 is arrested in an immature conformation during 60S biogenesis, which most likely is not able to bind to tRNAs (Figure 3.2B,C).

Active rearrangement of helix 89 appears to be blocked by Nog1, which pierces through the base of helix 89 with its N-domain, therefore preventing movement to the mature position (Figure 3.2B,C). Nevertheless, it is possible, that the Rea1 power stroke, via Nsa2, could induce rearrangements of the helix 89 tip, which might be a requirement for further maturation. Additionally, Rea1 could liberate the Nsa2 N-domain, which would remove one restriction of helix 89 movement (see section 3.1). As the cage is sequentially disassembled during 60S biogenesis, with Nog1 being the last assembly factor to leave, helix 89 likely assumes its final conformation after Nog1 has been released. Therefore, it is highly interesting that the Nsa2 N-domain contacts Nog1 at its GTPase domain, which implies, that Nsa2 could regulate Nog1 GTP hydrolysis (V in Figure 3.1B,C). The Nsa2 N-domain contacts Nog1 at two distinct sites, which together enclose and arrest the switch I region of the Nog1 GTPase domain (appendix Figure A.9). The switch I region is important for GTPase activity, as it moves during hydrolysis. It is also known as 'effector loop' of GTPases and is often bound by proteins in the GTP-bound state (the 'ON' state). Indeed, Nog1 contains GTP in its active center, which is evident from the structure of the Nog2 pre-ribosome. The interaction with Nsa2 therefore likely prevents GTP hydrolysis by restricting the flexibility of the switch I region. The importance of this possible regulation is highlighted by the Nsa2$^{\Delta 14}$ mutant, which is lacking the N-terminal 14 amino acids, that are contacting Nog1. This mutant is able to assemble into pre-ribosomes like the wild type, but is unable to support growth in the absence of the wild type protein

(Figure 2.14B and Figure 2.15A).

Nog1 activation appears to be an important checkpoint in 60S assembly, as the GTPase domain is contacted by a second biogenesis factor, Nog2, which binds closely to the switch II region of Nog1, that also undergoes structural rearrangement during GTP hydrolysis (appendix Figure A.9). Therefore, Nsa2 and Nog2 cooperate to form an inhibitory clamp at the GTPase domain of Nog1, which appears to inhibit essential movements of the switch regions and which generally arrests the GTPase domain in relation to the N-domain. I therefore propose, that the final function of Nsa2 in 60S maturation is to release an inhibition on the Nog1 GTPase domain, which comes to pass, when Nsa2 is removed from the 60S pre-ribosome, or alternatively, when the N-domain is released and moved away from Nog1 (Figure 3.1C). Additionally, the removal of Nsa2 might involve a coordinated rearrangement of the Nog1 N-domain together with helix 89, which are both bound by the Nsa2 β-barrel (Figure 3.2B). This rearrangement of the Nog1 N-domain might be the structural signal that induces GTP hydrolysis in Nog1, which might trigger final Nog1 release. Subsequently, helix 89 would be free to move into its mature position, which would allow further maturation steps, like the recruitment of Rpl10 (uL16) and Rpl40 (eL40), that are both associated with helix 89 in mature 60S subunits.

3.3 Recruitment of Nsa2 to the pre-ribosome

Nsa2 binds to pre-60S subunits at an intermediate maturation step, that is characterized by the presence of the early assembly factor Ssf1 (Figure 2.14A and Ulbrich et al. 2009). The Ssf1-Nsa2 split purification shows, that Nsa2 is exclusive to Rrp5 and other early assembly factors, which suggests, that the Ssf1-purification contains at least two major pre-ribosomal particles (Figure 2.14A). Rrp5 is an early maturation factor, that is involved in the maturation of both ribosomal subunits, which forms a subcomplex with 60S assembly factors Noc1 and Noc2 (Dragon et al. 2002; Hierlmeier et al. 2013; Lebaron, A. Segerstolpe, et al. 2013). Unpublished work from the lab of Dr. Sander Granneman demonstrates by chemical modification of pre-ribosomal RNA, that the modification pattern of rRNA changes drastically from a Rrp5-associated to a Nsa2-associated pre-ribosome. This analysis highlights differences in accessibility of rRNA to modification, which suggests a significant change in rRNA conformation from Rrp5 to Nsa2-associated pre-ribosomes, that is likely a requirement for Nsa2 binding to the pre-60S subunit.

It has been demonstrated, that the recruitment of Nsa2 depends on the assembly factors Nog1, Rlp24, Tif6, Dbp10, and the Nop2/Nip7 subcomplex, that are likely involved

in stabilizing the maturing A-site and the P stalk, which form the binding site for Nsa2 (Talkish et al. 2012 and section 2.4). Older data and a recent high resolution structure of the Nog2-particle suggest, that Nog1 plays a major role in Nsa2 recruitment, as it contacts Nsa2 on the pre-ribosome (Lebreton et al. 2006; Wu, Tutuncuoglu, et al. 2016 and Figure 3.1A). Tif6 is located away from Nsa2 and is necessary for the association of Nog1 and Rlp24. Its effect on Nsa2 recruitment is therefore likely indirect, similarly to Rlp24, which is also required for Nog1 association (Saveanu et al. 2003; Talkish et al. 2012). The helicase Dbp10 is found on Nsa2-particles and is associated with the Nsa2 fraction of the Ssf1-Nsa2 split purification, which indicates, that it binds to similar pre-ribosomes as Nsa2 (Figure 2.6 and Figure 2.14A). CRAC experiments show, that Dbp10 localizes to the same region as Nsa2 on the pre-ribosome, which implies, that its helicase activity might be necessary for Nsa2 recruitment or that it physically recruits Nsa2 (Manikas et al. 2016). Finally, the Nop2/Nip7 subcomplex might be directly involved in Nsa2 association, as Nop2 catalyzes methylation of cytosine 2870 in the 25S rRNA, which is probed by the C-domain of Nsa2 (S. Sharma et al. 2013; Wu, Tutuncuoglu, et al. 2016 and PDB code: 3JCT). Therefore, the formation of the Nsa2 binding pocket might depend on rRNA methylation by Nop2, or Nop2 might directly recruit Nsa2 as it associates at an adjacent location on the pre-ribosome. Nip7 is a requirement for Nop2 binding, which does not rule out a direct involvement in Nsa2 recruitment, as it has been found to interact with Nsa2 in a PCA screen (Tarassov et al. 2008). Furthermore, Nsa2 recruitment depends on the r-proteins Rpl17 (uL22), Rpl35 (uL29), and Rpl37 (eL37), which are located at the solvent side of the large subunit and are involved in intermediate assembly steps of the exit tunnel, leading up to C_2 cleavage (Gamalinda et al. 2013 and Figure 1.12). These r-proteins are located away from Nsa2, which rules out a direct role in its recruitment to the pre-ribosome. It is therefore more likely, that they stabilize parts of the large subunit that are necessary for formation of the Nsa2 binding site and which are probably undergoing drastic rearrangements just before the recruitment of Nsa2 (see above).

Through cryo-EM analysis, it has become clear, that Nsa2 binds to two separate rRNA regions on the large subunit with two distinct domains. Truncation analysis revealed that the N-domain is necessary for association with the pre-ribosome, as sedimentation analysis of the N-terminal truncation mutants Nsa2$^{\Delta 34}$, Nsa2$^{\Delta 59}$, and Nsa2$^{\Delta 84}$ shows a gradual shift from the associated to the free state (Figure 2.15A). Additionally, N-terminal fragments of Nsa2 can bind specifically to pre-60S subunits, as the Nsa2$^{1\text{-}34}$, Nsa2$^{1\text{-}59}$, and Nsa2$^{1\text{-}84}$ fragments are found in the same gradient fractions as the wild type protein and precipitate stoichiometric pre-ribosomes (Figure 2.15A,B,D). This implies, that the first 34 amino acids of Nsa2 contain the association signal for pre-60S ribosomes and

that the C-domain of Nsa2, despite its intimate interaction with rRNA in the bound state, cannot recruit Nsa2 to the pre-ribosome alone. This could indicate, that the C-domain is not initially bound to rRNA, as only a late pre-ribosomal structure with bound Nsa2 is available, that most likely does not recapitulate the earlier rRNA arrangement. Therefore, the rRNA binding pocket for the C-domain might form after recruitment of Nsa2 by the N-domain.

The initial association of Nsa2 via the N-domain is supported by the Dbp10 CRAC data, which localizes Dbp10 to the P stalk region, where the Nsa2 N-domain is bound (Manikas et al. 2016). It is therefore possible, that the helicase activity of Dbp10 forms a rRNA conformation, that can be recognized by the Nsa2 N-domain or alternatively, that Dbp10 directs the N-domain to the P stalk.

3.4 Does Rsa4 have an extra-ribosomal function?

Rsa4 is a ribosome assembly factor, which has been initially identified as being involved in Notch signaling in *Drosophila* and *Xenopus* where it binds to the cytoplasmic domain of Notch (Royet et al. 1998). It is therefore a good candidate for additional extra ribosomal functions, which are hinted at by the Y448E, N406K, and G164L mutants, that I generated. These fail to interact with Nsa2 *in vitro* and show reduced association with pre-ribosomes (Figure 2.8B). Instead, they co-purify multiple extra bands, which include Mec1 (genome integrity checkpoint protein and PI kinase superfamily member), Sgs1 (RecQ family nucleolar DNA helicase), Rpo31 (RNA polymerase III largest subunit C160), Mph1 (3'-5' DNA helicase involved in error-free bypass of DNA lesions), Rfa1 and Rfa2 (Subunits of heterotrimeric Replication Protein A, RPA), Mgm101 (Mitochondrial Genome Maintenance protein), and Rim1 (ssDNA-binding protein essential for mitochondrial genome maintenance) (Figure 2.9B, definitions from SGD). All of these proteins are associated with DNA, either in DNA damage repair, transcription, or mitochondrial DNA maintenance, which raises the possibility that Rsa4 is involved in one of these processes. It is likely, that most of these proteins stick to DNA and were co-purified by a potential binding partner of Rsa4, or that Rsa4 can directly associate with DNA. Direct DNA binding by β-propellers has been demonstrated at least in two cases: Human DDB2 and bacterial YncE have been shown to bind to DNA via aromatic amino acids at the top side of the β-propeller, which might be a common occurrence in DNA binding by β-propellers (Kagawa et al. 2011; Yeh et al. 2012).

The DNA related function of Rsa4 would most likely involve single stranded DNA, as two ssDNA binding proteins, Rim1 and Rfa1 are the most prominent bands that are

purified by the Rsa4 mutants (Figure 2.9B). Rim1 even appears to be over-stoichiometric, which is most likely explained by the fact, that it forms homo-tetramers, which then bind to DNA (Van Dyck et al. 1992). Therefore, I investigated the potential interaction of Rsa4 and Rim1. Yeast two hybrid analysis and *in vitro* binding assays failed to recapitulate the interaction, although the possibility remains, that Rim1 requires a specific DNA substrate, like ssDNA, to assemble into a conformation that can be recognized by Rsa4 (data not shown). *In silico* analysis using HH-Pred demonstrates, that Rim1 is structurally related to Rfa1, and to a lesser degree Rfa2, which raises the possibility, that both proteins could interact with Rsa4 via similar structural features (Söding et al. 2005). This would indicate, that Rsa4 could be associated with two extra ribosomal functions. These would likely involve DNA pathways that have a ssDNA intermediate like replication, recombination, transcription, telomere maintenance, or DNA repair. It is therefore highly interesting, that Rsa4 displays a synthetic lethal genetic interaction with Sgs1 and Chl1, two helicases, which highlights a potential involvement of Rsa4 in DNA helicase activity (Pel et al. 2013).

It therefore remains to be seen, if Rsa4 is indeed involved in novel functions outside of ribosome biogenesis, which would be an attractive way for the cell to reuse cellular machinery, which has already been demonstrated for ribosomal proteins, like e.g. the regulation of the MDM2-p53 feedback loop by RPL5 (uL18) and RPL11 (uL5) (Dai and Lu 2004; Lohrum et al. 2003; Marechal et al. 1994; Nicolas et al. 2016; Y. Zhang et al. 2003).

3.5 Evolutionary origins of Nsa2

Nsa2 has been classified as a member of the S8e protein family, which contains homologs of Rps8 and Nsa2, and I have shown, that the C-terminal domain of Nsa2 shares significant sequence identity with Rps8 (subsection 2.3.2 and appendix Figure A.6). This conservation is strongest between archaeal Rps8 homologs and Nsa2, which argues for a common origin of Nsa2 and Rps8 in archaea (Figure 2.12B).

The similarity is further highlighted on the structural level by the NMR structure of the Nsa2 C-domain, which closely resembles the β-barrel of Rps8 homologs (Figure 2.11). The NMR structure of the Nsa2 N-domain reveals no obvious similarity to the N-domain of Rps8, although both contain highly charged amino acids. The N-domain of Nsa2 consists of α-helices, whereas the N-domain of Rps8 is mostly unstructured and forms a lasso-like arrangement (Figure 2.10B and Figure 2.11). The precise association of Nsa2 with the rRNA has been revealed by a recent high resolution structure of the Nog2 pre-ribosome and bears striking similarities to the rRNA interactions of Rps8 (Figure 3.3B).

This structure revealed, that the N-domains of Nsa2 and Rps8 share functional homology, as both engage in intimate rRNA contacts, that anchor the protein to the ribosome (section 2.5 and PDB code: 3JCT). Furthermore, the conserved β-barrel of Nsa2 and Rps8 is bound to highly similar rRNA environments (Figure 3.3B). It is primarily bound to one rRNA helix (helix 89 of the 25S for Nsa2 and helix 9 of the 18S for Rps8), which is oriented perpendicular to the β-barrel (Figure 3.3B). Additional interacting rRNA helices are oriented in the same angles around the β-barrels of Nsa2 and Rps8. It is worth noting, that the full rRNA pocket for Rps8 is only formed in 80S ribosomes, as both subunits contribute rRNA helices to the binding site, whereas Nsa2 is exclusively bound to a similar pocket on the pre-60S subunit. Furthermore, a flexible loop, which is seen in the Nsa2 β-barrel solution structure, is folded into the same α-helical turn, that is seen in ribosome-bound Rps8, which indicates an even higher structural conservation between the two proteins (Figure 3.3B).

It is therefore conceivable, that Nsa2 originated from a promiscuously binding Rps8, which could be stably incorporated into small ribosomal subunits, while also binding transiently to large subunits during maturation (Figure 3.3A). As extant archaea do not possess a Nsa2 homolog, Nsa2 must have evolved after eukaryogenesis, or specifically in the archaeal host of eukaryotes. Because Nsa2 shares more sequence similarity with archaeal than eukaryotic Rps8, it must have originated before Rps8 diverged from the ancestral sequence in evolution.

The idea that ancestral Rps8 could have displayed a promiscuous binding behavior to rRNA is supported by the fact, that many extant archaeal r-protein display such a promiscuous binding, which is not seen in eukaryotic ribosomes (Armache et al. 2013). For example, *Pyrococcus furiosus* and *Thermococcus kodakaraensis* 70S ribosomes contain two copies each of eS24 and eL14 as well as three copies of eL8. These are bound to specific locations, as S24e binds to both ribosomal subunits, L14e to two distinct places on the large subunit and L8e to two locations on the large and one on the small subunit (Armache et al. 2013). This is contrasted by eukaryotic ribosomes, which, with the exception of P stalk proteins, contain only one copy of each r-protein. Therefore, it is likely, that the archaeal host cell, which gave rise to eukaryotes, contained a homolog of Rps8, that showed the mentioned promiscuous binding pattern on the small and large subunit. This raises the interesting question, if extant archaeal Rps8 still binds to the pre-50S subunit during maturation and if this interaction is associated with a function in ribosome biogenesis (Figure 3.3A). Because Nsa2 displays more sequence similarity with archaeal than eukaryotic Rps8, it is possible that the archaeal sequence retains two distinct functionalities, that were split up after the gene duplication (appendix Figure A.6). Subsequently, both copies could evolve towards their specific functional niche, which

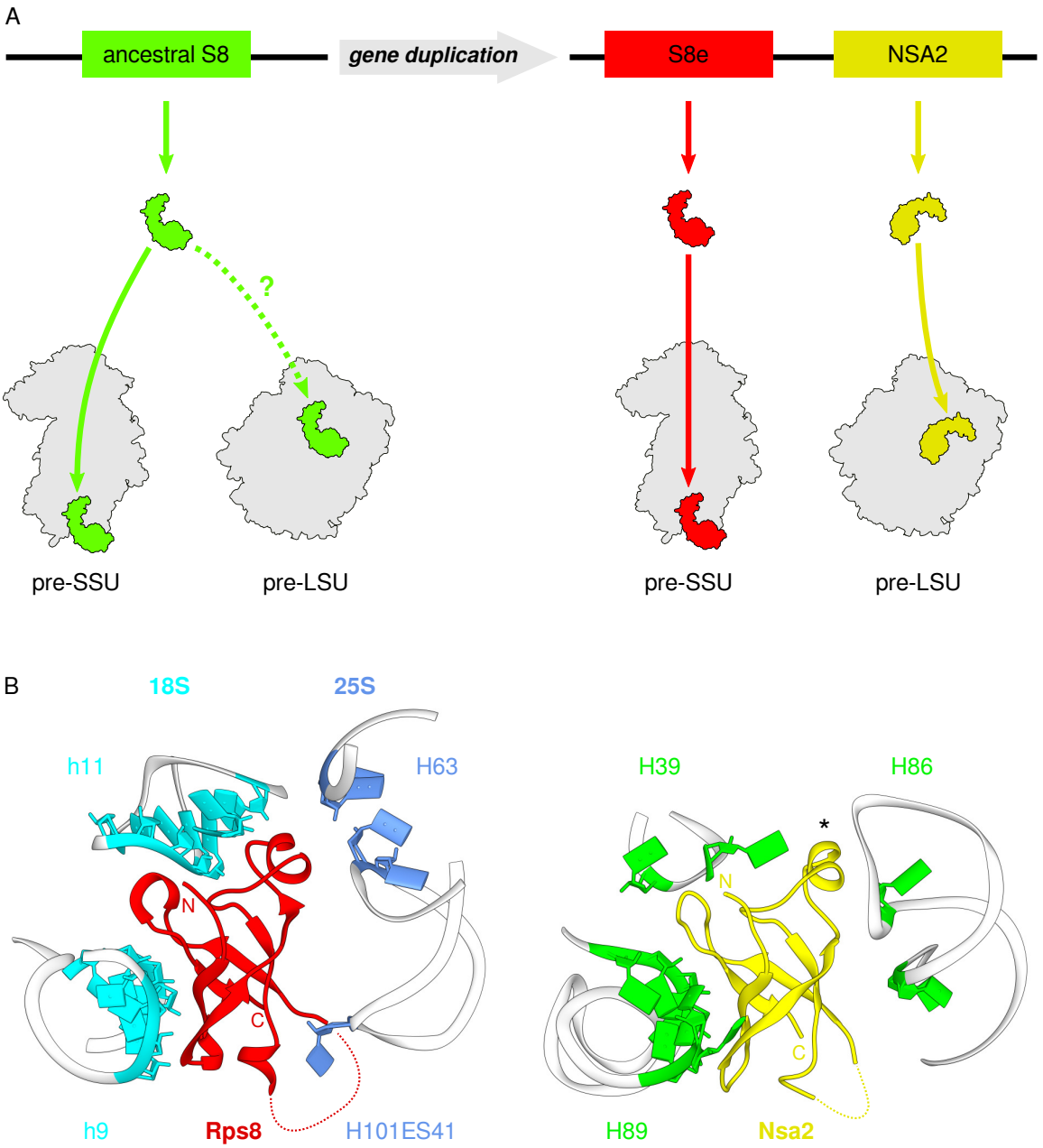

Figure 3.3: Evolutionary connection of Nsa2 and Rps8 A) Nsa2 and S8e likely originated as a gene duplication from an ancestral S8. Ancestral S8 was able to bind stably to the small subunit and possibly transiently to the large subunit. This functionality was split after the gene duplication, leading to functional niches for S8e and Nsa2. SSU = small subunit, LSU = large subunit. B) The β-barrels of Nsa2 and Rps8 are bound to highly similar rRNA pockets. Adjacent rRNA helices are arranged in the same angles around the β-barrels and contact similar parts of the barrel. RNA interactions are organized around one major rRNA helix (h9 and H89, respectively), whereas Rps8 forms additional RNA contacts, that appear less evident in Nsa2. 18S rRNA helices are labeled with 'h', 25S rRNA helices with 'H'. The β-barrel insertion loop in Nsa2, which is unstructured in solution, assumes the same fold as Rps8 in the bound state (indicated by an asterisk). Additional barrel insertions, that do not share sequence similarity between Rps8 and Nsa2 are indicated by dashed lines. N = N-terminus. C = C-terminus.

lead to mutations in regions of eukaryotic Rps8, that were retained in Nsa2.

It is worth mentioning, that *Lokiarchaeum*, a member of the Asgard superphylum, that comprises the closest known archaeal relatives of eukaryotes known to date, contains two copies of Rps8. One copy possesses a N-terminal extension, that is not seen in any other member of the S8e family and might represent an annotation mistake. The homologous region of the two variants is also not identical, as it deviates at several amino acids, which collectively do not amount to significant sequence differences (GenBank identifiers: KKK41658.1 and KKK42752.1). Further studies of extant archaeal ribosomes and archaeal 50S pre-ribosomes are therefore necessary to reveal, if extant archaeal Rps8 displays a promiscuous binding behavior and if it takes part in large subunit maturation, which would shed light on the evolution of Nsa2 and its associated function in eukaryotic ribosome biogenesis. Since archaeal Rps8 does not contain the Rsa4 interacting motif and archaea do not contain homologs of Rsa4 and Rea1, it is possible that Nsa2 acquired this functionality in addition to an existing role in large subunit formation.

4 Materials and Methods

4.1 Molecular biology techniques

4.1.1 Cloning

DNA cloning, including digestion, ligation and electrophoresis was performed according to Sambrook et al. 1989.

DNA inserts for *Saccharomyces cerevisiae* genes and promoters were excised from existing plasmids or amplified by PCR from existing plasmids or genomic DNA. DNA inserts for *Chaetomium thermophilum* ctNsa2 truncations were amplified from a plasmid (pRSFDuet1–Nsa2Ct No-tag - Hurt lab collection), which was created by Rizos-Georgios Manikas. DNA oligos for PCR amplification were obtained from Sigma and PCR amplification was performed using Phusion polymerase (NEB), according to the manufacturer's instructions. Subsequent DNA digestion was carried out using restriction enzymes from NEB and Thermo Fisher Scientific. Digested DNA was separated by agarose gel electrophoresis, stained with SERVA DNA stain G (SERVA), and extracted from the agarose gels using the QIAquick Gel Extraction kit (QIAGEN). For DNA ligation, T4 DNA Ligase (NEB) was used. Ligations were transformed into chemically competent DH5αcells, that had been prepared according to Inoue et al. 1990. Plasmid DNA was purified from DH5α transformants using the GenElute^{TM} HP Plasmid Miniprep Kit (Sigma) and verified by test digest, as well as DNA sequencing (Eurofins MWG-Operon; Ebersberg, Germany).

4.1.2 Plasmid construction

Plasmids used in this study are listed in Table 4.1.

pET Duet1 rsa4 $\triangle$136 was constructed by digesting pET Due1 with NcoI-BamHI and ligation of a PCR fragment comprised of NcoI ATG Rsa4 aa 137-516 STOP BamHI. pET24d HIS-TEV-ctnsa2 1-84 & pET24d HIS-TEV-ctnsa2 168-261 were constructed by digesting pET24d HIS-TEV with NdeI-BamHI and ligation of a PCR fragment comprised of NdeI ATG ctNsa2 variants STOP BamHI. pET24d HIS-TEV-RSA4 and variants were constructed by digestion of pET24d HIS-TEV with NdeI-BamHI and ligation of NdeI-

BamHI inserts from YCp111-P.Rsa4-TAP(Flag)2-RSA4 and mutant variants. pETM43 MBP-PRE-NSA2 and variants were constructed by digestion of pETM43 MBP-PRE with NcoI-BamHI and ligation of a PCR fragment comprised of NcoI ATG Nsa2 variants STOP BamHI. pETMBPxray_V43 MBP-nsa2 81-101 & pETMBPxray_V43 MBP-nsa2 84-96 were constructed by digestion pETMBPxray_V43 with NcoI-BamHI and ligation of annealed oligos comprised of NcoI Nsa2 BamHI. pRS315 nsa2 point mutants were generated by site-directed mutagenesis of pRS315 NSA2. pRSF Duet1 GST-TEV-NSA2 HIS-TEV-RSA4 and variants were generated by digesting pRSF Duet1 with NcoI-BamHI and ligation of a PCR fragment comprised of NcoI Nsa2 variants BamHI, followed by digestion with NdeI-XhoI and ligation of a PCR fragment comprised of NdeI HIS-TEV-Rsa4 XhoI. The GST-tag was added by insertion of a PCR fragment comprised of NcoI GST-TEV NcoI into the NcoI site in front of the Nsa2 ORF. YCplac111 NSA2-FTpA and variants were constructed by digestion of YCplac111 FTpA with EcoRI-BamHI and ligation of a PCR fragment comprised of EcoRI pNSA2-NSA2-(Linker)-$\triangle$stop BamHI. For the nsa2 $\triangle$86-90 and $\triangle$85-98 variants joint PCRs were performed, only constructs, that contain the Nsa2 C-domain were cloned with the linker ASSYTAPQPGLGGS. YCplac111 pGAL NSA2-FTpA and variants were constructed by digestion of YCplac111 NSA2-FTpA with EcoRI-BamHI and ligation of a PCR fragment comprised of EcoRI pGAL Nsa2-Linker $\triangle$stop BamHI. Subsequently the $\triangle$86-90 and $\triangle$85-98 fragments were amplified by joint PCR and ligated into the NcoI-BamHI sites. YCplac111 TAP-FLAG-rsa4 point mutants were generated by site-directed mutagenesis of YCplac111 TAP-FLAG-RSA4. YCplac22 NSA2-FTpA and variants were generated by subcloning EcoRI-XhoI fragments from YCplac111 NSA2-FTpA into YCplac22. For nsa2 variants PCRs of EcoRI pNSA2-nsa2-Linker-$\triangle$stop BamHI were cloned into YCplac22 NSA2-FTpA. YCplac22 NSA2-HA and variants were constructed by insertion of a NdeI-site between the promoter and the Nsa2 ORF in YCplac22 pNsa2 Nsa2-L-HA, the resulting vector was used for ligation of PCR fragments comprised of NdeI NSA2-(Linker)-BamHI, only constructs, that contain the Nsa2 C-domain were cloned with the linker ASSYTAPQPGLGGS. YCplac22 pGAL NSA2-HA and variants were constructed by digesting of YCplac22 pNSA2 NdeI NSA2-HA and variants with EcoRI-NdeI and ligation of a EcoRI pGAL NdeI insert. YEplac112 pGAL NSA2 and variants were constructed by digestion of YEplac112 pGAL Nug2K328N$\triangle$i (obtained from Rizos-Georgios Manikas) with NcoI-XhoI and ligation of NcoI-XhoI inserts from pETM43 MBP-PRE-NSA2 and variants. YEplac112 pGAL RSA4 and variants were constructed by digestion of YEplac112 pGAL Gle2 (obtained from Matthias Thoms) with NdeI-BamHI and insertion of NdeI-BamHI inserts from TAP-FLAG-RSA4 and variants. YEplac181 pGAL NSA2 pGAL tc-apt-2xHA-TAG-RPL25-FTpA and variant were constructed by 1) creation of a pre-vector: YEplac181-P2.3-IPI1

(obtained from Matthias Thoms) was digested with NdeI-BamHI and ligated with a PCR fragment comprised of NdeI Nsa2 STOP BamHI 2) The Asc1-PmeI inserts of the pre-vectors were subcloned into YEplac181-P2.2-GFP-rsa4E114D-T.ADH1-P1-P.Gal1-10-tc-apt-2xHA-STOP-Rpl25-Flag-ProtA (obtained from Matthias Thoms).

Table 4.1: Plasmids used in this study

Plasmid	Relevant information	Source
pEcOmeTyr/ectRNA$_{CUA}$	CEN, expression of amber suppressor ectRNA$_{CUA}$ and aminoacyl ectRNA$_{CUA}$ synthetase	Chin et al. 2003
pET Duet1 rsa4 Δ136	AmpR, p*T7*, rsa4 ΔN, Δ136 amino acids	Baßler et al. 2014
pET24d HIS-TEV-ctnsa2 1-84	KanR, p*T7*, His$_6$-TEV-ctnsa2 ΔC, 1-84 amino acids, *Chaetomium thermophilum* Nsa2	Baßler et al. 2014
pET24d HIS-TEV-ctnsa2 168-261	KanR, p*T7*, His$_6$-TEV-ctnsa2 ΔN, 168-261 amino acids, *Chaetomium thermophilum* Nsa2	Baßler et al. 2014
pET24d HIS-TEV-RSA4	KanR, p*T7*, His$_6$-TEV-Rsa4	Baßler et al. 2014
pET24d HIS-TEV-rsa4 K130E R134E	KanR, p*T7*, His$_6$-TEV-rsa4 K130E R134E	Baßler et al. 2014
pET24d HIS-TEV-rsa4 G164L	KanR, p*T7*, His$_6$-TEV-rsa4 G164L	This study
pET24d HIS-TEV-rsa4 T175R T177R	KanR, p*T7*, His$_6$-TEV-rsa4 T175R T177R	Baßler et al. 2014
pET24d HIS-TEV-rsa4 N406K	KanR, p*T7*, His$_6$-TEV-rsa4 N406K	This study
pET24d HIS-TEV-rsa4 Y448E	KanR, p*T7*, His$_6$-TEV-rsa4 Y448E	Baßler et al. 2014
pETM43 MBP	KanR, empty vector, p*T7*, Maltose binding protein control	EMBL core facility
pETM43 MBP-PRE-NSA2	KanR, p*T7*, MBP-PreScission-Nsa2	Baßler et al. 2014
pETM43 MBP-PRE-nsa2 Y90A	KanR, p*T7*, MBP-PreScission-nsa2 Y90A	Baßler et al. 2014
pETM43 MBP-PRE-nsa2 Y90F	KanR, p*T7*, MBP-PreScission-nsa2 Y90F	Baßler et al. 2014
pETMBPxray_V43	KanR, p*T7*, MBP (optimized for carrier driven crystallization: D82A, K83A, K239A, E359A, K362A, D363A), MBP-linker (AAAA) NcoI	Baßler et al. 2014
pETMBPxray_V43 MBP-nsa2 81-101	see above, Nsa2 amino acids 81-101	Baßler et al. 2014
pETMBPxray_V43 MBP-nsa2 84-96	see above, Nsa2 amino acids 84-96	Baßler et al. 2014
pRS315 NSA2	CEN, *LEU2*, AmpR, p*NSA2 NSA2*	Baßler et al. 2014
pRS315 nsa2 P88A	CEN, *LEU2*, AmpR, p*NSA2 nsa2* P88A	This study
pRS315 nsa2 Y90A	CEN, *LEU2*, AmpR, p*NSA2 nsa2* Y90A	Baßler et al. 2014
pRS315 nsa2 Y90F	CEN, *LEU2*, AmpR, p*NSA2 nsa2* Y90F	Baßler et al. 2014
pRSF Duet1 GST-TEV-NSA2 HIS-TEV-RSA4	KanR, p*T7 GST-TEV-NSA2*, p*T7 HIS$_6$-TEV-RSA4*	Baßler et al. 2014
pRSF Duet1 GST-TEV-nsa2 Δ85-98 HIS-TEV-RSA4	KanR, p*T7 GST-TEV-nsa2* Δ85-98, p*T7 HIS$_6$-TEV-RSA4*	Baßler et al. 2014
pRSF Duet1 GST-TEV-nsa2 Δ86-90 HIS-TEV-RSA4	KanR, p*T7 GST-TEV-nsa2* Δ86-90, p*T7 HIS$_6$-TEV-RSA4*	Baßler et al. 2014

Table 4.1: (continued)

Plasmid	Relevant information	Source
pT7 HIS-rsa4 ΔN	KanR, p*T7*, His_6-rsa4 ΔN, amino acids 112-516	Baßler et al. 2014
YCplac111 NSA2-FTpA	CEN, *LEU2*, AmpR, p*NSA2* Nsa2-Linker-FLAG-TEV-pA, Linker: AS-SYTAPQPGLGGS	Baßler et al. 2014
YCplac111 nsa2-FTpA Δ85-98	see above, nsa2 Δ85-98 amino acids	Baßler et al. 2014
YCplac111 nsa2-FTpA Δ86-90	see above, nsa2 Δ86-90 amino acids	Baßler et al. 2014
YCplac111 nsa2-FTpA 1-34	see above but no linker, nsa2 1-34 amino acids	This study
YCplac111 nsa2-FTpA 1-59	see above but no linker, nsa2 1-59 amino acids	This study
YCplac111 nsa2-FTpA 1-84	see above but no linker, nsa2 1-84 amino acids	This study
YCplac111 nsa2-FTpA 1-98	see above but no linker, nsa2 1-98 amino acids	This study
YCplac111 nsa2-FTpA Δ34	see above, Linker: ASSYTAPQPGLGGS, nsa2 Δ34	This study
YCplac111 nsa2-FTpA Δ58	see above, Linker: ASSYTAPQPGLGGS, nsa2 Δ58	This study
YCplac111 nsa2-FTpA Δ84	see above, Linker: ASSYTAPQPGLGGS, nsa2 Δ84	This study
YCplac111 pGAL NSA2-FTpA	CEN, *LEU2*, AmpR, p*GAL1-10* Nsa2-Linker-FLAG-TEV-pA, Linker: ASSYTAPQPGLGGS	Baßler et al. 2014
YCplac111 pGAL nsa2-FTpA Δ85-98	CEN, *LEU2*, AmpR, p*GAL1-10* nsa2-Linker-FLAG-TEV-pA, Linker: ASSYTAPQPGLGGS, nsa2 Δ85-98 amino acids	Baßler et al. 2014
YCplac111 pGAL nsa2-FTpA Δ86-90	CEN, *LEU2*, AmpR, p*GAL1-10* nsa2-Linker-FLAG-TEV-pA, Linker: ASSYTAPQPGLGGS, nsa2 Δ86-90 amino acids	Baßler et al. 2014
YCplac111 TAP-FLAG-RSA4	CEN, *LEU2*, AmpR, p*RSA4* pA-CBP-2xFLAG-Rsa4	Baßler et al. 2014
YCplac111 TAP-FLAG-rsa4 K130E R134E	CEN, *LEU2*, AmpR, p*RSA4* pA-CBP-2xFLAG-rsa4 K130E R134E	Baßler et al. 2014
YCplac111 TAP-FLAG-rsa4 G164L	CEN, *LEU2*, AmpR, p*RSA4* pA-CBP-2xFLAG-rsa4 G164L	This study
YCplac111 TAP-FLAG-rsa4 T175R T177R	CEN, *LEU2*, AmpR, p*RSA4* pA-CBP-2xFLAG-rsa4 T175R T177R	Baßler et al. 2014
YCplac111 TAP-FLAG-rsa4 N406K	CEN, *LEU2*, AmpR, p*RSA4* pA-CBP-2xFLAG-rsa4 N406K	This study
YCplac111 TAP-FLAG-rsa4 Y448E	CEN, *LEU2*, AmpR, p*RSA4* pA-CBP-2xFLAG-rsa4 Y448E	Baßler et al. 2014
YCplac22 NSA2-FTpA	CEN, *TRP1*, AmpR, p*NSA2*, Nsa2-Linker-FLAG-TEV-pA, Linker: AS-SYTAPQPGLGGS	Baßler et al. 2014
YCplac22 nsa2-FTpA P88A	see above, nsa2 P88A	Baßler et al. 2014
YCplac22 nsa2-FTpA Y90A	see above, nsa2 Y90A	Baßler et al. 2014
YCplac22 nsa2-FTpA Y90F	see above, nsa2 Y90F	Baßler et al. 2014
YCplac22 NSA2-HA	CEN, *TRP1*, AmpR, p*NSA2*, Nsa2-Linker-2xHA, Linker: ASSY-TAPQPGLGGS	This study
YCplac22 nsa2-HA 1-14	CEN, *TRP1*, AmpR, p*NSA2*, nsa2-2xHA, Nsa2 amino acids 1-14	This study
YCplac22 nsa2-HA 1-34	see above, Nsa2 amino acids 1-34	This study
YCplac22 nsa2-HA 1-59	see above, Nsa2 amino acids 1-59	This study
YCplac22 nsa2-HA 1-84	see above, Nsa2 amino acids 1-84	This study
YCplac22 nsa2-HA 1-98	see above, Nsa2 amino acids 1-98	This study

Table 4.1: (continued)

Plasmid	Relevant information	Source
YCplac22 nsa2-HA △14	CEN, *TRP1*, AmpR, p*NSA2*, nsa2-Linker-2xHA, Linker: ASSY-TAPQPGLGGS, Nsa2 △14	This study
YCplac22 nsa2-HA △34	see above, Nsa2 △34	This study
YCplac22 nsa2-HA △59	see above, Nsa2 △59	This study
YCplac22 nsa2-HA △84	see above, Nsa2 △84	This study
YCplac22 pGAL NSA2-HA	CEN, *TRP1*, AmpR, p*GAL1-10*, Nsa2-Linker-2xHA, Linker: ASSY-TAPQPGLGGS	This study
YCplac22 pGAL nsa2-HA 1-14	CEN, *TRP1*, AmpR, p*GAL1-10*, Nsa2-2xHA, Nsa2 amino acids 1-14	This study
YCplac22 pGAL nsa2-HA 1-34	see above, Nsa2 amino acids 1-34	This study
YCplac22 pGAL nsa2-HA 1-59	see above, Nsa2 amino acids 1-59	This study
YCplac22 pGAL nsa2-HA 1-84	see above, Nsa2 amino acids 1-84	This study
YCplac22 pGAL nsa2-HA 1-98	see above, Nsa2 amino acids 1-98	This study
YCplac22 pGAL nsa2-HA △14	CEN, *TRP1*, AmpR, p*GAL1-10*, Nsa2-Linker-2xHA, Linker: ASSY-TAPQPGLGGS, Nsa2 △14	This study
YCplac22 pGAL nsa2-HA △34	see above, Nsa2 △34	This study
YCplac22 pGAL nsa2-HA △59	see above, Nsa2 △59	This study
YCplac22 pGAL nsa2-HA △84	see above, Nsa2 △84	This study
YEplac112 pGAL NSA2	2µ, *TRP1*, AmpR, p*GAL1-10 NSA2*	Baßler et al. 2014
YEplac112 pGAL nsa2 P88A	2µ, *TRP1*, AmpR, p*GAL1-10 nsa2* P88A	This study
YEplac112 pGAL nsa2 Y90A	2µ, *TRP1*, AmpR, p*GAL1-10 nsa2* Y90A	Baßler et al. 2014
YEplac112 pGAL RSA4	2µ, *TRP1*, AmpR, p*GAL1-10 RSA4*	Baßler et al. 2014
YEplac112 pGAL rsa4 K130E R134E	2µ, *TRP1*, AmpR, p*GAL1-10 rsa4* K130E R134E	Baßler et al. 2014
YEplac112 pGAL rsa4 G164L	2µ, *TRP1*, AmpR, p*GAL1-10 rsa4* G164L	This study
YEplac112 pGAL rsa4 T175R T177R	2µ, *TRP1*, AmpR, p*GAL1-10 rsa4* T175R T177R	Baßler et al. 2014
YEplac112 pGAL rsa4 N406K	2µ, *TRP1*, AmpR, p*GAL1-10 rsa4* N406K	This study
YEplac112 pGAL rsa4 Y448E	2µ, *TRP1*, AmpR, p*GAL1-10 rsa4* Y448E	Baßler et al. 2014
YEplac181 pGAL NSA2 pGAL tc-apt-2xHA-TAG-RPL25-FTpA	2µ, *LEU2*, AmpR, p*GAL1-10 NSA2*, p*GAL1-10* tetracycline-aptamer-2x*HA*-amber-*RPL25-FLAG-TEV-pA*	Baßler et al. 2014
YEplac181 pGAL nsa2 Y90A pGAL tc-apt-2xHA-TAG-RPL25-FTpA	2µ, *LEU2*, AmpR, p*GAL1-10 nsa2* Y90A, p*GAL1-10* tetracycline-aptamer-2x*HA*-amber-*RPL25-FLAG-TEV-pA*	Baßler et al. 2014

4.2 Yeast techniques

4.2.1 Yeast strains

Saccharomyces cerevisiae strains used in this study are listed in Table 4.2.

Yeast were transformed according to the LiOAc/PEG protocol (Gietz and Woods 2002). After transformation, cells were streaked onto selective media plates and transformants were subsequently grown on selective media plates or in liquid cultures, depending on the experiment.

Table 4.2: Yeast strains used in this study

Strain	Relevant information	Source
DS1-2b	MATα, his3-Δ200, leu2-Δ1, trp1-Δ63, ura3-52	Nissan et al. 2002
W303a	MATa, ade2-1, can1-100, his3-11,15, leu2-3,112, trp1-1, ura3-1	B. J. Thomas and Rothstein 1989
Nsa2 shuffle	W303a-derived, MATa, ade2-1, can1-100, his3-11,15, leu2-3,112, trp1-1, ura3-1, *NSA2*::*kanMX6*, pRS316 *NSA2*	Baßler et al. 2014
Nsa2-FTpA	W303a-derived, MATa, ade2-1, can1-100, his3-11,15, leu2-3,112, trp1-1, ura3-1, p*NSA2-NSA2-LINKER-FLAG-TEV-pA*::*natNT2*, linker = ASSYTAPQPGLGGS	Baßler et al. 2014
Rsa4 shuffle	W303a-derived, MATa, ade2-1, can1-100, his3-11,15, leu2-3,112, trp1-1, ura3-1, *RSA4*::*kanMX6*, pRS316 *RSA4*	Ulbrich et al. 2009
TAP-FLAG-Rsa4	W303a-derived, MATa, ade2-1, can1-100, his3-11,15, leu2-3,112, trp1-1, ura3-1, *RSA4*::*natNT2*-p*RSA4-TAP-FLAG-RSA4*, N-terminal TAP = 2xpA-TEV-CBP	Baßler et al. 2014
Ssf1-TAP Nsa2-FLAG	W303a-derived, MATa, ade2-1, can1-100, his3-11,15, leu2-3,112, trp1-1, ura3-1, *NSA2*::*NSA2-LINKER-FLAG-natNT2*, linker = ASSY-TAPQPGLGGS, *SSF1*::*SSF1-TAP-HIS3MX*, C-terminal TAP = CBP-TEV-2xpA	This study

4.2.2 Yeast media

Yeast growth media were prepared according to Sherman 1991:

YPD (yeast extract peptone dextrose): 1% (w/v) yeast extract (MP), 2% (w/v) Bacto^{TM} peptone (BD), 2%(w/v) glucose (Merck), pH 5.5

SDC-XY (synthetic dextrose complete): 2% (w/v) glucose (Merck), 0.67% (w/v) yeast nitrogen base w/o amino acids, complemented with amino acids lacking XY (CSM drop-out, Formedium), pH 5.5

SRC-XY (synthetic raffinose complete): 2% (w/v) raffinose (MP), 0.67% (w/v) yeast nitrogen base w/o amino acids, complemented with amino acids lacking XY (CSM drop-

out, Formedium), pH 5.5

YPG (rich galactose medium): 1% (w/v) yeast extract (MP), 2% (w/v) Bacto^{TM} peptone (BD), 2%(w/v) galactose (Sigma), pH 5.5

For plates, the media was supplied with 22g/l agar.

4.2.3 Growth assays

For growth analysis, yeast cells were spotted in 10-fold dilution on selective media plates with a starting OD of 1 (except for Figure 2.14, where an OD of 3 was used) and grown at 23 °C , 30 °C , and 37 °C for the indicated number of days.

4.2.4 Non-radioactive pulse chase

Description adapted from Baßler et al. 2014: The yeast strain DS1-2b was transformed with pEcOmeTyr/ectRNA$_{CUA}$ (carrying the amber 'TAG' suppressor tRNA and its corresponding tRNA synthetase; Chin et al. 2003) and YEplac181 pGAL NSA2 pGAL tc-apt-2xHA-TAG-RPL25-FTpA for galactose-inducible overexpression of Rpl25-FTpA and Nsa2 (wild type or Y90A mutant). Expression of *NSA2* and *HA-RPL25-FTpA* mRNA was induced for 60 min by the addition of galactose. Then, the translation of HA-Rpl25-FTpA was pulsed for 7 min by the addition of O-methyl-tyrosine. Subsequently, the expression and translation of HA-Rpl25-FTpA were shut down by the addition of tetracycline and glucose for 20 min (chase). For subsequent analysis, Rpl25 was purified using the standard TAP protocol (see below). The eluates were analyzed by SDS-PAGE on 4–12% NuPAGE gels (Thermo Fisher Scientific). Associated proteins were identified by mass spectrometry. For details see Stelter and Hurt 2014; Stelter et al. 2012.

4.3 Biochemical techniques

4.3.1 Tandem affinity purification

For TAP purification, cells were grown in either YPD (Figure 2.6) or SDC-LEU media (Figure 2.7D, Figure 2.9B, and Figure 2.15D) to an OD_{600} of ~1.5-2. For each purification a pellet of a 2-liter yeast culture was used. Affinity purification was carried out as described in Rigaut et al. 1999. Cells were lysed in a buffer consisting of 100 mM NaCl, 50 mM Tris/Cl pH 7.5 (at 4 °C), 5 mM $MgCl_2$, 1 mM DTT, 5% glycerol (v/v), 0.1% NP-40 (v/v) and FY complete protease inhibitor (SERVA). After initial centrifugation for 5 minutes at maximum speed in a falcon tabletop centrifuge, the lysate was cleared

for 20 minutes at 16.000 rpm in a JA 25.50 rotor (RCF_{avg} = 21002) (Beckman-Coulter). Afterwards, the supernatant was mixed with IgG-Sepharose (IgG-Sepharose^{TM} 6 Fast Flow, GE Healthcare) in batch and incubated for 90 min at 4 °C on a rotating wheel. Then, the beads were transferred to a Mobicol (MobiTec), washed, and eluted by incubation with tobacco etch virus (TEV) protease for 120 min at 16 °C . The TEV-eluate was then incubated with anti-FLAG M2 Affinity Gel (Sigma-Aldrich) for 45 minutes at 4 °C and bound pre-ribosomes were eluted after washing with 1 x FLAG-peptide (45 minute incubation at 4 °C). Eluates were precipitated with 10% TCA and analyzed on 4–12% NuPAGE gels (Thermo Fisher Scientific).

4.3.2 Western blotting

After SDS-PAGE, proteins were transferred onto a nitrocellulose membrane (Protran membrane, Whatman) by semi-dry blotting using transfer buffer consisting of 48 mM Tris, 39 mM glycine, 1.3 mM SDS and 20% methanol (v/v). The transfer was performed for 45 minutes at 12 V and the membrane was subsequently stained by Ponceau S (SERVA) to analyze the transfer efficiency and indicate the protein marker on the membrane. Blocking of the membrane was performed by a solution consisting of 1 x PBS, 0.1% Tween (v/v), and 5% milk powder (w/v) for 30 minutes at room temperature on a rocker. The primary antibody was applied diluted in blocking solution and incubated with the membrane for 45 minutes at room temperature and subsequently washed three times for 10 minutes with 1 x PBS containing 0.1% Tween (v/v). The secondary antibody was applied diluted in blocking solution and incubated with the membrane for 45 minutes at room temperature and subsequently washed three times for 10 minutes with 1 x PBS containing 0.1% Tween (v/v). Visualization of bands was then performed using ECL detection solution (GE Healthcare) and the Image Quant LAS 4000 (GE Healthcare).

4.3.3 Purification of recombinantly expressed proteins from *E.coli*

Recombinant proteins used in binding assays, as well as in crystallization trials were produced in BL21 codon plus (DE3) cells (EMD Millipore) by IPTG induction for 3 h at 37 °C or overnight at 16 °C . Electro-competent BL21 codon plus cells were prepared according to Sambrook et al. 1989. Cells were grown in Luria-Bertani (LB) medium (0.5% yeast extract (w/v) (MP), 1% tryptone (w/v) (MP), 0.5% NaCl (w/v), and pH 7.2) with antibiotics added as necessary (ampicillin (100 μg/ml), kanamycin (10μg/ml) or cloramphenicol (34μg/ml). Cells were harvested an frozen in liquid nitrogen and then stored at -20 °C . Cell lysis was performed with a microfluidizer (Microfluidics) and the

lysates were cleared by centrifugation for 20 minutes at 16.000 rpm in a JA 25.50 rotor (RCF_{avg} = 21002) (Beckman-Coulter). Proteins were subsequently purified in batch with the corresponding affinity resins.

Descriptions below are adapted from Baßler et al. 2014:

Purification of MBP-scNsa2 variants. Frozen E. coli pellets were resuspended in $NaCl_{200}$ buffer (20 mM Hepes pH 7.5, 200 mM NaCl, and 1 mM DTT). The cleared lysate was incubated with SP Sepharose (Sigma-Aldrich) for 1 h to reduce ribosomal contamination. After extensive washing ($NaCl_{200}$), MBP-scNsa2 was eluted with $NaCl_{600}$ buffer (20 mM Hepes, pH 7.5, and 600 mM NaCl). The eluates were incubated with Amylose Resin (New England Biolabs, Inc.) for 1 h. After extensive washing ($NaCl_{200}$), the beads were resuspended in $NaCl_{200}$ buffer and used for binding assays. MBP control and MBP-scNsa2 peptide were purified accordingly, without the SP Sepharose step.

Purification of HIS-TEV-scRsa4 variants. Frozen pellets were resuspended in buffer $NaCl_{200}$ (20 mM Hepes pH 7.5, 200 mM NaCl, and 1 mM DTT). After lysis, imidazole, pH 8.0, was added to a final concentration of 10 mM. The cleared lysate was then incubated with NiNTA (Macherey-Nagel) for 1 h. After extensive washing ($NaCl_{200}$), the proteins were eluted with $NaCl_{200}$ buffer containing 200 mM imidazole.

4.3.4 *In vitro* reconstitution of the Nsa2-Rsa4 interaction

Description adapted from Baßler et al. 2014: Binding assays were performed using Micro Bio-Spin columns (Bio-Rad Laboratories). To reduce nonspecific binding, *E. coli* lysate was used as a competitor in all binding assays. Because *E. coli* express endogenous maltose-binding protein (MBP), the lysate was depleted of MBP with amylose resin before use. For binding studies, MBP-bait proteins bound to amylose resin were incubated with a 5x excess of Rsa4 variants mixed with *E. coli* lysate at 4 °C . After 45 minutes of incubation, the beads were washed with buffer $NaCl_{200}$ (20 mM Hepes pH 7.5, 200 mM NaCl, and 1 mM DTT). Bound proteins were eluted by incubating the beads for 10 min at 65 °C with SDS sample buffer.

For binding assays of scNsa2 deletion constructs, GST-Nsa2 and HIS-Rsa4 were coexpressed. Frozen pellets were resuspended in buffer $NaCl_{250}$ (20 mM Hepes pH 7.5, 250 mM NaCl, and 0.01% NP-40 (v/v)). The cleared lysate was incubated with Glutathione Sepharose Resin (Macherey-Nagel) for 1 h at 4 °C . After extensive washing ($NaCl_{250}$), the beads were resuspended in $NaCl_{250}$ buffer containing 1 mM DTT. Bound proteins were released by TEV cleavage for 1 h at 16 °C and the eluates were precipitated with 10 % TCA.

4.3.5 Crystallization of the minimal Rsa4-Nsa2 complex

Description adapted from Baßler et al. 2014: For crystallization of the minimal scNsa2–scRsa4 complex, scNsa2 (81–101 aa) was recombinantly expressed as an MBP fusion protein. To facilitate crystallization, a modified version of the original MBP sequence was used, which had been optimized for carrier driven crystallization by surface entropy reduction, according to Moon et al. 2010 (mutations in MBP: D82A, K83A, K239A, E359A, K362A, D363A), MBP-linker (AAAA) NcoI). For crystallization trials the Nsa2-Rsa4 complex was reconstituted in $NaCl_{200}$ buffer (20 mM Hepes pH 7.5, 200 mM NaCl, and 1 mM DTT). First, MBP-Nsa2 was bound to amylose resin and incubated with an *E. coli* lysate containing scRsa4$\triangle$136. After washing, the complex was eluted with $NaCl_{200}$ buffer containing 10 mM maltose and further purified by size-exclusion chromatography on a HiLoad 16/60 Superdex200 column (GE Healthcare) equilibrated in $NaCl_{200}$ buffer (Figure 2.3A,B). Peak fractions containing the complex were collected, concentrated and used for crystallization trials (see Figure 2.3C,D). The purified complex was concentrated to 46 mg/ml and hanging drops were set up with 2 μl of Nsa2-Rsa4 complex and 0.5 μl precipitant consisting of 200 mM NH_4SO_4 and 20 % PEG 3350 (w/v). After 57 days at 18 °C , needle-shaped crystals were discovered.

Crystals were cryo-protected and diffraction data were collected under cryogenic conditions (100 K) at the European Synchrotron Radiation Facility (ESRF) by members of the lab of Dr. Irmi Sinning. X-ray data collection and structure determination are described in detail in Baßler et al. 2014. Data collection and refinement statistics of the Nsa2-Rsa4 crystal structure are shown in Table 4.3.

4.3.6 Sucrose gradient analysis

Yeast cultures were grown to OD_{600} of 0.5-0.8 and incubated with 100μg/ml cycloheximide for 10 minutes on ice prior to lysis. Cells were harvested and lysis was performed with lysis buffer consisting of 100 mM KCl, 50 mM Tris/Cl pH 7.5 at 4 °C , 12 mM $MgCl_2$, and 100μg/ml cycloheximide by vortexing six times for 30S with glass beads. The lysates were then clarified in an Eppendorf centrifuge at maximum speed for a few seconds to pellet the beads and subsequently the supernatant was centrifuged at 10.000 rpm for 5 minutes at 4 °C in an Eppendorf centrifuge. The cleared lysates were applied to 10–50% sucrose gradients (w/v) and centrifuged for 2:45 h at 39,000 rpm in a SW40 rotor (RCF_{avg} = 192072) (Beckman-Coulter). Gradients were fractionated by using 'Foxy junior' from Isco with Peak TRAK software.

Table 4.3: Data collection and refinement statistics of the Nsa2-Rsa4 crystal structure.

Adapted from Baßler et al. 2014.

Criteria	scNsa2 peptide + scRsa4
Data collection	
Space group	C2
Cell dimensions	
α, β, χ (Å)	198.58, 96.49, 196,45
α, β, γ (°)	90, 115.45, 90
Resolution (Å)	48.98–3.20 (3.30–3.20)[a]
R_{merge}	0.168 (0.875)
$\mathbf{I}/\sigma\mathbf{I}$	15.6 (3.1)
Completeness (%)	100 (100)
Redundancy	11.4 (11.5)
Refinement	
Resolution (Å)	48.98–3.20
No. reflections	55659
R_{work}/R_{free}	0.2184/ 0.2571
No. atoms	
Protein	23533
Water	142
B-factors	
Protein	27.80
Water	17.80
Rms deviations	
Bond lengths (Å)	0.002
Bond angles (°)	0.64
Validation	
Ramachandran plot (%)	
Favored	96.2
Allowed	3.7
Outliers	0.1
MolProbity clash score	5.46

One crystal was used for structure solution.
[a]Highest resolution shell is shown in parenthesis.

4.4 *In silico* analysis

Multiple sequence alignments were generated using Clustal Omega, except for appendix Figure A.6 and Figure 2.12, where MSAProbs was used (Liu et al. 2010; Sievers et al. 2014). Alignments were displayed using Jalview and secondary structure was predicted using the JNet server (Drozdetskiy et al. 2015; Waterhouse et al. 2009).

Molecular graphics and analyses, including rigid body fitting of the Nsa2-Rsa4 crystal structure into EM-volumes, were performed with the UCSF Chimera package (Pettersen et al. 2004). Chimera is developed by the Resource for Biocomputing, Visualization, and Informatics at the University of California, San Francisco (supported by NIGMS P41-GM103311). Electrostatic surface potential was calculated using PDB2PQR and APBS (Baker et al. 2001; Dolinsky et al. 2007; Dolinsky et al. 2004).

Table 4.4: Statistics of NMR structures. Adapted from Baßler et al. 2014.

Criteria	ctNsa2-C	ctNsa2-N
NOE-derived distance contraints		
Sequential $[(i-j)=1]$	766	
Medium Range $[1<(i-j)\leq 5]$	176	
Long Range $[(i-j)>5]$	400	
Total	1,342	
Dihedral angle constraints		
φ	53	
ψ	56	
H-bonding constraints	28	
Number of constraints per residue	15.7	
Number of long-range constraints per residue	4.3	
Average RMSD to the mean CYANA coordinates [Å]		
All heavy atoms	1.3	
Backbone heavy atom (178-204, 215-224, 235-261)	0.80	
PROCHECK Z-scores (φ and ψ / all dihedral angles)	−1.41/ −1.42	
MOLPROBITY mean score/clash score	11.08/ 2.20	
Ramachandran plot summary for ordered residues [%]		
Most favored regions	98.7	
Additionally allowed regions	1.3	
Disallowed regions	0.0	
Restraint violations		
CYANA target function [Å]	0.27	
Average number of distance violations per CYANA conformer [Å] > 0.5	0	
Average number of dihedral-angle violations per CYANA conformer [degrees]	0	
Average number of Van der Waal violations per CYANA conformer [Å] > 0.5	0	
CS-Rosetta input		
$^{13}C^{\alpha}$ shifts		77
$^{13}C^{\beta}$ shifts		73
$^{13}C'$ shifts		68
^{15}N shifts		69
$^{1}H^{N}$ shifts		69
$^{1}H^{\alpha}$ shifts		45

Publications included in this thesis:

1. Baßler, J.*, H. Paternoga*, I. Holdermann, M. Thoms, S. Granneman, C. Barrio-Garcia, A. Nyarko, W. Lee, G. Stier, S. A. Clark, D. Schraivogel, M. Kallas, R. Beckmann, D. Tollervey, E. Barbar, I. Sinning, and E. Hurt (2014). “A network of assembly factors is involved in remodeling rRNA elements during preribosome maturation.” J Cell Biol 207.4, pp. 481–498. * co-first author

Bibliography

Agmon, I., A. Bashan, R. Zarivach, and A. Yonath (2005). “Symmetry at the active site of the ribosome: structural and functional implications”. *Biological Chemistry* 386.9.

Allfrey, V., M. M. Daly, and A. E. Mirsky (1953). “Synthesis of protein in the pancreas. II. The role of ribonucleoprotein in protein synthesis.” *J Gen Physiol* 37.2, pp. 157–175.

Allmang, C., J. Kufel, G. Chanfreau, P. Mitchell, E. Petfalski, and D. Tollervey (1999). “Functions of the exosome in rRNA, snoRNA and snRNA synthesis.” *EMBO J* 18.19, pp. 5399–5410.

Allmang, C., P. Mitchell, E. Petfalski, and D. Tollervey (2000). “Degradation of ribosomal RNA precursors by the exosome”. *Nucleic Acids Research* 28.8, pp. 1684–1691.

Altvater, M., Y. Chang, A. Melnik, L. Occhipinti, S. Schütz, U. Rothenbusch, P. Picotti, and V. G. Panse (2012). “Targeted proteomics reveals compositional dynamics of 60S pre-ribosomes after nuclear export.” *Mol Syst Biol* 8, p. 628.

Amlacher, S., P. Sarges, D. Flemming, V. van Noort, R. Kunze, D. P. Devos, M. Arumugam, P. Bork, and E. Hurt (2011). “Insight into structure and assembly of the nuclear pore complex by utilizing the genome of a eukaryotic thermophile.” *Cell* 146.2, pp. 277–289.

Anger, A. M., J.-P. Armache, O. Berninghausen, M. Habeck, M. Subklewe, D. N. Wilson, and R. Beckmann (2013). “Structures of the human and Drosophila 80S ribosome.” *Nature* 497.7447, pp. 80–85.

Aravind, L. and E. V. Koonin (2000). “Eukaryote-specific Domains in Translation Initiation Factors: Implications for Translation Regulation and Evolution of the Translation System”. *Genome Research* 10.8, pp. 1172–1184.

Armache, J.-P., A. M. Anger, V. Márquez, S. Franckenberg, T. Fröhlich, E. Villa, O. Berninghausen, M. Thomm, G. J. Arnold, R. Beckmann, and D. N. Wilson (2013). “Promiscuous behaviour of archaeal ribosomal proteins: implications for eukaryotic ribosome evolution.” *Nucleic Acids Res* 41.2, pp. 1284–1293.

Arnaout, M. A., B. Mahalingam, and J.-P. Xiong (2005). “Integrin structure, allostery, and bidirectional signaling.” *Annu Rev Cell Dev Biol* 21, pp. 381–410.

Asano, N., K. Kato, A. Nakamura, K. Komoda, I. Tanaka, and M. Yao (2015). “Structural and functional analysis of the Rpf2-Rrs1 complex in ribosome biogenesis”. *Nucleic Acids Research* 43.9, pp. 4746–4757.

Axt, K., S. L. French, A. L. Beyer, and D. Tollervey (2014). “Kinetic Analysis Demonstrates a Requirement for the Rat1 Exonuclease in Cotranscriptional Pre-rRNA Cleavage”. *PLoS ONE* 9.2. Ed. by B. Tian, e85703.

Bachellerie, J. P., J. Cavaillé, and A. Hüttenhofer (2002). “The expanding snoRNA world.” *Biochimie* 84.8, pp. 775–790.

Baker, N. A., D. Sept, S. Joseph, M. J. Holst, and J. A. McCammon (2001). “Electrostatics of nanosystems: application to microtubules and the ribosome.” *Proc Natl Acad Sci U S A* 98.18, pp. 10037–10041.

Ban, N., P. Nissen, J. Hansen, P. B. Moore, and T. A. Steitz (2000). "The complete atomic structure of the large ribosomal subunit at 2.4 A resolution." *Science* 289.5481, pp. 905–920.

Bange, G., G. Murat, I. Sinning, E. Hurt, and D. Kressler (2013). "New twist to nuclear import: When two travel together". *Communicative & Integrative Biology* 6.4, e24792.

Barrio-Garcia, C., M. Thoms, D. Flemming, L. Kater, O. Berninghausen, J. Baßler, R. Beckmann, and E. Hurt (2016). "Architecture of the Rix1-Rea1 checkpoint machinery during pre-60S-ribosome remodeling." *Nat Struct Mol Biol* 23.1, pp. 37–44.

Bassler, J., I. Klein, C. Schmidt, M. Kallas, E. Thomson, M. A. Wagner, B. Bradatsch, G. Rechberger, H. Strohmaier, E. Hurt, and Bergl (2012). "The Conserved Bud20 Zinc Finger Protein Is a New Component of the Ribosomal 60S Subunit Export Machinery". *Molecular and Cellular Biology* 32.24, pp. 4898–4912.

Baßler, J., P. Grandi, O. Gadal, T. Leßmann, E. Petfalski, D. Tollervey, J. Lechner, and E. Hurt (2001). "Identification of a 60 S Preribosomal Particle that Is Closely Linked to Nuclear Export". *Molecular Cell* 8.3, pp. 517–529.

Bassler, J., M. Kallas, B. Pertschy, C. Ulbrich, M. Thoms, and E. Hurt (2010). "The AAA-ATPase Rea1 drives removal of biogenesis factors during multiple stages of 60S ribosome assembly." *Mol Cell* 38.5, pp. 712–721.

Baßler, J., H. Paternoga, I. Holdermann, M. Thoms, S. Granneman, C. Barrio-Garcia, A. Nyarko, W. Lee, G. Stier, S. A. Clark, D. Schraivogel, M. Kallas, R. Beckmann, D. Tollervey, E. Barbar, I. Sinning, and E. Hurt (2014). "A network of assembly factors is involved in remodeling rRNA elements during preribosome maturation." *J Cell Biol* 207.4, pp. 481–498.

Baudin-Baillieu, A., D. Tollervey, C. Cullin, and F. Lacroute (1997). "Functional analysis of Rrp7p, an essential yeast protein involved in pre-rRNA processing and ribosome assembly." *Molecular and Cellular Biology* 17.9, pp. 5023–5032.

Baxter-Roshek, J. L., A. N. Petrov, and J. D. Dinman (2007). "Optimization of Ribosome Structure and Function by rRNA Base Modification". *PLoS ONE* 2.1. Ed. by T. Preiss, e174.

Belin, S., A. Beghin, E. Solano-Gonzàlez, L. Bezin, S. Brunet-Manquat, J. Textoris, A.-C. Prats, H. C. Mertani, C. Dumontet, and J.-J. Diaz (2009). "Dysregulation of ribosome biogenesis and translational capacity is associated with tumor progression of human breast cancer cells." *PLoS One* 4.9, e7147.

Belousoff, M. J., C. Davidovich, E. Zimmerman, Y. Caspi, I. Wekselman, L. Rozenszajn, T. Shapira, O. Sade-Falk, L. Taha, A. Bashan, M. S. Weiss, and A. Yonath (2010). "Ancient machinery embedded in the contemporary ribosome." *Biochem Soc Trans* 38.2, pp. 422–427.

Ben-Shem, A., N. Garreau de Loubresse, S. Melnikov, L. Jenner, G. Yusupova, and M. Yusupov (2011). "The structure of the eukaryotic ribosome at 3.0 Å resolution." *Science* 334.6062, pp. 1524–1529.

Ben-Shem, A., L. Jenner, G. Yusupova, and M. Yusupov (2010). "Crystal structure of the eukaryotic ribosome." *Science* 330.6008, pp. 1203–1209.

Bernabeu, C. and J. A. Lake (1982). "Nascent polypeptide chains emerge from the exit domain of the large ribosomal subunit: immune mapping of the nascent chain." *Proc Natl Acad Sci U S A* 79.10, pp. 3111–3115.

Bokov, K. and S. V. Steinberg (2009). "A hierarchical model for evolution of 23S ribosomal RNA." *Nature* 457.7232, pp. 977–980.

Boocock, G. R., J. A. Morrison, M. Popovic, N. Richards, L. Ellis, P. R. Durie, and J. M. Rommens (2002). "Mutations in SBDS are associated with Shwachman–Diamond syndrome". *Nature Genetics* 33.1, pp. 97–101.

Borovjagin, A. V. and S. A. Gerbi (2001). "Xenopus U3 snoRNA GAC-Box A' and Box A Sequences Play Distinct Functional Roles in rRNA Processing". *Molecular and Cellular Biology* 21.18, pp. 6210–6221.

Borsook, H., C. L. Deasy, A. J. Haagensmit, G. Keighley, and P. H. Lowy (1950). "Metabolism of C14 labeled glycine, L-histidine, L-leucine, and L-lysine." *J Biol Chem* 187.2, pp. 839–848.

Brachet, J. (1942). "La localisation des acides pentosenucléiques dans les tissus animaux et les oeufs d'Amphibiens en voie de développement". *Archives de biologie* 53, pp. 207–257.

Bradatsch, B., J. Katahira, E. Kowalinski, G. Bange, W. Yao, T. Sekimoto, V. Baumgärtel, G. Boese, J. Bassler, K. Wild, R. Peters, Y. Yoneda, I. Sinning, and E. Hurt (2007). "Arx1 Functions as an Unorthodox Nuclear Export Receptor for the 60S Preribosomal Subunit". *Molecular Cell* 27.5, pp. 767–779.

Bradatsch, B., C. Leidig, S. Granneman, M. Gnädig, D. Tollervey, B. Böttcher, R. Beckmann, and E. Hurt (2012). "Structure of the pre-60S ribosomal subunit with nuclear export factor Arx1 bound at the exit tunnel." *Nat Struct Mol Biol* 19.12, pp. 1234–1241.

Brenner, S., F. Jacob, and M. Meselson (1961). "An unstable intermediate carrying information from genes to ribosomes for protein synthesis." *Nature* 190, pp. 576–581.

Brosius, J., T. J. Dull, and H. F. Noller (1980). "Complete nucleotide sequence of a 23S ribosomal RNA gene from Escherichia coli." *Proc Natl Acad Sci U S A* 77.1, pp. 201–204.

Brosius, J., M. L. Palmer, P. J. Kennedy, and H. F. Noller (1978). "Complete nucleotide sequence of a 16S ribosomal RNA gene from Escherichia coli." *Proc Natl Acad Sci U S A* 75.10, pp. 4801–4805.

Burwick, N., A. Shimamura, and J. M. Liu (2011). "Non-Diamond Blackfan anemia disorders of ribosome function: Shwachman Diamond syndrome and 5q- syndrome." *Semin Hematol* 48.2, pp. 136–143.

Bussiere, C., Y. Hashem, S. Arora, J. Frank, and A. W. Johnson (2012). "Integrity of the P-site is probed during maturation of the 60S ribosomal subunit". *The Journal of Cell Biology* 197.6, pp. 747–759.

Bystricky, K., T. Laroche, G. van Houwe, M. Blaszczyk, and S. M. Gasser (2005). "Chromosome looping in yeast: telomere pairing and coordinated movement reflect anchoring efficiency and territorial organization." *J Cell Biol* 168.3, pp. 375–387.

Calviño, F. R., S. Kharde, A. Ori, A. Hendricks, K. Wild, D. Kressler, G. Bange, E. Hurt, M. Beck, and I. Sinning (2015). "Symportin 1 chaperones 5S RNP assembly during ribosome biogenesis by occupying an essential rRNA-binding site." *Nat Commun* 6, p. 6510.

Carter, A. P. and R. D. Vale (2010). "Communication between the AAA+ ring and microtubule-binding domain of dynein." *Biochem Cell Biol* 88.1, pp. 15–21.

Carter, C. W. (2015). "What RNA World? Why a Peptide/RNA Partnership Merits Renewed Experimental Attention." *Life (Basel)* 5.1, pp. 294–320.

Caspersson, T. (1947). "The relations between nucleic acid and protein synthesis." *Symp Soc Exp Biol* 1, pp. 127–151.

Caspersson, T. (1941). "Studien über den Eiweißumsatz der Zelle". *Naturwissenschaften* 29.3, pp. 33–43.

Cate, J. H., A. R. Gooding, E. Podell, K. Zhou, B. L. Golden, A. A. Szewczak, C. E. Kundrot, T. R. Cech, and J. A. Doudna (1996). "RNA tertiary structure mediation by adenosine platforms." *Science* 273.5282, pp. 1696–1699.

Cech, T. R. and B. Zhang (1997). "Peptide bond formation by in vitro selected ribozymes." *Nature* 390.6655, pp. 96–100.

Chaker-Margot, M., J. Barandun, M. Hunziker, and S. Klinge (2016). "Architecture of the yeast small subunit processome". *Science* 355.6321, eaal1880.

Chaker-Margot, M., M. Hunziker, J. Barandun, B. D. Dill, and S. Klinge (2015). "Stage-specific assembly events of the 6-MDa small-subunit processome initiate eukaryotic ribosome biogenesis". *Nature Structural & Molecular Biology*.

Chantha, S.-C. and D. P. Matton (2007). "Underexpression of the plant NOTCHLESS gene, encoding a WD-repeat protein, causes pleitropic phenotype during plant development." *Planta* 225.5, pp. 1107–1120.

Chawla, M., R. Oliva, J. M. Bujnicki, and L. Cavallo (2015). "An atlas of RNA base pairs involving modified nucleobases with optimal geometries and accurate energies". *Nucleic Acids Research* 43.14, pp. 6714–6729.

Chen, S. S. and J. R. Williamson (2013). "Characterization of the ribosome biogenesis landscape in E. coli using quantitative mass spectrometry." *J Mol Biol* 425.4, pp. 767–779.

Chin, J. W., T. A. Cropp, J. C. Anderson, M. Mukherji, Z. Zhang, and P. G. Schultz (2003). "An Expanded Eukaryotic Genetic Code". *Science* 301.5635, pp. 964–967.

Clark, C. G., B. W. Tague, V. C. Ware, and S. A. Gerbi (1984). "Xenopus laevis 28S ribosomal RNA: a secondary structure model and its evolutionary and functional implications." *Nucleic Acids Res* 12.15, pp. 6197–6220.

Collins, E. T. (1900). "Cases with symmetrical congenital notches in the outer part of each lid and defective development of the malar bones". *Trans Ophthalmol Soc UK* 20, pp. 190–192.

Cox, C. J., P. G. Foster, R. P. Hirt, S. R. Harris, and T. M. Embley (2008). "The archaebacterial origin of eukaryotes." *Proc Natl Acad Sci U S A* 105.51, pp. 20356–20361.

Crick, F. H. (1968). "The origin of the genetic code." *J Mol Biol* 38.3, pp. 367–379.

Dai, M.-S. and H. Lu (2004). "Inhibition of MDM2-mediated p53 ubiquitination and degradation by ribosomal protein L5." *J Biol Chem* 279.43, pp. 44475–44482.

de la Cruz, J., K. Karbstein, and J. L. Woolford Jr (2015). "Functions of ribosomal proteins in assembly of eukaryotic ribosomes in vivo." *Annu Rev Biochem* 84, pp. 93–129.

de la Cruz, J., E. Sanz-Martinez, and M. Remacha (2005). "The essential WD-repeat protein Rsa4p is required for rRNA processing and intra-nuclear transport of 60S ribosomal subunits." *Nucleic Acids Res* 33.18, pp. 5728–5739.

Decatur, W. A. and M. J. Fournier (2002). "rRNA modifications and ribosome function." *Trends Biochem Sci* 27.7, pp. 344–351.

Dembowski, J. A., B. Kuo, and J. L. Woolford (2013). "Has1 regulates consecutive maturation and processing steps for assembly of 60S ribosomal subunits". *Nucleic Acids Research* 41.16, pp. 7889–7904.

Dez, C., J. Houseley, and D. Tollervey (2006). "Surveillance of nuclear-restricted pre-ribosomes within a subnucleolar region of Saccharomyces cerevisiae." *EMBO J* 25.7, pp. 1534–1546.

Dinman, J. D. (2016). "Pathways to Specialized Ribosomes: The Brussels Lecture." *J Mol Biol* 428.10 Pt B, pp. 2186–2194.

Dolinsky, T. J., P. Czodrowski, H. Li, J. E. Nielsen, J. H. Jensen, G. Klebe, and N. A. Baker (2007). "PDB2PQR: expanding and upgrading automated preparation of biomolecular structures for molecular simulations". *Nucleic Acids Research* 35.Web Server, W522–W525.

Dolinsky, T. J., J. E. Nielsen, J. A. McCammon, and N. A. Baker (2004). "PDB2PQR: an automated pipeline for the setup of Poisson-Boltzmann electrostatics calculations". *Nucleic Acids Research* 32.Web Server, W665–W667.

Dragon, F., J. E. G. Gallagher, P. A. Compagnone-Post, B. M. Mitchell, K. A. Porwancher, K. A. Wehner, S. Wormsley, R. E. Settlage, J. Shabanowitz, Y. Osheim, A. L. Beyer, D. F. Hunt, and S. J. Baserga (2002). "A large nucleolar U3 ribonucleoprotein required for 18S ribosomal RNA biogenesis." *Nature* 417.6892, pp. 967–970.

Drozdetskiy, A., C. Cole, J. Procter, and G. J. Barton (2015). "JPred4: a protein secondary structure prediction server". *Nucleic Acids Research* 43.W1, W389–W394.

Dutca, L. M. and G. M. Culver (2008). "Assembly of the 5' and 3' Minor Domains of 16S Ribosomal RNA as Monitored by Tethered Probing from Ribosomal Protein S20". *Journal of Molecular Biology* 376.1, pp. 92–108.

Eisinger, D. P., F. A. Dick, E. Denke, and B. L. Trumpower (1997). "SQT1, which encodes an essential WD domain protein of Saccharomyces cerevisiae, suppresses dominant-negative mutations of the ribosomal protein gene QSR1." *Molecular and Cellular Biology* 17.9, pp. 5146–5155.

Ellis, S. R. (2014). "Nucleolar stress in Diamond Blackfan anemia pathophysiology." *Biochim Biophys Acta* 1842.6, pp. 765–768.

Ellwood, M. and M. Nomura (1982). "Chromosomal locations of the genes for rRNA in Escherichia coli K-12." *J Bacteriol* 149.2, pp. 458–468.

Emery, B., J. De La Cruz, S. Rocak, O. Deloche, and P. Linder (2004). "Has1p, a member of the DEAD-box family, is required for 40S ribosomal subunit biogenesis in Saccharomyces cerevisiae†". *Molecular Microbiology* 52.1, pp. 141–158.

Engemann, S., E. Herfurth, U. Briesemeister, and B. Wittmann-Liebold (1995). "Amino acid sequence of the ribosomal protein HS23 from the halophilic Haloarcula marismortui and homology studies to other ribosomal proteins." *J Protein Chem* 14.4, pp. 189–195.

Eperon, I. C., S. Anderson, and D. P. Nierlich (1980). "Distinctive sequence of human mitochondrial ribosomal RNA genes." *Nature* 286.5772, pp. 460–467.

Eschrich, D., M. Buchhaupt, P. Kötter, and K.-D. Entian (2002). "Nep1p (Emg1p), a novel protein conserved in eukaryotes and archaea, is involved in ribosome biogenesis". *Current Genetics* 40.5, pp. 326–338.

Ettema, T. J. G., A.-C. Lindås, and R. Bernander (2011). "An actin-based cytoskeleton in archaea." *Mol Microbiol* 80.4, pp. 1052–1061.

Faber, A. W., H. R. Vos, J. C. Vos, and H. A. Raué (2006). "5'-End formation of yeast 5.8SL rRNA is an endonucleolytic event". *Biochemical and Biophysical Research Communications* 345.2, pp. 796–802.

Falahati, H., B. Pelham-Webb, S. Blythe, and E. Wieschaus (2016). "Nucleation by rRNA Dictates the Precision of Nucleolus Assembly". *Current Biology* 26.3, pp. 277–285.

Falahati, H. and E. Wieschaus (2017). "Independent active and thermodynamic processes govern the nucleolus assembly in vivo". *Proceedings of the National Academy of Sciences*, p. 201615395.

Fatica, A., A. D. Cronshaw, M. Dlakić, and D. Tollervey (2002). "Ssf1p prevents premature processing of an early pre-60S ribosomal particle." *Mol Cell* 9.2, pp. 341–351.

Feric, M., N. Vaidya, T. S. Harmon, D. M. Mitrea, L. Zhu, T. M. Richardson, R. W. Kriwacki, R. V. Pappu, and C. P. Brangwynne (2016). "Coexisting Liquid Phases Underlie Nucleolar Subcompartments". *Cell* 165.7, pp. 1686–1697.

Fernandez-Pevida, A., O. Rodriguez-Galan, A. Diaz-Quintana, D. Kressler, and J. de la Cruz (2012). "Yeast Ribosomal Protein L40 Assembles Late into Precursor 60 S Ribosomes and Is Required for Their Cytoplasmic Maturation". *Journal of Biological Chemistry* 287.45, pp. 38390–38407.

Ferreira-Cerca, S., G. Pöll, P.-E. Gleizes, H. Tschochner, and P. Milkereit (2005). "Roles of Eukaryotic Ribosomal Proteins in Maturation and Transport of Pre-18S rRNA and Ribosome Function". *Molecular Cell* 20.2, pp. 263–275.

Ferreira-Cerca, S., G. Pöll, H. Kühn, A. Neueder, S. Jakob, H. Tschochner, and P. Milkereit (2007). "Analysis of the In Vivo Assembly Pathway of Eukaryotic 40S Ribosomal Proteins". *Molecular Cell* 28.3, pp. 446–457.

Forterre, P. (2015). "The universal tree of life: an update." *Front Microbiol* 6, p. 717.

Foster, P. G., C. J. Cox, and T. M. Embley (2009). "The primary divisions of life: a phylogenomic approach employing composition-heterogeneous methods." *Philos Trans R Soc Lond B Biol Sci* 364.1527, pp. 2197–2207.

Fox, G. E. and C. R. Woese (1975). "5S RNA secondary structure." *Nature* 256.5517, pp. 505–507.

Fox, G. E. (2010). "Origin and evolution of the ribosome." *Cold Spring Harb Perspect Biol* 2.9, a003483.

French, S. L., Y. N. Osheim, F. Cioci, M. Nomura, and A. L. Beyer (2003). "In exponentially growing Saccharomyces cerevisiae cells, rRNA synthesis is determined by the summed RNA polymerase I loading rate rather than by the number of active genes." *Mol Cell Biol* 23.5, pp. 1558–1568.

Gadal, O., D. Strauss, J. Kessl, B. Trumpower, D. Tollervey, and E. Hurt (2001). "Nuclear export of 60s ribosomal subunits depends on Xpo1p and requires a nuclear export sequence-containing factor, Nmd3p, that associates with the large subunit protein Rpl10p." *Mol Cell Biol* 21.10, pp. 3405–3415.

Gamalinda, M., J. Jakovljevic, R. Babiano, J. Talkish, J. de la Cruz, and J. L. Woolford Jr (2013). "Yeast polypeptide exit tunnel ribosomal proteins L17, L35 and L37 are necessary to recruit late-assembling factors required for 27SB pre-rRNA processing." *Nucleic Acids Res* 41.3, pp. 1965–1983.

Gamalinda, M., U. Ohmayer, J. Jakovljevic, B. Kumcuoglu, J. Woolford, B. Mbom, L. Lin, and J. L. Woolford Jr (2014). "A hierarchical model for assembly of eukaryotic 60S ribosomal subunit domains." *Genes Dev* 28.2, pp. 198–210.

Ganot, P., M. L. Bortolin, and T. Kiss (1997). "Site-specific pseudouridine formation in preribosomal RNA is guided by small nucleolar RNAs." *Cell* 89.5, pp. 799–809.

Garbarino, J. E. and I. R. Gibbons (2002). "Expression and genomic analysis of midasin, a novel and highly conserved AAA protein distantly related to dynein." *BMC Genomics* 3, p. 18.

Gaspin, C., J. Cavaillé, G. Erauso, and J. P. Bachellerie (2000). "Archaeal homologs of eukaryotic methylation guide small nucleolar RNAs: lessons from the Pyrococcus genomes." *J Mol Biol* 297.4, pp. 895–906.

Gasse, L., D. Flemming, and E. Hurt (2015). "Coordinated Ribosomal ITS2 RNA Processing by the Las1 Complex Integrating Endonuclease, Polynucleotide Kinase, and Exonuclease Activities." *Mol Cell* 60.5, pp. 808–815.

Gaudet, P., P.-A. Michel, M. Zahn-Zabal, I. Cusin, P. D. Duek, O. Evalet, A. Gateau, A. Gleizes, M. Pereira, D. Teixeira, Y. Zhang, L. Lane, and A. Bairoch (2015). "The neXtProt knowledgebase on human proteins: current status". *Nucleic Acids Research* 43.D1, pp. D764–D770.

Gerbi, S. A. (1986). "The evolution of eukaryotic ribosomal DNA." *Biosystems* 19.4, pp. 247–258.

Gerbi, S. A. (1996). "Expansion segments: regions of variable size that interrupt the universal core secondary structure of ribosomal RNA." In: *Ribosomal RNA: Structure, Evolution, Processing and Function in Protein Synthesis*. Ed. by R. Zimmermann and A. Dahlberg. Telford - CRC Press, Boca Raton, FL, pp. 71–87.

Ghalei, H., F. X. Schaub, J. R. Doherty, Y. Noguchi, W. R. Roush, J. L. Cleveland, M. E. Stroupe, and K. Karbstein (2015). "Hrr25/CK1delta-directed release of Ltv1 from pre-40S ribosomes is necessary for ribosome assembly and cell growth". *The Journal of Cell Biology* 208.6, pp. 745–759.

Gietz, R. D. and R. A. Woods (2002). "Transformation of yeast by lithium acetate/single-stranded carrier DNA/polyethylene glycol method." *Methods Enzymol* 350, pp. 87–96.

Gigova, A., S. Duggimpudi, T. Pollex, M. Schaefer, and M. Koš (2014). "A cluster of methylations in the domain IV of 25S rRNA is required for ribosome stability". *RNA* 20.10, pp. 1632–1644.

Gilbert, W. (1986). "Origin of life: The RNA world". *Nature* 319.6055, pp. 618–618.

Gilbert, W. V. (2011). "Functional specialization of ribosomes?" *Trends Biochem Sci* 36.3, pp. 127–132.

Glader, B. E., K. Backer, and L. K. Diamond (1983). "Elevated erythrocyte adenosine deaminase activity in congenital hypoplastic anemia." *N Engl J Med* 309.24, pp. 1486–1490.

Glotz, C. and R. Brimacombe (1980). "An experimentally-derived model for the secondary structure of the 16S ribosomal RNA from Escherichia coli." *Nucleic Acids Res* 8.11, pp. 2377–2395.

Glotz, C., C. Zwieb, R. Brimacombe, K. Edwards, and H. Kössel (1981). "Secondary structure of the large subunit ribosomal RNA from Escherichia coli, Zea mays chloroplast, and human and mouse mitochondrial ribosomes." *Nucleic Acids Res* 9.14, pp. 3287–3306.

Graifer, D. and G. Karpova (2015). "Interaction of tRNA with eukaryotic ribosome." *Int J Mol Sci* 16.4, pp. 7173–7194.

Grandi, P., V. Rybin, J. Baßler, E. Petfalski, D. Strauß, M. Marzioch, T. Schäfer, B. Kuster, H. Tschochner, D. Tollervey, A. C. Gavin, and E. Hurt (2002). "90S Pre-Ribosomes Include the 35S Pre-rRNA, the U3 snoRNP, and 40S Subunit Processing Factors but Predominantly Lack 60S Synthesis Factors". *Molecular Cell* 10.1, pp. 105–115.

Gros, F., H. Hiatt, W. Gilbert, C. G. Kurland, R. W. Risebrough, and J. D. Watson (1961). "Unstable ribonucleic acid revealed by pulse labelling of Escherichia coli." *Nature* 190, pp. 581–585.

Gunderson, J. H., M. L. Sogin, G. Wollett, M. Hollingdale, V. F. de la Cruz, A. P. Waters, and T. F. McCutchan (1987). "Structurally distinct, stage-specific ribosomes occur in Plasmodium." *Science* 238.4829, pp. 933–937.

Gupta, V. and J. R. Warner (2014). "Ribosome-omics of the human ribosome." *RNA* 20.7, pp. 1004–1013.

Gutell, R. R., N. Larsen, and C. R. Woese (1994). "Lessons from an evolving rRNA: 16S and 23S rRNA structures from a comparative perspective." *Microbiol Rev* 58.1, pp. 10–26.

Guy, L. and T. J. G. Ettema (2011). “The archaeal ’TACK’ superphylum and the origin of eukaryotes.” *Trends Microbiol* 19.12, pp. 580–587.

Guy, L., J. H. Saw, and T. J. G. Ettema (2014). “The archaeal legacy of eukaryotes: a phylogenomic perspective.” *Cold Spring Harb Perspect Biol* 6.10, a016022.

Hackmann, A., T. Gross, C. Baierlein, and H. Krebber (2011). “The mRNA export factor Npl3 mediates the nuclear export of large ribosomal subunits”. *EMBO reports* 12.10, pp. 1024–1031.

Hage, A. E. and D. Tollervey (2004). “A surfeit of factors: why is ribosome assembly so much more complicated in eukaryotes than bacteria?” *RNA Biol* 1.1, pp. 10–15.

Hall, B. D. and P. Doty (1959). “The preparation and physical chemical properties of ribonucleic acid from microsomal particles”. *Journal of Molecular Biology* 1.2, pp. 111–126.

Halperin, D. S. and M. H. Freedman (1989). “Diamond-blackfan anemia: etiology, pathophysiology, and treatment.” *Am J Pediatr Hematol Oncol* 11.4, pp. 380–394.

Harnpicharnchai, P., J. Jakovljevic, E. Horsey, T. Miles, J. Roman, M. Rout, D. Meagher, B. Imai, Y. Guo, C. J. Brame, J. Shabanowitz, D. F. Hunt, and J. Woolford Jr (2001). “Composition and functional characterization of yeast 66S ribosome assembly intermediates.” *Mol Cell* 8.3, pp. 505–515.

Hashem, Y., A. des Georges, J. Fu, S. N. Buss, F. Jossinet, A. Jobe, Q. Zhang, H. Y. Liao, R. A. Grassucci, C. Bajaj, E. Westhof, S. Madison-Antenucci, and J. Frank (2013). “High-resolution cryo-electron microscopy structure of the Trypanosoma brucei ribosome.” *Nature* 494.7437, pp. 385–389.

Hedges, J., M. West, and A. W. Johnson (2005). “Release of the export adapter, Nmd3p, from the 60S ribosomal subunit requires Rpl10p and the cytoplasmic GTPase Lsg1p”. *The EMBO Journal* 24.3, pp. 567–579.

Held, W. A., B. Ballou, S. Mizushima, and M. Nomura (1974). “Assembly mapping of 30 S ribosomal proteins from Escherichia coli. Further studies.” *J Biol Chem* 249.10, pp. 3103–3111.

Held, W. A., S. Mizushima, and M. Nomura (1973). “Reconstitution of Escherichia coli 30 S ribosomal subunits from purified molecular components.” *J Biol Chem* 248.16, pp. 5720–5730.

Hellmich, U. A., B. L. Weis, A. Lioutikov, J. P. Wurm, M. Kaiser, N. A. Christ, K. Hantke, P. Kotter, K.-D. Entian, E. Schleiff, and J. Wöhnert (2013). “Essential ribosome assembly factor Fap7 regulates a hierarchy of RNA-protein interactions during small ribosomal subunit biogenesis”. *Proceedings of the National Academy of Sciences* 110.38, pp. 15253–15258.

Henras, A. K., C. Plisson-Chastang, M.-F. O’Donohue, A. Chakraborty, and P.-E. Gleizes (2015). “An overview of pre-ribosomal RNA processing in eukaryotes.” *Wiley Interdiscip Rev RNA* 6.2, pp. 225–242.

Hernandez-Verdun, D., P. Roussel, M. Thiry, V. Sirri, and D. L. J. Lafontaine (2010). “The nucleolus: structure/function relationship in RNA metabolism.” *Wiley Interdiscip Rev RNA* 1.3, pp. 415–431.

Hierlmeier, T., J. Merl, M. Sauert, J. Perez-Fernandez, P. Schultz, A. Bruckmann, S. Hamperl, U. Ohmayer, R. Rachel, A. Jacob, K. Hergert, R. Deutzmann, J. Griesenbeck, E. Hurt, P. Milkereit, J. Baßler, and H. Tschochner (2013). “Rrp5p, Noc1p and Noc2p form a protein module which is part of early large ribosomal subunit precursors in S. cerevisiae.” *Nucleic Acids Res* 41.2, pp. 1191–1210.

Higa-Nakamine, S., T. Suzuki, T. Uechi, A. Chakraborty, Y. Nakajima, M. Nakamura, N. Hirano, T. Suzuki, and N. Kenmochi (2011). "Loss of ribosomal RNA modification causes developmental defects in zebrafish". *Nucleic Acids Research* 40.1, pp. 391–398.

Ho, J. H., G. Kallstrom, and A. W. Johnson (2000). "Nmd3p is a Crm1p-dependent adapter protein for nuclear export of the large ribosomal subunit." *J Cell Biol* 151.5, pp. 1057–1066.

Hoagland, M. B., M. L. Stephenson, J. F. Scott, L. I. Hecht, and P. C. Zamecnik (1958). "A soluble ribonucleic acid intermediate in protein synthesis." *J Biol Chem* 231.1, pp. 241–257.

Hoagland, M. B., P. C. Zamecnik, and M. L. Stephenson (1957). "Intermediate reactions in protein biosynthesis." *Biochim Biophys Acta* 24.1, pp. 215–216.

Holzer, S., N. Ban, and S. Klinge (2013). "Crystal Structure of the Yeast Ribosomal Protein rpS3 in Complex with Its Chaperone Yar1". *Journal of Molecular Biology* 425.22, pp. 4154–4160.

Hopper, A. K. (2013). "Transfer RNA post-transcriptional processing, turnover, and subcellular dynamics in the yeast Saccharomyces cerevisiae." *Genetics* 194.1, pp. 43–67.

Hsiao, C., T. K. Lenz, J. K. Peters, P.-Y. Fang, D. M. Schneider, E. J. Anderson, T. Preeprem, J. C. Bowman, E. B. O'Neill, L. Lie, S. S. Athavale, J. J. Gossett, C. Trippe, J. Murray, A. S. Petrov, R. M. Wartell, S. C. Harvey, N. V. Hud, and L. D. Williams (2013). "Molecular paleontology: a biochemical model of the ancestral ribosome." *Nucleic Acids Res* 41.5, pp. 3373–3385.

Hsiao, C., S. Mohan, B. K. Kalahar, and L. D. Williams (2009). "Peeling the onion: ribosomes are ancient molecular fossils." *Mol Biol Evol* 26.11, pp. 2415–2425.

Hsiao, C. and L. D. Williams (2009). "A recurrent magnesium-binding motif provides a framework for the ribosomal peptidyl transferase center." *Nucleic Acids Res* 37.10, pp. 3134–3142.

Hughes, J. M. and M. Ares Jr (1991). "Depletion of U3 small nucleolar RNA inhibits cleavage in the 5' external transcribed spacer of yeast pre-ribosomal RNA and impairs formation of 18S ribosomal RNA." *EMBO J* 10.13, pp. 4231–4239.

Hughes, J. M. (1996). "Functional Base-pairing Interaction Between Highly Conserved Elements of U3 Small Nucleolar RNA and the Small Ribosomal Subunit RNA". *Journal of Molecular Biology* 259.4, pp. 645–654.

Hung, N.-J., K.-Y. Lo, S. S. Patel, K. Helmke, and A. W. Johnson (2007). "Arx1 Is a Nuclear Export Receptor for the 60S Ribosomal Subunit in Yeast". *Molecular Biology of the Cell* 19.2, pp. 735–744.

Hunziker, M., J. Barandun, E. Petfalski, D. Tan, C. Delan-Forino, K. R. Molloy, K. H. Kim, H. Dunn-Davies, Y. Shi, M. Chaker-Margot, B. T. Chait, T. Walz, D. Tollervey, and S. Klinge (2016). "UtpA and UtpB chaperone nascent pre-ribosomal RNA and U3 snoRNA to initiate eukaryotic ribosome assembly". *Nature Communications* 7, p. 12090.

Hury, J., U. Nagaswamy, M. Larios-Sanz, and G. E. Fox (2006). "Ribosome origins: the relative age of 23S rRNA Domains." *Orig Life Evol Biosph* 36.4, pp. 421–429.

Iadevaia, V., R. Liu, and C. G. Proud (2014). "mTORC1 signaling controls multiple steps in ribosome biogenesis." *Semin Cell Dev Biol* 36, pp. 113–120.

Inoue, H., H. Nojima, and H. Okayama (1990). "High efficiency transformation of Escherichia coli with plasmids." *Gene* 96.1, pp. 23–28.

Iouk, T. L., J. D. Aitchison, S. Maguire, and R. W. Wozniak (2001). "Rrb1p, a Yeast Nuclear WD-Repeat Protein Involved in the Regulation of Ribosome Biosynthesis". *Molecular and Cellular Biology* 21.4, pp. 1260–1271.

Jäkel, S., J.-M. Mingot, P. Schwarzmaier, E. Hartmann, and D. Görlich (2002). "Importins fulfil a dual function as nuclear import receptors and cytoplasmic chaperones for exposed basic domains". *The EMBO Journal* 21.3, pp. 377–386.

Jia, M. Z., S. Horita, K. Nagata, and M. Tanokura (2010). "An Archaeal Dim2-Like Protein and aDim2p and Forms a Ternary Complex with a/eIF2α and the 3' End Fragment of 16S rRNA". *Journal of Molecular Biology* 398.5, pp. 774–785.

Jomaa, A., N. Jain, J. H. Davis, J. R. Williamson, R. A. Britton, and J. Ortega (2014). "Functional domains of the 50S subunit mature late in the assembly process." *Nucleic Acids Res* 42.5, pp. 3419–3435.

Kagawa, W., T. Sagawa, H. Niki, and H. Kurumizaka (2011). "Structural basis for the DNA-binding activity of the bacterial beta-propeller protein YncE". *Acta Crystallogr D* 67.12, pp. 1045–1053.

Kandoth, C., M. D. McLellan, F. Vandin, K. Ye, B. Niu, C. Lu, M. Xie, Q. Zhang, J. F. McMichael, M. A. Wyczalkowski, M. D. M. Leiserson, C. A. Miller, J. S. Welch, M. J. Walter, M. C. Wendl, T. J. Ley, R. K. Wilson, B. J. Raphael, and L. Ding (2013). "Mutational landscape and significance across 12 major cancer types." *Nature* 502.7471, pp. 333–339.

Kappel, L., M. Loibl, G. Zisser, I. Klein, G. Fruhmann, C. Gruber, S. Unterweger, G. Rechberger, B. Pertschy, and H. Bergler (2012). "Rlp24 activates the AAA-ATPase Drg1 to initiate cytoplasmic pre-60S maturation." *J Cell Biol* 199.5, pp. 771–782.

Karbstein, K. (2011). "Inside the 40S ribosome assembly machinery". *Current Opinion in Chemical Biology* 15.5, pp. 657–663.

Kempers-Veenstra, A. E., J. Oliemans, H. Offenberg, A. F. Dekker, P. W. Piper, R. J. Planta, and J. Klootwijk (1986). "3'-End formation of transcripts from the yeast rRNA operon." *The EMBO Journal* 5.10, pp. 2703–2710.

Kent, T., Y. R. Lapik, and D. G. Pestov (2008). "The 5' external transcribed spacer in mouse ribosomal RNA contains two cleavage sites". *RNA* 15.1, pp. 14–20.

Khaitovich, P., A. S. Mankin, R. Green, L. Lancaster, and H. F. Noller (1999). "Characterization of functionally active subribosomal particles from Thermus aquaticus." *Proc Natl Acad Sci U S A* 96.1, pp. 85–90.

Kharde, S., F. R. Calviño, A. Gumiero, K. Wild, and I. Sinning (2015). "The structure of Rpf2–Rrs1 explains its role in ribosome biogenesis". *Nucleic Acids Research* 43.14, pp. 7083–7095.

Khoshnevis, S., I. Askenasy, M. C. Johnson, M. D. Dattolo, C. L. Young-Erdos, M. E. Stroupe, and K. Karbstein (2016). "The DEAD-box Protein Rok1 Orchestrates 40S and 60S Ribosome Assembly by Promoting the Release of Rrp5 from Pre-40S Ribosomes to Allow for 60S Maturation". *PLOS Biology* 14.6. Ed. by J. Cate, e1002480.

Kief, D. R. and J. R. Warner (1981). "Coordinate control of syntheses of ribosomal ribonucleic acid and ribosomal proteins during nutritional shift-up in Saccharomyces cerevisiae." *Mol Cell Biol* 1.11, pp. 1007–1015.

King, T. H., B. Liu, R. R. McCully, and M. J. Fournier (2003). "Ribosome structure and activity are altered in cells lacking snoRNPs that form pseudouridines in the peptidyl transferase center." *Mol Cell* 11.2, pp. 425–435.

Kiss-László, Z., Y. Henry, J. P. Bachellerie, M. Caizergues-Ferrer, and T. Kiss (1996). "Site-specific ribose methylation of preribosomal RNA: a novel function for small nucleolar RNAs." *Cell* 85.7, pp. 1077–1088.

Kobayashi, J. and Y. Matsuura (2013). "Structural basis for cell-cycle-dependent nuclear import mediated by the karyopherin Kap121p." *J Mol Biol* 425.11, pp. 1852–1868.

Koch, B., V. Mitterer, J. Niederhauser, T. Stanborough, G. Murat, G. Rechberger, H. Bergler, D. Kressler, and B. Pertschy (2012). "Yar1 Protects the Ribosomal Protein Rps3 from Aggregation". *Journal of Biological Chemistry* 287.26, pp. 21806–21815.

Koonin, E. V. and N. Yutin (2014). "The dispersed archaeal eukaryome and the complex archaeal ancestor of eukaryotes." *Cold Spring Harb Perspect Biol* 6.4, a016188.

Koplin, A., S. Preissler, Y. Ilina, M. Koch, A. Scior, M. Erhardt, and E. Deuerling (2010). "A dual function for chaperones SSB–RAC and the NAC nascent polypeptide–associated complex on ribosomes". *The Journal of Cell Biology* 189.1, pp. 57–68.

Kornprobst, M., M. Turk, N. Kellner, J. Cheng, D. Flemming, I. Koš-Braun, M. Koš, M. Thoms, O. Berninghausen, R. Beckmann, and E. Hurt (2016). "Architecture of the 90S Pre-ribosome: A Structural View on the Birth of the Eukaryotic Ribosome". *Cell* 166.2, pp. 380–393.

Korostelev, A., S. Trakhanov, M. Laurberg, and H. F. Noller (2006). "Crystal structure of a 70S ribosome-tRNA complex reveals functional interactions and rearrangements." *Cell* 126.6, pp. 1065–1077.

Kos, M. and D. Tollervey (2010). "Yeast pre-rRNA processing and modification occur cotranscriptionally." *Mol Cell* 37.6, pp. 809–820.

Kovacs, D., M. Rakacs, B. Agoston, K. Lenkey, K. Semrad, R. Schroeder, and P. Tompa (2009). "Janus chaperones: assistance of both RNA- and protein-folding by ribosomal proteins." *FEBS Lett* 583.1, pp. 88–92.

Kraft, C., A. Deplazes, M. Sohrmann, and M. Peter (2008). "Mature ribosomes are selectively degraded upon starvation by an autophagy pathway requiring the Ubp3p/Bre5p ubiquitin protease." *Nat Cell Biol* 10.5, pp. 602–610.

Kressler, D., G. Bange, Y. Ogawa, G. Stjepanovic, B. Bradatsch, D. Pratte, S. Amlacher, D. Strauß, Y. Yoneda, J. Katahira, I. Sinning, and E. Hurt (2012). "Synchronizing nuclear import of ribosomal proteins with ribosome assembly." *Science* 338.6107, pp. 666–671.

Kressler, D., E. Hurt, and J. Baßler (2010). "Driving ribosome assembly". *Biochimica et Biophysica Acta (BBA) - Molecular Cell Research* 1803.6, pp. 673–683.

Kressler, D., E. Hurt, H. Bergler, and J. Bassler (2012). "The power of AAA-ATPases on the road of pre-60S ribosome maturation–molecular machines that strip pre-ribosomal particles." *Biochim Biophys Acta* 1823.1, pp. 92–100.

Kressler, D., D. Roser, B. Pertschy, and E. Hurt (2008). "The AAA ATPase Rix7 powers progression of ribosome biogenesis by stripping Nsa1 from pre-60S particles." *J Cell Biol* 181.6, pp. 935–944.

Kruiswijk, T., R. J. Planta, and J. M. Krop (1978). "The course of the assembly of ribosomal subunits in yeast." *Biochim Biophys Acta* 517.2, pp. 378–389.

Kufel, J., B. Dichtl, and D. Tollervey (1999). "Yeast Rnt1p is required for cleavage of the pre-ribosomal RNA in the 3' ETS but not the 5' ETS." *RNA* 5.7, pp. 909–917.

Kurland, C. (1960). "Molecular characterization of ribonucleic acid from Escherichia coli ribosomes". *Journal of Molecular Biology* 2.2, pp. 83–91.

Lafontaine, D. L. J. (2015). "Noncoding RNAs in eukaryotic ribosome biogenesis and function". *Nature Structural & Molecular Biology* 22.1, pp. 11–19.

Lam, Y. W., A. I. Lamond, M. Mann, and J. S. Andersen (2007). "Analysis of nucleolar protein dynamics reveals the nuclear degradation of ribosomal proteins." *Curr Biol* 17.9, pp. 749–760.

Lamanna, A. C. and K. Karbstein (2009). “Nob1 binds the single-stranded cleavage site D at the 3’-end of 18S rRNA with its PIN domain”. *Proceedings of the National Academy of Sciences* 106.34, pp. 14259–14264.

LaRiviere, F. J., S. E. Cole, D. J. Ferullo, and M. J. Moore (2006). “A late-acting quality control process for mature eukaryotic rRNAs.” *Mol Cell* 24.4, pp. 619–626.

Lasek-Nesselquist, E. and J. P. Gogarten (2013). “The effects of model choice and mitigating bias on the ribosomal tree of life.” *Mol Phylogenet Evol* 69.1, pp. 17–38.

Lebaron, S., C. Schneider, R. W. van Nues, A. Swiatkowska, D. Walsh, B. Böttcher, S. Granneman, N. J. Watkins, and D. Tollervey (2012). “Proofreading of pre-40S ribosome maturation by a translation initiation factor and 60S subunits.” *Nat Struct Mol Biol* 19.8, pp. 744–753.

Lebaron, S., Å. Segerstolpe, S. L. French, T. Dudnakova, F. de lima Alves, S. Granneman, J. Rappsilber, A. L. Beyer, L. Wieslander, and D. Tollervey (2013). “Rrp5 Binding at Multiple Sites Coordinates Pre-rRNA Processing and Assembly”. *Molecular Cell* 52.5, pp. 707–719.

Lebaron, S., A. Segerstolpe, S. L. French, T. Dudnakova, F. de Lima Alves, S. Granneman, J. Rappsilber, A. L. Beyer, L. Wieslander, and D. Tollervey (2013). “Rrp5 binding at multiple sites coordinates pre-rRNA processing and assembly.” *Mol Cell* 52.5, pp. 707–719.

Lebreton, A., C. Saveanu, L. Decourty, A. Jacquier, and M. Fromont-Racine (2006). “Nsa2 is an unstable, conserved factor required for the maturation of 27 SB pre-rRNAs.” *J Biol Chem* 281.37, pp. 27099–27108.

Lecompte, O., R. Ripp, J.-C. Thierry, D. Moras, and O. Poch (2002). “Comparative analysis of ribosomal proteins in complete genomes: an example of reductive evolution at the domain scale.” *Nucleic Acids Res* 30.24, pp. 5382–5390.

Leidig, C., M. Thoms, I. Holdermann, B. Bradatsch, O. Berninghausen, G. Bange, I. Sinning, E. Hurt, and R. Beckmann (2014). “60S ribosome biogenesis requires rotation of the 5S ribonucleoprotein particle.” *Nat Commun* 5, p. 3491.

Lestrade, L. and M. J. Weber (2006). “snoRNA-LBME-db, a comprehensive database of human H/ACA and C/D box snoRNAs.” *Nucleic Acids Res* 34.Database issue, pp. D158–D162.

Li, N., Y. Chen, Q. Guo, Y. Zhang, Y. Yuan, C. Ma, H. Deng, J. Lei, and N. Gao (2013). “Cryo-EM structures of the late-stage assembly intermediates of the bacterial 50S ribosomal subunit”. *Nucleic Acids Research* 41.14, pp. 7073–7083.

Liang, X.-H., Q. Liu, and M. J. Fournier (2007). “rRNA modifications in an intersubunit bridge of the ribosome strongly affect both ribosome biogenesis and activity.” *Mol Cell* 28.6, pp. 965–977.

Liang, X.-H., Q. Liu, and M. J. Fournier (2009). “Loss of rRNA modifications in the decoding center of the ribosome impairs translation and strongly delays pre-rRNA processing.” *RNA* 15.9, pp. 1716–1728.

Lindås, A.-C., E. A. Karlsson, M. T. Lindgren, T. J. G. Ettema, and R. Bernander (2008). “A unique cell division machinery in the Archaea.” *Proc Natl Acad Sci U S A* 105.48, pp. 18942–18946.

Littauer, U. Z. and H. Eisenberg (1959). “Ribonucleic acid from Escherichia coli; preparation, characterization and physical properties.” *Biochim Biophys Acta* 32, pp. 320–337.

Littlefield, J. W., E. B. Keller, J. Gross, and P. C. Zamecnik (1955). “Studies on cytoplasmic ribonucleoprotein particles from the liver of the rat.” *J Biol Chem* 217.1, pp. 111–123.

Liu, Y., B. Schmidt, and D. L. Maskell (2010). “MSAProbs: multiple sequence alignment based on pair hidden Markov models and partition function posterior probabilities”. *Bioinformatics* 26.16, pp. 1958–1964.

Lo, K.-Y., Z. Li, C. Bussiere, S. Bresson, E. M. Marcotte, and A. W. Johnson (2010). "Defining the pathway of cytoplasmic maturation of the 60S ribosomal subunit." *Mol Cell* 39.2, pp. 196–208.

Loc'h, J., M. Blaud, S. Réty, S. Lebaron, P. Deschamps, J. Bareille, J. Jombart, J. Robert-Paganin, L. Delbos, F. Chardon, E. Zhang, C. Charenton, D. Tollervey, and N. Leulliot (2014). "RNA Mimicry by the Fap7 Adenylate Kinase in Ribosome Biogenesis". *PLoS Biology* 12.5. Ed. by G. A. Petsko, e1001860.

Lohrum, M. A. E., R. L. Ludwig, M. H. G. Kubbutat, M. Hanlon, and K. H. Vousden (2003). "Regulation of HDM2 activity by the ribosomal protein L11." *Cancer Cell* 3.6, pp. 577–587.

Luo, B.-H., C. V. Carman, and T. A. Springer (2007). "Structural basis of integrin regulation and signaling." *Annu Rev Immunol* 25, pp. 619–647.

Lygerou, Z., C. Allmang, D. Tollervey, and B. Séraphin (1996). "Accurate processing of a eukaryotic precursor ribosomal RNA by ribonuclease MRP in vitro." *Science* 272.5259, pp. 268–270.

Ma, C., S. Wu, N. Li, Y. Chen, K. Yan, Z. Li, L. Zheng, J. Lei, J. L. Woolford, and N. Gao (2017). "Structural snapshot of cytoplasmic pre-60S ribosomal particles bound by Nmd3, Lsg1, Tif6 and Reh1". *Nature Structural & Molecular Biology*.

Machnicka, M. A., A. Olchowik, H. Grosjean, and J. M. Bujnicki (2014). "Distribution and frequencies of post-transcriptional modifications in tRNAs". *RNA Biology* 11.12, pp. 1619–1629.

Madru, C., S. Lebaron, M. Blaud, L. Delbos, J. Pipoli, E. Pasmant, S. Réty, and N. Leulliot (2015). "Chaperoning 5S RNA assembly". *Genes & Development* 29.13, pp. 1432–1446.

Mahoney, S. J., J. M. Dempsey, and J. Blenis (2009). "Cell signaling in protein synthesis ribosome biogenesis and translation initiation and elongation." *Prog Mol Biol Transl Sci* 90, pp. 53–107.

Malkin, L. I. and A. Rich (1967). "Partial resistance of nascent polypeptide chains to proteolytic digestion due to ribosomal shielding." *J Mol Biol* 26.2, pp. 329–346.

Malyutin, A. G., S. Musalgaonkar, S. Patchett, J. Frank, and A. W. Johnson (2017). "Nmd3 is a structural mimic of eIF5A, and activates the cpGTPase Lsg1 during 60S ribosome biogenesis". *EMBO J*.

Manikas, R.-G., E. Thomson, M. Thoms, and E. Hurt (2016). "The K+-dependent GTPase Nug1 is implicated in the association of the helicase Dbp10 to the immature peptidyl transferase centre during ribosome maturation." *Nucleic Acids Res* 44.4, pp. 1800–1812.

Marechal, V., B. Elenbaas, J. Piette, J. C. Nicolas, and A. J. Levine (1994). "The ribosomal L5 protein is associated with mdm-2 and mdm-2-p53 complexes." *Mol Cell Biol* 14.11, pp. 7414–7420.

Markman, B., R. Dienstmann, and J. Tabernero (2010). "Targeting the PI3K/Akt/mTOR pathway–beyond rapalogs." *Oncotarget* 1.7, pp. 530–543.

Marmier-Gourrier, N., A. Clery, F. Schlotter, V. Senty-Segault, and C. Branlant (2011). "A second base pair interaction between U3 small nucleolar RNA and the 5'-ETS region is required for early cleavage of the yeast pre-ribosomal RNA". *Nucleic Acids Research* 39.22, pp. 9731–9745.

Mason, P. B. and K. Struhl (2005). "Distinction and Relationship between Elongation Rate and Processivity of RNA Polymerase II In Vivo". *Molecular Cell* 17.6, pp. 831–840.

Matsson, H., E. J. Davey, N. Draptchinskaia, I. Hamaguchi, A. Ooka, P. Levéen, E. Forsberg, S. Karlsson, and N. Dahl (2004). "Targeted disruption of the ribosomal protein S19 gene is lethal prior to implantation." *Mol Cell Biol* 24.9, pp. 4032–4037.

Matsuo, Y., S. Granneman, M. Thoms, R.-G. Manikas, D. Tollervey, and E. Hurt (2014). "Coupled GTPase and remodelling ATPase activities form a checkpoint for ribosome export." *Nature* 505.7481, pp. 112–116.

McGowan, K. A., J. Z. Li, C. Y. Park, V. Beaudry, H. K. Tabor, A. J. Sabnis, W. Zhang, H. Fuchs, M. H. de Angelis, R. M. Myers, L. D. Attardi, and G. S. Barsh (2008). "Ribosomal mutations cause p53-mediated dark skin and pleiotropic effects." *Nat Genet* 40.8, pp. 963–970.

McMahon, M. E., D. Stamenkovich, and T. D. Petes (1984). "Tandemly arranged variant 5S ribosomal RNA genes in the yeast Saccharomyces cerevisiae." *Nucleic Acids Res* 12.21, pp. 8001–8016.

McMahon, M., A. Contreras, and D. Ruggero (2014). "Small RNAs with big implications: new insights into H/ACA snoRNA function and their role in human disease". *Wiley Interdisciplinary Reviews: RNA* 6.2, pp. 173–189.

Mears, J. A., J. J. Cannone, S. M. Stagg, R. R. Gutell, R. K. Agrawal, and S. C. Harvey (2002). "Modeling a minimal ribosome based on comparative sequence analysis." *J Mol Biol* 321.2, pp. 215–234.

Melnikov, S., A. Ben-Shem, N. Garreau de Loubresse, L. Jenner, G. Yusupova, and M. Yusupov (2012). "One core, two shells: bacterial and eukaryotic ribosomes." *Nat Struct Mol Biol* 19.6, pp. 560–567.

Melnikov, S., A. Ben-Shem, G. Yusupova, and M. Yusupov (2015). "Insights into the origin of the nuclear localization signals in conserved ribosomal proteins." *Nat Commun* 6, p. 7382.

Méreau, A., R. Fournier, A. Grégoire, A. Mougin, P. Fabrizio, R. Lührmann, and C. Branlant (1997). "An in vivo and in vitro structure-function analysis of the Saccharomyces cerevisiae U3A snoRNP: protein-RNA contacts and base-pair interaction with the pre-ribosomal RNA". *Journal of Molecular Biology* 273.3, pp. 552–571.

Meyer, B., J. P. Wurm, S. Sharma, C. Immer, D. Pogoryelov, P. Kötter, D. L. J. Lafontaine, J. Wöhnert, and K.-D. Entian (2016). "Ribosome biogenesis factor Tsr3 is the aminocarboxypropyl transferase responsible for 18S rRNA hypermodification in yeast and humans." *Nucleic Acids Res* 44.9, pp. 4304–4316.

Miles, T. D., J. Jakovljevic, E. W. Horsey, P. Harnpicharnchai, L. Tang, and J. L. Woolford (2005). "Ytm1, Nop7, and Erb1 Form a Complex Necessary for Maturation of Yeast 66S Preribosomes". *Molecular and Cellular Biology* 25.23, pp. 10419–10432.

Miller Jr, O. and B. R. Beatty (1969). "Visualization of nucleolar genes." *Science* 164.3882, pp. 955–957.

Mitterer, V., N. Gantenbein, R. Birner-Gruenberger, G. Murat, H. Bergler, D. Kressler, and B. Pertschy (2016). "Nuclear import of dimerized ribosomal protein Rps3 in complex with its chaperone Yar1". *Scientific Reports* 6, p. 36714.

Mitterer, V., G. Murat, S. Réty, M. Blaud, L. Delbos, T. Stanborough, H. Bergler, N. Leulliot, D. Kressler, and B. Pertschy (2016). "Sequential domain assembly of ribosomal protein S3 drives 40S subunit maturation". *Nature Communications* 7, p. 10336.

Mizushima, S. and M. Nomura (1970). "Assembly mapping of 30S ribosomal proteins from E. coli." *Nature* 226.5252, p. 1214.

Monro, R. E. (1967). "Catalysis of peptide bond formation by 50 S ribosomal subunits from Escherichia coli." *J Mol Biol* 26.1, pp. 147–151.

Moon, A. F., G. A. Mueller, X. Zhong, and L. C. Pedersen (2010). "A synergistic approach to protein crystallization: combination of a fixed-arm carrier with surface entropy reduction." *Protein Sci* 19.5, pp. 901–913.

Mougey, E. B., M. O'Reilly, Y. Osheim, O. Miller Jr, A. Beyer, and B. Sollner-Webb (1993). "The terminal balls characteristic of eukaryotic rRNA transcription units in chromatin spreads are rRNA processing complexes." *Genes Dev* 7.8, pp. 1609–1619.

Mulder, A. M., C. Yoshioka, A. H. Beck, A. E. Bunner, R. A. Milligan, C. S. Potter, B. Carragher, and J. R. Williamson (2010). "Visualizing Ribosome Biogenesis: Parallel Assembly Pathways for the 30S Subunit". *Science* 330.6004, pp. 673–677.

Narla, A. and B. L. Ebert (2010). "Ribosomopathies: human disorders of ribosome dysfunction." *Blood* 115.16, pp. 3196–3205.

Nerurkar, P., M. Altvater, S. Gerhardy, S. Schütz, U. Fischer, C. Weirich, and V. G. Panse (2015). "Eukaryotic Ribosome Assembly and Nuclear Export." *Int Rev Cell Mol Biol* 319, pp. 107–140.

Neyer, S., M. Kunz, C. Geiss, M. Hantsche, V.-V. Hodirnau, A. Seybert, C. Engel, M. P. Scheffer, P. Cramer, and A. S. Frangakis (2016). "Structure of RNA polymerase I transcribing ribosomal DNA genes". *Nature*.

Ni, J., A. L. Tien, and M. J. Fournier (1997). "Small nucleolar RNAs direct site-specific synthesis of pseudouridine in ribosomal RNA." *Cell* 89.4, pp. 565–573.

Ni, X., J. H. Davis, N. Jain, A. Razi, S. Benlekbir, A. G. McArthur, J. L. Rubinstein, R. A. Britton, J. R. Williamson, and J. Ortega (2016). "YphC and YsxC GTPases assist the maturation of the central protuberance, GTPase associated region and functional core of the 50S ribosomal subunit". *Nucleic Acids Research* 44.17, pp. 8442–8455.

Nicholas, M. P., F. Berger, L. Rao, S. Brenner, C. Cho, and A. Gennerich (2015). "Cytoplasmic dynein regulates its attachment to microtubules via nucleotide state-switched mechanosensing at multiple AAA domains". *Proc Natl Acad Sci USA* 112.20, pp. 6371–6376.

Nicolas, E., P. Parisot, C. Pinto-Monteiro, R. de Walque, C. De Vleeschouwer, and D. L. J. Lafontaine (2016). "Involvement of human ribosomal proteins in nucleolar structure and p53-dependent nucleolar stress." *Nat Commun* 7, p. 11390.

Nicoloso, M., L. H. Qu, B. Michot, and J. P. Bachellerie (1996). "Intron-encoded, antisense small nucleolar RNAs: the characterization of nine novel species points to their direct role as guides for the 2'-O-ribose methylation of rRNAs." *J Mol Biol* 260.2, pp. 178–195.

Nierhaus, K. H. and F. Dohme (1974). "Total reconstitution of functionally active 50S ribosomal subunits from Escherichia coli." *Proc Natl Acad Sci U S A* 71.12, pp. 4713–4717.

Nirenberg, M. W. and J. H. Matthaei (1961). "The dependence of cell-free protein synthesis in E. coli upon naturally occurring or synthetic polyribonucleotides." *Proc Natl Acad Sci U S A* 47, pp. 1588–1602.

Nissan, T. A., J. Bassler, E. Petfalski, D. Tollervey, and E. Hurt (2002). "60S pre-ribosome formation viewed from assembly in the nucleolus until export to the cytoplasm." *EMBO J* 21.20, pp. 5539–5547.

Nissen, P., J. Hansen, N. Ban, P. B. Moore, and T. A. Steitz (2000). "The structural basis of ribosome activity in peptide bond synthesis." *Science* 289.5481, pp. 920–930.

Nissen, P., J. A. Ippolito, N. Ban, P. B. Moore, and T. A. Steitz (2001). "RNA tertiary interactions in the large ribosomal subunit: the A-minor motif." *Proc Natl Acad Sci U S A* 98.9, pp. 4899–4903.

Nomura, M. (1973). "Assembly of bacterial ribosomes." *Science* 179.4076, pp. 864–873.

O'Donohue, M.-F., V. Choesmel, M. Faubladier, G. Fichant, and P.-E. Gleizes (2010). "Functional dichotomy of ribosomal proteins during the synthesis of mammalian 40S ribosomal subunits". *The Journal of Cell Biology* 190.5, pp. 853–866.

Omer, A. D., T. M. Lowe, A. G. Russell, H. Ebhardt, S. R. Eddy, and P. P. Dennis (2000). "Homologs of small nucleolar RNAs in Archaea." *Science* 288.5465, pp. 517–522.

Orgel, L. E. (1968). "Evolution of the genetic apparatus." *J Mol Biol* 38.3, pp. 381–393.

Orsolic, I., D. Jurada, N. Pullen, M. Oren, A. G. Eliopoulos, and S. Volarevic (2016). "The relationship between the nucleolus and cancer: Current evidence and emerging paradigms." *Semin Cancer Biol* 37-38, pp. 36–50.

Osheim, Y. N., S. L. French, K. M. Keck, E. A. Champion, K. Spasov, F. Dragon, S. J. Baserga, and A. L. Beyer (2004). "Pre-18S Ribosomal RNA Is Structurally Compacted into the SSU Processome Prior to Being Cleaved from Nascent Transcripts in Saccharomyces cerevisiae". *Molecular Cell* 16.6, pp. 943–954.

Palade, G. E. (1955). "A small particulate component of the cytoplasm." *J Biophys Biochem Cytol* 1.1, pp. 59–68.

Pausch, P., U. Singh, Y. L. Ahmed, B. Pillet, G. Murat, F. Altegoer, G. Stier, M. Thoms, E. Hurt, I. Sinning, G. Bange, and D. Kressler (2015). "Co-translational capturing of nascent ribosomal proteins by their dedicated chaperones." *Nat Commun* 6, p. 7494.

Pel, D. M. van, P. C. Stirling, S. W. Minaker, P. Sipahimalani, and P. Hieter (2013). "Saccharomyces cerevisiae Genetics Predicts Candidate Therapeutic Genetic Interactions at the Mammalian Replication Fork". *G3; Genes|Genomes|Genetics* 3.2, pp. 273–282.

Pertschy, B., C. Schneider, M. Gnadig, T. Schafer, D. Tollervey, and E. Hurt (2009). "RNA Helicase Prp43 and Its Co-factor Pfa1 Promote 20 to 18 S rRNA Processing Catalyzed by the Endonuclease Nob1". *Journal of Biological Chemistry* 284.50, pp. 35079–35091.

Pertschy, B., C. Saveanu, G. Zisser, A. Lebreton, M. Tengg, A. Jacquier, E. Liebminger, B. Nobis, L. Kappel, I. van der Klei, G. Högenauer, M. Fromont-Racine, and H. Bergler (2007). "Cytoplasmic recycling of 60S preribosomal factors depends on the AAA protein Drg1." *Mol Cell Biol* 27.19, pp. 6581–6592.

Petfalski, E., T. Dandekar, Y. Henry, and D. Tollervey (1997). "Processing of the Precursors to Small Nucleolar RNAs and rRNAs Requires Common Components". *Molecular and Cellular Biology* 18.3, pp. 1181–1189.

Petrov, A. S., C. R. Bernier, B. Gulen, C. C. Waterbury, E. Hershkovits, C. Hsiao, S. C. Harvey, N. V. Hud, G. E. Fox, R. M. Wartell, and L. D. Williams (2014). "Secondary structures of rRNAs from all three domains of life." *PLoS One* 9.2, e88222.

Petrov, A. S., C. R. Bernier, E. Hershkovits, Y. Xue, C. C. Waterbury, C. Hsiao, V. G. Stepanov, E. A. Gaucher, M. A. Grover, S. C. Harvey, N. V. Hud, R. M. Wartell, G. E. Fox, and L. D. Williams (2013). "Secondary structure and domain architecture of the 23S and 5S rRNAs." *Nucleic Acids Res* 41.15, pp. 7522–7535.

Petrov, A. S., C. R. Bernier, C. Hsiao, A. M. Norris, N. A. Kovacs, C. C. Waterbury, V. G. Stepanov, S. C. Harvey, G. E. Fox, R. M. Wartell, N. V. Hud, and L. D. Williams (2014). "Evolution of the ribosome at atomic resolution." *Proc Natl Acad Sci U S A* 111.28, pp. 10251–10256.

Petrov, A. S., B. Gulen, A. M. Norris, N. A. Kovacs, C. R. Bernier, K. A. Lanier, G. E. Fox, S. C. Harvey, R. M. Wartell, N. V. Hud, and L. D. Williams (2015). "History of the ribosome and the origin of translation." *Proc Natl Acad Sci U S A* 112.50, pp. 15396–15401.

Pettersen, E. F., T. D. Goddard, C. C. Huang, G. S. Couch, D. M. Greenblatt, E. C. Meng, and T. E. Ferrin (2004). "UCSF Chimera–a visualization system for exploratory research and analysis." *J Comput Chem* 25.13, pp. 1605–1612.

Piekna-Przybylska, D., P. Przybylski, A. Baudin-Baillieu, J.-P. Rousset, and M. J. Fournier (2008). "Ribosome Performance Is Enhanced by a Rich Cluster of Pseudouridines in the A-site Finger Region of the Large Subunit". *Journal of Biological Chemistry* 283.38, pp. 26026–26036.

Piekna-Przybylska, D., W. A. Decatur, and M. J. Fournier (2008). "The 3D rRNA modification maps database: with interactive tools for ribosome analysis." *Nucleic Acids Res* 36.Database issue, pp. D178–D183.

Pillet, B., J. J. Garca-Gomez, P. Pausch, L. Falquet, G. Bange, J. de la Cruz, and D. Kressler (2015). "The Dedicated Chaperone Acl4 Escorts Ribosomal Protein Rpl4 to Its Nuclear Pre-60S Assembly Site." *PLoS Genet* 11.10, e1005565.

Pillet, B., V. Mitterer, D. Kressler, and B. Pertschy (2016). "Hold on to your friends: Dedicated chaperones of ribosomal proteins". *BioEssays*.

Porter, K. R. (1954). "Electron microscopy of basophilic components of cytoplasm." *J Histochem Cytochem* 2.5, pp. 346–375.

Ramaswamy, P. and S. A. Woodson (2009a). "Global stabilization of rRNA structure by ribosomal proteins S4, S17, and S20." *J Mol Biol* 392.3, pp. 666–677.

Ramaswamy, P. and S. A. Woodson (2009b). "S16 throws a conformational switch during assembly of 30S 5' domain." *Nat Struct Mol Biol* 16.4, pp. 438–445.

Ramesh, M. and J. L. Woolford Jr (2016). "Eukaryote-specific rRNA expansion segments function in ribosome biogenesis." *RNA* 22.8, pp. 1153–1162.

Rheinberger, H. J., H. Sternbach, and K. H. Nierhaus (1981). "Three tRNA binding sites on Escherichia coli ribosomes." *Proc Natl Acad Sci U S A* 78.9, pp. 5310–5314.

Rich, A. (1962). "On the problems of evolution and biochemical information transfer". In: *Horizons in biochemistry*. Ed. by P. B. Kasha M. Academic, New York, pp. 103–126.

Rigaut, G., A. Shevchenko, B. Rutz, M. Wilm, M. Mann, and B. Séraphin (1999). "A generic protein purification method for protein complex characterization and proteome exploration." *Nat Biotechnol* 17.10, pp. 1030–1032.

Rivera, M. C., R. Jain, J. E. Moore, and J. A. Lake (1998). "Genomic evidence for two functionally distinct gene classes." *Proc Natl Acad Sci U S A* 95.11, pp. 6239–6244.

Roberts, R. B. (1958). *Microsomal particles and protein synthesis; papers presented at the First Symposium of the Biophysical Society, at the Massachusetts Institute of Technology, Cambridge, February 5, 6, and 8, 1958.* Ed. by R. B. Roberts. New York, Published on behalf of the Washington Academy of Sciences, Washington, D.C., by Pergamon Press, p. 188.

Rosen, N. and Q.-B. She (2006). "AKT and cancer–is it all mTOR?" *Cancer Cell* 10.4, pp. 254–256.

Rout, M. P., G. Blobel, and J. D. Aitchison (1997). "A Distinct Nuclear Import Pathway Used by Ribosomal Proteins". *Cell* 89.5, pp. 715–725.

Royet, J., T. Bouwmeester, and S. M. Cohen (1998). "Notchless encodes a novel WD40-repeat-containing protein that modulates Notch signaling activity." *EMBO J* 17.24, pp. 7351–7360.

Ruggero, D., L. Montanaro, L. Ma, W. Xu, P. Londei, C. Cordon-Cardo, and P. P. Pandolfi (2004). "The translation factor eIF-4E promotes tumor formation and cooperates with c-Myc in lymphomagenesis." *Nat Med* 10.5, pp. 484–486.

Sambrook, J., E. Fritsch, and T. Maniatis (1989). *Molecular cloning: a laboratory manual*. Molecular Cloning: A Laboratory Manual Bd. 2. Cold Spring Harbor Laboratory.

Sardana, R., X. Liu, S. Granneman, J. Zhu, M. Gill, O. Papoulas, E. M. Marcotte, D. Tollervey, C. C. Correll, and A. W. Johnson (2015). "The DEAH-box Helicase Dhr1 Dissociates U3 from the Pre-rRNA to Promote Formation of the Central Pseudoknot". *PLOS Biology* 13.2. Ed. by J. Cate, e1002083.

Sarkar, A., M. Pech, M. Thoms, R. Beckmann, and E. Hurt (2016). "Ribosome-stalk biogenesis is coupled with recruitment of nuclear-export factor to the nascent 60S subunit". *Nature Structural & Molecular Biology* 23.12, pp. 1074–1082.

Sato, A., G. Kobayashi, H. Hayashi, H. Yoshida, A. Wada, M. Maeda, S. Hiraga, K. Takeyasu, and C. Wada (2005). "The GTP binding protein Obg homolog ObgE is involved in ribosome maturation." *Genes Cells* 10.5, pp. 393–408.

Saveanu, C., A. Namane, P.-E. Gleizes, A. Lebreton, J.-C. Rousselle, J. Noaillac-Depeyre, N. Gas, A. Jacquier, and M. Fromont-Racine (2003). "Sequential Protein Association with Nascent 60S Ribosomal Particles". *Molecular and Cellular Biology* 23.13, pp. 4449–4460.

Schäfer, T., B. Maco, E. Petfalski, D. Tollervey, B. Böttcher, U. Aebi, and E. Hurt (2006). "Hrr25-dependent phosphorylation state regulates organization of the pre-40S subunit". *Nature* 441.7093, pp. 651–655.

Schäfer, T., D. Strauß, E. Petfalski, D. Tollervey, and E. Hurt (2003). "The path from nucleolar 90S to cytoplasmic 40S pre-ribosomes". *The EMBO Journal* 22.6, pp. 1370–1380.

Schaper, S., M. Fromont-Racine, P. Linder, J. de la Cruz, A. Namane, and M. Yaniv (2001). "A yeast homolog of chromatin assembly factor 1 is involved in early ribosome assembly." *Curr Biol* 11.23, pp. 1885–1890.

Schluenzen, F., A. Tocilj, R. Zarivach, J. Harms, M. Gluehmann, D. Janell, A. Bashan, H. Bartels, I. Agmon, F. Franceschi, and A. Yonath (2000). "Structure of functionally activated small ribosomal subunit at 3.3 angstroms resolution." *Cell* 102.5, pp. 615–623.

Schnare, M. N., S. H. Damberger, M. W. Gray, and R. R. Gutell (1996). "Comprehensive comparison of structural characteristics in eukaryotic cytoplasmic large subunit (23 S-like) ribosomal RNA." *J Mol Biol* 256.4, pp. 701–719.

Schraivogel, D. (2009). "Charakterisierung der Interaktion von Rsa4 und Nsa2, zweier essentieller Faktoren bei der 60S-Biogenese". Diplomathesis. University Heidelberg, Heidelberg, Germany.

Schütz, S., U. Fischer, M. Altvater, P. Nerurkar, C. Peña, M. Gerber, Y. Chang, S. Caesar, O. T. Schubert, G. Schlenstedt, and V. G. Panse (2014). "A RanGTP-independent mechanism allows ribosomal protein nuclear import for ribosome assembly." *Elife* 3, e03473.

Schuwirth, B. S., M. A. Borovinskaya, C. W. Hau, W. Zhang, A. Vila-Sanjurjo, J. M. Holton, and J. H. D. Cate (2005). "Structures of the bacterial ribosome at 3.5 A resolution." *Science* 310.5749, pp. 827–834.

Selmer, M., C. M. Dunham, F. V. Murphy 4th, A. Weixlbaumer, S. Petry, A. C. Kelley, J. R. Weir, and V. Ramakrishnan (2006). "Structure of the 70S ribosome complexed with mRNA and tRNA." *Science* 313.5795, pp. 1935–1942.

Semrad, K., R. Green, and R. Schroeder (2004). "RNA chaperone activity of large ribosomal subunit proteins from Escherichia coli." *RNA* 10.12, pp. 1855–1860.

Senger, B., D. L. Lafontaine, J.-S. Graindorge, O. Gadal, A. Camasses, A. Sanni, J.-M. Garnier, M. Breitenbach, E. Hurt, and F. Fasiolo (2001). "The Nucle(ol)ar Tif6p and Efl1p Are Required for a Late Cytoplasmic Step of Ribosome Synthesis". *Molecular Cell* 8.6, pp. 1363–1373.

Shajani, Z., M. T. Sykes, and J. R. Williamson (2011). "Assembly of bacterial ribosomes." *Annu Rev Biochem* 80, pp. 501–526.

Shammas, C., T. F. Menne, C. Hilcenko, S. R. Michell, B. Goyenechea, G. R. B. Boocock, P. R. Durie, J. M. Rommens, and A. J. Warren (2005). "Structural and Mutational Analysis of the SBDS Protein Family: INSIGHT INTO THE LEUKEMIA-ASSOCIATED SHWACHMAN-DIAMOND SYNDROME". *Journal of Biological Chemistry* 280.19, pp. 19221–19229.

Sharma, K. and D. Tollervey (1999). "Base Pairing between U3 Small Nucleolar RNA and the 5' End of 18S rRNA Is Required for Pre-rRNA Processing". *Molecular and Cellular Biology* 19.9, pp. 6012–6019.

Sharma, S., J. Yang, P. Watzinger, P. Kotter, and K.-D. Entian (2013). "Yeast Nop2 and Rcm1 methylate C2870 and C2278 of the 25S rRNA, respectively". *Nucleic Acids Research* 41.19, pp. 9062–9076.

Sharma, S. and D. L. J. Lafontaine (2015). "'View From A Bridge': A New Perspective on Eukaryotic rRNA Base Modification." *Trends Biochem Sci* 40.10, pp. 560–575.

Sherman, F. (1991). "Getting started with yeast." *Methods Enzymol* 194, pp. 3–21.

Sievers, F., A. Wilm, D. Dineen, T. J. Gibson, K. Karplus, W. Li, R. Lopez, H. McWilliam, M. Remmert, J. Söding, J. D. Thompson, and D. G. Higgins (2014). "Fast, scalable generation of high-quality protein multiple sequence alignments using Clustal Omega". *Molecular Systems Biology* 7.1, pp. 539–539.

Sjostrand, F. S. and V. Hanzon (1954). "Membrane structures of cytoplasm and mitochondria in exocrine cells of mouse pancreas as revealed by high resolution electron microscopy." *Exp Cell Res* 7.2, pp. 393–414.

Slautterback, D. B. (1953). "Electron microscopic studies of small cytoplasmic particles (microsomes)." *Exp Cell Res* 5.1, pp. 173–186.

Söding, J., A. Biegert, and A. N. Lupas (2005). "The HHpred interactive server for protein homology detection and structure prediction." *Nucleic Acids Res* 33.Web Server issue, W244–W248.

Spang, A., J. H. Saw, S. L. Jørgensen, K. Zaremba-Niedzwiedzka, J. Martijn, A. E. Lind, R. van Eijk, C. Schleper, L. Guy, and T. J. G. Ettema (2015). "Complex archaea that bridge the gap between prokaryotes and eukaryotes." *Nature* 521.7551, pp. 173–179.

Steitz, T. A. (2008). "A structural understanding of the dynamic ribosome machine." *Nat Rev Mol Cell Biol* 9.3, pp. 242–253.

Stelter, P., F. M. Huber, R. Kunze, D. Flemming, A. Hoelz, and E. Hurt (2015). "Coordinated Ribosomal L4 Protein Assembly into the Pre-Ribosome Is Regulated by Its Eukaryote-Specific Extension." *Mol Cell* 58.5, pp. 854–862.

Stelter, P. and E. Hurt (2014). "A pulse-chase epitope labeling to study cellular dynamics of newly synthesized proteins: a novel strategy to characterize NPC biogenesis and ribosome maturation/export." *Methods Cell Biol* 122, pp. 147–163.

Stelter, P., R. Kunze, M. Radwan, E. Thomson, K. Thierbach, M. Thoms, and E. Hurt (2012). "Monitoring spatiotemporal biogenesis of macromolecular assemblies by pulse-chase epitope labeling." *Mol Cell* 47.5, pp. 788–796.

Stiegler, P., P. Carbon, M. Zuker, J. P. Ebel, and C. Ehresmann (1980). "[Secondary and topographic structure of ribosomal RNA 16S of Escherichia coli]." *C R Seances Acad Sci D* 291.12, pp. 937–940.

Strunk, B. S., C. R. Loucks, M. Su, H. Vashisth, S. Cheng, J. Schilling, C. L. Brooks, K. Karbstein, and G. Skiniotis (2011). "Ribosome Assembly Factors Prevent Premature Translation Initiation by 40S Assembly Intermediates". *Science* 333.6048, pp. 1449–1453.

Strunk, B. S., M. N. Novak, C. L. Young, and K. Karbstein (2012). "A translation-like cycle is a quality control checkpoint for maturing 40S ribosome subunits." *Cell* 150.1, pp. 111–121.

Sun, Q., X. Zhu, J. Qi, W. An, P. Lan, D. Tan, R. Chen, B. Wang, S. Zheng, C. Zhang, and et al. (2017). "Molecular architecture of the 90S small subunit pre-ribosome". *eLife* 6.

Sung, M.-K., T. R. Porras-Yakushi, J. M. Reitsma, F. M. Huber, M. J. Sweredoski, A. Hoelz, S. Hess, and R. J. Deshaies (2016). "A conserved quality-control pathway that mediates degradation of unassembled ribosomal proteins." *Elife* 5.

Sung, M.-K., J. M. Reitsma, M. J. Sweredoski, S. Hess, and R. J. Deshaies (2016). "Ribosomal proteins produced in excess are degraded by the ubiquitin-proteasome system." *Mol Biol Cell* 27.17, pp. 2642–2652.

Takagi, J. (2007). "Structural basis for ligand recognition by integrins." *Curr Opin Cell Biol* 19.5, pp. 557–564.

Talkish, J., J. Zhang, J. Jakovljevic, E. W. Horsey, and J. L. Woolford Jr (2012). "Hierarchical recruitment into nascent ribosomes of assembly factors required for 27SB pre-rRNA processing in Saccharomyces cerevisiae." *Nucleic Acids Res* 40.17, pp. 8646–8661.

Tarassov, K., V. Messier, C. R. Landry, S. Radinovic, M. M. S. Molina, I. Shames, Y. Malitskaya, J. Vogel, H. Bussey, and S. W. Michnick (2008). "An in Vivo Map of the Yeast Protein Interactome". *Science* 320.5882, pp. 1465–1470.

Thiry, M. and D. L. J. Lafontaine (2005). "Birth of a nucleolus: the evolution of nucleolar compartments." *Trends Cell Biol* 15.4, pp. 194–199.

Thomas, B. J. and R. Rothstein (1989). "Elevated recombination rates in transcriptionally active DNA". *Cell* 56.4, pp. 619–630.

Thomas, F. and U. Kutay (2003). "Biogenesis and nuclear export of ribosomal subunits in higher eukaryotes depend on the CRM1 export pathway". *J. Cell Sci.* 116.12, pp. 2409–.

Thoms, M., E. Thomson, J. Baßler, M. Gnädig, S. Griesel, and E. Hurt (2015). "The Exosome Is Recruited to RNA Substrates through Specific Adaptor Proteins". *Cell* 162.5, pp. 1029–1038.

Thomson, E. and D. Tollervey (2009). "The Final Step in 5.8S rRNA Processing Is Cytoplasmic in Saccharomyces cerevisiae". *Molecular and Cellular Biology* 30.4, pp. 976–984.

Timasheff, S. N., R. A. Brown, J. S. Colter, and M. Davies (1958). "The molecular weight of ribonucleic acid prepared from ascites-tumor cells." *Biochim Biophys Acta* 27.3, pp. 662–663.

Ting, Y.-H., T.-J. Lu, A. W. Johnson, J.-T. Shie, B.-R. Chen, S. Kumar S., and K.-Y. Lo (2016). "Bcp1 Is the Nuclear Chaperone of Rpl23 inSaccharomyces cerevisiae". *Journal of Biological Chemistry* 292.2, pp. 585–596.

Tissieres, A. and J. D. Watson (1958). "Ribonucleoprotein particles from Escherichia coli." *Nature* 182.4638, pp. 778–780.

Trapman, J., J. Retèl, and R. J. Planta (1975). "Ribosomal precursor particles from yeast." *Exp Cell Res* 90.1, pp. 95–104.

Traub, P. and M. Nomura (1968). “Structure and function of E. coli ribosomes. V. Reconstitution of functionally active 30S ribosomal particles from RNA and proteins.” *Proc Natl Acad Sci U S A* 59.3, pp. 777–784.

Trotta, C. R., E. Lund, L. Kahan, A. W. Johnson, and J. E. Dahlberg (2003). “Coordinated nuclear export of 60S ribosomal subunits and NMD3 in vertebrates.” *EMBO J* 22.11, pp. 2841–2851.

Ts’o, P. O., J. Bonner, and H. Dintzis (1958). “On the similarity of amino acid composition of microsomal nucleoprotein particles.” *Arch Biochem Biophys* 76.1, pp. 225–227.

Turowski, T. W. and D. Tollervey (2014). “Cotranscriptional events in eukaryotic ribosome synthesis”. *Wiley Interdisciplinary Reviews: RNA* 6.1, pp. 129–139.

Tutuncuoglu, B., J. Jakovljevic, S. Wu, N. Gao, and J. L. Woolford Jr (2016). “The N-terminal extension of yeast ribosomal protein L8 is involved in two major remodeling events during late nuclear stages of 60S ribosomal subunit assembly.” *RNA*.

Udem, S. A. and J. R. Warner (1972). “Ribosomal RNA synthesis in Saccharomyces cerevisiae.” *J Mol Biol* 65.2, pp. 227–242.

Udem, S. A. and J. R. Warner (1973). “The cytoplasmic maturation of a ribosomal precursor ribonucleic acid in yeast.” *J Biol Chem* 248.4, pp. 1412–1416.

Ulbrich, C., M. Diepholz, J. Bassler, D. Kressler, B. Pertschy, K. Galani, B. Böttcher, and E. Hurt (2009). “Mechanochemical removal of ribosome biogenesis factors from nascent 60S ribosomal subunits.” *Cell* 138.5, pp. 911–922.

Van Dyck, E., F. Foury, B. Stillman, and S. J. Brill (1992). “A single-stranded DNA binding protein required for mitochondrial DNA replication in S. cerevisiae is homologous to E. coli SSB.” *The EMBO Journal* 11.9, pp. 3421–3430.

Van Etten, R. A., M. W. Walberg, and D. A. Clayton (1980). “Precise localization and nucleotide sequence of the two mouse mitochondrial rRNA genes and three immediately adjacent novel tRNA genes.” *Cell* 22.1 Pt 1, pp. 157–170.

Veith, T., R. Martin, J. P. Wurm, B. L. Weis, E. Duchardt-Ferner, C. Safferthal, R. Hennig, O. Mirus, M. T. Bohnsack, J. Wohnert, and E. Schleiff (2011). “Structural and functional analysis of the archaeal endonuclease Nob1”. *Nucleic Acids Research* 40.7, pp. 3259–3274.

Veith, T., J. P. Wurm, E. Duchardt-Ferner, B. Weis, R. Martin, C. Safferthal, M. T. Bohnsack, E. Schleiff, and J. Wöhnert (2011). “Backbone and side chain NMR resonance assignments for an archaeal homolog of the endonuclease Nob1 involved in ribosome biogenesis”. *Biomolecular NMR Assignments* 6.1, pp. 47–50.

Velculescu, V. E., L. Zhang, W. Zhou, J. Vogelstein, M. A. Basrai, D. Bassett Jr, P. Hieter, B. Vogelstein, and K. W. Kinzler (1997). “Characterization of the yeast transcriptome.” *Cell* 88.2, pp. 243–251.

Venema, J. and D. Tollervey (1996). “RRP5 is required for formation of both 18S and 5.8S rRNA in yeast.” *The EMBO Journal* 15.20, pp. 5701–5714.

Venema, J. and D. Tollervey (1999). “Ribosome synthesis in Saccharomyces cerevisiae.” *Annu Rev Genet* 33, pp. 261–311.

Voss, N. R., M. Gerstein, T. A. Steitz, and P. B. Moore (2006). “The geometry of the ribosomal polypeptide exit tunnel.” *J Mol Biol* 360.4, pp. 893–906.

Warner, J. R. (1999). “The economics of ribosome biosynthesis in yeast.” *Trends Biochem Sci* 24.11, pp. 437–440.

Warner, J. R., P. M. Knopf, and A. Rich (1963). “A multiple ribosomal structure in protein synthesis.” *Proc Natl Acad Sci U S A* 49, pp. 122–129.

Warner, J. R. and K. B. McIntosh (2009). “How common are extraribosomal functions of ribosomal proteins?” *Mol Cell* 34.1, pp. 3–11.

Waterhouse, A. M., J. B. Procter, D. M. A. Martin, M. Clamp, and G. J. Barton (2009). “Jalview Version 2–a multiple sequence alignment editor and analysis workbench.” *Bioinformatics* 25.9, pp. 1189–1191.

Watkins, N. J. and M. T. Bohnsack (2011). “The box C/D and H/ACA snoRNPs: key players in the modification, processing and the dynamic folding of ribosomal RNA”. *Wiley Interdisciplinary Reviews: RNA* 3.3, pp. 397–414.

Weis, F., E. Giudice, M. Churcher, L. Jin, C. Hilcenko, C. C. Wong, D. Traynor, R. R. Kay, and A. J. Warren (2015). “Mechanism of eIF6 release from the nascent 60S ribosomal subunit.” *Nat Struct Mol Biol* 22.11, pp. 914–919.

West, M., J. B. Hedges, A. Chen, and A. W. Johnson (2005). “Defining the Order in Which Nmd3p and Rpl10p Load onto Nascent 60S Ribosomal Subunits”. *Molecular and Cellular Biology* 25.9, pp. 3802–3813.

Wettstein, F. O. and H. Noll (1965). “Binding of transfer ribonucleic acid to ribosomes engaged in protein synthesis: number and properties of ribosomal binding sites.” *J Mol Biol* 11, pp. 35–53.

Williams, T. A., P. G. Foster, C. J. Cox, and T. M. Embley (2013). “An archaeal origin of eukaryotes supports only two primary domains of life.” *Nature* 504.7479, pp. 231–236.

Williams, T. A., P. G. Foster, T. M. W. Nye, C. J. Cox, and T. M. Embley (2012). “A congruent phylogenomic signal places eukaryotes within the Archaea.” *Proc Biol Sci* 279.1749, pp. 4870–4879.

Wimberly, B. T., D. E. Brodersen, W. Clemons Jr, R. J. Morgan-Warren, A. P. Carter, C. Vonrhein, T. Hartsch, and V. Ramakrishnan (2000). “Structure of the 30S ribosomal subunit.” *Nature* 407.6802, pp. 327–339.

Winker, S. and C. R. Woese (1991). “A definition of the domains Archaea, Bacteria and Eucarya in terms of small subunit ribosomal RNA characteristics.” *Syst Appl Microbiol* 14.4, pp. 305–310.

Woese, C. R. (1987). “Bacterial evolution.” *Microbiol Rev* 51.2, pp. 221–271.

Woese, C. R. (2000). “Interpreting the universal phylogenetic tree.” *Proc Natl Acad Sci U S A* 97.15, pp. 8392–8396.

Woese, C. R., L. J. Magrum, R. Gupta, R. B. Siegel, D. A. Stahl, J. Kop, N. Crawford, J. Brosius, R. Gutell, J. J. Hogan, and H. F. Noller (1980). “Secondary structure model for bacterial 16S ribosomal RNA: phylogenetic, enzymatic and chemical evidence.” *Nucleic Acids Res* 8.10, pp. 2275–2293.

Woese, C. R. (1967). *The genetic code : the molecular basis for genetic expression*. New York: Harper & Row.

Woodson, S. A. (2011). “RNA folding pathways and the self-assembly of ribosomes.” *Acc Chem Res* 44.12, pp. 1312–1319.

Woolford Jr, J. L. and S. J. Baserga (2013). “Ribosome biogenesis in the yeast Saccharomyces cerevisiae.” *Genetics* 195.3, pp. 643–681.

Wu, S., D. Tan, J. L. Woolford Jr, M.-Q. Dong, and N. Gao (2016). “Atomic modeling of the ITS2 ribosome assembly subcomplex from cryo-EM together with mass spectrometry-identified protein-protein crosslinks.” *Protein Sci*.

Wu, S., B. Tutuncuoglu, K. Yan, H. Brown, Y. Zhang, D. Tan, M. Gamalinda, Y. Yuan, Z. Li, J. Jakovljevic, C. Ma, J. Lei, M.-Q. Dong, J. L. Woolford Jr, and N. Gao (2016). “Diverse roles of

assembly factors revealed by structures of late nuclear pre-60S ribosomes". *Nature* 534.7605, pp. 133–137.

Wurm, J. P., B. Meyer, U. Bahr, M. Held, O. Frolow, P. Kotter, J. W. Engels, A. Heckel, M. Karas, K. D. Entian, and J. Wöhnert (2010). "The ribosome assembly factor Nep1 responsible for Bowen-Conradi syndrome is a pseudouridine-N1-specific methyltransferase". *Nucleic Acids Research* 38.7, pp. 2387–2398.

Xue, S. and M. Barna (2012). "Specialized ribosomes: a new frontier in gene regulation and organismal biology." *Nat Rev Mol Cell Biol* 13.6, pp. 355–369.

Yang, C. H., E. J. Lambie, J. Hardin, J. Craft, and M. Snyder (1989). "Higher order structure is present in the yeast nucleus: autoantibody probes demonstrate that the nucleolus lies opposite the spindle pole body." *Chromosoma* 98.2, pp. 123–128.

Yao, W., D. Roser, A. Köhler, B. Bradatsch, J. Bassler, and E. Hurt (2007). "Nuclear export of ribosomal 60S subunits by the general mRNA export receptor Mex67-Mtr2." *Mol Cell* 26.1, pp. 51–62.

Yeh, J. I., A. S. Levine, S. Du, U. Chinte, H. Ghodke, H. Wang, H. Shi, C. L. Hsieh, J. F. Conway, B. Van Houten, and V. Rapić-Otrin (2012). "Damaged DNA induced UV-damaged DNA-binding protein (UV-DDB) dimerization and its roles in chromatinized DNA repair". *Proceedings of the National Academy of Sciences* 109.41, E2737–E2746.

Yusupov, M. M., G. Z. Yusupova, A. Baucom, K. Lieberman, T. N. Earnest, J. H. Cate, and H. F. Noller (2001). "Crystal structure of the ribosome at 5.5 A resolution." *Science* 292.5518, pp. 883–896.

Yusupova, G., L. Jenner, B. Rees, D. Moras, and M. Yusupov (2006). "Structural basis for messenger RNA movement on the ribosome." *Nature* 444.7117, pp. 391–394.

Yutin, N. and E. V. Koonin (2012). "Archaeal origin of tubulin." *Biol Direct* 7, p. 10.

Yutin, N., P. Puigbò, E. V. Koonin, and Y. I. Wolf (2012). "Phylogenomics of prokaryotic ribosomal proteins." *PLoS One* 7.5, e36972.

Zaremba-Niedzwiedzka, K., E. F. Caceres, J. H. Saw, D. Bäckström, L. Juzokaite, E. Vancaester, K. W. Seitz, K. Anantharaman, P. Starnawski, K. U. Kjeldsen, M. B. Scott, T. Nunoura, J. F. Banfield, A. Schramm, B. J. Baker, A. Spang, and T. J. G. Ettema (2017). "Asgard archaea illuminate the origin of eukaryotic cellular complexity". *Nature* 541.7637, pp. 353–358.

Zhang, H., X. Ma, T. Shi, Q. Song, H. Zhao, and D. Ma (2010). "NSA2, a novel nucleolus protein regulates cell proliferation and cell cycle." *Biochem Biophys Res Commun* 391.1, pp. 651–658.

Zhang, J., P. Harnpicharnchai, J. Jakovljevic, L. Tang, Y. Guo, M. Oeffinger, M. P. Rout, S. L. Hiley, T. Hughes, and J. L. Woolford Jr (2007). "Assembly factors Rpf2 and Rrs1 recruit 5S rRNA and ribosomal proteins rpL5 and rpL11 into nascent ribosomes." *Genes Dev* 21.20, pp. 2580–2592.

Zhang, L., C. Wu, G. Cai, S. Chen, and K. Ye (2016). "Stepwise and dynamic assembly of the earliest precursors of small ribosomal subunits in yeast". *Genes & Development* 30.6, pp. 718–732.

Zhang, X., K. Yan, Y. Zhang, N. Li, C. Ma, Z. Li, Y. Zhang, B. Feng, J. Liu, Y. Sun, Y. Xu, J. Lei, and N. Gao (2014). "Structural insights into the function of a unique tandem GTPase EngA in bacterial ribosome assembly." *Nucleic Acids Res* 42.21, pp. 13430–13439.

Zhang, Y., G. W. Wolf, K. Bhat, A. Jin, T. Allio, W. A. Burkhart, and Y. Xiong (2003). "Ribosomal protein L11 negatively regulates oncoprotein MDM2 and mediates a p53-dependent ribosomal-stress checkpoint pathway." *Mol Cell Biol* 23.23, pp. 8902–8912.

Zhou, X., W.-J. Liao, J.-M. Liao, P. Liao, and H. Lu (2015). “Ribosomal proteins: functions beyond the ribosome.” *J Mol Cell Biol* 7.2, pp. 92–104.

Zhu, J., X. Liu, M. Anjos, C. C. Correll, and A. W. Johnson (2016). “Utp14 Recruits and Activates the RNA Helicase Dhr1 To Undock U3 snoRNA from the Preribosome”. *Molecular and Cellular Biology* 36.6, pp. 965–978.

Zuker, M. (2003). “Mfold web server for nucleic acid folding and hybridization prediction.” *Nucleic Acids Res* 31.13, pp. 3406–3415.

Appendix

A.1 Salt stability of the Nsa2-Rsa4 interaction

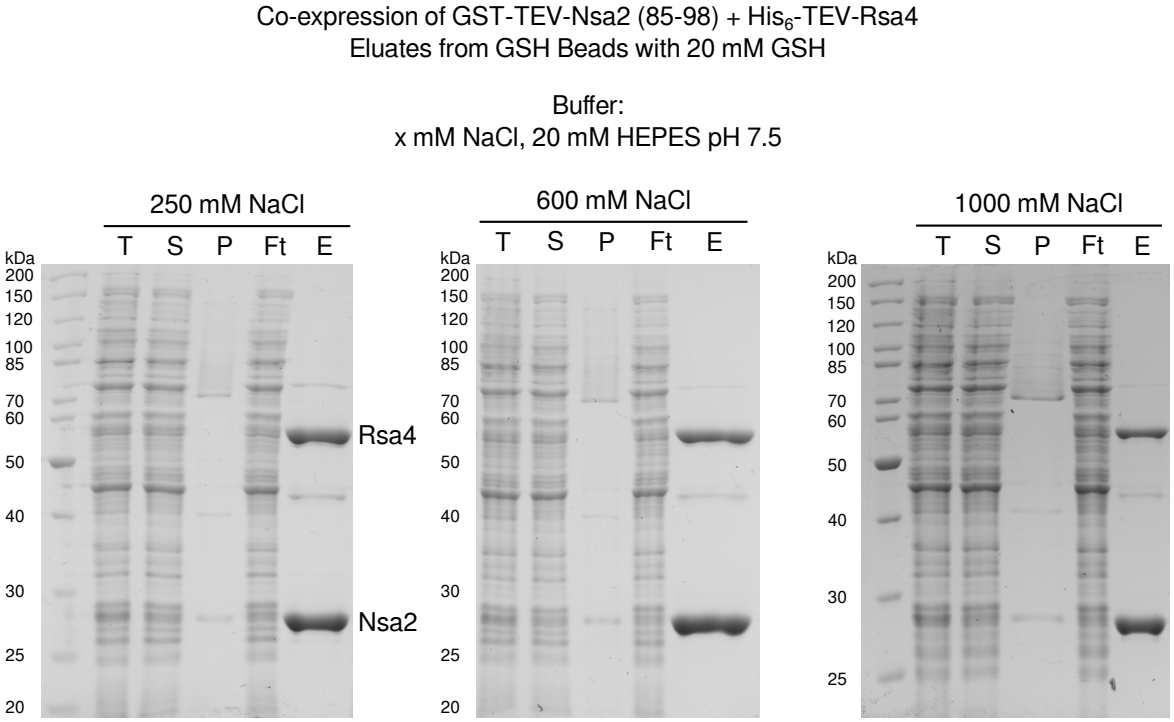

Figure A.1: The interaction of Nsa2 and Rsa4 is resistant to high salt concentrations The Nsa2-Rsa4 heterodimer was purified with increasing salt concentrations. The GST-TEV-tagged peptide of Nsa2 (amino acids 85-98) was co-expressed with His_6-Rsa4 in *E. coli*. Purifications were performed in a buffer containing 20 mM HEPES pH 7.5 and 250 mM, 600 mM, and 1000 mM NaCl, respectively. After washing, the complex was eluted with buffer containing 20 mM GSH and samples were analyzed by SDS-PAGE. T = Total. S = Supernatant, P = Pellet. Ft = Flow through. E = Eluate.

A.2 *In vitro* degradation of ctNsa2

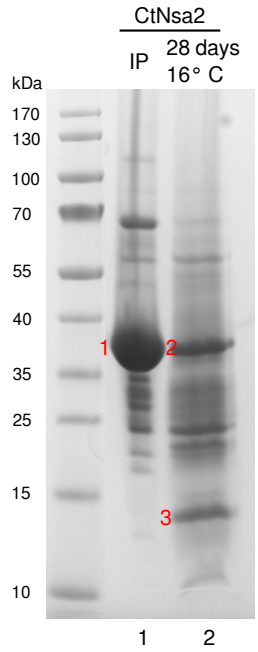

Buffer:
150 mM NaCl
25 mM HEPES pH 7.5
3% Glycerol (v/v)

Sequence coverage of mass specced bands

1 CtNsa2 - fulllength - 0 days @ 16° C

Matched peptides shown in **Bold Red**

```
  1 MPQNEYIERH RKLHGRRLDA EERARKKAAR EGHKNSENAQ NLRGLRAKLY
 51 AKQRHAQKIQ MRKAIKQHEE RNVKGRPAEK EPSDPIPSYL LDRANPTTAK
101 ALSSQIKNKR AEKAARFSVP IPKVRGISEE EMFKVVKTGK KTHKKGWKRI
151 VTKPTFVGPD FTRRPVKYER FIRPMGLRYK KANVTHPTLN VTVQLPILSV
201 KKNPSNPLYT QLGVLTKGTI IEVNVSDLGI VTASGKIAWG RYAQITNNPE
251 NDGCVNAVLL V
```

2 CtNsa2 - fulllength - 28 days @ 16° C

Matched peptides shown in **Bold Red**

```
  1 MPQNEYIERH RKLHGRRLDA EERARKKAAR EGHKNSENAQ NLRGLRAKLY
 51 AKQRHAQKIQ MRKAIKQHEE RNVKGRPAEK EPSDPIPSYL LDRANPTTAK
101 ALSSQIKNKR AEKAARFSVP IPKVRGISEE EMFKVVKTGK KTHKKGWKRI
151 VTKPTFVGPD FTRRPVKYER FIRPMGLRYK KANVTHPTLN VTVQLPILSV
201 KKNPSNPLYT QLGVLTKGTI IEVNVSDLGI VTASGKIAWG RYAQITNNPE
251 NDGCVNAVLL V
```

3 CtNsa2 - fragment - 28 days @ 16° C

Matched peptides shown in **Bold Red**

```
  1 MPQNEYIERH RKLHGRRLDA EERARKKAAR EGHKNSENAQ NLRGLRAKLY
 51 AKQRHAQKIQ MRKAIKQHEE RNVKGRPAEK EPSDPIPSYL LDRANPTTAK
101 ALSSQIKNKR AEKAARFSVP IPKVRGISEE EMFKVVKTGK KTHKKGWKRI
151 VTKPTFVGPD FTRRPVKYER FIRPMGLRYK KANVTHPTLN VTVQLPILSV
201 KKNPSNPLYT QLGVLTKGTI IEVNVSDLGI VTASGKIAWG RYAQITNNPE
251 NDGCVNAVLL V
```

Figure A.2: The N-domain of ctNsa2 is unstable and readily degraded *in vitro* Full length ctNsa2 was incubated for 28 days at 16 °C , which mimicked the conditions that produced initial crystals in the crystallization trials. The buffer consisted of 150 mM NaCl, 25 mM HEPES pH 7.5, and 3% glycerol (v/v). The input sample was compared to the incubated sample by SDS-PAGE (left side). The incubated sample showed a band at ~14 kDa, which is not seen in the control, and which corresponds to the size of the protein fragment, that was found in the initial crystals (data not shown). The bands, which represent the full length and stable fragments, were analyzed by mass spectrometry. Sequence coverage for the three analyzed bands is shown on the right side. The full length bands display a peptide coverage of the whole protein sequence, whereas the stable fragment only contains C-domain derived peptides.

A.3 Crystallization finescreen for the Nsa2-Rsa4 complex

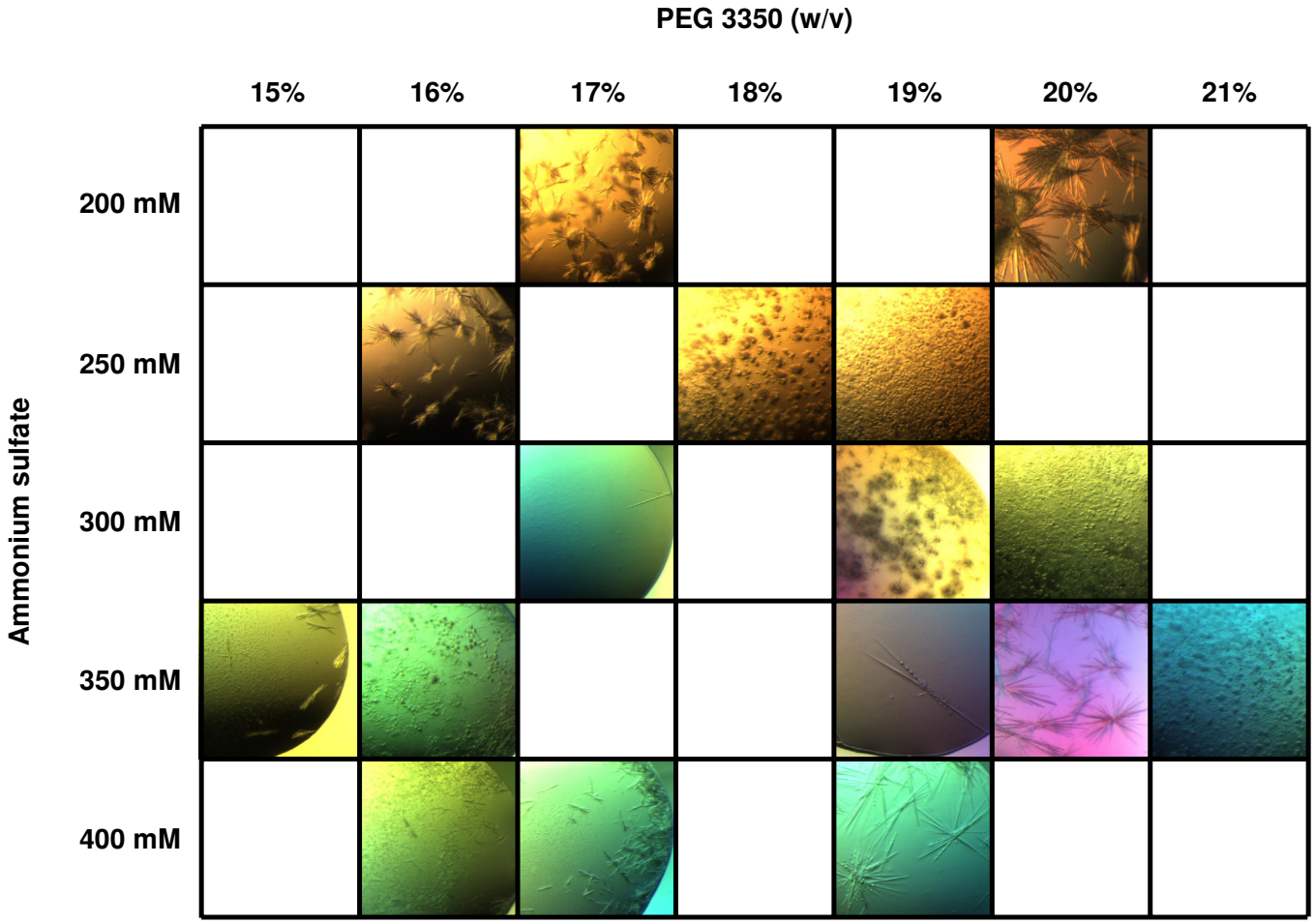

Figure A.3: Crystallization fine screen of the Nsa2-Rsa4 minimal complex The minimal complex, consisting of MBP-Nsa2 (amino acids 81-101) and the Rsa4 Δ136 truncation, was concentrated to 20 mg/ml and sitting drops were set up with 0.2 µl of protein and 0.2 µl of precipitant. Indicated wells showed crystals after seven days of incubation at 18 °C .

A.4 Rsa4 alignment

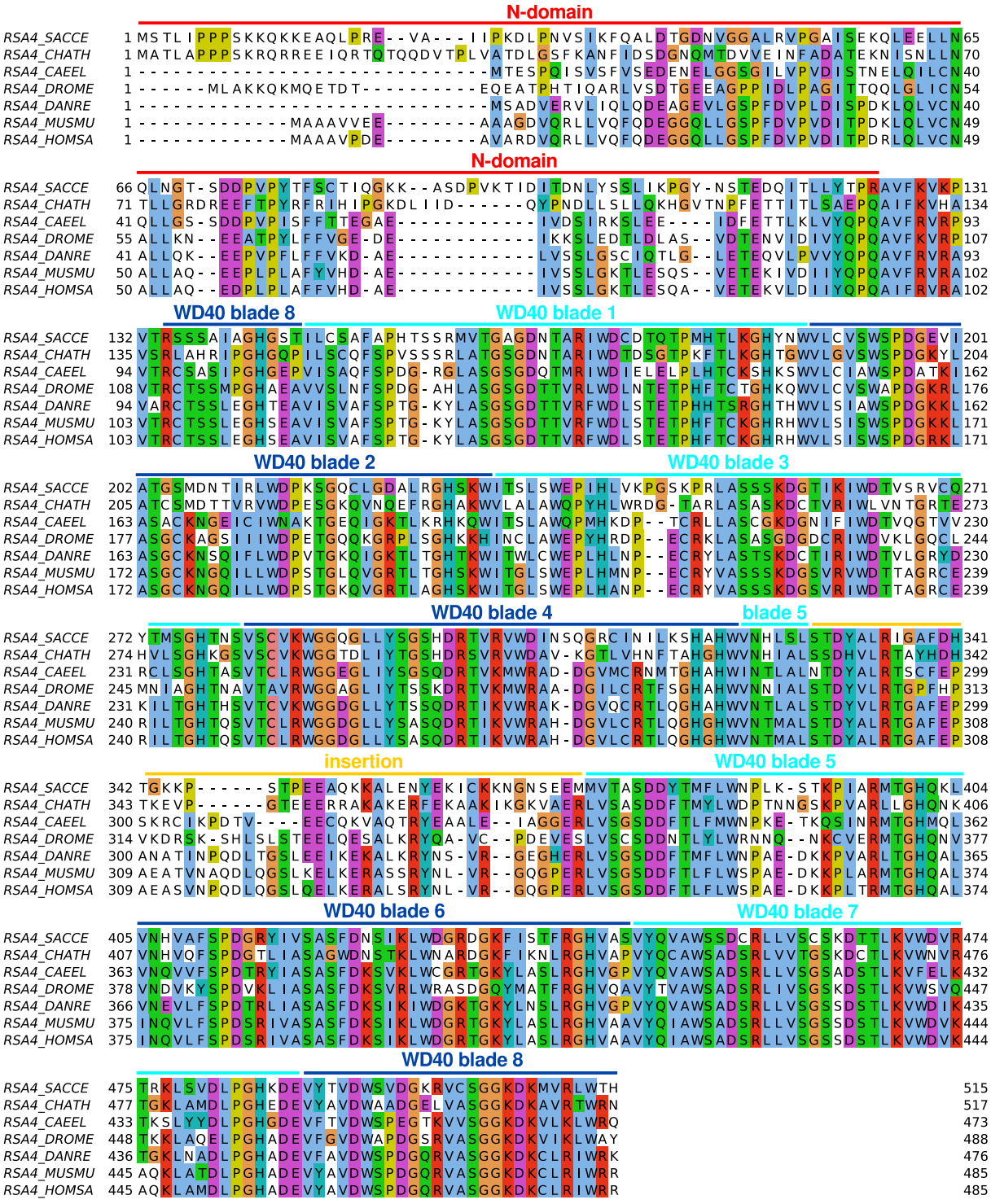

Figure A.4: Annotated multiple sequence alignment of Rsa4 homologs SACCE = *Saccharomyces cerevisiae*, CHATH = *Chaetomium thermophilum*, CAEEL = *Caenorhabditis elegans*, DROME = *Drosophila melanogaster*, DANRE = *Danio rerio*, MUSMU = *Mus musculus*, HOMSA = *Homo sapiens*.

A.5 The S8E family

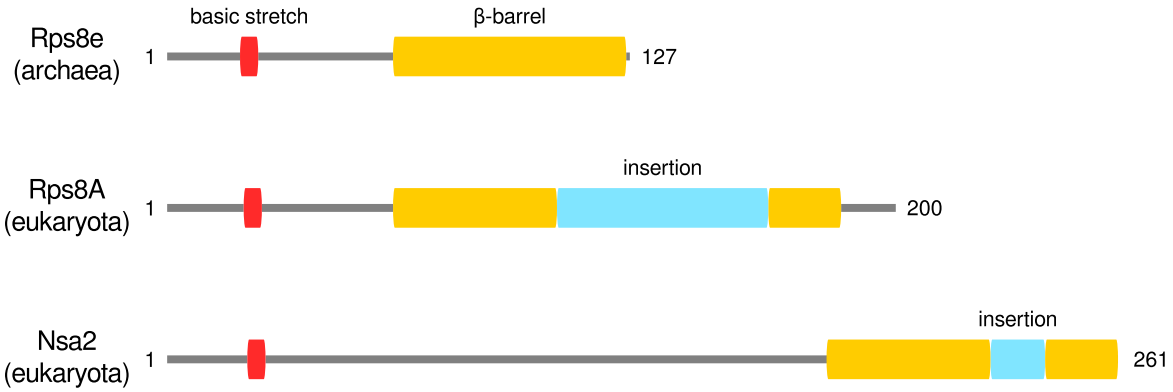

Figure A.5: The S8e family Representative members of the S8e family are depicted. Rps8e from *Pyrococcus horikoshii*, Rps8A and Nsa2 from *Saccharomyces cerevisiae*. Defining features of the S8e family are indicated: Red = basic stretch. Yellow = β-barrel. Cyan = eukaryotic β-barrel insertions.

A.6 S8E family alignment

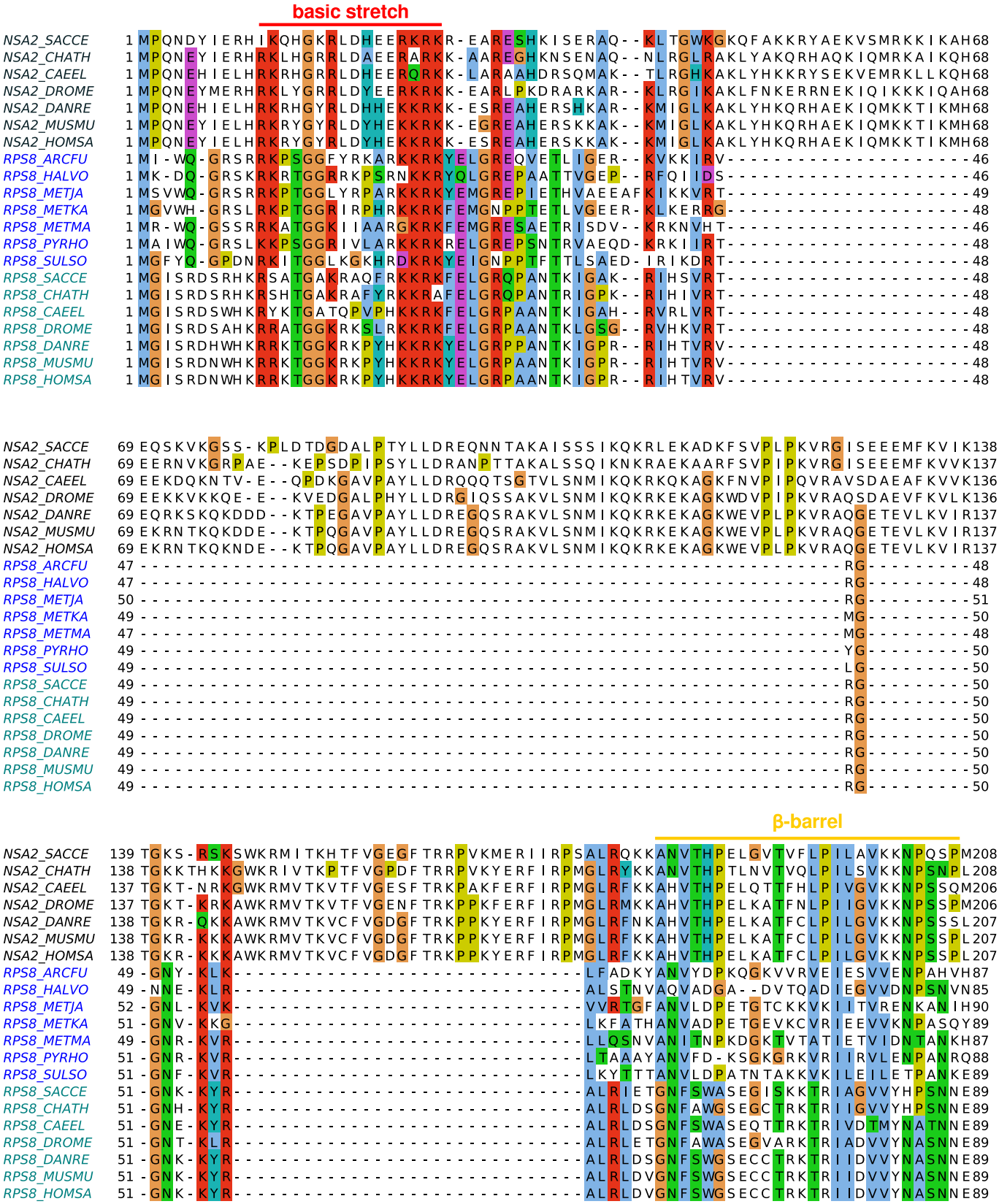

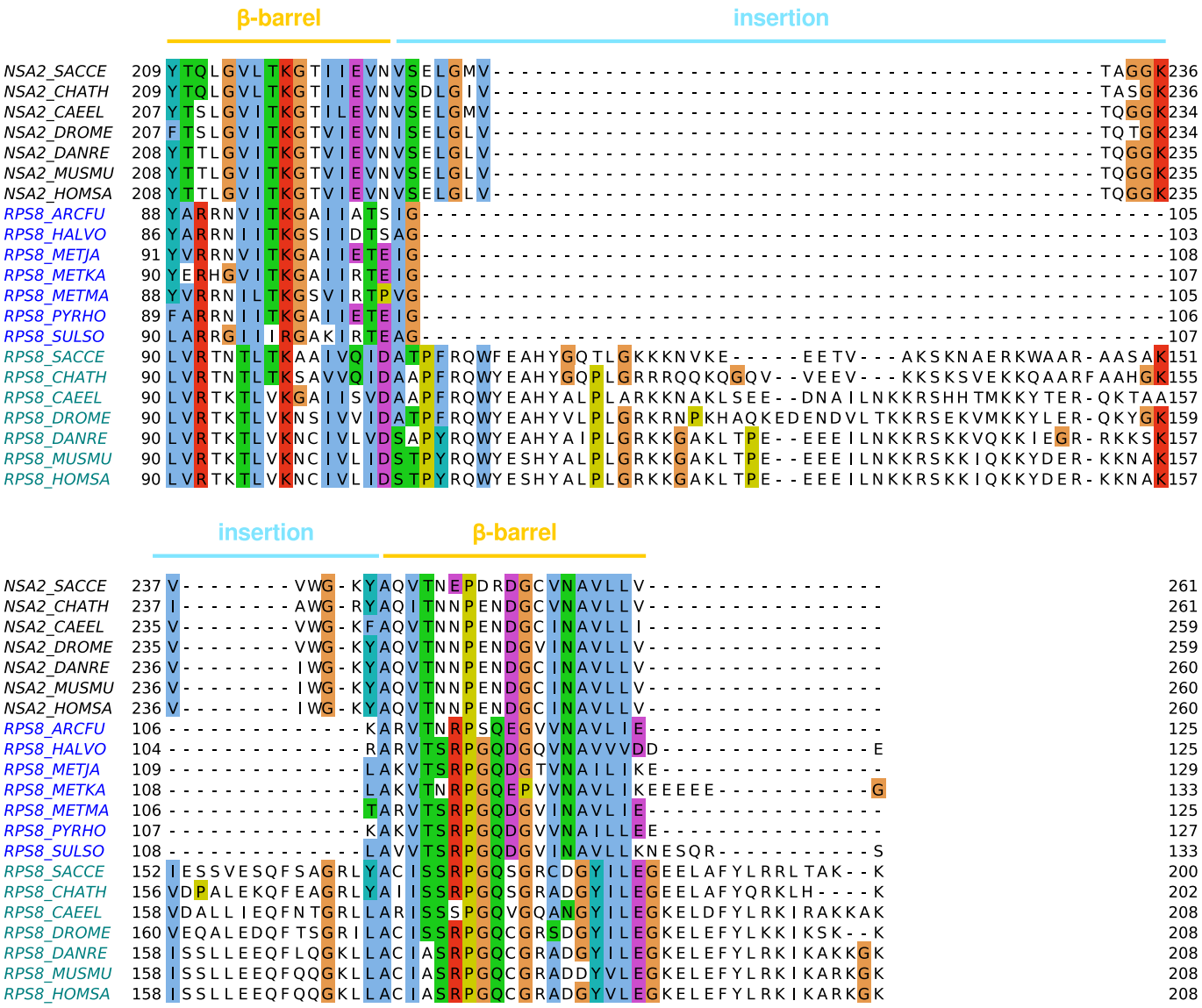

Figure A.6: Annotated multiple sequence alignment of Rps8e family homologs Rps8e homologs were aligned using MSAProbs. Black font = Nsa2 homologs. Blue font = Archaeal Rps8 homologs. Sea green = eukaryotic Rps8 homologs. Sequence features are indicated above the alignment. Basic stretch = defining feature of the PROSITE family 'RIBOSOMAL_S8E' (PROSITE entry PDOC00918), as described by Engemann et al. 1995. β-barrel = second defining feature of the S8E family, not mentioned in the PROSITE database, but is present in all members of the S8E family. Alignment of the β-barrel demonstrates sequence conservation between archaeal Rps8 and Nsa2, which is less evident between eukaryotic Rps8 and Nsa2. Nevertheless, eukaryotic Rps8 and Nsa2 contain an insertion in the β-barrel, at the same position, but of varying length and sequence. SACCE = *Saccharomyces cerevisiae*, CHATH = *Chaetomium thermophilum*, CAEEL = *Caenorhabditis elegans*, DROME = *Drosophila melanogaster*, DANRE = *Danio rerio*, MUSMU = *Mus musculus*, HOMSA = *Homo sapiens*, ARCFU = *Archaeoglobus fulgidus*, HALVO = *Haloferax volcanii*, METJA = *Methanocaldococcus jannaschii*, METKA = *Methanopyrus kandleri*, METMA = *Methanosarcina mazei*, PYRHO = *Pyrococcus horikoshii*, SULSO = *Sulfolobus solfataricus*.

A.7 Nsa2 alignment

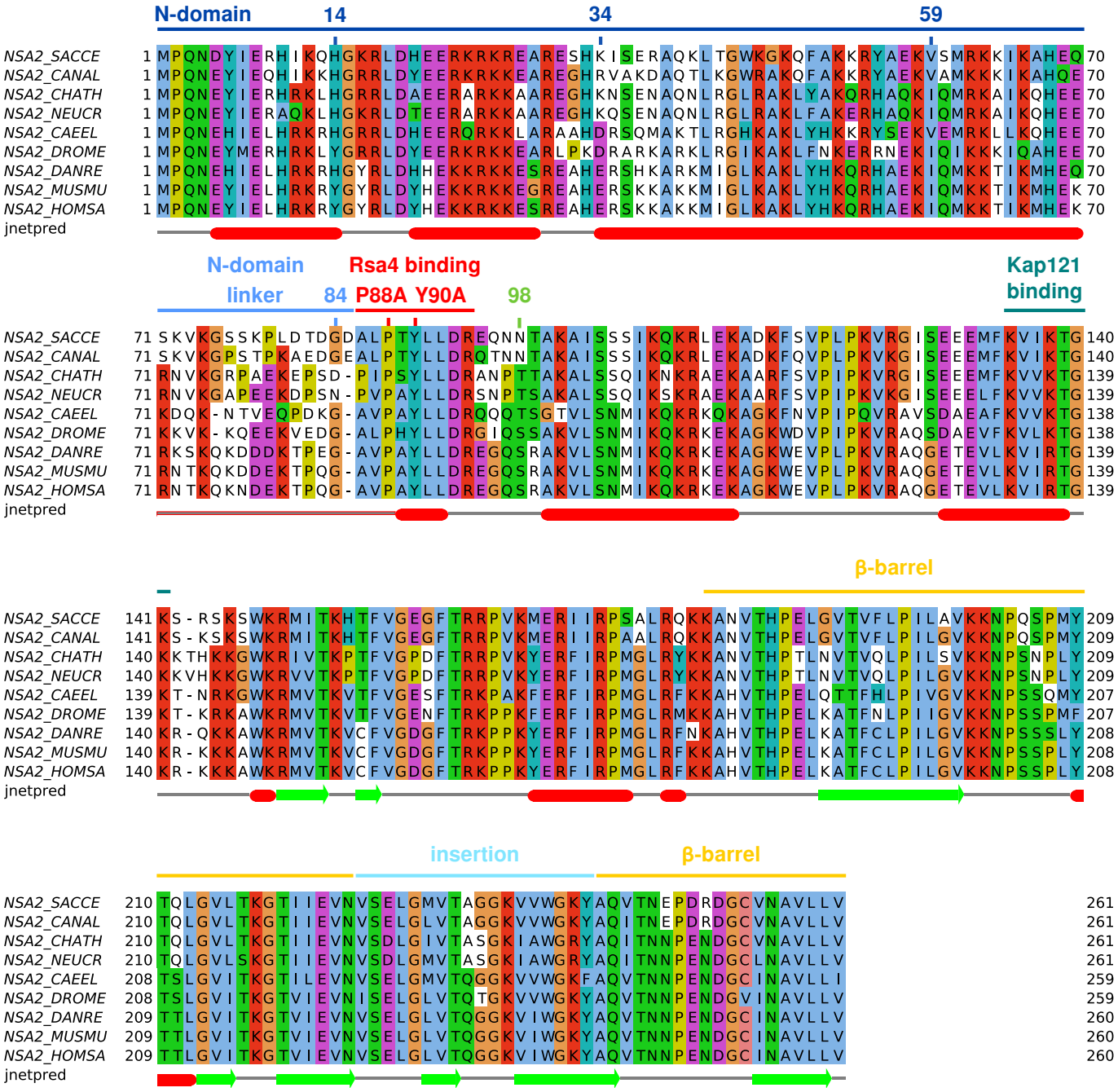

Figure A.7: Annotated multiple sequence alignment of Nsa2 homologs Nsa2 homologs were aligned with Clustal Omega. The secondary structure was predicted by jnetpred for 'NSA2_SACCE'. Functional regions of Nsa2 are indicated above the alignment. The P88A and Y90A mutant are depicted at the Rsa4 binding motif. SACCE = *Saccharomyces cerevisiae*, CANAL = *Candida albicans*, CHATH = *Chaetomium thermophilum*, NEUCR = *Neurospore crassa*, CAEEL = *Caenorhabditis elegans*, DROME = *Drosophila melanogaster*, DANRE = *Danio rerio*, MUSMU = *Mus musculus*, HOMSA = *Homo sapiens*.

A.8 The β-barrel insertion and the linker of Nsa2 are essential

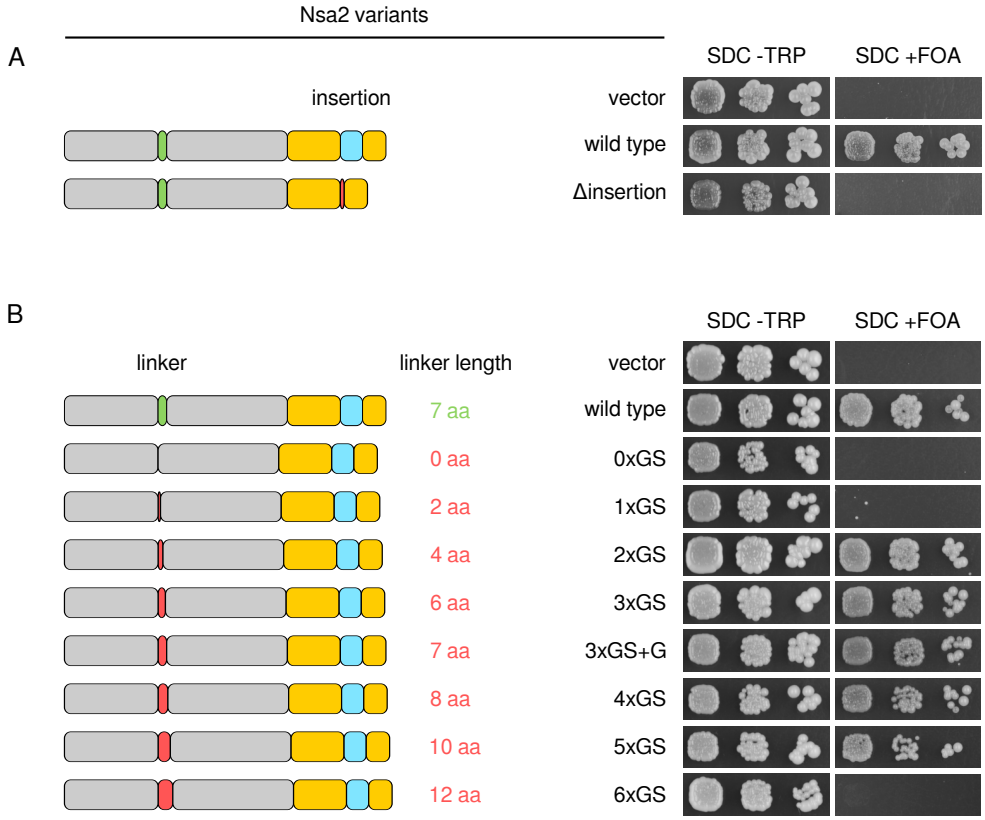

Figure A.8: The β-barrel insertion and the linker of Nsa2 are essential A) Deletion of the insertion in the β-barrel of Nsa2 is inviable. A *NSA2* shuffle strain was transformed with plasmids expressing indicated Nsa2 variants under control of the endogenous *NSA2* promoter. Transformants were spotted on 5-FOA containing plates and grown for four days at 30 °C . The deletion created orphan β-strands in the β-barrel, which were connected by a three amino acid long linker with the sequence 'Ile-Gly-Leu', that was derived from archaeal sequences of Rps8. B) The length of the linker between the Nsa2 N-domain and Rsa4 is important for viability. The endogenous sequence can be replaced by glycine and serine containing peptides of varying length. Linkers smaller than four amino acids and larger than 10 amino acids are inviable. A *NSA2* shuffle strain was transformed with plasmids expressing indicated Nsa2 variants under control of the endogenous *NSA2* promoter. Transformants were spotted on 5-FOA containing plates and grown for three days at 30 °C .

A.9 Nog1 N-domain alignment

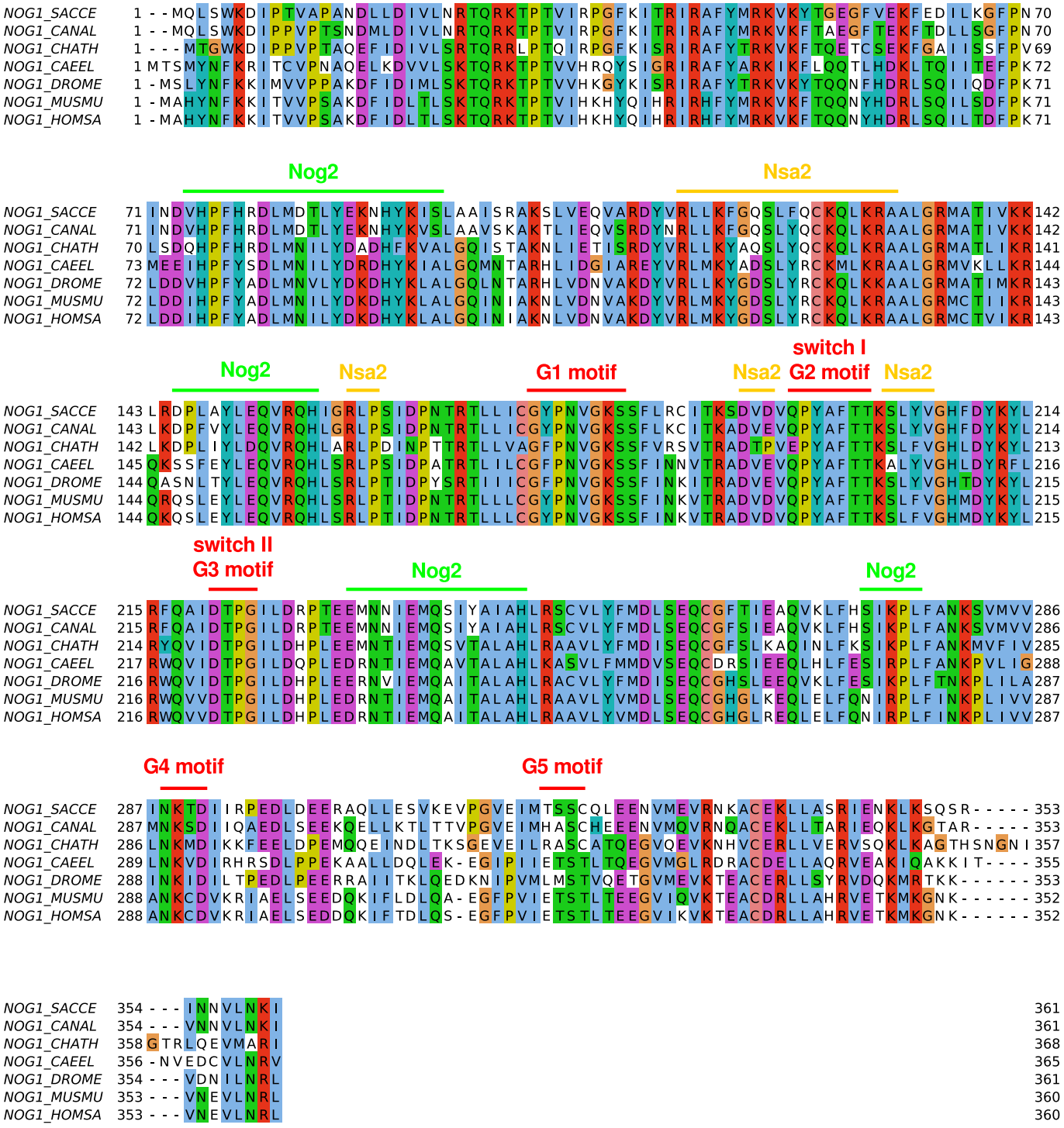

Figure A.9: Multiple sequence alignment of the Nog1 N-domain with binding sites of Nsa2 and Nog2 Red = GTPase consensus motifs. Yellow = Nsa2 binding. Green = Nog2 binding, according to PDB code: 3JCT. SACCE = *Saccharomyces cerevisiae*, CANAL = *Candida albicans*, CHATH = *Chaetomium thermophilum*, CAEEL = *Caenorhabditis elegans*, DROME = *Drosophila melanogaster*, MUSMU = *Mus musculus*, HOMSA = *Homo sapiens*.

List of abbreviations

AAA ATPase associated with diverse cellular activities
AF assembly factor
ATP Adenosine triphosphate
CP central protuberance
CRAC cross-linking and analysis of cDNA
ES expansion segment
ETS external transcribed spacer
GTP Guanosine triphosphate
IGS intergenic spacer
ITS internal transcribed spacer
kDa kilodalton
LUCA last universal common ancestor (of all cells)
MBP maltose-binding protein
MIDAS metal ion–dependent adhesion site
NAC nascent polypeptide–associated complex
NLS nuclear localization signal
NTS non-transcribed spacer
NPC nuclear pore complex
NMR nuclear magnetic resonance
mRNA messenger RNA
PTC peptidyl transferase center
RNA ribonucleic acid
RNP ribonucleoprotein
r-protein ribosomal protein
SDS-PAGE SDS polyacrylamide gel electrophoresis
SEC size-exclusion chromatography
rRNA ribosomal RNA
snoRNA small nucleolar RNA
TEV tobacco etch virus
tRNA transfer RNA

List of Figures

1.1 Secondary structure of the small subunit of *Saccharomyces cerevisiae* . 7
1.2 Secondary structure of the large subunit of *Saccharomyces cerevisiae* . 8
1.3 80S ribosome of *Saccharomyces cerevisiae* 10
1.4 Ribosomal subunits of *Saccharomyces cerevisiae* 11
1.5 Peptidyl transferase center of *Saccharomyces cerevisiae* 13
1.6 Expansion of rRNA in evolution 16
1.7 Ribosome biogenesis in *Saccharomyces cerevisiae* 19
1.8 rDNA gene of *Saccharomyces cerevisiae* 20
1.9 cryo-EM tomography analysis of rDNA transcription 21
1.10 Box C/D and H/ACA snoRNAs 24
1.11 rRNA processing in *Saccharomyces cerevisiae* 26
1.12 Major steps in eukaryotic ribosome assembly 33
1.13 Depletion phenotypes of ribosomal proteins correlate with their location on the ribosome 34
1.14 Late steps in 60S subunit assembly 37
1.15 The AAA-ATPase Rea1 38
1.16 The role of Rea1 in 60S biogenesis 39

2.1 13 amino acids of Nsa2 interact with the Rsa4 β-propeller 45
2.2 The Rsa4-interacting motif of Nsa2 is essential for cell growth 46
2.3 Crystallization of the Nsa2-Rsa4 minimal complex 48
2.4 Crystal structure of the Nsa2-Rsa4 complex 50
2.5 Interaction of the Nsa2 peptide with the Rsa4 β-propeller 51
2.6 Tandem affinity purification of Nsa2 and Rsa4 52
2.7 The Y90A mutant of Nsa2 abolishes the interaction with Rsa4 55
2.8 Mutations in the Rsa4 β-propeller disrupt the interaction with Nsa2 . . . 57
2.9 Rsa4 point mutants are associated with DNA damage repair factors . . . 58
2.10 NMR structure of the Nsa2 N-domain 61
2.11 The C-domain of Nsa2 forms the S8E family β-barrel 62
2.12 Sequence alignment of defining features of the S8e family 63

2.13 Location of Nsa2 and Rsa4 on the Arx1-particle 66
2.14 Nsa2 association to Ssf1-particles and truncation analysis of the N-domain 69
2.15 Pre-ribosome association of Nsa2 depends on its N-domain 70

3.1 Assembly factor network of Nsa2 on late 60S pre-ribosomes 75
3.2 Nsa2 functions in rRNA domain stabilization and helix 89 maturation . . 78
3.3 Evolutionary connection of Nsa2 and Rps8 85

A.1 The interaction of Nsa2 and Rsa4 is resistant to high salt concentrations 125
A.2 The N-domain of ctNsa2 is unstable and readily degraded *in vitro* 126
A.3 Crystallization fine screen of the Nsa2-Rsa4 minimal complex 127
A.4 Annotated multiple sequence alignment of Rsa4 homologs 128
A.5 The S8e family 129
A.6 Annotated multiple sequence alignment of Rps8e family homologs . . . 131
A.7 Annotated multiple sequence alignment of Nsa2 homologs 132
A.8 The β-barrel insertion and the linker of Nsa2 are essential 133
A.9 Multiple sequence alignment of the Nog1 N-domain with binding sites of Nsa2 and Nog2 134